

Dissertation for the Doctor's degree
submitted to the Faculty of Chemistry and Pharmacy
at the Ludwig-Maximilians-University of Munich

**I-Modified Nucleosides as DNA-Sugar Centered Radical
Precursors**

II-DNA Excess Electron Transfer Studies

**III-A new Direct DNA Detection Method:
DNA-Photography**

Antonio Manetto
from
Messina/Italy

2007

Erklärung

Diese Dissertation wurde im Sinne von § 13 Abs. 3 bzw. 4 der Promotionsordnung vom 29. Januar 1998 von Herrn Prof. Dr. Thomas Carell betreut.

Ehrenwörtliche Versicherung

Diese Dissertation wurde selbstständig, ohne unerlaubte Hilfe erarbeitet.

München, am 19.04.2007



(Antonio Manetto)

Dissertation eingereicht am 19.04.2007

1. Gutachter Prof. Thomas Carell

2. Gutachter Prof. Hendrik Zipse

Mündliche Prüfung am 14.05.2007

Dedicato alla mia Famiglia in Sicilia, a *Susanne*, a *Giulia* e al mio piccolo maschietto.

Dedicated to my Sicilian Family, *Susanne*, *Giulia* and to my little boy.

Ci sono alcuni, oh re Gelone, che ritengono i granelli di sabbia essere una moltitudine infinita.
There are some people, oh king Gelone, which consider the grain of sand as an endless flurry.

Archimede, (287-212 a.C.), Syracuse (Sicily)

La semplicità è la più complessa delle sofisticazioni.
Simplicity is the ultimate sophistication.

Leonardo Da Vinci, (1452-1519), Italy.

Ho finito!
Ich habe fertig!

Giovanni Trapattoni, (1939), Italy

Acknowledgements

I'm really grateful to Prof. Dr. *Thomas Carell* who allowed me to enjoy his group and his valuable scientific and personal experience. I'm equally grateful to Dr. *Chryssostomos Chatgililoglu* for introducing me to the fascinating world of scientific research, advising me with his professionalism and his friendship.

I'm grateful to Prof. Dr. *Hendrik Zipse* for his enthusiasm in reading and correcting my thesis and for his availability to be the co-referee of this work.

I want to thank all the members of the commission of my final examination, Prof. Dr. *Heinz Langhals*, Prof. Dr. *Ingo-Peter Lorenz* and Prof. Dr. *Konstantin Karaghiosoff*.

I'm grateful to Prof. *Pier Carlo Montecvecchi* for offering me the initial PhD position in Bologna.

Frau *Slava Gärtner* helped me in every bureaucratic issue with her infinite patience. Thank you.

The English of this thesis would have sound much more "Italian" without the strong effort of *Philipp Gramlich*, which not only translated the summary in German language and corrected my grammar mistakes, but advised me with helpful and useful suggestions. I almost feel sorry that my Italy won against his Germany 2:0 in the last Soccer World Championship. Almost! I'm very grateful to Dr. *Sébastien Bareyt* and Dr. *Ulrich Hennecke* for read-proofing my thesis and for their precious advices. I want to thank *Heiko Müller* and *Christian Wirges* as well for their correction in the first draft of the thesis.

Two more special people took part in the correction of this thesis: Professoressa *Franca-Concetta Pantò* in *Manetto*, my beloved mother and Dr. *Susanne Manetto*, my sweet wife, which helped me to translate the summary and organise the thesis final version as well.

During my PhD I closely worked with many colleagues. They gave me experience, advices, new skills and overall friendship and good working atmosphere. I want to thank all the members of the *Chatgililoglu* group with whom I spent a great time in Bologna. Among them my laboratory mates Dr. *Clara Caminal*, *Liliana Jimenez*, Dr. *Inmaculada Andreu*, Dr. *Abdelouahid Samadi*, Dr. *Immacolata Manco*, *Antonio D'Aurizio* and an ideal scientific guide, Dr. *Carla Ferreri*. I'm really grateful to the co-workers of CNR-Bologna as well, for their scientific advices and their friendship.

At the beginning of my work in Munich I found immediately two "native fellows" which taught me the perfect Bavarian behaviour, *Philipp (Litzka) Gramlich* and *Simon Warncke*, my two Fk lab-mates. With them I spent hours not only drinking "the best beer in the world", but

discussing about chemistry and science in general as well. They have always been available for any kind of help I needed, inside and outside the working place. Thank you.

During my staying in Munich I could enjoy the friendship of many other people, mainly from the Ak-Carell group. With *Aaron Alt* I experienced the “authentic Israelian Sushi” and the genuine “Israelian lame excuse to avoid the Praktikum correction”. The time during our Network meetings and his availability as baby-sitter let him become like my little-older brat brother anyway. In *Sébastien Bareyt* I immediately discovered a friend with his integrity and his “Mediterranean” behaviour. With *Maria Izquierdo* I nicely spent relaxing time in the parks of Munich and less relaxing time in front of the Capillary Electrophoresis. I enjoyed her friendship and her meticulous scientific preparation. My lab-mate *Eva-Maria Jahn* has always been a perfect advisor in chemistry as well as in private life. I want to thank her for listening my “ideas” and “stories” with realistic interest. *Sascha (Paule) Breeger* introduced me to my topic and taught me how to deal with many lab-equipments. He has been a great co-worker in the EET studies and has always been available for any discussions. *Johannes Gierlich* has not only been very helpful in solving computer related problems, but in every scientific field I was involved, he could be ready to lend a hand. I shortly collaborated with *Guido Clever* on the M-MEET topic. His scientific preparation can be compared only with his amusing behave, both great. Thanks to Dr. *Carsten Pieck*, *Melanie Maul* and Dr. *Markus Müller* for their “bio-advices”. *Stephanie Schorr* allowed me to finish my thesis by replacing me in the last “Praktikum”, thank you. Frau *Sabine Voß* helped me to appropriately deal with the German language, offering me a welcoming smile every morning as well. The whole *Carell* group has been very helpful for my work, in a way or another. I want to thank all of them.

Many thanks are for my friends in Messina (*Carlo, Simone, Oreste, Giovanni, Valentina* and *Lia* among others) and in Bologna (*Maurizio, Alessandro, Davide, Frank, Stefano, Vito* and *Le Comari* just to cite some of them). They daily supported me with their valuable friendship.

Special thanks are for my Family in Italy. My mother and my father always supported me, financially and with their love. My three sisters, *Giovanna, Chiara* and *Elena* and their partners have always been lovely and helpful with me. My niece *Francesca* and my new-born nephew *Lorenzo* gave me happiness and motivation. I own to all of them my enthusiasm in doing my work as well.

My deepest thanks are for my little Family. My lovely and helpful wife *Susanne*, my adored two-years old daughter *Giulia* and my little boy, still in mamma’s belly, are my inspiration, my happiness and my life. They helped me in this work more than any text-book and scientific article I ever read. *Giulia*’s smile gave me the power to deal with any problem and her unaware love fills my life with precious happiness.

Parts of this work have been published in the following peer-reviewed journals and congresses:

Manetto, A.; Chatgililoglu, C.; Giese, B.; Carell, T.; The Kind of Electron Injection into DNA Determines the Chemistry: Only Ground state Donors Trigger with one Electron two Reaction. *Manuscript in preparation*.

Hammond, D. M.* **Manetto, A.*** Gierlich, J.; Azov, V. A.; Gramlich, P. M. A.; Burley, G. A.; Maul, M.; Carell, T., Click-Chemistry Combined with Black-and-White Photography allows Ultra-sensitive DNA Detection by Eye. *Angew. Chem. Int. Ed.*, **2007**, *46*, 4184-4187.

Manetto, A.; Georganakis, D.; Gimisis, T.; Leondiadis, L.; Carell, T.; Chatgililoglu, C., Independent Generation of C5'-Nucleosidyl Radicals in Thymidine and 2'-Deoxyguanosine. *J. Org. Chem.*, **2007**, *72*, 3659 -3666.

Manetto, A.; Breeger, S.; Chatgililoglu, C.; Carell, T., Complex Sequence Dependence by Excess-Electron Transfer through DNA with Different Strength Electron Acceptors. *Angew. Chem. Int. Ed.*, **2006**, *45*, 318-321.

Navacchia, M. L.; **Manetto, A.**; Montevecchi, P. C.; Chatgililoglu, C., Radical Cyclization Approach to Cyclonucleosides. *Eur. J. Org. Chem.*, **2005**, 4640-4648.

Montevecchi, P. C.; **Manetto, A.**; Navacchia, M. L.; Chatgililoglu, C., Thermal decomposition of the tert-butyl perester of thymidine-5'-carboxylic acid. Formation and fate of the pseudo-C4' radical. *Tetrahedron*, **2004**, *60*, 4303-4308.

CLUSTOXDNA V EU-Meeting, Oct. 2006, Gandia, Spain.

Authors: Manetto, A. Gimisis, T. Chatgililoglu, C. Carell, T.

Titel: "Independent Generation of C5'-Nucleosidyl Radicals in Thymidine and 2'-Deoxyguanosine"

Contribution: Oral talk

CLUSTOXDNA Mid-Term EU-Meeting, May. 2006, Oxford, UK.

Authors: Manetto, A. Carell, T.

Titel: "EET and M-MEET. through DNA"

Contribution: Oral talk

Cerlib 2006, Mar. 2006, Annecy, France.

Authors: Manetto, A. Breeger, S. Chatgililoglu, C. Carell, T.

Titel: "EET. through DNA Investigated with Differently Strong Electron Acceptors"

Contribution: Poster

CLUSTOXDNA IV EU-Meeting, Mar. 2006, Annecy, France.

Authors: Manetto, A. Clever, G. Carell, T.

Titel: "M-MEET. Metal mediated excess electron transfer through DNA"

Contribution: Oral talk

CLUSTOXDNA III EU-Meeting, Oct. 2005, Athens, Greece.

Authors: Manetto, A. Breeger, S. Chatgililoglu, C. Carell, T.

Titel: "Excess Electron Transfer Through DNA Investigated with Differently Strong Electron Acceptors Reveals Complex Sequence Dependence"

Contribution: Oral talk

CLUSTOXDNA II EU-Meeting, Feb. 2005, München, Germany.

Authors: Manetto, A. Breeger, S. Chatgililoglu, C. Carell, T.

Titel: "8-Br-purines: new electron acceptors for the EET in DNA"

Contribution: Oral talk

ISOFR 9th, June 2004, Porto Vecchio, Corsica, France.

Authors: Manetto, A. Montevecchi, P. C. Navacchia, M. L. Chatgililoglu, C.

Titel: "Radical Cyclization Approach to Cyclonucleosides"

Contribution: Poster

3th SAYCS and COFEM 2003, May 2003, Riccione, Italy.

Authors: Manetto, A.

Titel: "Radical decomposition of the *tert*-butyl perestere of the thymidinoic acid: the fate of *pseudo*-C4' radical."

Contribution: Oral communication and Poster

XV International Round Table Nucleosides, Nucleotides and Nucleic acids Sept. 2002, Leuven, Belgium.

Authors: Manetto, A. Montevecchi, P. C. Navacchia, M. L. Chatgililoglu, C.

Titel: "Model studies on the fate of C-5' radicals under aerobic conditions: the case of *pseudo*-C4' radical"

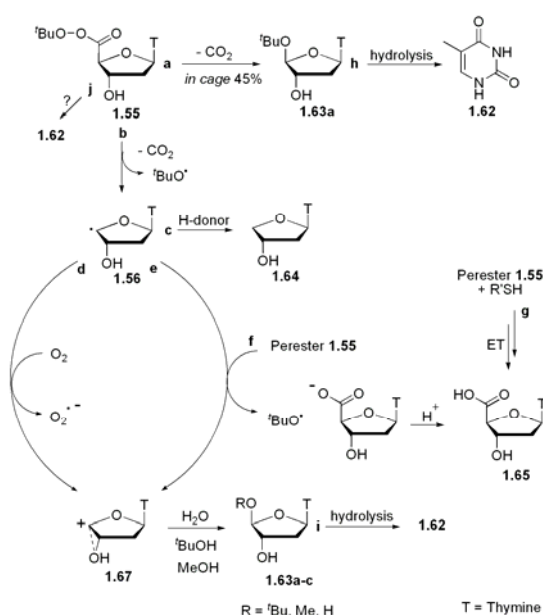
Contribution: Poster

Table of contents

Summary.....	I
Zusammenfassung	V
General.....	1
1 Nucleoside models for the study of C5'-radicals fate	2
1.1 Introduction	2
1.1.1 Aim of Chapter 1	20
1.2 Results and Discussion.....	21
1.2.1 Formation and fate of the <i>pseudo</i> C4'-radical.....	21
1.2.2 Radical Cyclisation Approach to Cyclonucleosides	33
1.2.3 Independent Generation of C5'-Nucleosidyl Radicals in Thymidine	46
1.3 Conclusions	53
2 Electron Transfer Through DNA	54
2.1 Introduction	54
2.1.1 Aim of Chapter 2.....	76
2.2 Results and Discussion.....	82
2.2.1 Flavin / Br-nucleoside model systems	82
2.2.2 SED: Single electron donor and multiple acceptors.....	108
2.2.3 M-MEET: Metal-Mediated Excess Electron Transfer	127
2.3 Conclusions	137
3 Molecular Beacons for DNA-Photography. Selective Detection of a Target	138
3.1 Introduction	138
3.2 Results and Discussion.....	143
3.3 Conclusions and Outlook.....	153
4 Experimental Section	154
4.1 Nucleoside models for the study of C5'-radicals fate associated with oxidative damage of DNA	155
4.1.1 Formation and fate of the <i>pseudo</i> C4'-radical.....	155
4.1.2 Radical Cyclization Approach to Cyclonucleosides	162
4.1.3 Independent Generation of C5'-Nucleosidyl Radicals in Thymidine	169
4.2 Electron Transfer through DNA.....	186
4.2.1 Sequence dependence studies.....	186
4.2.2 Single electron donor and two acceptors.....	193
4.3 M-MEET. High resolution mass	194
4.4 Molecular beacon for DNA-photography	198
5 Abbreviations	200
6 References	203
7 Curriculum Vitae.....	223

Summary

During cellular metabolism of oxygen to water in the mitochondria, a small fraction of the oxygen is reductively converted into superoxide ($O_2^{\cdot-}$) as a by-product. Through complex biochemical processes, superoxide may be converted into various reactive oxygen species (ROS), e.g. hydroxyl radicals ($\cdot OH$), H_2O_2 , 1O_2 , etc. These ROS and in particular the highly diffusible $\cdot OH$ are known to cause chemical modifications on DNA through the formation of strand breaks and nucleobase modifications. DNA damage and strand breaks may also be induced through other environmental influences such as ionizing radiation, photooxidation and naturally occurring or synthetic chemical mutagens. Oxidative DNA damage can be

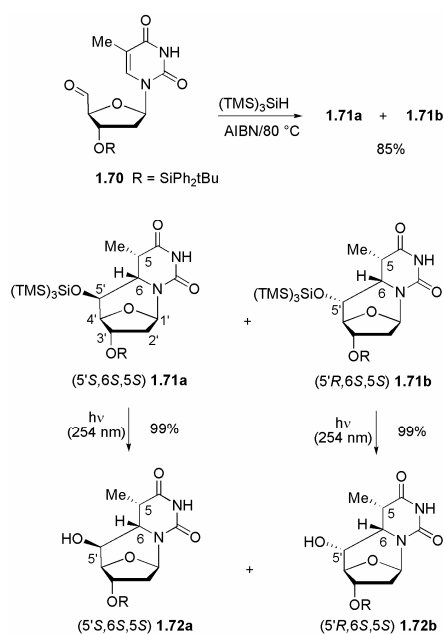


S.-Fig. 1

produced by the oxidation of the nucleobases or of the sugar units. In the last case carbon centered radicals are formed by direct or indirect hydrogen abstraction. In the first part of this thesis (Chapter 1), the fate of the carbon centered radicals C5' and *pseudo*-C4' of the sugar was investigated at the nucleoside level. The syntheses of new thermal or photolabile C5' and *pseudo*-C4' radical precursors were achieved to this end and the mechanistic aspects were studied under various conditions. Kinetic data were obtained as well and the access to biological lesions was possible through these studies. In section 1.2.1, the synthesis of a novel perester radical precursor (**1.55**) was achieved. The unprecedented selective generation of the *pseudo*-C4' radical was established as well. The radical was studied in solution under various conditions and the pathways of base releasing and degradation were proved and described (S.-Fig. 1).

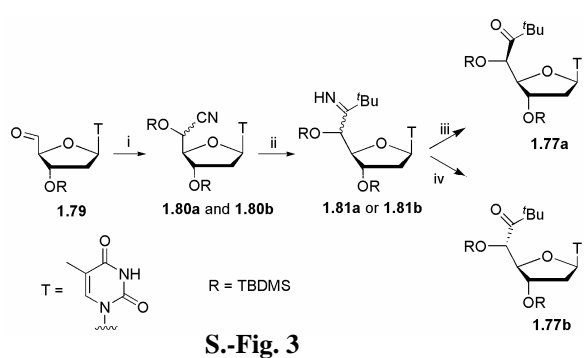
In section 1.2.2 a short and efficient synthetic sequence for the preparation of cyclonucleosides **1.72a-b** has been disclosed, based on consecutive

produced by the oxidation of the nucleobases or of the sugar units. In the last case carbon centered radicals are formed by direct or indirect hydrogen abstraction. In the first part of this thesis (Chapter 1), the fate of the carbon centered radicals C5' and *pseudo*-C4' of the sugar was investigated at the nucleoside level. The syntheses of new thermal or photolabile C5' and *pseudo*-C4' radical precursors were achieved to this end and the mechanistic aspects were studied under various conditions. Kinetic data were obtained as well and the access to



S.-Fig. 2

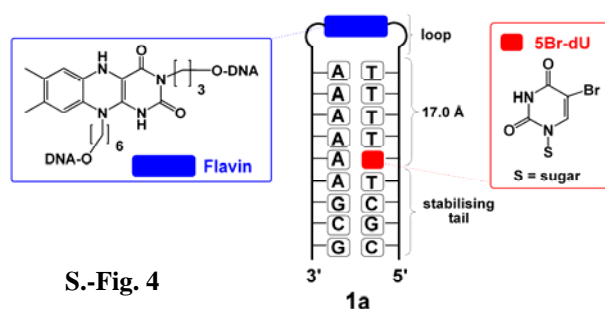
radical reactions followed by a photochemical desilylation (S.-Fig. 2). The C5' radicals, generated by the addition of a $(\text{TMS})_3\text{Si}^\bullet$ radical to the corresponding 5'-carboxaldehyde, are the key intermediates in these transformations. The rate constant k_C of the subsequent cyclisation reaction was estimated for the first time in such systems through a radical clock reaction setup. The value of $k_C = 7 \times 10^3 \text{ s}^{-1}$ at 25 °C found here is strictly correlated with the C5'-radical repair reaction.



In section 1.2.3 a new synthetic route for the preparation of (5'*R*)-*tert*-butyl ketones **1.77a** and **1.77b** was disclosed (S.-Fig. 3). Photolysis experiments selectively afforded the corresponding C5' radical. In the presence of a physiological concentration of alkanethiol, the thymidin-5'-yl radical is efficiently reduced.

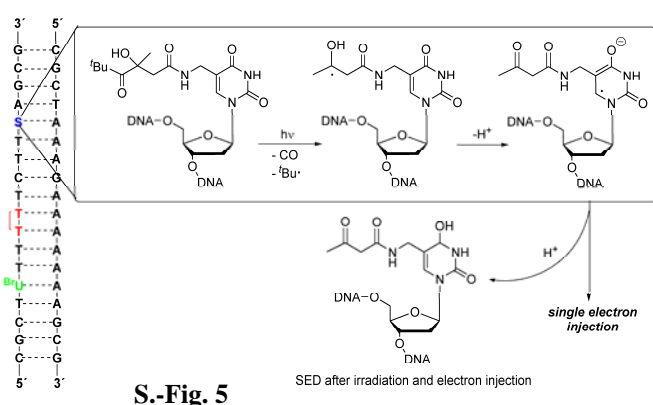
Under these conditions the half-life of **1.77a** was calculated to be $t_{1/2} = 6.6 \text{ min.}$ without any cyclisation product being observed. The resulting C5' radical could be obtained either by *Norrish* Type I photocleavage or by initial formation of an acyl radical that decarbonylates with a rate constant in the range of $10^5\text{--}10^6 \text{ s}^{-1}$. The presence of a thiol prevents subsequent reactions such as the intramolecular attack onto the C6–C5 double bond of thymine.

When an electron donor injects electrons into a duplex, negative charges move to an acceptor site in DNA. Investigations on how charges move through DNA and studies of how the electron transfer can be accelerated and controlled is an active field of research. In the second part of the thesis (Chapter 2) the study of the excess electron transfer (EET) through the DNA was undertaken. A flavin used as electron donor was alternated with a single electron injector in order to establish diverse EET features. A CPD lesion (T=T dimer) and one of three bromo-nucleosides were used as electron acceptors enabling the evaluation of the sequence dependence and the donor/acceptor system influence on the EET. Three series of five flavin-containing hairpins were prepared. They contained the flavin electron injector



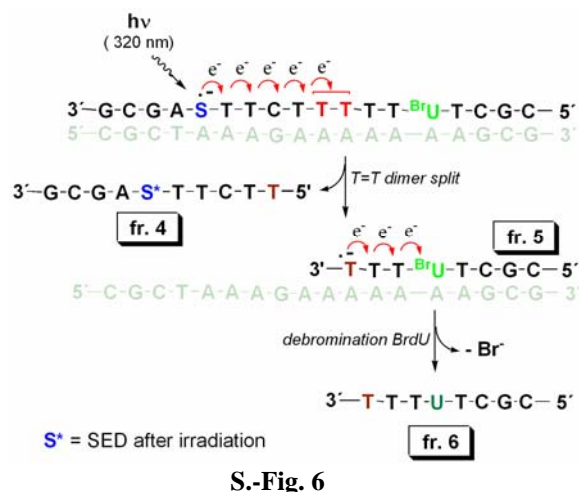
placed in the loop region of the hairpin and one of the three electron acceptors positioned in the stem region at a distance of about 17 Å to the flavin. The hairpin **1a** is reported as example in S.-Fig. 4.

The nature of the acceptor influences the debromination yield and therefore the EET process analysis. Moreover, the differences shown by the traps indicate that the reduction of the acceptor can indeed be the rate determining step. Thus, in the process of electron migration through DNA, which involves electron injection, migration and capture, the latter step might determine the final efficiency of the whole process. As a result of these studies, a G:C bp between the donor and the acceptor reduces the excess electron transfer efficiency approximately by a factor of two. More important is the unprecedented observation that the position of G:C base pairs between the donor and the acceptor strongly influences the efficiency of the process. Although every G:C bp reduces the EET efficiency by about 50 %, the position of a single G:C bp in proximity to the trap can decrease the efficiency by more than 85 %.



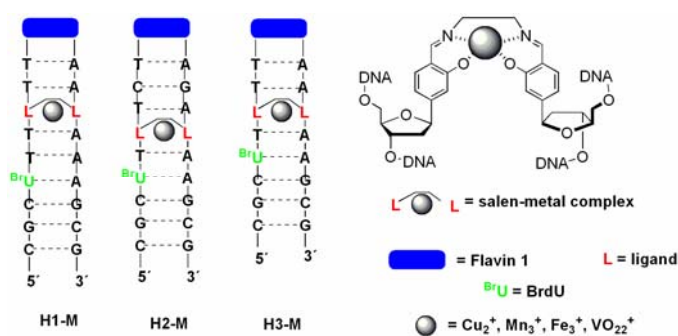
To further investigate the EET through DNA, it was chosen to initiate the process by the injection of one single electron per strand using a single electron donor (SED). In section 2.2.2 the use of the flavin donor in systems containing two

electron acceptors in a row. The irradiation at 320 nm of SED-containing dsS1 initiates a cascade of homolysis, charge translocation and deprotonation enabling the final electron injection into the DNA base stack. This process is initiated by a *Norrish* type I photolysis of the *tert*-butyl α -hydroxy ketone of the SED moiety (S.-Fig. 5). On the other hand, the results observed upon irradiation of a flavin-containing hairpin, provide an astonishing outcome. The chemistry that is triggered by a charge in DNA depends on how the charge was initially injected. In excited state systems, the injected electron feels the efficient charge recombination process, which seems to limit and bias charge propagation. If, however, ground state chemistry is employed to inject the charge, no recombination trap is present. In this case, the charge can move freely. Excess electrons injected by such a system can trigger more than one



reaction, establishing a catalytic electron, and they can hop over acceptors if their triggering mechanism is slower than the hopping step (S.-Fig. 6).

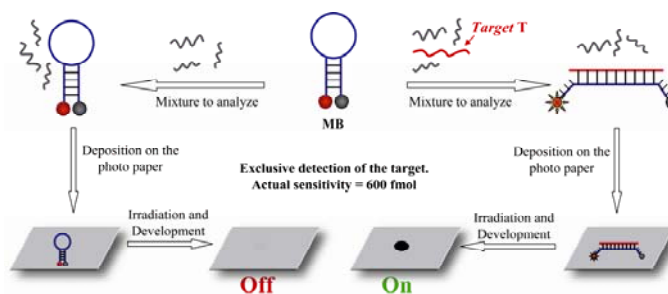
Strong efforts are under way to create DNA-based nanoelectronic materials with self-organizing properties. The long-term goal is that such a novel material may self assemble



S.-Fig. 7

into complex conductive nano-wire networks with computing or diagnostic potential. Recently, a controlled assembly of metallised DNA in which one or more natural base pairs are replaced by nucleosides carrying flat metal complexes was reported. The design and the synthesis of DNA structures containing an internal metal complex between an electron donor and an acceptor opened the access to the study of EET through metal base pairs (metal-mediated EET, M-MEET). A series of DNA hairpins containing the light dependent flavin electron donor and the fast electron acceptor BrdU were designed. A salen-metal complex between the donor and the electron acceptor was introduced via the oligonucleotide solid phase synthesis in order to establish the influence of one metal in the electron transfer process. The design of hairpins **H1-M**, **H2-M** and **H3-M** in S.-Fig. 7 was aimed at exploring the electron transfer through the salen-metal complexes in the context of mixed sequences. The effect of only one metal per DNA was investigated in this proof of concept study, in which only the nature of the metal and the irradiation conditions were systematically changed.

In the third part of the thesis (Chapter 3) a new direct DNA detection method was established based on the principle of the black-and-white photography, called DNA-photography, DP. A detection

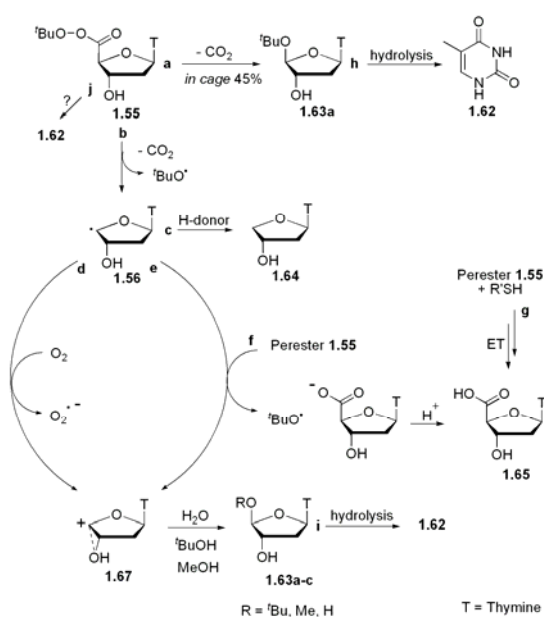


S.-Fig. 8

limit lower than 300 attomoles of DNA (10^{-18} moles) was achieved with a simple setup in a photography dark room. Moreover the detection of 600 femtomoles (10^{-15} mole of a sequence associated with a gene of *Y. pestis*, which causes the mortal disease *plague*, was achieved. In the latter case, molecular beacons (MBs) were used in order to use the FRET principle together with the DP method (S.-Fig. 8).

Zusammenfassung

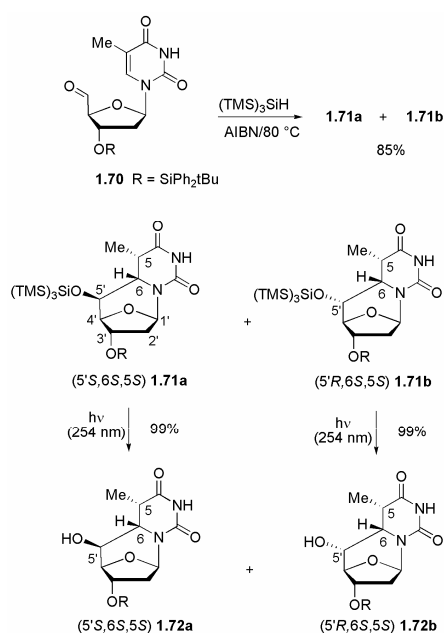
Über die mitochondriale Atmungskette setzen Zellen durch Metabolisierung von Sauerstoff zu Wasser als Nebenprodukte stets kleine Menge reduzierten Sauerstoffs in Form von Superoxid ($O_2^{\cdot-}$) frei. Durch komplexe biochemische Prozesse kann Superoxid im Folgenden in eine Vielzahl reaktiver Sauerstoffverbindungen (ROS) wie $\cdot OH$, H_2O_2 , 1O_2 , etc. umgewandelt werden. Diese ROS, im Speziellen das stark diffusionsfähige $\cdot OH$, können chemische Veränderungen an der DNA unter Bildung von Strangbrüchen und Modifikationen



Z.-Abb. 1

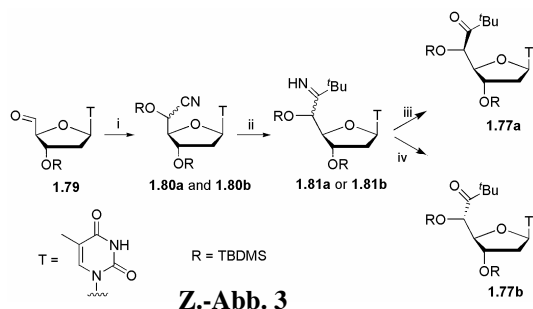
einzelner Nucleobasen bewirken. Ebenso können DNA-Schäden durch Umwelteinflüsse wie ionisierende Strahlung, Photooxidation, sowie durch natürliche und chemische Mutagene hervorgerufen werden. Oxidative Schäden können durch die Oxidation der Nucleobasen oder der entsprechenden Zuckereinheiten entstehen. Im letzteren Fall kommt es durch direkte oder indirekte H-Abstraktion zur Bildung Kohlenstoff-zentrierter Radikale. Im ersten Teil dieser Arbeit (Kapitel 1) wurde das Schicksal Kohlenstoff-zentrierter C5' und *pseudo*-C4' Radikale des Zuckers am Nucleosid untersucht. Zu diesem Zweck wurden die Synthesen neuer thermo- oder photolabiler C5' und *pseudo*-C4' Radikalvorläufer durchgeführt und mechanistische Aspekte unter verschiedenen Bedingungen untersucht. Auch kinetische Daten konnten ermittelt werden und der Zugang zu biologischen Schäden war im Verlauf der Untersuchungen ebenfalls möglich. In Kapitel 1.2.1 wurde die Synthese eines neuen Perester Radikalvorläufers (1.55) beschrieben. Weiterhin konnte das *pseudo*-C4' Radikal erstmals selektiv hergestellt werden. Die Radikaleigenschaften wurden in Lösung unter verschiedenen Bedingungen analysiert, sowie die Freisetzung und der Abbau der Nucleobasen nachgewiesen und beschrieben (Z.-Abb. 1).

einzelner Nucleobasen bewirken. Ebenso können DNA-Schäden durch Umwelteinflüsse wie ionisierende Strahlung, Photooxidation, sowie durch natürliche und chemische Mutagene hervorgerufen werden. Oxidative Schäden können durch die Oxidation der Nucleobasen oder der entsprechenden Zuckereinheiten entstehen. Im letzteren Fall kommt es durch direkte oder indirekte H-Abstraktion zur Bildung Kohlenstoff-zentrierter Radikale. Im ersten Teil dieser Arbeit (Kapitel 1) wurde das Schicksal Kohlenstoff-zentrierter C5' und *pseudo*-C4'



Z.-Abb. 2

In Kapitel 1.2.2 konnte eine kurze und effektive Synthese zur Herstellung von Cyclonucleosiden **1.72a-b** durch aufeinander folgende Radikalreaktionen und eine anschließende photochemische Desilylierung aufgezeigt werden (Z.-Abb. 2). Die durch die Addition eines $(\text{TMS})_3\text{Si}^\bullet$ Radikals an das entsprechende 5'-Carboxyaldehyd generierten C5' Radikale sind die entscheidenden Zwischenprodukte dieser Umwandlungen. Die Geschwindigkeitskonstante k_C der anschließenden Zyklisierungsreaktion wurde erstmals in



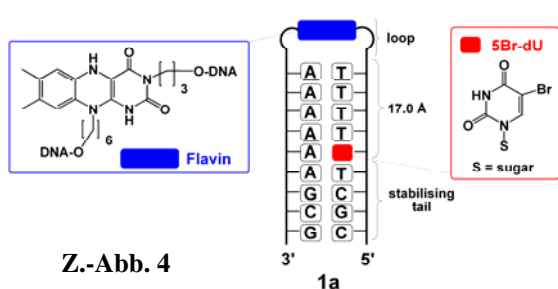
Z.-Abb. 3

solch einem System durch eine Radikaluhr bestimmt. Der hier bei 25 °C ermittelte Wert von $k_C = 7 \times 10^3 \text{ s}^{-1}$ steht in engem Zusammenhang mit der Reparatur des C5' Radikals.

In Kapitel 1.2.3 konnte ein neuer Syntheseweg für die Herstellung von (5'R)-tert-Butylketonen **1.77a** und **1.77b** gezeigt werden (Z.-Abb. 3).

Photolyseexperimente ermöglichten die selektive Generierung des entsprechenden C5' Radikals. In Anwesenheit einer physiologischen Konzentration an Alkanthiol wurde das Thymidin-5'-yl Radikal hierbei effizient reduziert. Unter diesen Bedingungen wurde die Halbwertszeit von **1.77a** mit $t_{1/2} = 6.6 \text{ min.}$ berechnet, ohne dass ein Zyklisierungsprodukt beobachtet werden konnte. Das gebildete C5' Radikal könnte über eine *Norrish* Typ I Photospaltung oder durch die Bildung eines Acylradikals, welches mit einer Geschwindigkeitskonstante im Bereich von $10^5\text{--}10^6 \text{ s}^{-1}$ decarboxyliert, entstehen. Die Anwesenheit eines Thiols beugt hierbei Folgereaktionen wie dem intramolekularen Angriff an der C6–C5 Doppelbindung des Thymins vor.

Wenn über einen Donor Elektronen in die Doppelhelix injiziert werden, bewegen sich diese negativen Ladungen zu einem Akzeptor in der DNA. Untersuchungen zur Bewegung, Beschleunigung und Kontrolle von Ladungen in der DNA sind ein wichtiges und aktuelles Forschungsgebiet. Im zweiten Teil dieser Arbeit (Kapitel 2) wurden Studien zum Überschusselektronentransfer (EET) in DNA durchgeführt. Flavin als Elektronendonator oder



Z.-Abb. 4

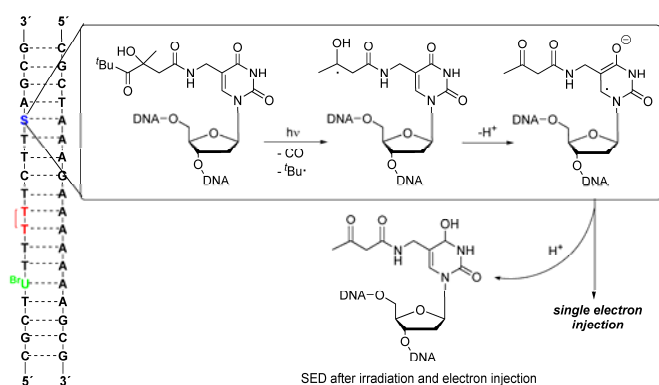
ein Einelektronendonator wurden eingebaut, um verschiedene Merkmale des EET zu ermitteln. Ein CPD Schaden (T=T Dimer) und eines von drei Bromnucleosiden wurden als Elektronenakzeptoren eingesetzt, so dass eine

Bewertung der Sequenzabhängigkeit und des Donor/Akzeptor-Einflusses auf den EET möglich war. Hierzu wurden drei Serien von fünf Flavin-haltigen Haarnadelstrukturen hergestellt. Diese enthielten den Flavin Elektronendonator in der Schlaufenregion der Haarnadelstruktur und einen der drei Elektronenakzeptoren im Stammbereich, mit einem Abstand von 17 Å zum Flavin. Haarnadelstruktur **1a** ist als Beispiel hierfür in Z.-Abb. 4 dargestellt.

Die Eigenschaften des Akzeptors beeinflussen hierbei die Debrominierungsausbeute und somit die Analyse des EET Prozesses. Darüber hinaus zeigen die Unterschiede bei den verschiedenen Elektronenfallen, dass die Reduktion des Akzeptors in der Tat der geschwindigkeitsbestimmende Schritt sein kann. Dadurch kann letzterer Schritt für die Effizienz des gesamten Prozesses, der aus Elektroneninjektion, Wanderung und Einfangen besteht, bestimmend sein. Aus diesen Studien ergibt sich, dass ein G:C Basenpaar zwischen dem Donor und dem Akzeptor die Effizienz des Elektronentransfers in etwa um den Faktor zwei reduziert. Wichtiger noch ist die bislang noch nie da gewesene Beobachtung, dass die Position des G:C Basenpaares zwischen dem Donor und dem Akzeptor die Effizienz des Prozesses stark beeinflusst. Obwohl jedes G:C Basenpaar die Effizienz des EET um etwa 50% absenkt, kann die Position eines einzelnen G:C Basenpaares in der Nähe der Elektronenfälle diese um mehr als

85% verringern.

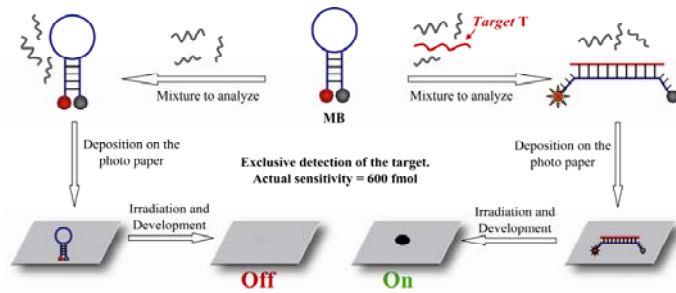
Um den EET durch DNA weiter zu untersuchen, wurde der Prozess durch Injektion eines einzelnen Elektrons pro Strang durch Benutzung eines Einelektronendonors (SED) initiiert. In Kapitel 2.2.2 wurde abwechselnd der SED und ein Flavin



Z.-Abb. 5

als Donoren in Systeme mit zwei Akzeptoren hintereinander eingebaut. Die Belichtung bei 320 nm des SED enthaltenden dsS1 löst eine Kaskade von Homolyse, Ladungswanderung und Deprotonierung aus, was die Elektroneninjektion in DNA ermöglicht. Dieser Prozess wird durch eine *Norrish* Typ I Photolyse des *tert*-Butyl- α -hydroxyketons der SED Einheit ausgelöst (Z.-Abb. 5). Auf der anderen Seite stellen die Ergebnisse, die bei der Belichtung einer Flavin enthaltenden Haarnadelstruktur erhalten wurden, einen erstaunlich Befund dar. Die Chemie, die in DNA durch eine Ladung ausgelöst wird, hängt davon ab, wie die Ladung injiziert wurde. In angeregten Systemen kann das injizierte Elektron durch effiziente Ladungs

Im dritten Teil der Arbeit (Kapitel 3) wurde eine neue Methode der Detektion von DNA eingeführt, die auf dem Prinzip der Schwarz-Weiss Photographie beruht (DNA Photographie, DP). Eine Nachweisgrenze von weniger als 300 attomol DNA (10^{-18} mol) wurde durch einen



Z.-Abb. 8

Krankheit *Pest* verursacht. Im letzteren Fall wurden *molecular beacons* (MB) verwendet, um das FRET Prinzip mit der DP Methode zu verknüpfen (Z.-Abb. 8).

einfachen Aufbau in einer photographischen Dunkelkammer erreicht. Darüber hinaus gelang der Nachweis von 600 femtomol (10^{-15} mol) einer Sequenz, des Gens von *Y. pestis*, welches die tödliche

General

The work reported here was carried out in three different institutes of two cities. The first part was achieved in the laboratories of the Department of Organic Chemistry in the Faculty of Industrial Chemistry of the University of Bologna, Italy, supervised by Prof. *Pier Carlo Montevocchi* (January-May 2002) as well as in the Institute for Organic Synthesis and Photoreactivity (ISOF) of the National Council of Research (CNR), Bologna, Italy, under the supervision of Dr. *Chryssostomos Chatgililoglu* (May 2002-March 2004). The second and third part were done in the Department of Chemistry and Pharmacy, of the Ludwig Maximilians University (LMU), München, Germany, under the supervision of Prof. Dr. *Thomas Carell* (March 2004-December 2006).

This PhD thesis is divided in five distinct chapters:

1. Nucleoside models for the study of C5'-radicals fate.
2. Electron transfer through DNA.
3. Detection of DNA by light-sensitive surfaces.
4. Experimental part.
5. References.

Three different high connected topics associated with DNA oxidative damage, DNA biochemical and physical properties and DNA detection are discussed in Chapters 1, 2 and 3. In Chapter 4 the whole experimental part of this PhD thesis is reported. In Chapter 5 the complete bibliography of this work is listed.

A general brief introduction about the DNA, its structure and some correlated topics relevant for this work are given in section 1.1 and not repeated in the next Chapters.

1 Nucleoside models for the study of C5'-radicals fate

1.1 Introduction

The DNA

The technical aspects of life involve the complex chemical interactions that take place among several thousand different kinds of molecules found within any living cell. Of these, the deoxyribonucleic acid (DNA) is the master molecule in whose structure is encoded all of the information needed to create and direct the chemical machinery of life. Solving the structure of DNA was surely one of the most important biological discoveries of the 20th century. *James Watson* and *Francis Crick*, in their 1953 letter to *Nature*,^[1] assembled pieces of a chemical puzzle that had been accumulating for more than 80 years.

DNA was already discovered in 1869 by a German doctor, *Friedrich Miescher*,^[2] isolating a substance, he called “nuclein” from the nuclei of white blood cells. By 1900 the basic chemistry of nuclein had been understood. It was known to be a long molecule composed of three distinct chemical subunits: a five-carbon sugar, acidic phosphate and five types of nitrogen-rich bases (adenine, thymine, guanine, cytosine and uracil). By the 1920s, two forms of nucleic acid were differentiated by virtue of their sugar composition: ribonucleic acid (RNA) and deoxyribonucleic acid (DNA).^[3,4] These forms were also found to differ slightly in base composition; thymine is found exclusively in DNA, whereas uracil is found only in RNA. The structure of the nucleosides was elucidated at the end of the 1940s.^[5,6] In 1950, *Erwin Chargaff* of Columbia University discovered a consistent one-to-one ratio of adenine-to-thymine (A-T) and guanine-to-cytosine (G-C) in DNA samples from a variety of organisms.^[7] A few years later *Rosalind Franklin* obtained well-resolved X-ray diffraction photographs of DNA.^[8] The diffraction patterns strongly suggested a helical molecule with a repeat of 34 angstrom ($\text{\AA} = 10^{-10} \text{ m}$) and a width of 20 \AA . The structure *Watson* and *Crick* arrived at by manipulating paper and then metal models, was elegant in its simplicity. The DNA molecule they proposed is an α -helix and resembles a twisted ladder (Figure 1.1). The rails of the ladder, which run in antiparallel directions, contains alternating double units of deoxyribose sugar and phosphate. The aromatic nucleobases stack tightly on top one another, forming the rungs of the helical ladder. Each rung is composed of a pair of nucleotides (a base pair, bp) held together by hydrogen bonds (Figure 1.2). There are 10 bps *per* turn of the helix,

with an interplanar distance of 3.4 Å. In agreement with *Chargaff's* observation, adenine always pairs with thymine and cytosine always pairs with guanine.^[7] Thus, the nucleotide sequence on one half of the DNA helix determines the sequence of the other half.

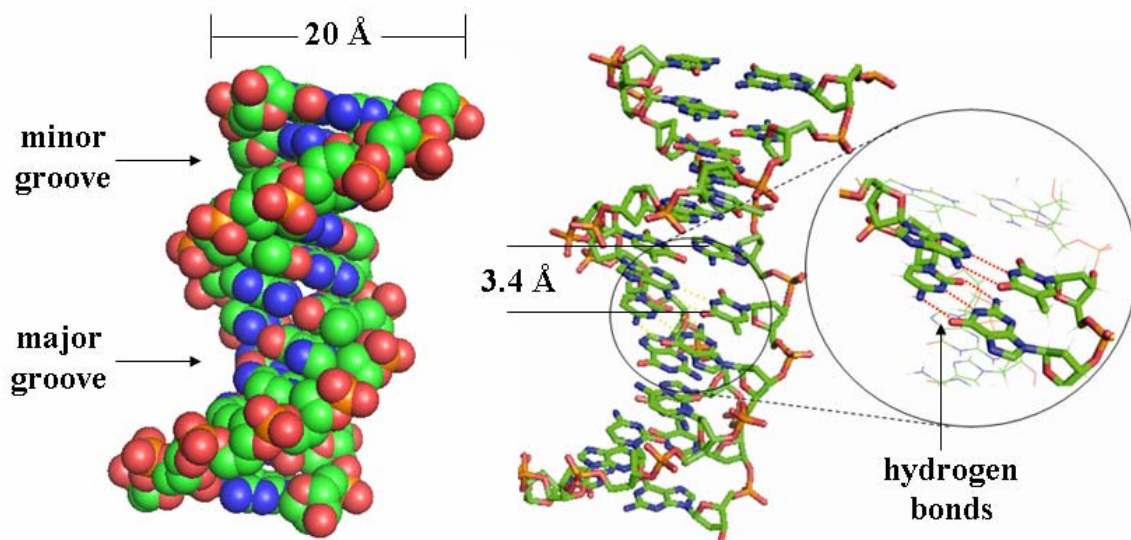


Figure 1.1 Structure of a B-DNA duplex in a “ball” (left) and “stick” (right) representation.

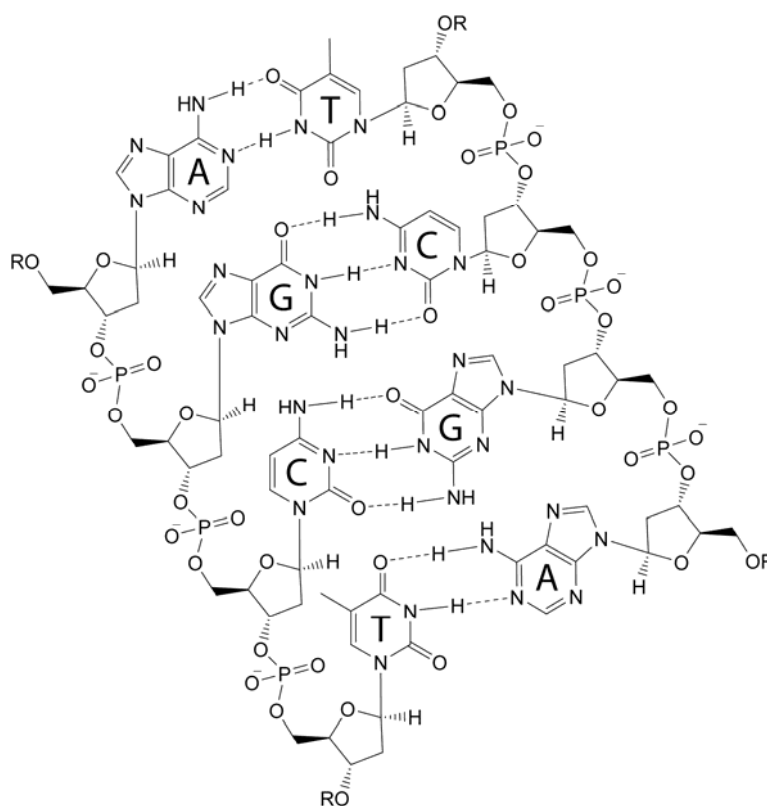
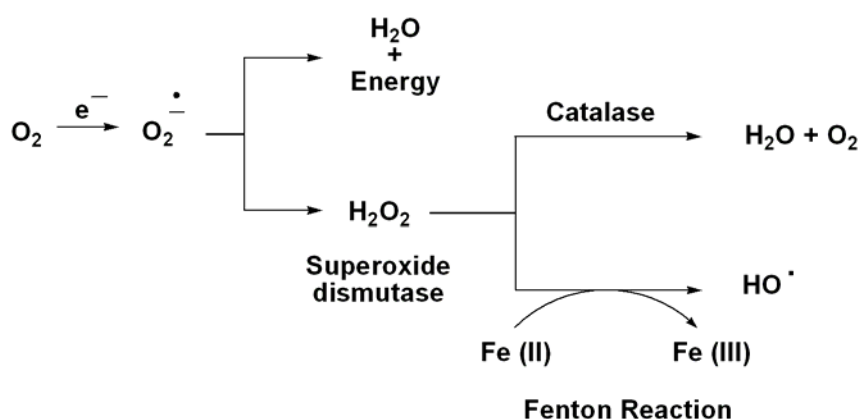


Figure 1.2 DNA structure. Structure of the nucleotides and the *Watson-Crick* hydrogen bonds between GC and AT.

Oxidation of DNA: H-abstraction from the sugar unit

During cellular metabolism of oxygen to water in the mitochondria, a small fraction of the oxygen is reductively converted into superoxide as a by-product.^[9] Through complex biochemical processes, superoxide may be converted into various reactive oxygen species (ROS), e.g. hydroxyl radicals ($\bullet\text{OH}$), H_2O_2 , $^1\text{O}_2$, *etc.* These ROS and in particular the highly diffusible $\bullet\text{OH}$ are known to cause chemical modifications on DNA through the formation of strand breaks and nucleobase modifications.^[10]



Scheme 1.1 Formation of superoxide, its enzymatic deactivation and the generation of $\bullet\text{OH}$ by a Fenton reaction.

DNA damage and strand breaks may also be induced through other environmental influences such as ionizing radiation, photooxidation and naturally occurring or synthetic chemical mutagens.^[11]

Maintaining the integrity of DNA is essential for every living organism. To this end evolution designed specific enzymes. Repair and protection of DNA is consequently performed by DNA repair enzymes via several routes. A majority of cells possess defence mechanisms against the harmful effects of ROS. The superoxide dismutase and catalase systems (Scheme 1.1) are able to quench radicals and other oxidising species. The endogenous glutathione (a γ -glutamylcysteinylglycine tripeptide, GSH) or the exogenous vitamins are smaller molecules that can drastically reduce the amount of ROS before they can damage the DNA. Lesions formed in DNA can be repaired by mismatch repair enzymes, error-prone repair enzymes, nucleotide excision repair process (NER) or base excision repair process (BER). The latter two are accomplished by several enzymes which recognise and

repair the DNA lesion. A simplified example of their working principle is illustrated in Figure 1.3. However, deleterious genetic alterations may accumulate in cells with age through errors in repair and recombination when the oxidative damages are poorly repaired. In addition, the level of repair enzymes may decrease with the age of the cell. DNA damage can eventually cause cell death or the modification of its functionality, as in the case of tumor cells. Thus, there is a great interest in the study of the mechanisms of DNA damage formation and effects on the cell and the repair systems involved in these processes. In addition, DNA damage is used in medical applications, i.e. in cancer therapies. Many cytostatic cancer drugs target the DNA of cells inducing apoptosis through DNA damage.

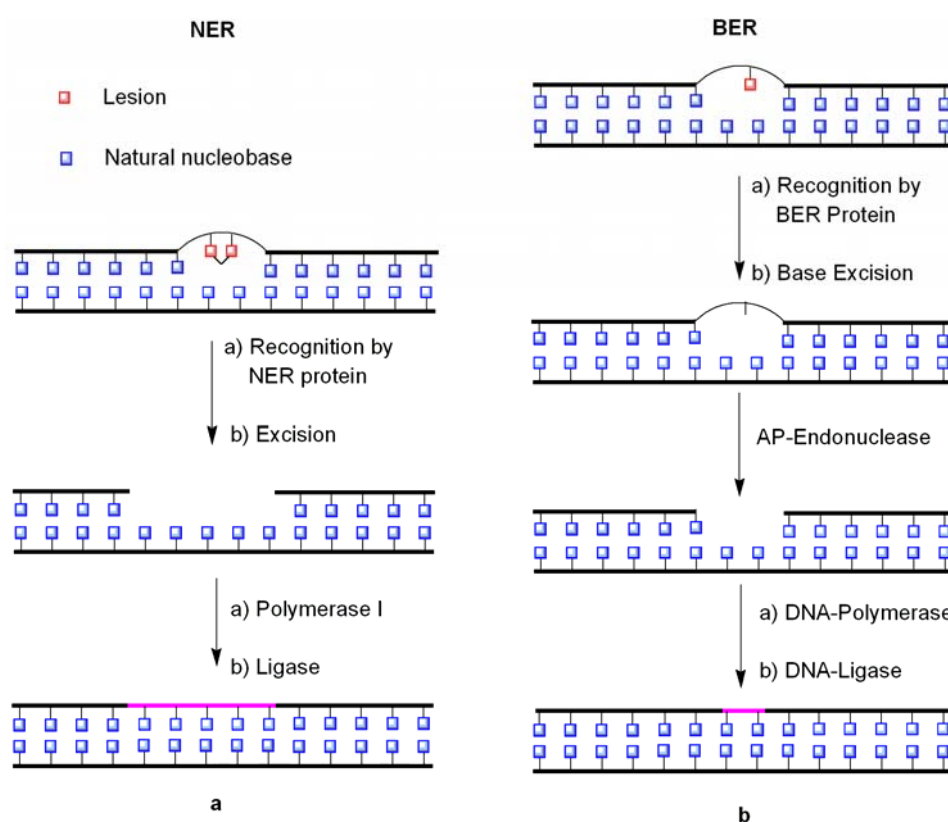


Figure 1.3 Schematic working principle of NER and BER processes.

Oxidative DNA damage can be produced by the oxidation of nucleobase or sugar units. More than 80 modified purines and pyrimidines resulting from oxidative damage have been identified. This base damage threatens the genomic integrity and is the origin of lethal effects or mutations in DNA. Damage to deoxyribose leads to the loss of one base and/or a strand break on DNA. Both kinds of damage eventually result in lethal lesions, especially when an oxidative process produces a double-strand break (DSB), that is two single strand breaks

(SSBs) on opposite strands. Furthermore a few examples of damage that involve both, the nucleobase and the sugar unit, are known. Cyclopurine and cyclopyrimidine lesions are observed among the decomposition products of DNA when exposed to ionising radiations or to certain antitumor agents.^[12-19] Two examples, described later in this Chapter 1, are the 5',6-cyclo-5,6-dihydrothymidine and the 5',8-cyclo-2'-deoxyadenosine. They possess an additional bond between the C6 position of pyrimidine or C8 position of purine and the C5' position of the 2'-deoxyribose.

All the sugar degradation processes are initiated by H-abstractions, since the aliphatic nature of deoxyribose does not favour oxidation by electron abstraction as in the case of the nucleobases. Subsequently, the generated sugar free radical can repair itself by hydrogen atom abstraction from glutathione (GSH), leading to modifications of the sugar unit (DNA-damage), or to strand-breakage.^[11,14,20] Although all seven hydrogen atoms of deoxyribose are believed to be reactive toward oxidising species and free radicals, not all are equally likely to be abstracted from DNA. The H-abstraction pathway is determined by the helical structure of DNA and on the relative orientation of the oxidant to the sugar. According to the structures obtained by X-ray crystallography of several oligonucleotides, the 5'-, 4'- and 1'-positions of B-form double strand DNA (dsDNA) are accessible from the minor groove, while the 3'- and 2'-positions are accessible from the major groove. One 5'-hydrogen atom (*pro-S*) points directly into the minor groove; the other points away from the backbone (see Figure 1.4).^[21]

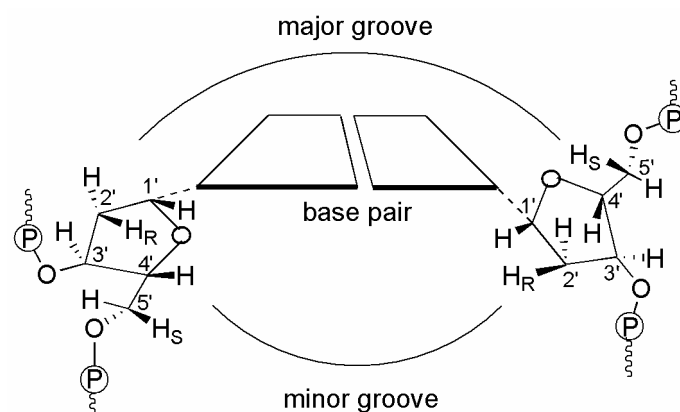


Figure 1.4 All seven C-H bonds of deoxyribose are prone to oxidation, but four point into the minor groove (indicated by wedge-shaped bonds), and three into the major groove (H_R and H_S refer to the absolute configuration –*pro-R* and *pro-S*– of hydrogen atoms at C2' and C5').

In the formation of a strand break, which of the seven hydrogen atoms is abstracted is the key question in elucidating mechanisms of nucleic acid degradation. *Osman* and co-workers calculated the energy of hydrogen abstraction initiated by the hydroxyl radical for the positions 1', 2', 3', and 4' of the model sugar 2-deoxy-*D*-ribose and found that the theoretical probability of abstraction is correlated with C-H bond strength.^[22] They also determined that, aside from the C2'-H, the abstraction of every hydrogen bond requires a similar amount of energy, presumably because the resulting radical is stabilized by the α -oxygen atom. When similar studies were performed on double-stranded B-DNA, solvent accessibility became an additional critical factor. In this case the hydrogen of C1' is virtually "hidden" by the local bulkiness, whereas the C4'-H and the C5'-H are significantly more exposed to solvent, making them much more likely to be abstracted.^[23,24]

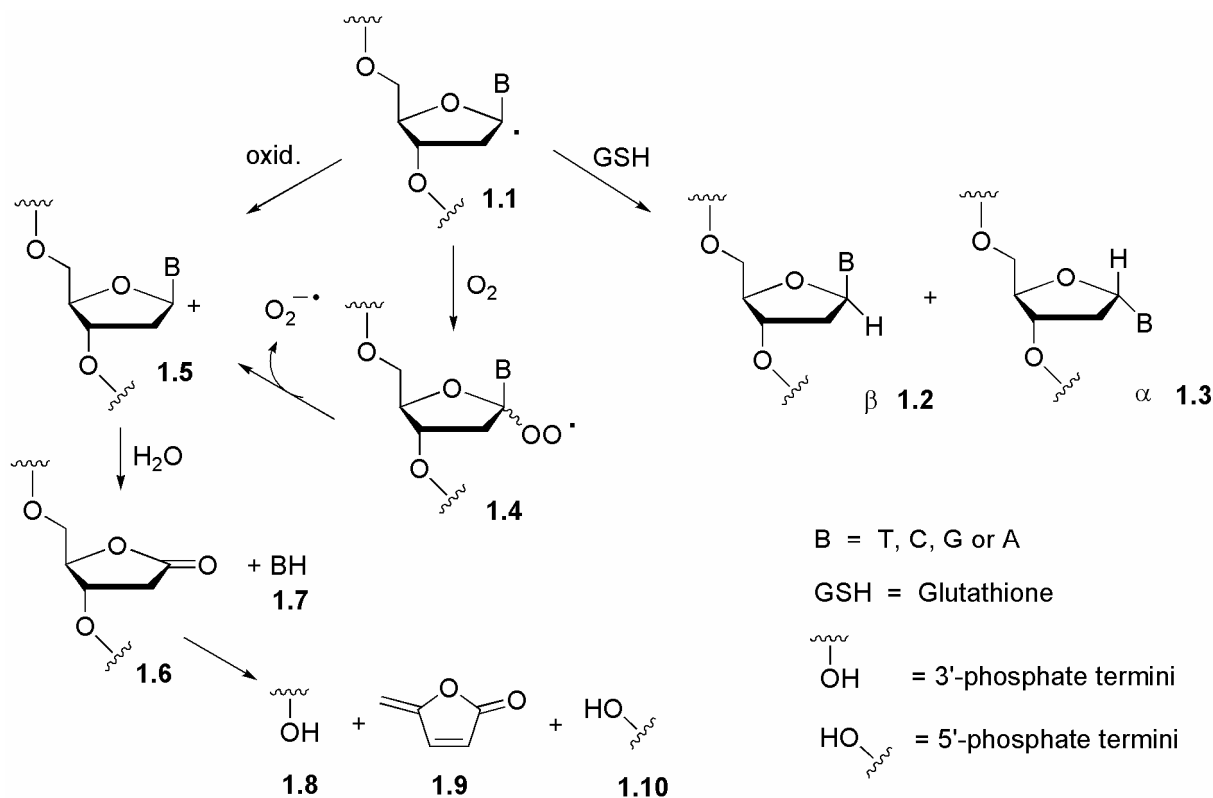
Another important point is that not all oxidation events lead to immediate strand cleavage. Several pathways result in the formation of metastable sugars or sites that can be hydrolysed *via* base-catalyzed reactions. Furthermore, the formation of a radical on the sugar unit can lead to stable nucleotide modifications by interaction with adjacent nucleobases of the same DNA strand (*intra*-strand cross-linking) or with the counter strand (*inter*-strand cross-linking). In addition, as in the case of the above-mentioned cyclopurines and cyclopyrimidines, the reaction can be *intra*-molecular. In fact, it has been verified that the C5' radical, initially generated by hydrogen abstraction, intramolecularly attacks the double bond of the nucleobase moiety to form a cyclonucleotide as the final product after oxidation or reduction (see also Scheme 1.6, pag. 18).^[25-27]

Here I briefly describe the chemistry of radicals formed by hydrogen abstraction from the sugar unit of DNA. The cases of the five sugar positions will be discussed focusing first on the C5'-H abstraction. The C5' radical generation and study of its fate represent the topic of Chapter 1. The molecules used by researchers to abstract hydrogen atoms from the sugar unit with a different degree of selectivity and/or the technique they used for the generation and detection of the intermediate and final products will only be described in this thesis for the C5' position. The reader is referred to excellent reviews for more details on this topic.^[11,14,20,28]

C1' radicals

The C1'-centered radical **1.1** can be generated by hydrogen abstraction through the interaction of DNA, oligonucleotides or nucleosides with ionizing radiation (γ -radiolysis), metal complexes (Mn-TMPyP, Cu(oP)₂ and anticancer drugs such as enediynes). Photolysis of photoreactive groups that are specific C1' radical precursors have been used by *Greenberg* and *Chatgialoglu* for kinetic and product studies.^[29-31] In addition the photoreaction of 5-halouracil-containing oligonucleotides gives rise to C1'- (and C2'-) centered radicals. The latter photoreaction has been extensively used in different fields of research as proliferation-marker^[32] or as electron acceptor in DNA excess electron transfer studies,^[33-35] and as DNA-structure probe.^[36] An example of radical generation via photoreaction of halouracil is reported for the C2'-radical in Scheme 1.3. More recently, *Sevilla* and co-workers reported the generation of sugar radicals using UV-A / visible photo-excitation of the guanosine radical cation (G^{•+}). According to the authors, selective radical generation is possible when optimised reaction parameters are employed. Specifically C1'-radicals have been observed in dsDNA under exposure to light (310-480 nm), whereas other radicals have been formed with longer wavelengths of irradiation (C3'- and C5'-radicals).^[37]

The C1' radical **1.1** abstracts a hydrogen atom from a thiol to give a mixture of β -anomer **1.2** (repairing reaction), and α -anomer **1.3** (Scheme 1.2). The latter belongs to a class of nucleotides that have been shown to be premutagenic *in vitro* when generated during γ -radiolysis of DNA under anaerobic conditions.^[38,39] In the presence of oxygen or metal complexes, radical **1.1** leads to abasic site damage, through the formation of the instable peroxyradical **1.4** resulting in the formation of a 2-deoxyribonolactone residue **1.6** and the corresponding free base BH **1.7**.^[11] This lesion is alkaline-labile and results in strand scission with formation of 3'-phosphate **1.8**, 5'-phosphate **1.10** and 5-methylene furanone (5-MF) **1.9**. In a biological environment, oxygen and GSH trapping of C1' radicals are competitive processes, due to the μM oxygen concentration (but high rate constant of $1 \times 10^9 \text{ M}^{-1} \text{ s}^{-1}$) in the nucleus. Once the peroxy radical is formed, the C1' peroxy radical **1.4** expels a superoxide radical anion with a rate constant of ca. $2 \times 10^4 \text{ s}^{-1}$. The resulting C1' cation **1.5** leads to the formation of the ribonolactone much faster than it is trapped by GSH. The H-abstraction from the thiol to give the hydroperoxide, has in fact a rate constant $\leq 400 \text{ M}^{-1} \text{ s}^{-1}$. Direct oxidation to cation **1.5** is also observed in the presence of metal complexes.



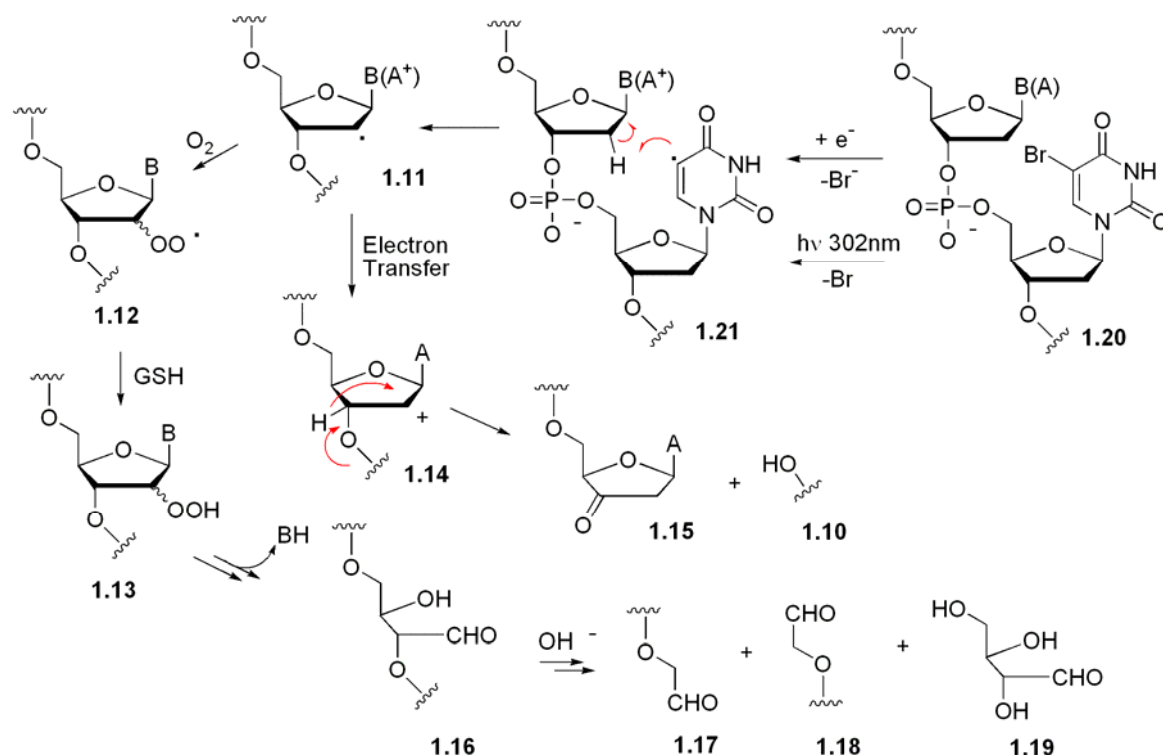
Scheme 1.2 Fate of the C1'-radical under different conditions.^[14]

C2' radicals

The 2'-position of deoxyribose is less prone to H-abstraction, either because of the low accessibility or the low reactivity of these hydrogens in the dsDNA.^[20] However, as already mentioned for the C1' radical generation, photoreaction of oligonucleotides containing halogenated uracil give rise to hydrogen abstraction from the C2'-position with generation of the C2' radical **1.11** as shown in Scheme 1.3. In the presence of oxygen this C2' radical can be trapped to the peroxy radical **1.12**, consequently being reduced to the hydroperoxide **1.13** by GSH. The hydroperoxide can undergo homolytic or heterolytic cleavage. Subsequently, the free base BH is released and the erythrose-containing site **1.16** is observed. This fragment is responsible for the formation, upon alkaline treatment, of the species **1.17**, **1.18** and to a certain extent **1.19**. A different pathway that gives rise to the furanone terminus **1.15** invokes an electron transfer between the photoactivated adenosine radical cation and the sugar unit. The C2' cation **1.14** hydrolyses to the observed fragments with consequent strand break.

Generally abstraction from the C2'-position does not contribute greatly to most pathways of DNA strand scission. Nevertheless abstraction of a C2'-H may be facilitated in RNA due to

the presence of the additional OH-group or, eventually by the presence of adjacent halogenated bases.

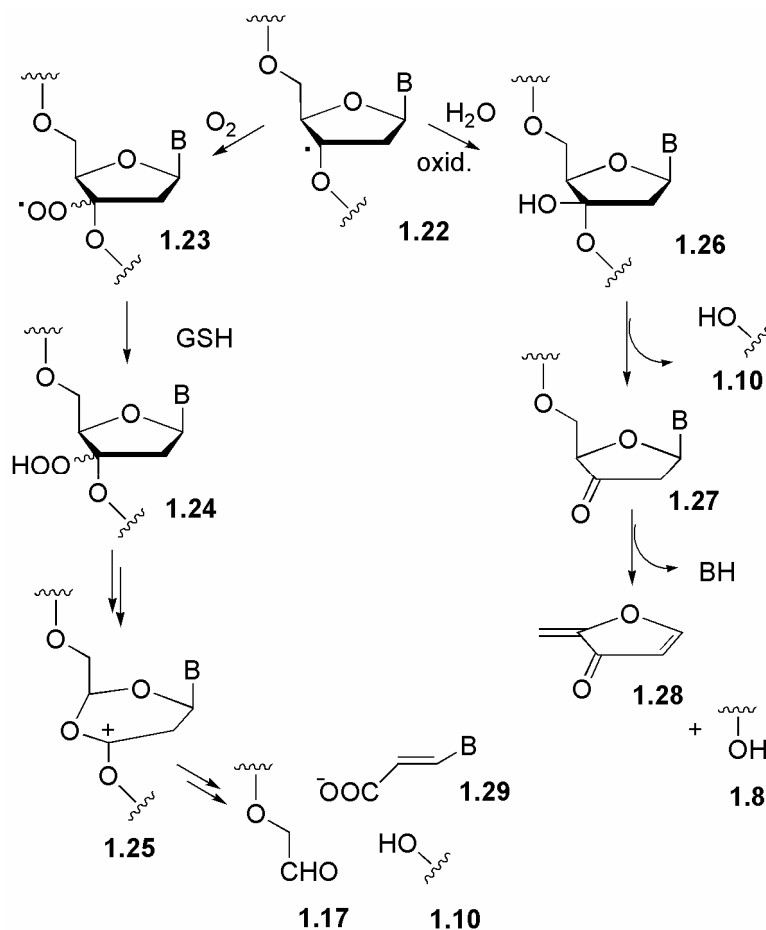


Scheme 1.3 Generation and fate of C2'-radical.

C3' radicals

The majority of known oxidative cleavage agents bind in the minor groove of the DNA. The C3'-H, which points into the major groove, seems to be only partially involved in the pathways leading to the scission of DNA. However, photoactive rhodium complexes have shown a specificity toward hydrogen abstraction from the C3'-position.^[40] These complexes made studies possible, in which the pathway of degradation starting from a C3'-centered radical (Scheme 1.4) was elucidated. In anaerobic conditions, the radical **1.22** is presumably oxidised by the rhodium complex itself. The addition of water yields an alcohol (**1.26**) which undergoes β -elimination of the phosphate and release of the free base, through the formation of a C3'-ketone terminus (**1.27**). This mechanism gives rise to the detected sugar lactone derivative **1.28**, the 2-methylene 3-furanone. In the presence of oxygen the formation of hydroperoxide **1.24** is followed by a rearrangement resulting in the insertion of an oxygen atom into the ribose ring (**1.25**). Successive decomposition of **1.25** yields the base propenoic

acid **1.17** and DNA fragments with 5'-phosphate (**1.10**) or 3'-phosphoglytaldehyde terminus **1.29**.



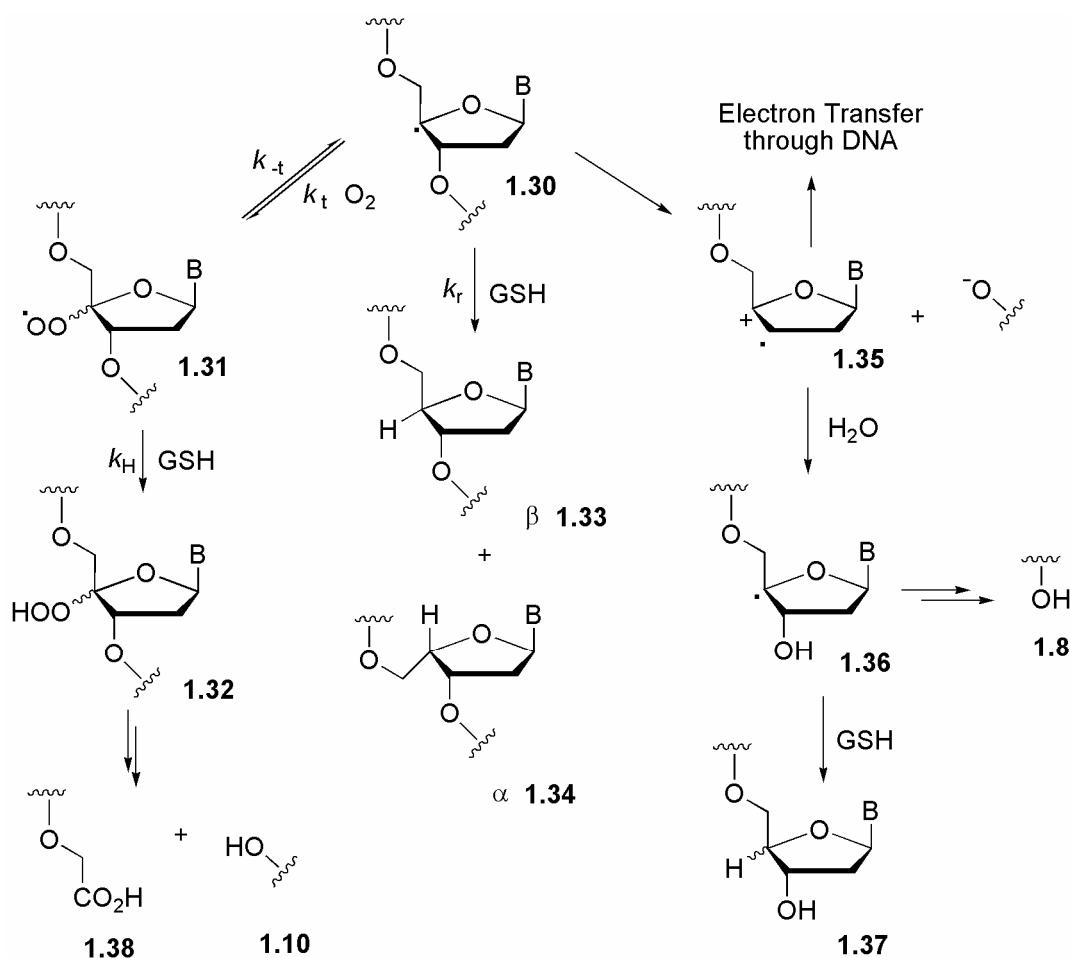
Scheme 1.4 Fate of the C3'-radical in aerobic (left) and anaerobic conditions (right).

C4' radicals

The C4'-position is believed to be highly accessible in B-DNA. Therefore several pathways and many final products are described, which are derived from the C4'-radical. DNA damage initiated from C4'-hydrogen abstraction has been proposed to take place after ionizing radiation, reaction with Fe(II) complexes, *Fenton* generated hydroxyl radicals and drugs like bleomycin, calicheamicin, neocarzinostatin and other enediines.^[11,20] More recently cyclopentadienyl metal complexes have been used to cleave DNA strands by hydrogen abstraction from the positions C4' and C5'.^[41] The synthesis of photoreactive model compounds that are specific C4' radical precursors were achieved by *Giese* and co-workers.^[42] In this case a 4'-pivaloyl substituted nucleoside was prepared as a precursor of a C4'-radical. This substrate, incorporated into an oligonucleotide, was used as radical cation

donor for charge transfer studies through DNA. Specifically, the C4'-radical **1.30** undergoes β -elimination generating the intermediate radical cation species **1.35** (Scheme 1.5). This is able to oxidize a guanine nucleobase to G^{+} , which in turn transfers the charge to another guanine. This process is then repeated resulting in a transfer of the positive charge (hole transfer) through the DNA. Some features of this process are covered in more detail in Chapter 2.

Trapping of the radical cation **1.35** by water generates radical **1.36**, which undergoes a second heterolytic cleavage to yield the phosphate end and sugar fragments. In the presence of GSH, radical **1.30** is reduced with a rate constant of $k_r = 1.9 \times 10^6 \text{ M}^{-1} \text{ s}^{-1}$ yielding a mixture of anomers β (**1.33**) / α (**1.34**) = 1.5 in single strand DNA (ssDNA) and $\beta/\alpha = 9$ in dsDNA.^[43] The heterolytic cleavage of radical **1.30** is in competition with hydrogen abstraction from GSH, when GSH is present in milli-molar levels. Therefore, in the presence of a hydrogen-donor such as GSH, radical **1.36** can be reduced to the alcohol terminus **1.37** (Scheme 1.5).



Scheme 1.5 Fate of the C4'-radical.

Under aerobic conditions, radical **1.30** is trapped very rapidly with a rate constant of $k_t = 2 \times 10^9 \text{ M}^{-1} \text{ s}^{-1}$ yielding the peroxy radical (**1.31**). This reaction with molecular oxygen is reversible, with a rate constant for the back reaction of $k_{-t} = 1.0 \text{ s}^{-1}$ at ambient temperature. The product of hydrogen abstraction from GSH, the hydroperoxide **1.32**, has been isolated and characterized.^[44] This reaction proceeds with a rate constant of ca. $k_H = 400 \text{ M}^{-1} \text{ s}^{-1}$. Hydroperoxide **1.32** may give 3'- and 5'-cleavage *via* a *Criegee*-rearrangement.^[45] Therefore, strand cleavage depends on the concentration of the hydrogen donor. At low GSH concentration, strand scission is the result of the spontaneous heterolytic cleavage occurring even under aerobic conditions.^[14]

C5'-radicals

The two hydrogen atoms attached to the C5' are also highly accessible in a B-DNA helix. Furthermore, while both hydrogen atoms are accessible from the minor groove, it should be noted that one hydrogen (the so-called *pro-S*) points away from the groove directly toward solvent molecules (see previous Figure 1.4, pag. 7). Pathways involving the abstraction of hydrogen from the C5'-position have been proposed for DNA scission mediated by enediyne antibiotics, Fenton-generated hydroxy radicals, γ -radiolysis, cationic metal porphyrins and perhydroxy radicals.^[20]

As reported in the introduction to Chapter 1, cyclonucleotides as **1.48**, **1.49** and **1.50** (Figure 1.5) have been observed among the decomposition products of DNA when irradiated in deaerated aqueous solutions.^[18,46,47] They were also identified in mammalian cellular DNA *in vivo*, where their level can be enhanced under conditions of oxidative stress.^[48] These compounds are formed after an intramolecular cyclisation starting from the C5'-radical **1.39** (Scheme 1.6), through the formation of the base-radical (an aminyl-radical for purines) **1.45**. Depending on the substrate and the experimental conditions, the ratio of the two diastereomers (i.e. (5'*S*)- and (5'*R*)-isomer) changes substantially. For example, with adenine derivatives the (5'*R*)-isomer predominates in ssDNA whereas the (5'*S*)-isomer slightly prevails in dsDNA.^[14] The incorporation of the synthetically prepared 5',8-cyclo-2'-deoxypurines **1.49** and **1.50** into plasmid DNA, depicted in Figure 1.5, showed that the (5'*R*)-isomer is more efficiently repaired by the human nucleotide excision-repair complex than the (5'*S*)-isomer.^[49] The difficulty of repair and the propensity to induce mutations render these lesions biologically significant and the study of their formation necessary.^[50-52]

Kinetic studies revealed that the 2'-deoxyadenosin-5'-yl radical undergoes cyclisation with a rate constant of $k_C = 2.5 \times 10^5 \text{ s}^{-1}$ at ambient temperature.^[26] On the other hand, the rate

constant for the reaction of the C5' radical **1.39** with the GSH, the “repair reaction”, to give the natural nucleobase is poorly understood, but expected to be of the order of $k_H \approx 10^6\text{-}10^7 \text{ M}^{-1} \text{ s}^{-1}$. Since the intracellular concentration of GSH in diverse mammalian cells ranges between 0.5-10 mM, the repair reaction and the cyclisation process should be similarly effective (i.e. $k_H = 10 \text{ mM} \times 10^7 \text{ M}^{-1} \text{ s}^{-1} = 10^5 \text{ s}^{-1} \approx k_C$).^[14]

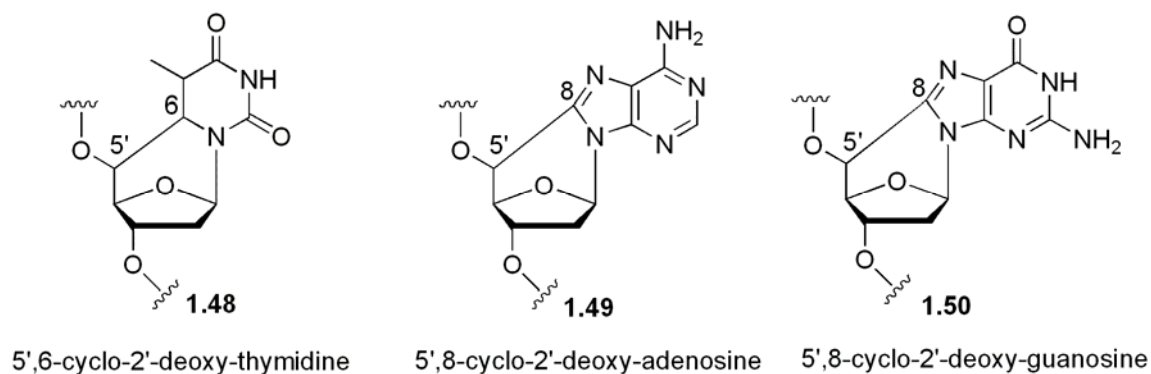
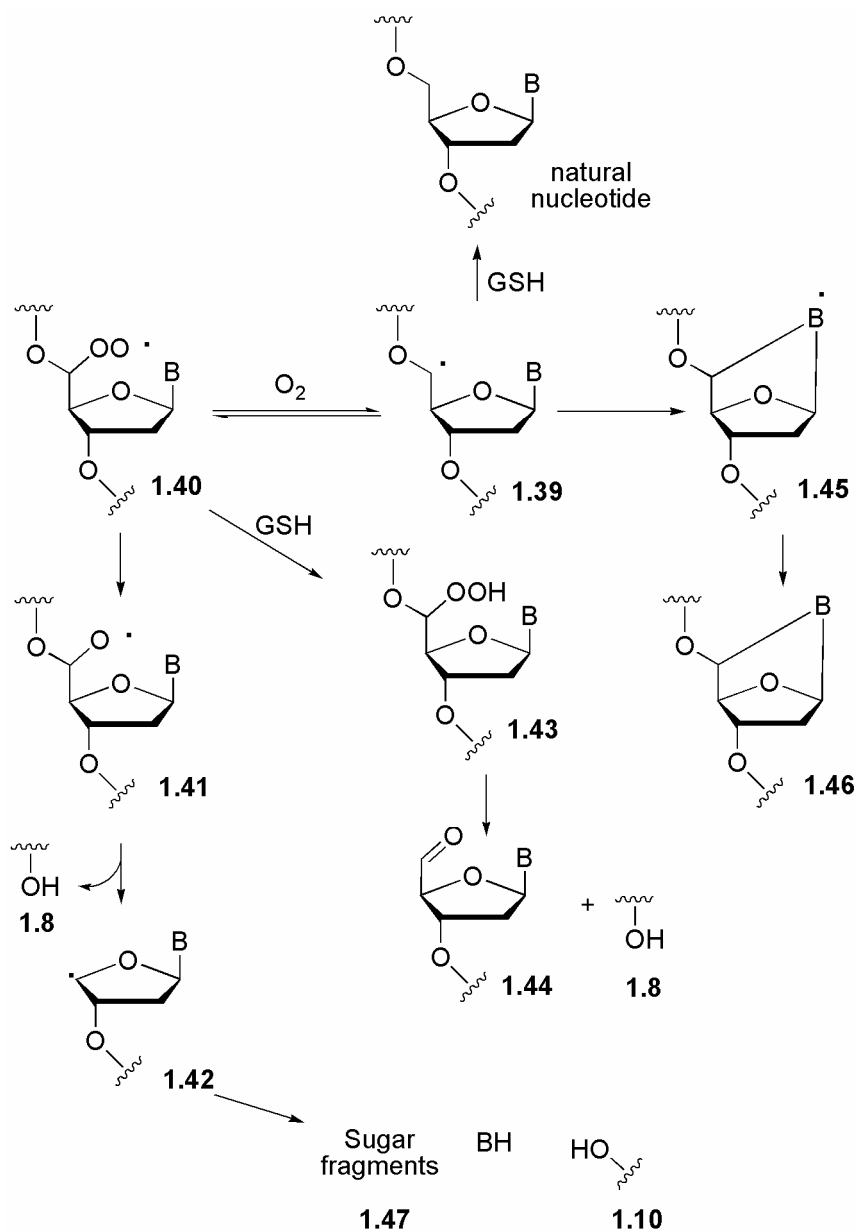


Figure 1.5 Cyclonucleosides derived from C5'-radical through intramolecular cyclisation.

Selective generation of C5'-radicals through irradiation (UV and γ -radiolysis) of 8-bromo-adenosine was reported by *Chatgililoglu* and co-workers.^[25-27] The authors exploited the ability of the C8-radical, generated after debromination of the reduced or photoexcited 8-bromo-purine, to transfer the radical intramolecularly. The C8-radical abstracts a hydrogen from the C5' sugar position, generating a C5'-radical. This sugar radical adds to the C8 of the base yielding, after oxidation, a cyclic-nucleoside. The analogous sequence of reactions for 8-bromo-2'-deoxyguanosine does not operate because the electron adduct undergoes protonation at C8 to afford the one-electron oxidized 2'-deoxyguanosine.^[35,53,54] Only recently a selective generation of 5',8-cyclo-deoxyguanosine, starting from the C5'-radical, was achieved (Section 1.2.3).^[55]

Scheme 1.6 depicts the pathways yielding the products and the strand scission generated after the formation of C5'-radicals. Under aerobic conditions, radical **1.39** is trapped reversibly by oxygen leading to strand scission or formation of an abasic site as the final DNA damage products. A DNA strand terminated with a 5'-aldehyde group (**1.44**) is unique to agents that oxidize the C5'-position and can serve as a marker for this pathway.^[20]



Scheme 1.6 Fate of the C5'-radical in presence and absence of oxygen.

In order to facilitate studies of the lesions derived from this pathway, *Greenberg* and *Kodama* recently reported the preparation and analysis of ODNs containing lesions resulting from C5' hydrogen abstraction.^[56] Nevertheless, the fate of C5'-radicals in the presence of oxygen is not yet completely understood, due to the lack of model compounds and to the absence of a method allowing selective generation of this damage-associated radical. Despite this lack of information, many of the proposed mechanisms for strand-cleavage include the initial formation of C5'-radicals. Specifically, most of the studies carried out to decipher the fate of the sugar radicals came from rationalisation of products derived from degradation of DNA by nucleolytic agents, which initiate the cleavage process by hydrogen abstraction from

the C5'-position. Many of these agents include enediynes, a family of anticancer antibiotics drugs. In particular neocarcinostatin (NCS) is an antitumor antibiotic consisting of a non-protein chromophore (NCS-C) tightly, but non-covalently bound ($K_D \sim 10^{-10}$ M) to its carrier protein ($M_r = 11000$).^[57] NCS-C, whose structure is depicted in Figure 1.6, binds to dsDNA *via* intercalation of its naphthoate moiety and interaction of the diendiyne bicyclic core with the minor groove.^[58]

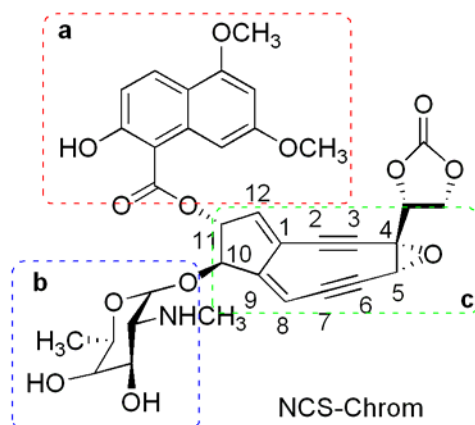
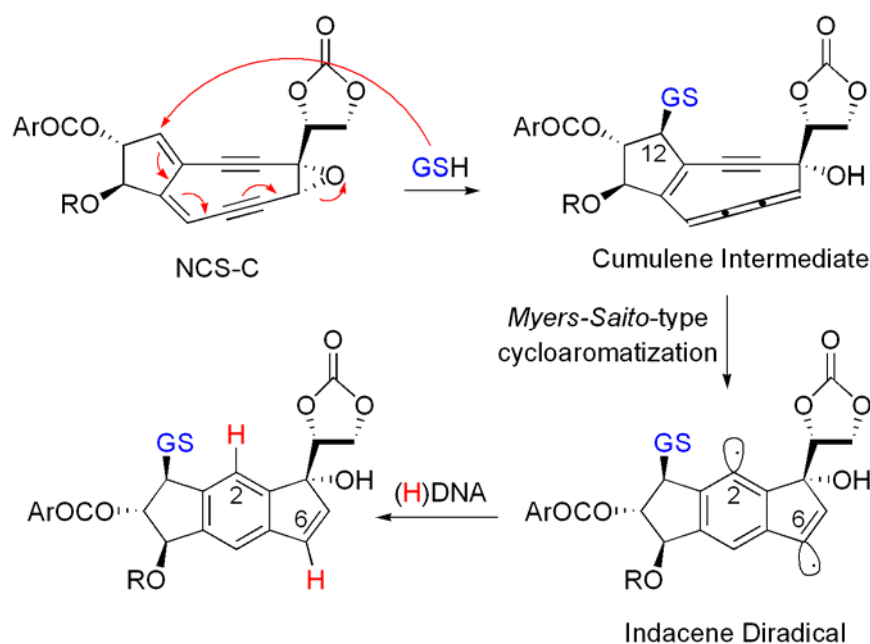


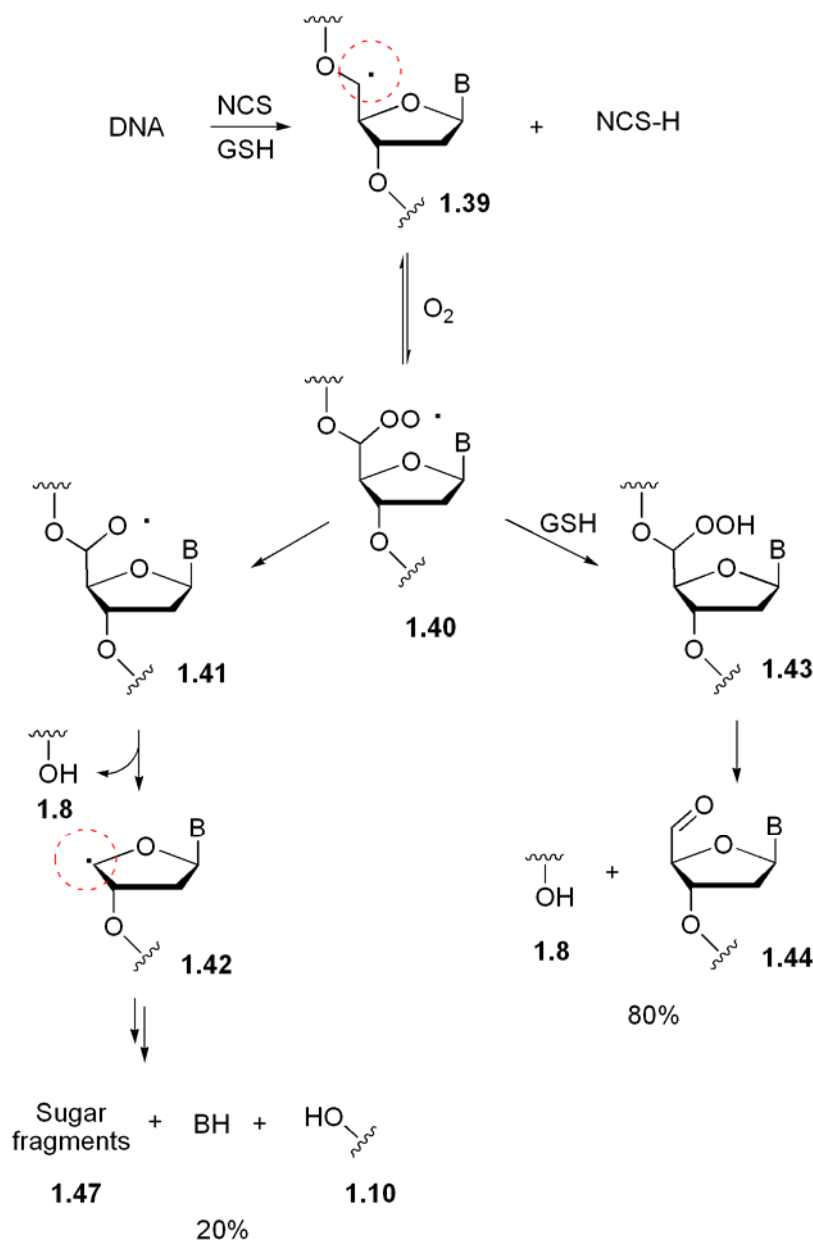
Figure 1.6 NCS-Chrom and its principal functionalities: **a.** Naphthoate group: intercalation into the major groove of DNA. **b.** Amino-sugar: *N*-methyl- α -D-fucosamine. **c.** Diendiyne bicyclic core: epoxy bicyclo[7,3,0]dodecadienediyne, interaction with the minor groove of DNA and generation of a diradical through a *Myers-Saito*-type cycloaromatisation.^[59,60]

NCS-C undergoes irreversible reaction with thiols, as shown in Scheme 1.7, to generate through a *Myers-Saito*-type cycloaromatisation a diradical species.^[59,60] This diradical is capable of cleaving DNA via hydrogen abstraction from the sugar backbone with a high degree of base specificity in single strands (ss) ($T > A \gg C \sim G$) and sequence specificity in double strands (ds) upon aerobic incubation.^[57,61,62] The intercalation of the active diradical species in the minor groove leads to a H-abstraction with the following preference: $H5' > H1' > H4' \gg H3' > H2'$.^[63]



Scheme 1.7 The mechanism of action of NCS-Chrom was intensively studied and a nucleophilic activation was proposed as the first step of a cascade reaction leading to the active diradical species. This activation step is reported here for the glutathion (GSH).

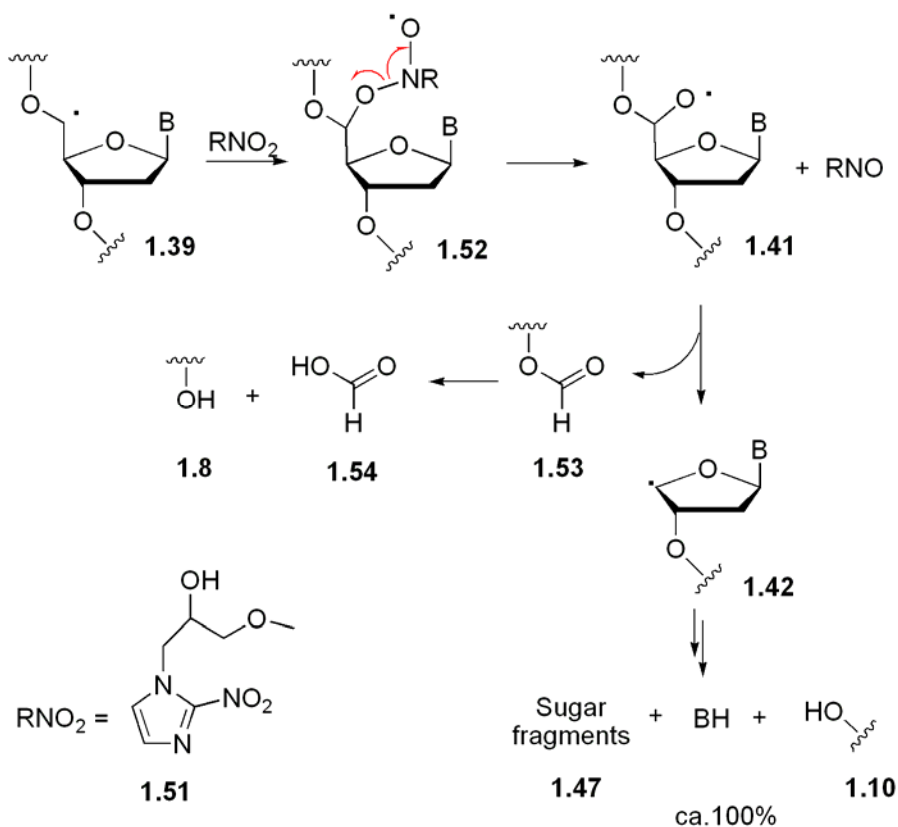
The proposed mechanism reported in Scheme 1.8 refers to the interaction of DNA with NCS-C in the presence of GSH under aerobic conditions.^[11,57] Explicitly, trapping of the C5'-radical **1.39** by dioxygen leads to the peroxy radical **1.40**, which can react in two different ways: i) hydrogen abstraction from GSH leading to the hydroperoxide **1.43**, which reacts to aldehyde **1.44** by loss of the phosphate unit (80%); ii) formation of the oxy radical **1.41** (mechanism not yet fully understood), and then β -fragmentation to give the *pseudo* C4'-radical **1.42**. The *pseudo* C4'-radical **1.42** is assumed to be responsible for the observed fragmentation products (20%), i.e. BH, RO_3PO^- , and unidentified sugar fragments.^[64,65]



Scheme 1.8 Proposed mechanism for the fate of the C5'-radical formed by NCS-mediated hydrogen abstraction under aerobic conditions. Highlighted into dashed circles are the carbon-centered radicals C5' and *pseudo*-C4'.

In addition, when misonidazole (**1.51**) replaces oxygen as oxidant, the degradation products related to this pathway increase from 20% to nearly 100% of the DNA fragments.^[66,67] *Goldberg* and co-workers explained these findings with the mechanism described in Scheme 1.9. Thus, the C5'-radical generated by hydrogen abstraction reacts anaerobically with misonidazole to create a nitroxyl radical adduct **1.52**, which fragments to produce the oxy radical at C5' (**1.41**). The addition of carbon-centered radicals to the oxygen of a nitro group of tetranitromethane and nitrobenzenes to give intermediate nitroxide radicals

has been documented by electron spin-resonance spectroscopy (EPR) and pulse radiolysis methods.^[68,69] Such radicals can undergo fragmentation to form oxy radicals and the nitroso reduction product of misonidazole. Subsequent β -fragmentation results in cleavage between C5' and C4' with generation of the above-mentioned *pseudo* C4'-radical **1.42** and the 3'-formyl phosphate terminated DNA **1.53**, which spontaneously hydrolyzes, releasing formate (**1.54**) and creating the 3'-phosphate terminus **1.8** (Scheme 1.9).



Scheme 1.9 Mechanism of misonidazole (**1.51**) action toward the NCS-C generated C5' radical **1.39** under anaerobic conditions.^[57]

1.1.1 Aim of Chapter 1

Model studies are required in order to clearly elucidate the pathways involved in the fate of sugar-centered radicals. Nucleoside models, able to generate such radicals selectively, have been previously reported for the sugar-positions C1',^[29,30] and C4'.^[42] Nevertheless, in the case of C5'-position such studies were lacking.

This work described in Chapter 1 was aimed at developing nucleoside models for the selective generation and study of radicals centered at the C5'-position (**1.39**) and radicals associated with it such as the *pseudo* C4'-radical **1.42** (Figure 1.7).

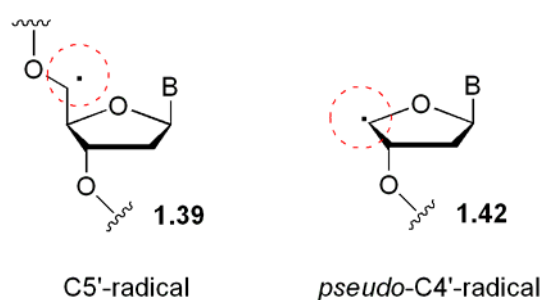


Figure 1.7 Sugar-centered radicals associated with oxidative damage of DNA.

The synthesis of a selective precursor of the *pseudo* C4'-radical was achieved and the mechanistic pathways of its degradation were studied (Section 1.2.1). Furthermore, the synthetic and kinetic aspects of the above-mentioned cyclisation reaction starting from a C5'-radical were investigated (Section 1.2.2). Finally, the synthesis of a selective C5'-radical precursor is reported (Section 1.2.3).

1.2 Results and Discussion

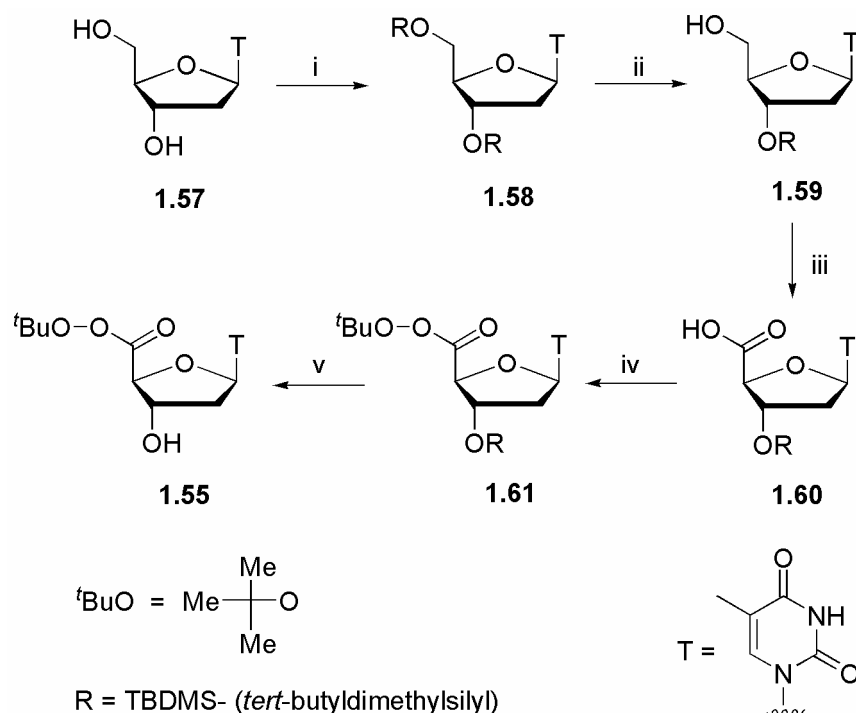
1.2.1 Formation and fate of the *pseudo* C4'-radical

General

Model studies on the fate of the postulated *pseudo* C4'-radical intermediate **1.42** are not available yet. In order to design a model valid for the radical-based DNA damage associated with the C5'-position, a model study was undertaken on the fate of the *pseudo* C4'-radical (**1.56** in Scheme 1.11) of the nucleoside thymidine. This nucleotide represents the main target for the cancer drug NCS-C among the four DNA bases.

Synthesis of the *tert*-butyl perester of C5' thymidinoic acid

The *tert*-butyl perester of C5' thymidinoic acid **1.55** was chosen as a possible precursor of the *pseudo* C4'-radical **1.56** through a homolytic cleavage as illustrated in Scheme 1.11. Perester **1.55** has been obtained in 25 % overall yield through the five-step synthesis depicted in Scheme 1.10. Specifically, the 3'-*O*-TBDMS-protected thymidine **1.59** was obtained by *tert*-butyldimethylsilyl chloride (TBDMS-Cl) full protection followed by a 5'-selective deprotection. The alcohol **1.59** was oxidized to the thymidinoic acid **1.60** in almost quantitative yield by a tetramethylpiperidinium-*N*-oxide (TEMPO)-based procedure in presence of water.^[70] The esterification to compound **1.61** with *tert*-butyl hydroperoxide was then achieved in high yields in tetrahydrofuran (THF) in presence of carbodiimide (CDI). As the radical studies were to be undertaken in water, the nucleoside had to be deprotected in the final step. The yields in this case could not be increased to more than 50 % due to the intrinsic instability of the perester **1.55**.



Scheme 1.10 Synthesis of the *tert*-butyl perester of C5' thymidinoic acid. Conditions: i) THF / DMF, TBDMS-Cl, Imidazole, AgNO₃, 98%; ii) MeOH, PPTS, 60%; iii) MeCN / H₂O, TEMPO, BAIB, 98%; iv) THF, CDI, ^tBuOOH, 90%; v) THF, TBAF, 50%.

Thermolysis of the *tert*-butyl perester of C5' thymidinoic acid

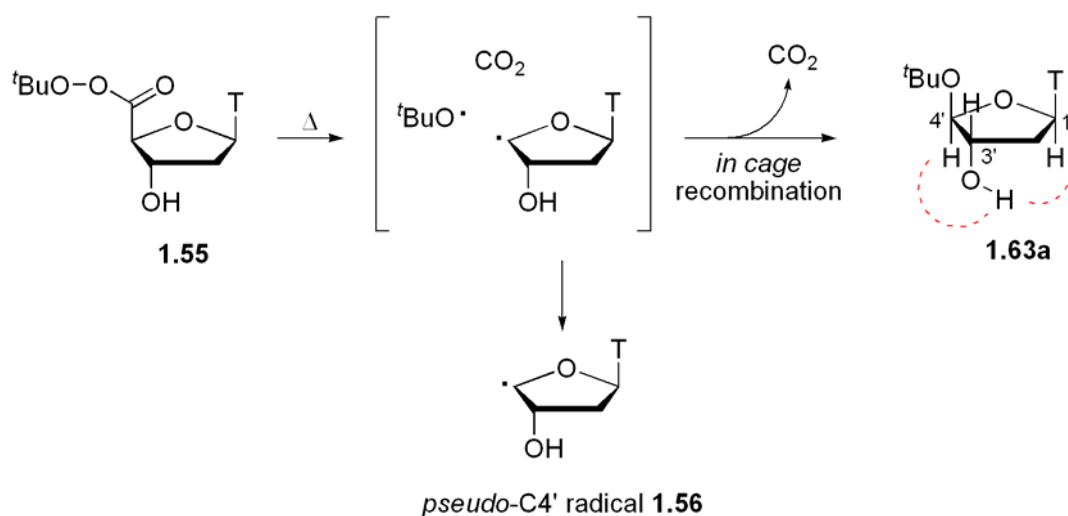
The decomposition of **1.55** was performed at 85 °C in various solvents such as THF, *tert*-butanol (^tBuOH), methanol (MeOH), and water (H₂O). The thermolysis were achieved in the absence and in the presence of a thiol such as thiophenol (PhSH) or GSH in order to measure both the capability of **1.55** for behaving as precursor of radical **1.56** and to investigate the fate of radical **1.56** under different reaction conditions. Complete disappearance of **1.55** was monitored within 1 h at the operating temperature of 85 °C. The rapid thermal decomposition of **1.55** as compared with other *tert*-butyl peresters, should be ascribable to the presence of the α -oxy substituent.^[71] The products of thermolysis, when not otherwise specified, are stable under the conditions of the experiments. The quantitative analysis of the products of thermolysis are reported in Table 1.1 at the end of this section.

Thermolysis in THF

The decomposition of **1.55** in THF resulted in the release of the free base thymine **1.62** (46%) and formation of the *tert*-butyl acetal **1.63a** (25%) as major products together with minor amounts (14%) of the reduced product **1.64** (Table 1.1, entry 1).

The acetal **1.63a** was isolated as (4'*S*) diastomer. The (4'*S*) configuration was supported by the ¹H-NMR spectrum through analysis of coupling constants in addition to NOE experiments. In particular, in CDCl₃ solution the coupling constant between H3' and H4' was found to be zero. This indicates a dihedral angle H3' ^ H4' of nearly 90°. Moreover, resonance on the C3'-OH proton caused a nuclear Overhauser enhancement of H4' and H3' protons, and minor enhancements of *tert*-butyl and H1' protons (Scheme 1.11).

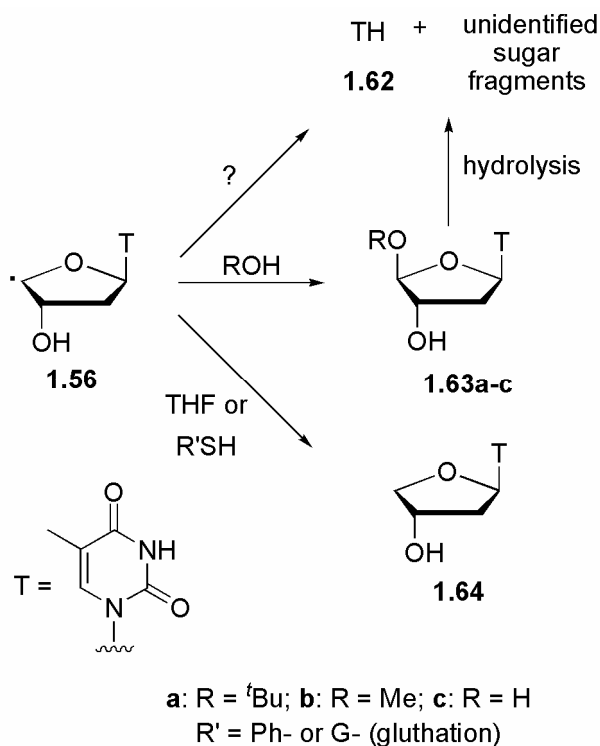
No evidence of any sugar fragments, expected to accompany the formation of thymine, could be obtained both by GC-MS and HPLC analysis of the reaction mixture. In addition, the reaction mixture was reacted with TMS-Cl following the procedure of Corey.^[72] Also in this case subsequent GC-MS analysis did not show the presence of any plausible sugar fragment.



Scheme 1.11 Thermolysis of perester **1.55** and formation of the free radical **1.56** after homolytic cleavage and decarboxylation. The acetal **1.63a** is generated in THF through an *in cage* recombination between the *tert*-butoxy radical ($t\text{BuO}\cdot$) and the radical **1.56**. The dashed red curves indicate the NOE correlation that allowed the assignment of the (4'*S*) configuration for the acetal **1.63a**.

Compound **1.64** in Scheme 1.12 is a reduction product and it is assumed to be formed from the *pseudo* C4'-radical **1.56** through hydrogen atom abstraction reaction. It represents a reliable radical probe for the radical under investigation. The hydrogen abstraction reaction by

1.56 occurred from the THF solvent, as proven by a strong deuterium isotope effect ($k_H/k_D = 7$) observed when the decomposition of **1.55** is carried out in *d8*-THF. In this deuterated solvent the yield of the reduction product **1.64** dropped down from 14% to 2%, as evidenced by HPLC analysis of the reaction mixture. This hydrogen atom abstraction reaction is an example of an “identity reaction”,^[73] since both the abstracting radical **1.56** and the resulting radical (THF[•]) are tetrahydrofuran-2-yl radicals.



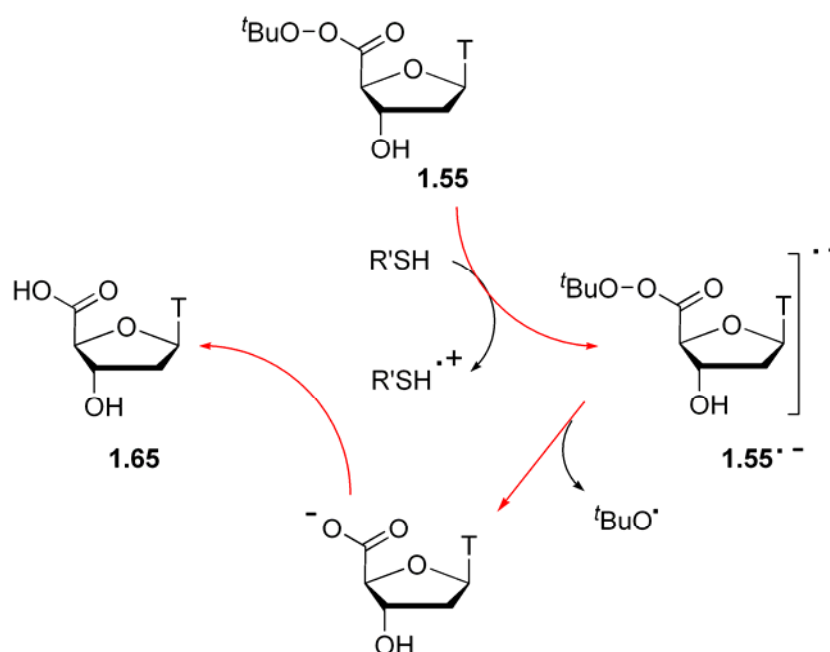
Scheme 1.12 Fate of the free radical **1.56** generated by thermolysis of **1.55** in different solvents.

Thermolysis in THF with a thiol

When the decomposition of perester **1.55** was performed in THF in the presence of a 5-fold excess of PhSH (a strong hydrogen donor) the yield of the reduction product **1.64** increased from 14% to 58% at the expense of thymine **1.62**, whereas the yield of the acetal **1.63a** remained unchanged (Table 1.1, entry 2). These findings clearly indicate that the thermal decomposition of perester **1.55** in THF can lead to radical **1.56**, which is responsible for both the free base thymine **1.62** and the reduction product **1.64**. On the contrary, the acetal **1.63a** was not formed from *free* radicals **1.56**. It was most likely derived from thermal decomposition of **1.55** with the loss of carbon dioxide and *in cage* coupling of the resulting

radicals (Scheme 1.11). Thus the *tert*-butoxy radical (${}^t\text{BuO}^\bullet$), formed by homolysis of perester **1.55**, couples with the radical **1.56** before it diffuses in the solvent. The *in cage* decomposition of *tert*-butyl peresters is well documented.^[74]

Small amounts of the thymidinoic acid **1.65** were also detected in the reaction when carried out in the presence of PhSH. The acid **1.65** was probably formed by a single electron transfer (SET) process between perester **1.55** and PhSH. The perester radical anion ${}^{\bullet-}\text{1.55}$ eventually yielded **1.65** by loss of ${}^t\text{BuO}^\bullet$ (Scheme 1.13). Similar SET processes between peresters and the sulfur atom of sulfides^[75] and thiols^[76] have already been reported.



Scheme 1.13 SET reaction between perester **1.55** and RSH to elucidate the formation of **1.65**.

Thermolysis in *tert*-butanol with a thiol

The decomposition of perester **1.55** was then carried out in ${}^t\text{BuOH}$ in the presence of a 5-fold excess of PhSH. The reduction product **1.64** and the *in cage* product, the acetal **1.63a** were formed together with minor amounts of the free base thymine **1.62** and acid **1.65** (Table 1.1, entry 4). The decomposition, repeated in the absence of the thiol as hydrogen donor, led to suppression of the radical product in favour of the acetal **1.63a** (Table 1.1, entry 3). The acetal **1.63a** was produced as (4'*S*) diastereomer regardless of the presence of a thiol

On this basis we can infer that, similar to the reaction carried out in THF, the decomposition of perester **1.55** in ${}^t\text{BuOH}$ furnishes both the *in cage* product **1.63a** and the

free radical **1.56**. In both solvents and in the presence of thiols, the free radical **1.56** affords the reduction product **1.64**. But, in contrast to the reactions conducted in THF, in ^tBuOH and in the absence of thiol, the free radical **1.56** mainly gives the acetal **1.63a** instead of thymine **1.62**.

The formation of the acetal **1.63a** as derived from the reaction of radical **1.56** with ^tBuOH is an unpredicted result. In fact, no reaction was expected between a radical species and a nucleophilic solvent.

Thermolysis in methanol

The latter finding was supported by results obtained by decomposition of perester **1.55** carried out in MeOH, which led to the formation of both *tert*-butylacetal **1.63a** and methylacetal **1.63b** (Figure 1.8). The former is formed by *in cage* decomposition, the latter from the free radical **1.56** (Table 1.1, entry 5).

When the reaction was carried out in the presence of PhSH, the reduction product **1.64** was formed at the expense of the acetal **1.63b**, but not the acetal **1.63a**, (Scheme 1.12 and Table 1.1, entry 6). Thus the *in cage* acetal **1.63a** remain constant and its concentration does not depend on the concentration of generated free radicals **1.56**.

In addition, in the thermolysis conducted in MeOH the major product was the methyl ester **1.66** (Figure 1.8). This product was formed from the perester **1.55** in methanol at room temperature as well (50% conversion after ca. 2h). It probably derives from a *trans*-esterification reaction.

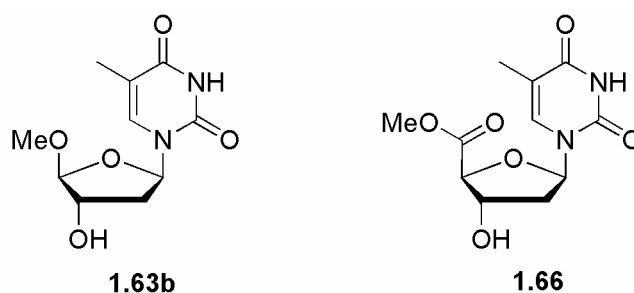


Figure 1.8 Methyl acetal **1.63a** and methyl ester **1.66**.

The methyl acetal **1.63b** and the methyl ester **1.66** in Figure 1.8 generate a mixture inseparable both by HPLC and column chromatography. As a consequence, the methyl acetal **1.63b** was not obtained as a pure product. Its identification was achieved by ¹H NMR spectral comparison of the mixture (**1.63b** + **1.66**) with a pure sample of **1.66**. In support of the

assigned structures, negative- and positive-ion ESI-MS spectra of the mixture clearly show both peaks for the acetal **1.63b** and the ester **1.66**.

In addition to these products, the acid **1.65** was found both in the absence and, to a greater extent, in the presence of PhSH. The formation of acid **1.65** in the absence of reducing species, such as thiols, is still unclear.

Thermolysis in water / *tert*-butanol 3:1 mixture

In order to investigate the effect of water on the behaviour of perester **1.55** (and radical **1.56**), the decomposition of **1.55** was carried out in a 3:1 H₂O / *t*BuOH mixture. The presence of *t*BuOH as a co-solvent was necessary due to the low solubility of perester **1.55** in H₂O.

The complete disappearance of **1.55** occurred within 1 h with concomitant formation of thymine **1.62** and *tert*-butyl acetal **1.63a**, whose ratio is determined by the reaction time. After prolonged heating of the reaction mixture (ca. 3 h) the free base thymine **1.62** was found as the only product in 87% yield (Table 1.1, entry 7). A separate experiment with the isolated acetal **1.63a** was undertaken in order to confirm the degradation of the acetal to thymine. Acetal **1.63a**, when heated at 85 °C in 3:1 H₂O / *t*BuOH yields thymine as the only product.

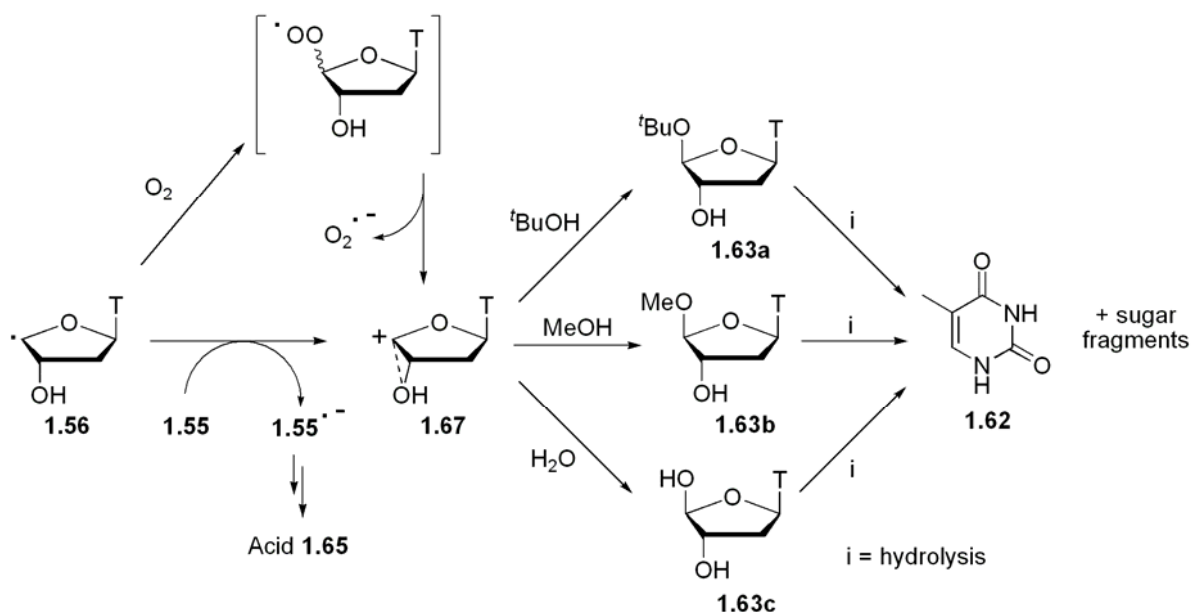
Thermolysis in water / *tert*-butanol 3:1 with a thiol

Thermal decomposition of perester **1.55** was repeated in the presence of GSH as hydrogen donor. After 1 h heating, thymine **1.62**, *tert*-butyl acetal **1.63a**, the reduction product **1.64** and small amounts of the acid **1.65** were formed. After prolonged heating (3 h), HPLC analysis showed the complete disappearance of the acetal **1.63a**, due to its hydrolysis with subsequent release of thymine. Thus, the free base thymine **1.62** and the reduction product **1.64** were the major products, together with minor amounts of acid **1.65** (Table 1.1, entries 8,9). The acid **1.65** was most probably is formed by **1.55** through SET reduction by GSH.^[76] In fact, as expected, the yield of acid **1.65** increased with increasing the GSH concentration.

These findings can be easily rationalized by the conclusion that the chemical behavior of perester **1.55** (and radical **1.56**) in H₂O / *t*BuOH is strictly related to that exhibited in neat alcohols. That is, perester **1.55** can undergo both the *in cage* decomposition leading to *tert*-butyl acetal **1.63a** and thermal fragmentation leading to radical **1.56** (Scheme 1.11). The latter can be reduced to **1.64** through hydrogen atom abstraction from GSH. In the absence of the thiol, the free radical **1.56** can be trapped by the nucleophilic solvent, *t*BuOH or H₂O, to

give acetal **1.63a** and hemiacetal **1.63c** respectively. These acetals can eventually give rise of thymine **1.62** by hydrolysis and successive fragmentation (Scheme 1.12). In addition, perester **1.55** can be reduced to acid **1.65** by a thiol (PhSH or GSH, Scheme 1.13).

The formation of acetal **1.63** from the reaction between the nucleophilic solvent and the free radical **1.56** must include an oxidation step. Under the reaction conditions employed and in the absence of any thiol, the free radical **1.56** can be oxidised by oxygen to cations **1.67**. This oxidation step probably occurs through the intermediacy of a peroxy radical followed by loss of superoxide radical anion, $O_2^{\cdot-}$. A similar mechanism has been previously proposed for the 2'-deoxyuridin-1'-yl radical.^[30,77] The formation of acetals **1.63a-c** is likely to proceed through a nucleophilic attack to the cations **1.67** by the solvent. The stereoselective formation of (4'*S*)-**1.63a** indicates that the nucleophilic attack occurs from the side opposite to the C3'-OH group. This finding might suggest that cation **1.67** can be stabilized through an oxiranium structure (Scheme 1.13).



Scheme 1.14 Oxidation of the *pseudo* C4'-radical **1.56** by dioxygen or by the perester **1.55** leads to the acetal (or hemiacetal) **1.63a-c**.

Thermolysis in water / *tert*-butanol 3:1 in absence of O₂

To obtain evidence of the role played by oxygen, reactions in H₂O / ^tBuOH in oxygen-free argon atmosphere were performed. In the absence of GSH, thymine **1.62** was formed in only 60 % yield together with acid **1.65** (10 %, Table 1.1, entry 10). On the contrary, thymine **1.62** was the only product formed in the presence of air (87%, Table 1.1, entry 7). Thus, in the absence of oxygen, radical **1.56** can be oxidized by perester **1.55** itself, with eventual formation of acid **1.65**. On the other hand, the oxygen concentration did not have an influence on reactions carried out in the presence of GSH, as expected, since oxidation of radical **1.56** is prevented by the hydrogen atom abstraction from the thiol H-donor (Table 1.1, entries 11-13).

Table 1.1 Products (%) from thermal decomposition of 1.5 mM solutions of perester **1.55**

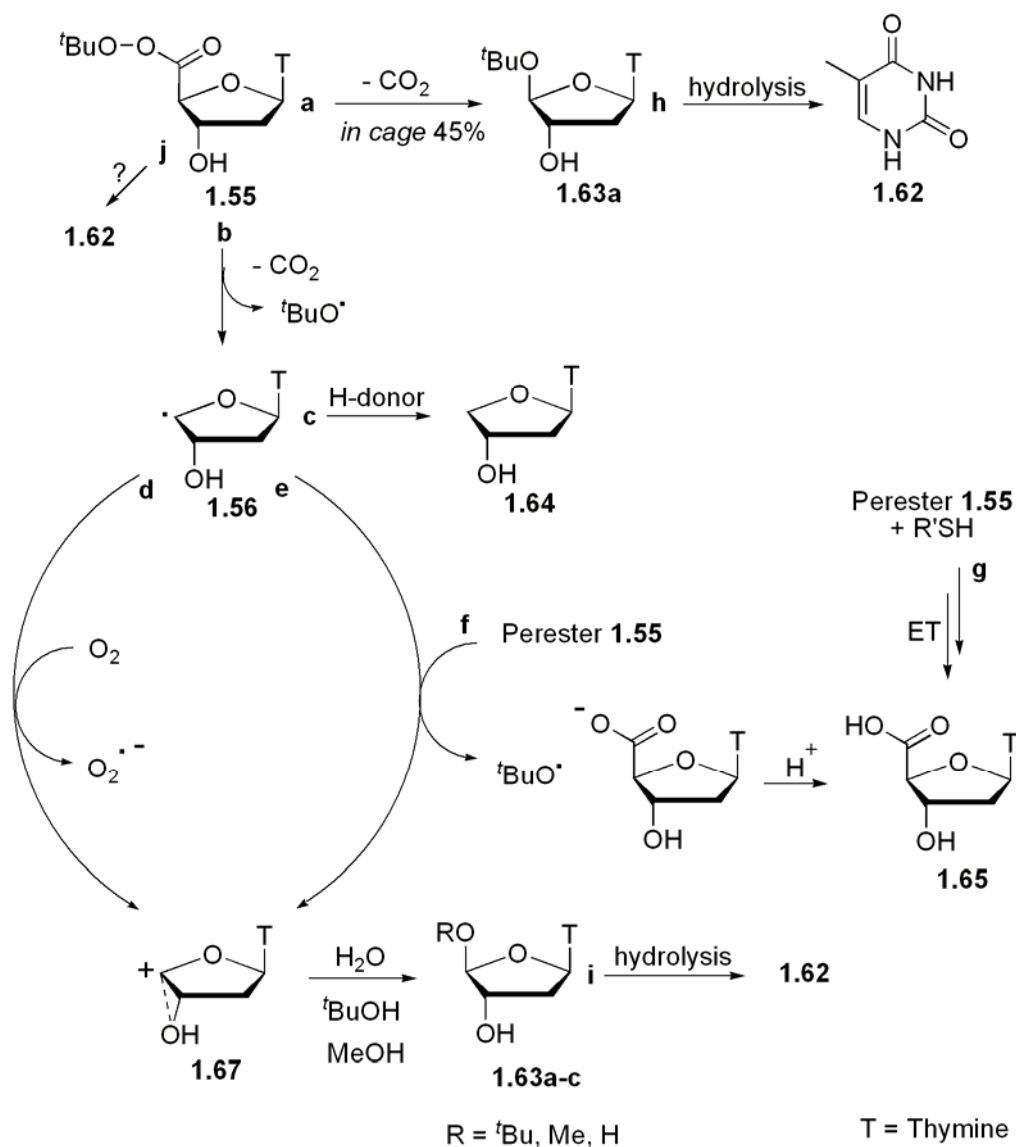
Entry	Conditions	Thymine 1.62 , %	Acetal 1.63a , %	Product 1.64 , %	Others (%)
1	THF, air	46	25	14	<i>none</i>
2	THF, air, PhSH (5 mol. equiv.)	7	24	58	1.65 (7)
3	^t BuOH, air	12	73	n.d.	none
4	^t BuOH, air, PhSH (5 mol. equiv.)	15	33	35	1.65 (8)
5	MeOH, air	7	12	n.d.	1.65 (10), 1:3 mixture of 1.63b + 1.66 (42)
6	MeOH, air, PhSH (5 mol. equiv.)	5	10	10	1.65 (20), 1.66 (30)
7	H ₂ O / ^t BuOH, air	87	n.d.	n.d.	<i>none</i>
8	H ₂ O / ^t BuOH, air, GSH (1 mol. equiv.)	46	n.d.	27	1.65 (4)
9	H ₂ O / ^t BuOH, air, GSH (5 mol. equiv.)	40	n.d.	23	1.65 (13)
10	H ₂ O / ^t BuOH, argon	60	n.d.	n.d.	1.65 (10)
11	H ₂ O / ^t BuOH, 10% oxygen, GSH (5 mol. equiv.)	44	n.d.	25	1.65 (13)
12	H ₂ O / ^t BuOH, 1% oxygen, GSH (5 mol. equiv.)	45	n.d.	26	1.65 (10)
13	H ₂ O / ^t BuOH, argon, GSH (5 mol. equiv.)	45	n.d.	28	1.65 (12)

Conclusions

In conclusion, it was shown that perester **1.55** undergoes thermal decomposition leading to both the *in cage* acetal **1.63a** and the free radical **1.56** (Scheme 1.15). The free radical undergoes H-abstraction by hydrogen atom abstraction from a thiol or from THF, if they are present, to form **1.64** or can be oxidized to cation **1.67** by oxygen. In absence of oxygen the radical **1.56** can be oxidised by perester **1.55**. In turn, cation **1.67** can be stereoselectively trapped by the nucleophilic solvent to give acetals **1.63a-c**. These acetals are subsequently hydrolysed by water, releasing the free base thymine **1.62**. The oxidation of the radical **1.56** by perester **1.55** eventually yields acid **1.65** by initial SET reaction. The acid **1.65** is also formed through analogous SET reaction between perester **1.55** and the thiol, PhSH or GSH.

In THF and in the absence of a thiol, radical **1.56** undergoes both *identity* hydrogen atom abstraction from the solvent and thermal fragmentation to thymine **1.62**. The mechanism of this reaction still remains unclear, since attempts to obtain evidence of the nature of the sugar fragments failed.

In summary, the unprecedented selective generation of the *pseudo-C4'* radical was established. The radical was studied in solution in various conditions and the pathways of base releasing and degradation were proved and described.



Scheme 1.15 Perester **1.55** thermally decomposes through pathways **a** and **b**. The pseudo C4'-radical **1.56** can be trapped by the H-donor (pathway **c**) or oxidized to cation **1.67** by oxygen in **d** or, under anaerobic conditions, by the perester in **e**. The acid **1.65** is generated from the perester through the pathway **f** in the absence of a thiol and through **g** in presence of a thiol for the electron transfer reaction. Thymine **1.62** is generated by hydrolysis of the *in cage* acetal **1.63a** (pathway **h**), by hydrolysis of acetals **1.63a-c** (pathway **i**) or directly from the perester in a poorly understood mechanism (pathway **j**).

1.2.2 Radical Cyclisation Approach to Cyclonucleosides

General

A generic method of cyclisation has been established in order to explore the ability of C5' centered radicals to undergo an intramolecular cyclisation, as described in the introduction to Chapter 1. Two nucleoside models were successfully synthesized: thymidine and adenosine (Figure 1.9). The studies connected with the thymidine and its cyclised products are described here, while the complete work, including studies on 2'-deoxyribo-adenosine (dA), has been recently published.^[78] The result concerning the dA cyclisation will be shortly illustrated at the end of this section.

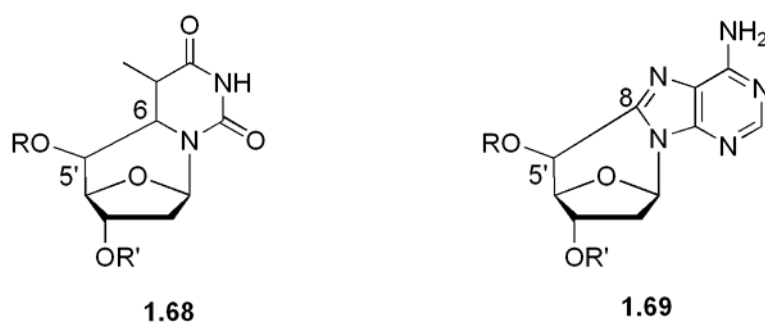


Figure 1.9 Examples of 5',6-cyclopyrimidine (**1.68**) and 5',8-cyclopurine (**1.69**) lesions (see also Figure 1.5).

Synthesis of modified 2'-deoxynucleosides containing specific DNA lesions and their incorporation into a defined sequence of oligonucleotides was an important approach to investigate their biological consequences. Synthetic ODNs containing the modified nucleosides **1.68**^[79] or **1.69**^[80,81] as well as other similar cyclopurine^[80] and cyclopyrimidine^[82,83] moieties were prepared by *Cadet* and co-workers. The synthesis of **1.68** in a diastereoisomeric ratio (5'*S*,6*S*,5'*R*)/(5'*S*,6*S*,5'*S*) = 1:2.7 was accomplished by these researchers, by tributyltin radical (Bu₃Sn[•]) mediated intramolecular cyclisation of the corresponding 5'-carboxaldehyde.^[79] The (5'*S*)-isomer of **1.69** was prepared by the same group in seven steps starting from a protected dA.^[81] The preparation of the (5'*R*)-isomer of **1.69** was further achieved by two additional steps, involving inversion of the configuration at the C5' position.^[80]

Recent studies have shown that the chemical synthesis of these lesions and their incorporation on specific sites of DNA are of considerable importance for the investigation of the details of biochemical and biophysical features of the double helix lesions.^[48,51,52,84,85]

A synthetically useful radical cascade process has been developed by *Chatgialoglu* and co-workers, which allows the conversion of 8-bromo-2'-deoxyadenosine (8BrdA) to cyclic **1.69** in a one-pot procedure. Using γ -irradiation as a source of solvated electrons (e_{aq}^-) in water, a diastereoisomeric ratio (5'R)/(5'S) = 6:1 was obtained. The overall yield, based on the recovered starting bromide, was 70%,^[25] whereas UV-irradiation in acetonitrile afforded a ratio (5'R)/(5'S) = 1.7:1 in 65% overall yield.^[27] However, attempts to obtain the corresponding phosphoramidite required for the automated synthesis of oligonucleotides, failed due to the difficulties in differentiating the two secondary hydroxyl groups by protecting group chemistry.

In summary, synthetic approaches to obtain the cyclo-nucleotides have up to now been hampered by several difficulties:

- low yields affect an efficient ODN synthesis.
- diastereoselectivity of the synthesis frequently can not be controlled.
- discrimination between the two secondary alcohol moieties in 3' and 5' is not practical.

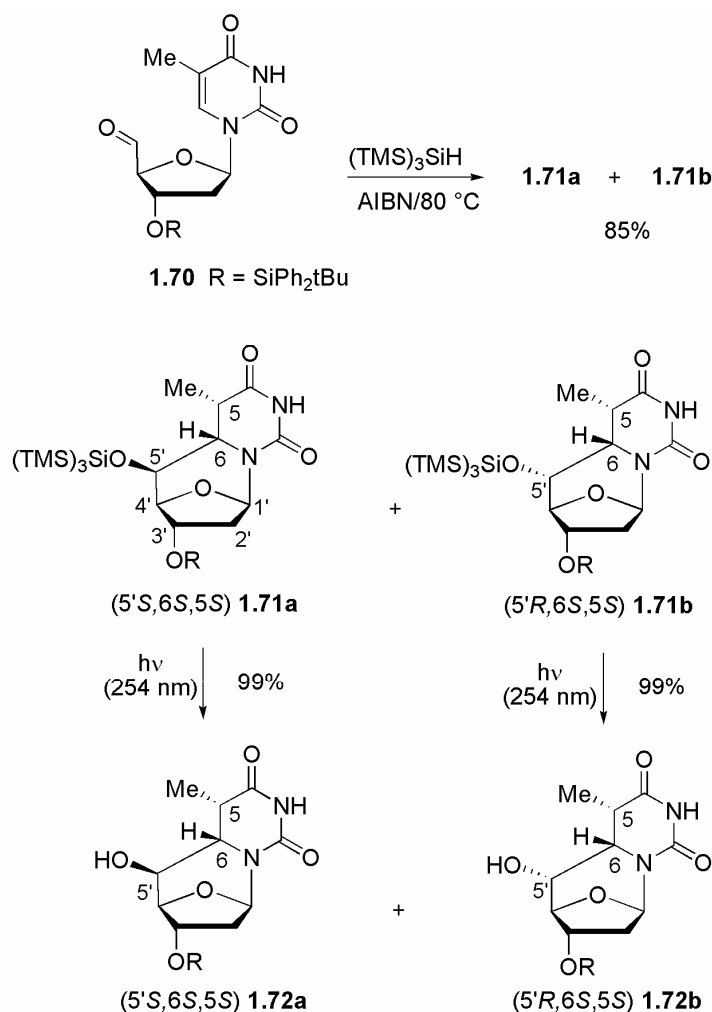
Therefore, the cyclisation of 5'-carboxaldehydes **1.70** with tris(trimethylsilyl)silane ((TMS)₃SiH, TTMS) as a radical mediator^[86,87] under a variety of conditions is described in this section. The main objective was to obtain a procedure for the preparation of 5',6-cyclo-5,6-dihydro thymidine (cyclo-dhT) **1.68**, which overcomes the limitations of the existing approaches, mainly the low yield of recently employed multiple-step syntheses and the discrimination between the alcohol moieties. In addition, a kinetic study of C5'-radical cyclisation using free-radical clock methodology is reported here.^[88,89]

Cyclisation reaction

Aldehyde **1.70** was obtained from *O*3'-(*tert*-butyldiphenylsilyl)-thymidine using a *Moffat* oxidation method in anhydrous DMSO,^[90] which turned out to be superior to other existing approaches.^[79,83]

The cyclisation reactions were tested employing TTMS as radical mediator and azobisisobutyronitrile (AIBN) as radical initiator. In a typical experiment a deoxygenated solution of **1.70** (0.01 M) in benzene (PhH) was treated with 5 equivalents (equ.) of TTMS

and 0.2 equ. AIBN. The resulting mixture was stirred at 80 °C until the starting aldehyde was reacted off, usually in less than 2 h at 80 °C. Under the same conditions, but in absence of TTMSS and AIBN, the aldehyde **1.70** is stable over a period of 3 h. After evaporation of the solvent, ¹H-NMR spectroscopic analysis showed two diastereoisomers of the cyclonucleoside (**1.71a** and **1.71b**) as the only products, in a 3:7 ratio (Scheme 1.16). These compounds were isolated by flash chromatography in 25% and 60% yield, respectively. Subsequently, a 20 mM solution of each cyclonucleosides in a 8:3 CH₂Cl₂/CH₃OH mixture was exposed to UV irradiation for 30 min at room temperature using a low-pressure mercury lamp (254 nm, 5.5 W).^[91] The quantitative formation of the mono-desilylated products **1.72a** and **1.72b** was observed. The highly selective photo-deprotection allows for the discrimination of the two secondary alcohols of the sugar moiety. This is a crucial point in the preparation of phosphoramidite derivatives. Thus, the short and high-yielding sequence of reactions presented here, gives an easy access to the standard protection steps required for the automated DNA synthesis. In addition, it has been reported that (TMS)₃SiCl can be used for the protection of primary and secondary alcohols.^[91] These silyl ethers are stable to the usual conditions employed in organic synthesis for the deprotection of other silyl groups and can be deprotected using photolysis at 254 nm, in yields ranging from 62 to 95%. The findings of the work described here point out the strength of this method if combined with radical reactions. Using an aldehydic function in consecutive radical reactions followed by deprotection could be a new approach for the formation of new stereogenic centers based on the properties of the (TMS)₃Si-group.^[86,87]



Scheme 1.16 Product studies of the reaction of aldehyde **1.70** with TTMSS under free radical conditions and subsequent photochemical deprotection. Cyclo-dhT **1.71a** and **1.71b** are formed in a 3:7 ratio.

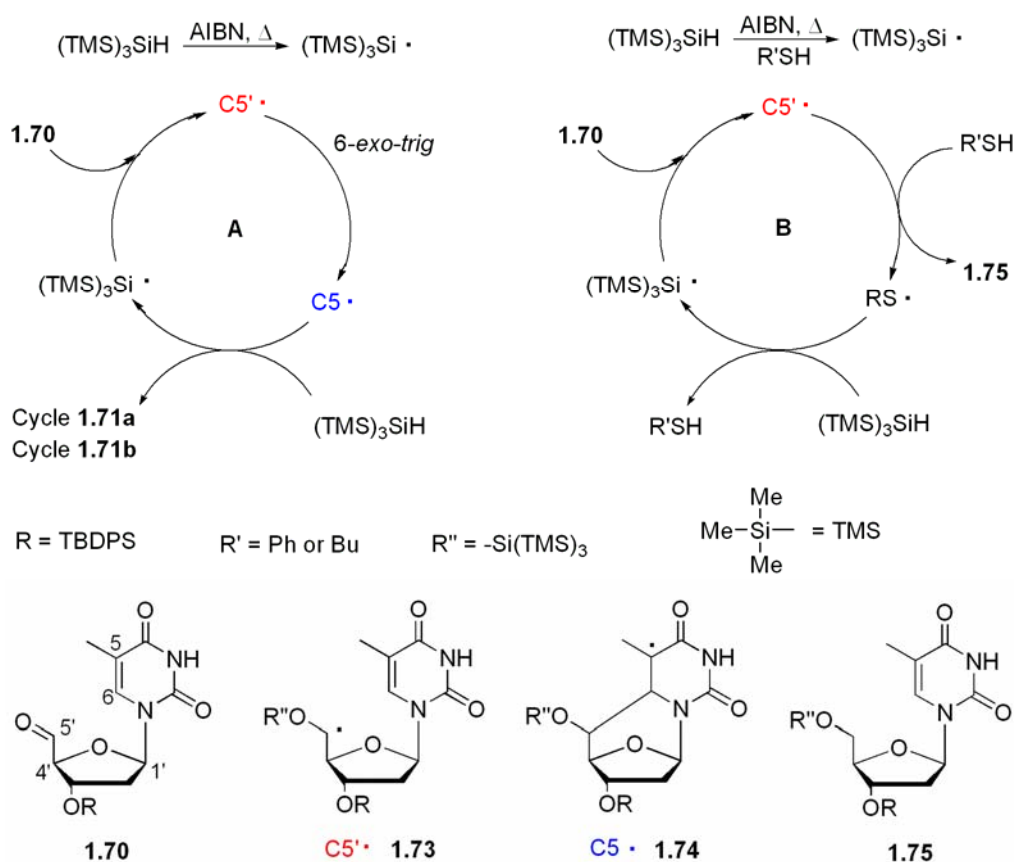
The stereochemistry of the products

In the cyclisation reaction three new stereocenters are formed at C5', C5 and C6. Among the eight possible isomers (2³), only two are produced. The stereochemistry of these two isomers was gathered from NMR analysis. The following observations led to the assignment of **1.71a** as (5'S,6S,5S)-isomer: (i) the large $J_{5',6} = 9.2$ Hz indicating that H5' and H6 are in a *trans*-diaxial arrangement, (ii) NOE on H2' (2 %) and H3' (6 %) upon irradiation of H6. Thus, a correlation is observed between H6 and H2'/H3', and (iii) NOE on H4' (8 %) observed only upon irradiation of H5. The assignment of (5'R,6S,5S) configuration to the isomer **1.71b** can be deduced from (i) the small $J_{5',6} = 2.0$ Hz indicating that H5' and H6 are in an equatorial and axial arrangement, respectively, (ii) NOEs on H2' (2 %), H5' (5 %) and H6 (4 %) upon

irradiation of H3', and (iii) irradiation of H5 caused an enhancement on H6 (4%), indicating that H5 and H6 are in an equatorial/axial and not in a trans-diaxial arrangement as could instead be deduced by the $J_{5,6}$ value of 7.6 Hz.

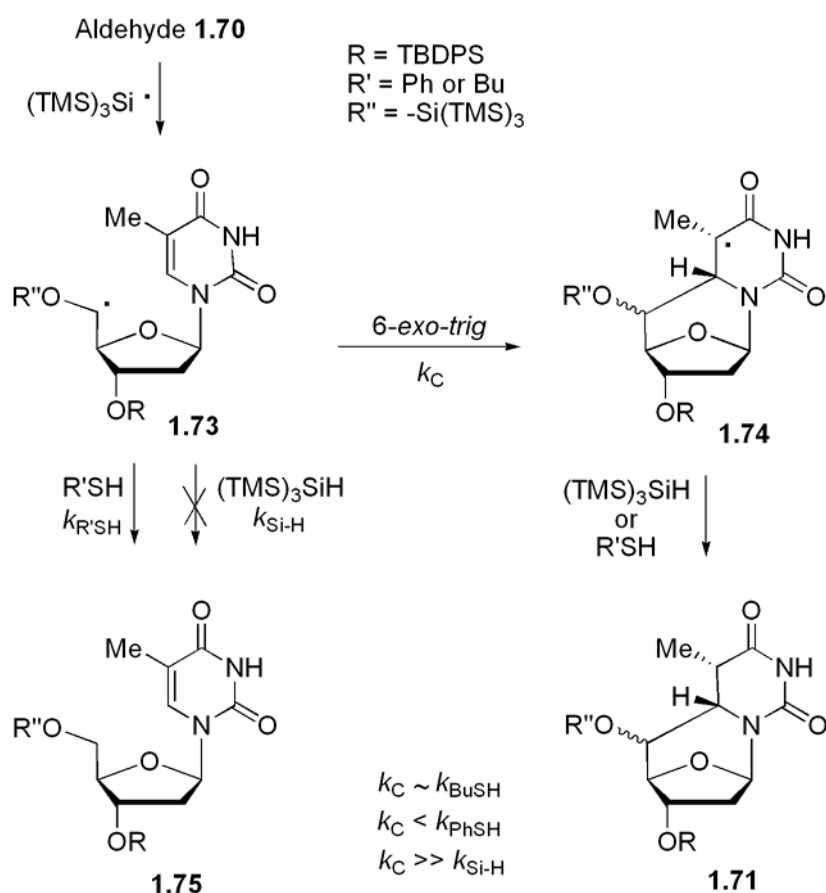
The mechanism

In Scheme 1.17 two radical chain reactions are described. Specifically, in the upper side of both chains, the initiator AIBN, after thermal decomposition, abstracts a hydrogen from the radical mediator TTMSS which generates a silyl radical $(\text{TMS})_3\text{Si}\cdot$. The latter adds to the aldehyde **1.70** (left side of both chains) giving the C5'-radical **1.73** (in red). The fate of this radical depends on the conditions. In absence of any thiol (chain A) C5'-radical undergoes a 6-*exo-trig* cyclisation adding to the double bond of the base. The resulting C5-radical (in blue) abstracts hydrogen from the silane, yielding the cyclic compounds **1.71a-b** while completing the radical chain. In the presence of a thiol (chain B) the C5'-radical is reduced to **1.75** via H-abstraction. The resulting thiyl radical $\text{R}'\text{S}\cdot$ abstracts hydrogen from the silane closing the chain.



Scheme 1.17 Radical chains A (left) and B (right) for the formation of cyclic compounds **1.71a-b** and the C5'-reduction product **1.75**.

Attempts to obtain the hydrosilylated product **1.75**, using high concentrations (5 M) of TTMSS, did not yield the desired product (Scheme 1.18). Thus, the C5'-radical **1.73** abstracts hydrogen from the silane with a rate that is much lower than the rate of cyclisation ($k_C \gg k_{\text{Si-H}}$). This is probably due to the high steric hindrance of the C5'-radical and the silane bearing both a $(\text{TMS})_3\text{Si}$ -group. Indeed, when the above-described typical experiment was carried out in the presence of 0.1 M PhSH, the $^1\text{H-NMR}$ spectrum showed a quantitative formation of the reduction product **1.75**, which was isolated by flash chromatography in 95% yield (Scheme 1.18). At such a concentration of PhSH the cyclisation reaction is slower than the hydrogen abstraction ($k_C < k_{\text{PhSH}}$).



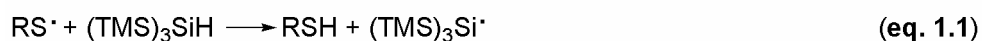
Scheme 1.18 Chemical studies on the fate of C5'-radical **1.73** under a variety of experimental conditions and formation of reduction product **1.75** in the presence of a thiol. The C5'-radical **1.73** abstracts hydrogen from the thiol (PhSH or BuSH) but not from the silane. Moreover the H-abstraction from PhSH is very fast, while from BuSH it proceeds with a rate similar to the cyclisation rate (depending on the BuSH concentration).

Radical clock reaction

At this point the relevance of the yet unknown rate constant k_C of the cyclisation reaction became evident. The products of this cyclisation are lesions of the genome within the DNA. From the kinetic data of this cyclization it could be possible to estimate the biological conditions, such as the thiol concentration, in which C5'-radicals lead to cyclo-lesions or are repaired to the natural nucleobase. Such kinetic data for cyclo-dhT are not yet available in literature.

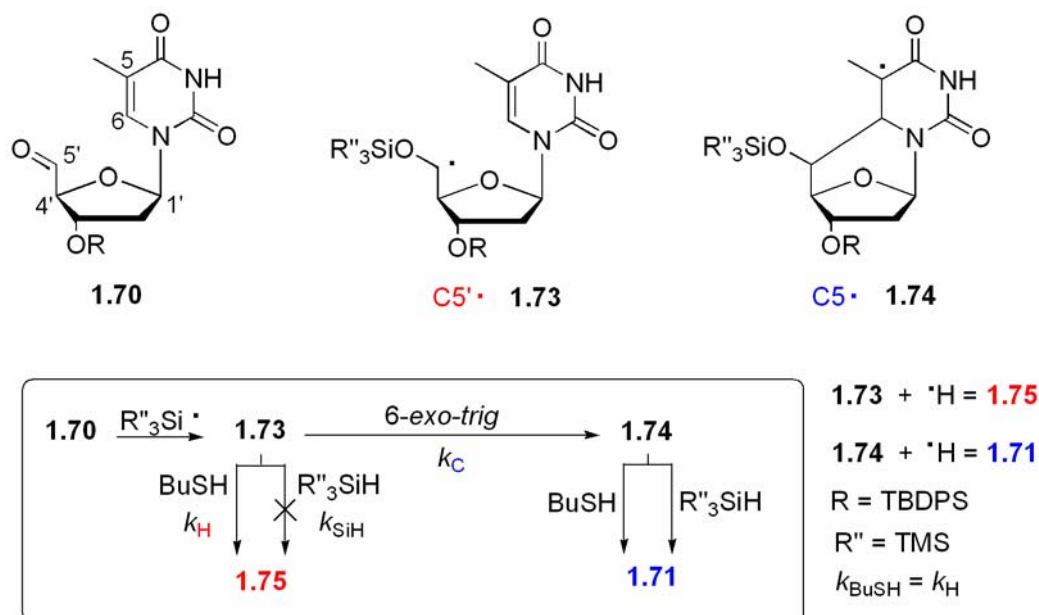
Standard methods employed to measure the rates of radical reactions include electron spin resonance (ESR), laser flash photolysis and pulse radiolysis. Another tool for investigating the rate of radical reactions is the radical clock methodology, introduced more than two decades ago by *Griller and Ingold*.^[88] Since then, the radical clock became a very popular method because no special instrumentation is required. Radical clocks are compounds that undergo a radical reaction at a known rate. The use of these compounds in competition experiments with another reaction allows the measurement of unknown rates, thus functioning as a molecular “clock”. Classic examples of radical clock reactions include cyclisations, ring openings and 1,2-radical migrations. The application of a radical clock allows the rate constant (k) of a reaction to be calculated from reactant concentrations, product ratio and the known rate constant for the radical clock reaction.

In the case of the aforementioned cyclisation of thymidine, there are two competitive irreversible reactions starting from the same intermediate, the C5'-radical **1.73** (Scheme 1.18). In the absence of any hydrogen donor the C5'-radical yields the cyclo-dhT isomers, as already described. In the presence of 0.1 M PhSH, the C5'-radical yields the reduction product **1.75**. The thiol acts as an effective hydrogen donor and the resulting thiyl radical (PhS \cdot) is able to abstract hydrogen from the silane TTMSS, thus completing the cycle of this chain reaction [Equation **1.1** and radical chain **B** in Scheme 1.17].^[92]



A rate constant k_C for the 6-*exo-trig* cyclisation can be provided when intermediate C5'-radical **1.73** can react via both reaction channels outlined in Scheme 1.18 and Scheme 1.19, that is the reaction with a hydrogen atom donor and the 6-*exo-trig* cyclisation.^[88,89] This scenario can be achieved by replacing PhSH with 1-butanethiol (BuSH), which is a weaker hydrogen donor. The homolytic bond dissociation energies (BDE)

for these species are reported to be $\text{PhS-H} = 79 \text{ kcal/mol}$, $\text{RS-H} \approx 87 \text{ kcal/mol}$ ($\text{R} = \text{alkyl group}$), $(\text{TMS})_3\text{Si-H} = 84 \text{ kcal/mol}$ and $\alpha\text{-oxy CH-H} = 92\text{-}93 \text{ kcal/mol}$.^[93] Moreover, the 6-*exo-trig* cyclization, yielding the radical **1.74**, is an irreversible reaction in this case. Therefore, the rate of the following reactions (**1.74**→**1.71** in Scheme 1.19), yielding exclusively **1.71**, does not affect the calculation of k_C . Thus, the formation of cyclo-dhT **1.71** can be directly compared with the formation of the reduction product **1.75**. A series of experiments was conducted in which the aldehyde **1.70** was treated with a mixture of TTMSS and BuSH. By varying the BuSH concentrations at various temperatures and in the presence of 50 mM TTMSS and a radical initiator, it was possible to set up a radical clock reaction (Scheme 1.19).^[88,93]



Scheme 1.19 Radical clock reaction. Rate constant of H-abstraction from BuSH = k_{H} . Rate constant of cyclisation reaction k_C .

To determine the kinetics under pseudo-first-order conditions, a series of experiments were conducted, in which aldehyde **1.70** was treated with a large excess of TTMSS and BuSH in known concentrations. The quantities of the reduction product **1.75** and the cyclo-dhT **1.71** were determined by $^1\text{H-NMR}$ and LC/MS, following the thermally initiated radical reaction. Figure 1.10 shows the linear regression analysis at different temperatures of the ratio $[\mathbf{1.75}]/[\mathbf{1.71}]$ vs $[\text{RSH}]$ by keeping the TTMSS concentration $[\text{TMS}_3\text{SiH}]$ constant. Since the thiol concentration remained essentially constant during the reaction under our experimental conditions (*pseudo*-first-order conditions),^[94] equation **1.2** can be applied.^[89] The slopes of the

lines, listed in Table 1.2, give the ratio k_H/k_C for each considered temperature. Kinetic data can be also obtained from the intercepts of the lines in Figure 1.10, based on equation 1.2, although large errors are associated with these values.^[93]

$$\frac{[1.75]}{[1.71]} = \frac{k_{SiH}}{k_C} [R''_3SiH] + \frac{k_H}{k_C} [BuSH] \quad (\text{eq. 1.2})$$

A concentration of BuSH in the range 0.6-40 mM was chosen so that the ratio $[1.75]/[1.71]$ ranged between 1:1 and 5:1. Specifically, the 6-*exo-trig* cyclisation is favoured at high temperature, suggesting a high activation energy for this process. Furthermore, the diastereomeric ratio between the final cyclo-dhT isomeric products $1.71a/1.71b = 30:70$ does not depend on the temperature of the experiment, highlighting the stereoselectivity of this 6-*exo-trig* cyclo-addition.

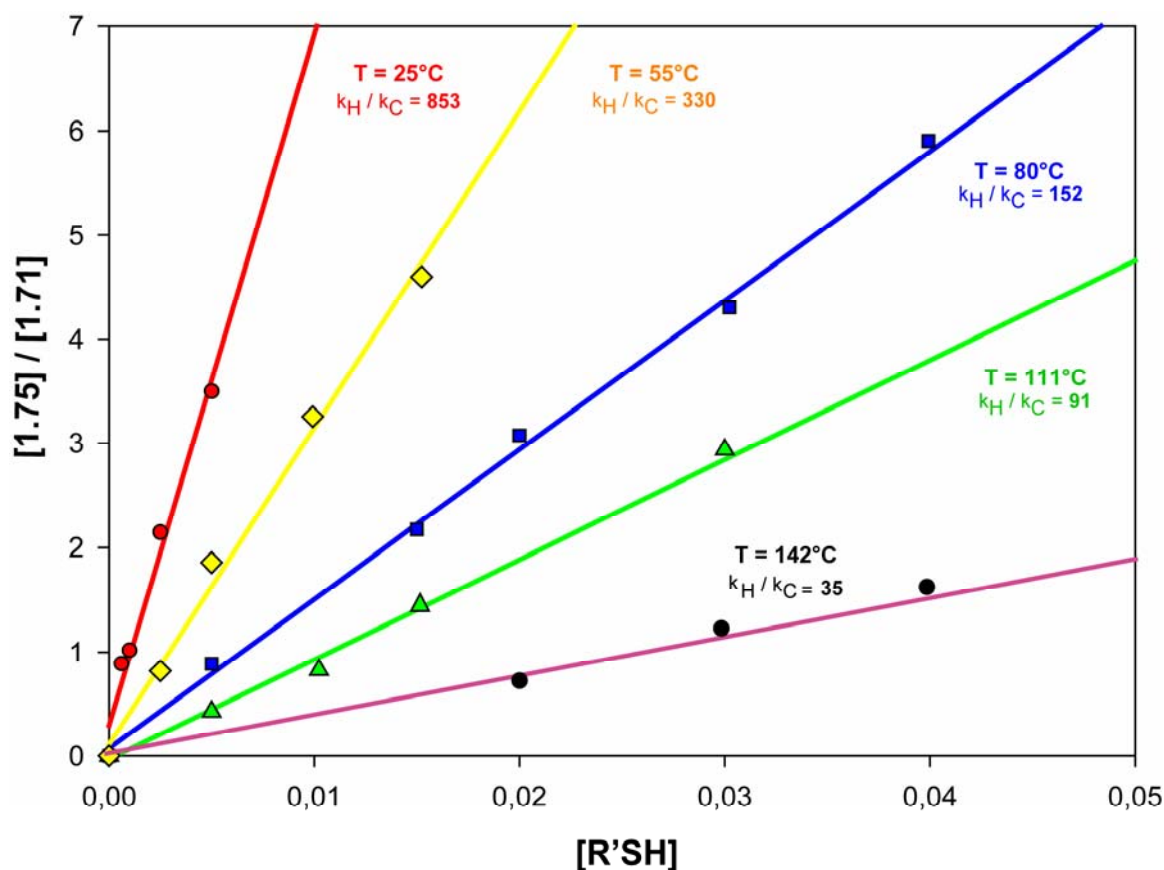


Figure 1.10 The k_H/k_C values reported in Table 1.2 were obtained as the average of at least three different experiments. The errors, reported in Table 1.2, correspond to a standard deviation.

The initial step for the experiments conducted at 25 °C involve the presence of oxygen (in traces). The radical initiator triethylboron (Et₃B) used at this temperature, reacts efficiently with molecular oxygen to yield peroxide. The subsequent reduction, utilizing unoxidized boron-carbon bonds, gives rise to ethyl radical (Et•), which initiates the radical chain.^[95]

In all the other experiments, the initiation step involves the homolytic thermolysis of (i) C-N bonds in case of di-*tert*-butyl hyponitrite (*t*-BuONNO*t*-Bu, TBHN) and AIBN, (ii) O-O bonds in case of *tert*-butyl peroxybenzoate (PhC(O)OO*t*-Bu, TBPB) and di-*tert*-butyl peroxide (*t*-BuOO*t*-Bu, DTBP).

The dependence of the rate constants on the temperature of the reaction can be estimated considering the k_H/k_C ratio. The values for temperatures and initiators used can be found in Table 1.2.

Table 1.2 Kinetic data for the reaction of aldehyde **1.70** with TTMSS/BuSH in benzene^[a]

T [°C]	Initiator	k_H/k_C , [M ⁻¹] ^[b]
25	Et ₃ B	853 ± 160 (4)
55	<i>t</i> -BuONNO <i>t</i> -Bu	330 ± 29 (4)
80	AIBN	152 ± 14 (5)
111	PhC(O)OO <i>t</i> -Bu ^[c]	91 ± 5 (4)
142	<i>t</i> -BuOO <i>t</i> -Bu ^[d]	35 ± 4 (3)

[a] Conditions: Aldehyde **1.70** 0.01 M, TTMSS 50 mM, BuSH concentration in the range 0.6-40 mM and initiator 2 mM (0.2 equ.). [b] Errors correspond to a standard deviation; reactions were repeated 3-5 times (in parenthesis) for each temperature. [c] In toluene. [d] In *o*-xylene.

Calculation of Arrhenius parameters

In order to calculate the kinetic parameters for the cyclisation reaction, the Arrhenius equation **1.3** is applied in its decimal logarithm form (eq. **1.4**).

$$k = A e^{-E_a / RT} \quad (\text{eq. 1.3})$$

$$\log(k) = \log(A) - \frac{E_a}{2.3 RT} \quad (\text{eq. 1.4})$$

The ratio k_H/k_C can be written in terms of $\log(k)$ as in the equation **1.5**.

$$\log \frac{k_H}{k_C} = \log \frac{A_H}{A_C} - \frac{(E_a^H - E_a^C)}{2.3 RT} \quad (\text{eq. 1.5})$$

The plot of the $\log k_H/k_C$ vs the temperature T gives rise to equation **1.6** after linear regression of the data (Figure 1.11). The intercept of this line is the $\log A_H/A_C$ and the slope is the $(E_a^H - E_a^C) / 2.3 R$ value, with $2.3 R = 4.576 \text{ kcal/mol}$.

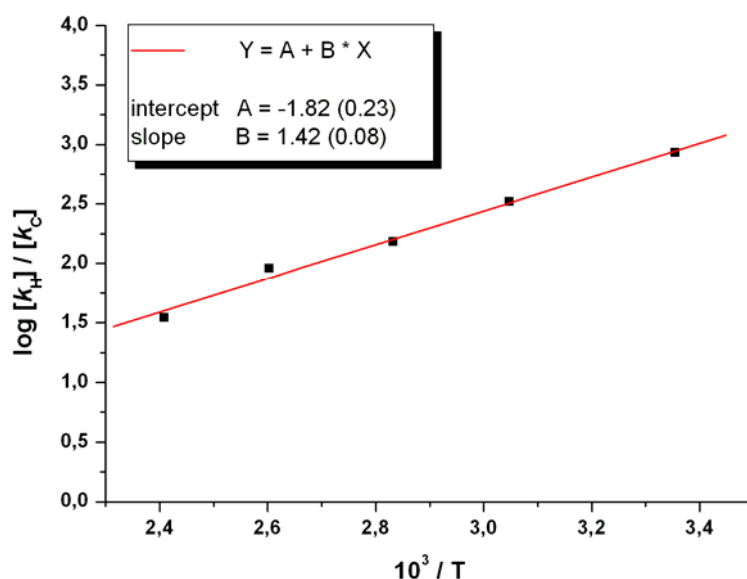


Figure 1.11 Linear regression analysis of a $\log(k_H/k_C)$ vs $1/T$ plot yields the relative *Arrhenius* parameters given in equation **1.6** in kcal/mol.

$$\log \frac{k_H}{k_C} = - (1.82 \pm 0.23) + \frac{(6.50 \pm 0.08)}{2.3 RT} \quad (\text{eq. 1.6})$$

The rate constant k_H for the reaction of the α -silyloxy secondary carbon-centered radical **1.73** with BuSH and its temperature dependence are unknown, although they are required in order to obtain the *Arrhenius* expression for k_C from equation **1.6**. However, *Newcomb* and coworkers have determined rate constants very close to $2.0 \times 10^7 \text{ M}^{-1} \text{ s}^{-1}$ for the reactions between octadecanethiol and primary alkyl- or α -methoxy secondary alkyl radicals in THF at $30 \text{ }^\circ\text{C}$.^[96] This rate can be used also for the similarly structured C5' radical of this work.

The *Arrhenius* parameters for the reaction of primary alkyl radicals with ^tBuSH are:^[97]

- $\log(A) = 8.15$ (A in $M^{-1} s^{-1}$)
- $E_a = 1.86$ kcal/mol.

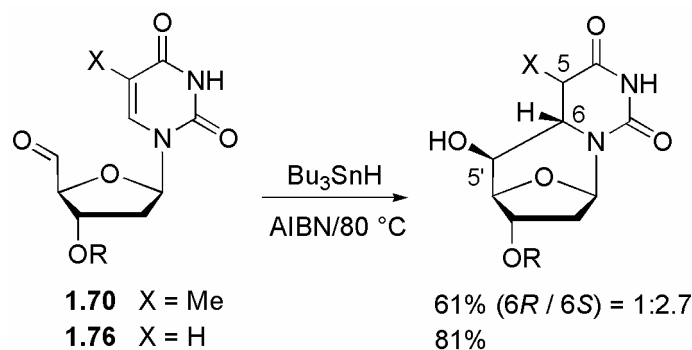
The combination of these data with equation **1.6** consequently yields:

- $\log(A) = 10.0$ (A in $M^{-1} s^{-1}$)
- $E_a = 8.4$ kcal/mol

for the cyclisation reaction in Schemes 1.18 and 1.19. The value of k_C can be calculated for the first time as $7 \times 10^3 s^{-1}$ at 25 °C.^[98]

Comparison with previous studies

It is interesting to compare the present results with the findings of *Cadet* and coworkers on similar reactions using Bu_3SnH as the reducing agent.^[79,83] They reported that both aldehydes **1.70** and **1.76** afford analogous cyclonucleosides exclusively having (*S*)-configuration at C5' position in the sugar but that only aldehyde **1.70** affords two diastereoisomers ($5R/5S = 1:2.7$, Scheme 1.19). The different chemical behavior exhibited by TTMSS and Bu_3SnH prompted us to re-investigate the reaction of aldehyde **1.70** with Bu_3SnH under the conditions reported by *Cadet* and co-workers.^[79] The ¹H-NMR analyses on the reaction mixture revealed the presence of three cyclonucleosides in a 15:65:20 ratio. Two of these are identical with *Cadet's* work. That is, the diastereoisomers having (*S*)-configuration at the C5' position and differing in the configuration at C5 ($5R/5S = 1:4.3$). The third one is the diastereoisomer **1.72b** (Scheme 1.16), having (*R*)-configuration at C5' position. Therefore, the cyclisation of the Bu_3Sn -adduct radical occurred with a diastereomeric ratio ($5'S)/(5'R) = 80:20$, whereas the cyclisation of the corresponding silyl substituted radical **1.73** occurred with a ratio ($5'S)/(5'R) = 30:70$. The inverted diastereoselectivity observed for the two reducing agents is probably due to the different steric demand of the $(TMS)_3Si$ and Bu_3Sn groups.^[86,87]



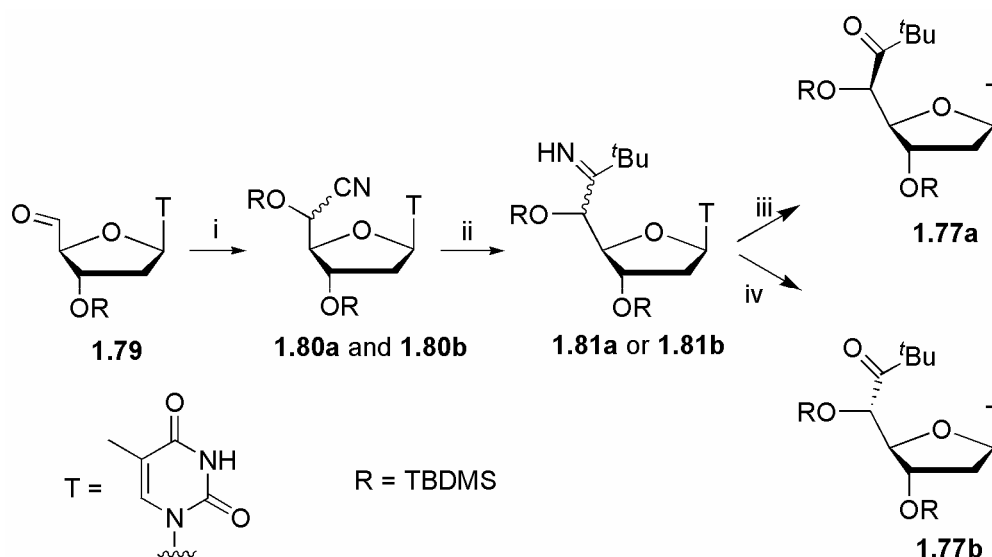
Scheme 1.20 Product studies following the procedure described by *Cadet* and co-workers.^[79,83]

Conclusion

In this section a short and efficient synthetic sequence for the preparation of cyclonucleosides **1.72a-b** has been disclosed, based on consecutive radical reactions followed by a photochemical desilylation. The C5' radicals, generated by the addition of a (TMS)₃Si radical to the corresponding 5'-carboxaldehyde, are the key intermediates in these transformations. The rate constant k_C of the subsequent cyclisation reaction was estimated for the first time in such systems through a radical clock reaction setup. The value of $k_C = 7 \times 10^3 \text{ s}^{-1}$ at 25 °C found here is strictly correlated with the C5'-radical repair reaction. The 6-*exo-trig* cyclisation is effective with both pyrimidine and purine derivatives with the generation of 5',6-cyclo-5,6-dihydro-2'-deoxythymidine **1.68** and 5',8-cyclo-2'-deoxyadenosine **1.69** respectively (Figure 1.9, pag. 34). In the case of the cyclisation on the 2'-deoxyadenosine system a rate constant $k_C = 3.5 \times 10^5 \text{ s}^{-1}$ at 86 °C was calculated in the research group of *Chatgialoglu*,^[78] following the procedure described above for the thymidine system. For comparison, an absolute rate constant $k_C = 1.6 \times 10^5 \text{ s}^{-1}$ at 22 °C is obtained by pulse radiolysis for the corresponding unprotected radical C5' in water.^[25,26] Moreover, a $k_C = 7.7 \times 10^4 \text{ s}^{-1}$ at 86 °C is calculated for the cyclization of the thymidine C5' radical **1.73**, which is nearly five times slower than the cyclization of the C5' radical of dA. These findings furnish a molecular basis for forthcoming experiments at DNA level.

The crude product consisted of a 3:2 mixture of two isomers, **1.80a** and **1.80b** (Scheme 1.20). The diastereomers were separated by chromatography. The assignment of absolute configurations by 2D-NMR spectroscopy failed due to rotation of C4'-C5' bond.

During the α -cyanohydrin formation, under not perfectly anhydrous conditions or in the presence of an excess of LiOEt, the 5' hydroxy position remained unprotected. In this case, an additional step for the *in-situ* 5'-TBDMS protection was achieved by a standard procedure (TBDMS-Cl, AgNO₃, imidazole).



Scheme 1.21. Synthesis of the ketones **1.77a** and **1.77b**: (i) TBDMS-CN, LiOEt, THF, 0 °C, 30 min, 82%. (ii) *t*BuLi, THF, -78 °C, 2-5 min., 43% (**1.81a**), 38% (**1.81b**). (iii) for **1.77a**: THF/H₂O/2N HCl (40:20:1), 3h, 88%. (iv) for **1.77b**: CDCl₃, 30 min., 70%. R = *tert*-butyldimethylsilyl (TBDMS), T = Thymine.

Hydrolysis of imines.

A mixture of **1.80a** and **1.80b** was treated with *tert*-butyl lithium (*t*BuLi) at -78 °C. The reaction yields the *tert*-butylketone **1.77a** as a single product in 45 % yield. The high resolution mass of **1.77a** is reported in Figure 1.13 and its configuration (5'*R*) was later assigned by crystal structure determination of the corresponding 3'-acetate (*vide infra*). The product yield, together with the absence of the (5'*S*)-isomer **1.77b**, indicated that the addition reaction products exhibit different stability when originating from either diastereomer **1.80a** or **1.80b**. Indeed, each isomer, after chromatographic separation, was used for the *t*BuLi addition under identical conditions. The reaction was monitored by TLC and ¹H-NMR

analysis. This led to the identification of two intermediate imine products **1.81a** and **1.81b** (Scheme 1.21). The acid-free NMR solvent acetone-*d*₆ was used for the characterisation in order to avoid hydrolysis of the imines. The imine **1.81b** readily decomposes even in the presence of slightly acidic solvents such as CDCl₃, when used for the NMR analysis. The corresponding ketone (**1.77b**) could not be isolated as it slowly decomposes in acidic media to unidentified fragments. Nevertheless ketone **1.77b** was fully characterized in a mixture with ketone **1.77a**. On the other hand, acidic hydrolysis conditions applied to the imine **1.81a** led to a slow but quantitative conversion to the stable ketone **1.77a** (Scheme 1.22).



Scheme 1.22. Reactivity of nitriles **1.80a-b**. i) Pathway and products of the major isomer **1.80a** and ii) of the isomer **1.80b**. The compounds present only in traces are depicted in red.

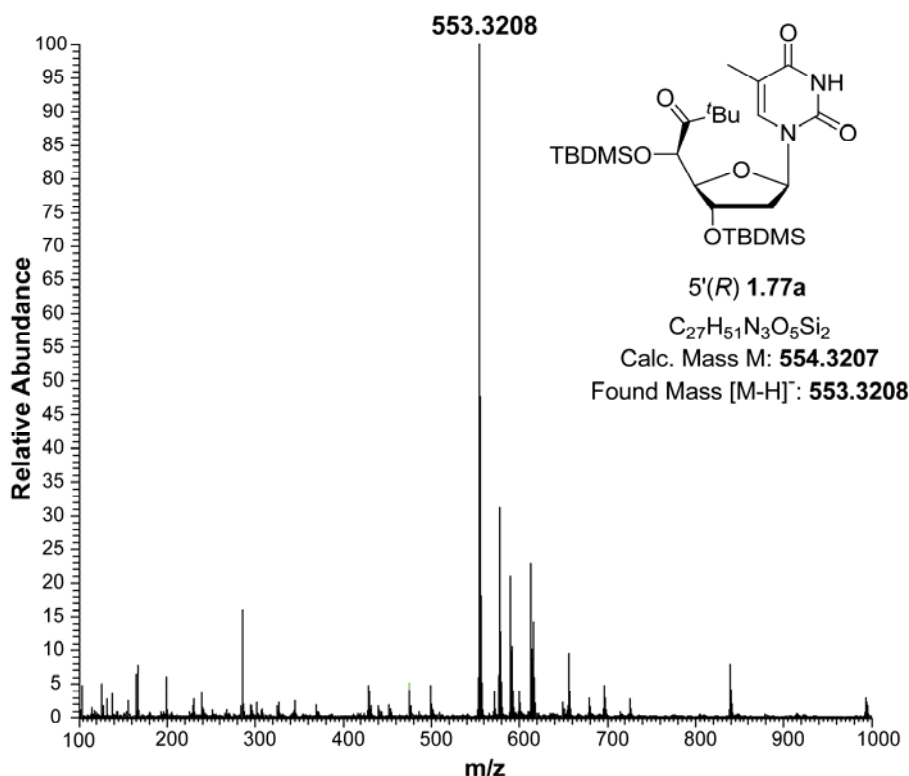
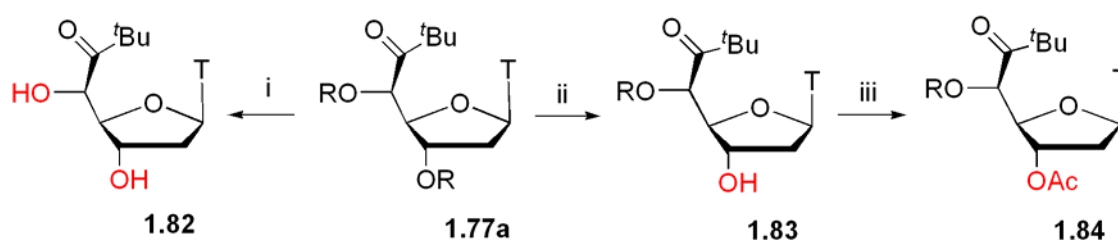


Figure 1.13 High-resolution mass (FTMS-ESI) of ketone **1.77a**.

Stereochemistry

The full deprotection of bis-silylether **1.77a** led to the ketone **1.82** as described in Scheme 1.23. Ketone **1.83** could be obtained from ketone **1.77a** through a selective deprotection. This compound was then protected to the 3'-acetate **1.84** and single crystals, suitable for X-ray crystallography, were obtained from a saturated solution in ethyl acetate. The resolution of the structure, as reported in Figure 1.14, allowed the assignment of the (5'*R*) configuration for the ketone **1.84**. Since the 5'-stereocenter was not involved in the protecting group conversions, we could extrapolate the assignment of the same configuration to the imine **1.81a** and its cyanohydrin precursor **1.80a** (which change to the (*S*) notation according to the CIP rules).



Scheme 1.23. Deprotection-protection strategy for the synthesis of **1.84**: (i) TBAF, MeOH, reflux, 5h, 60%. (ii) TBAF, THF, -15° C, 24h, 55%. (iii) Ac₂O, py, r.t., 24 h, 82%. R = TBDMS, T = thymine.

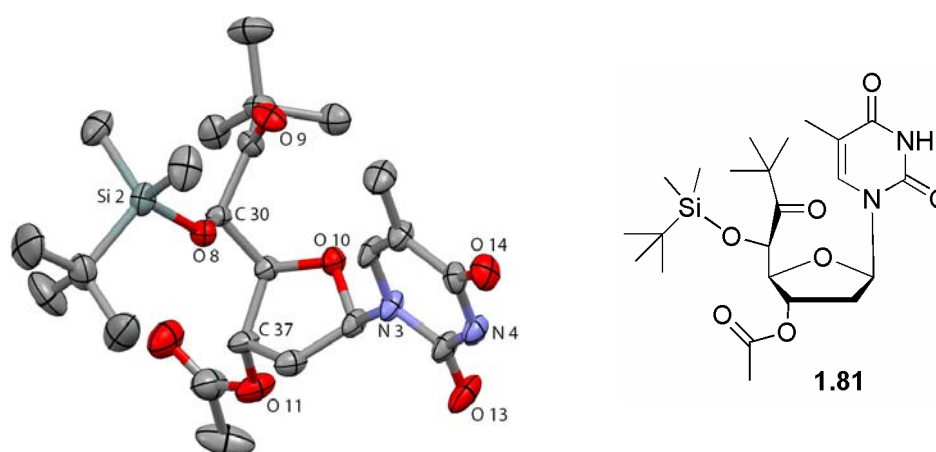


Figure 1.14. Crystal structure of **1.84** (left side) and chemical structure (right side), hydrogen atoms are omitted for clarity; selected distances [Å] and angles [°] (standard deviation in parenthesis): Si2 O8 1.659(4), O8 C30 1.419(6), O9 C31 1.206(6), N3 C39 1.466(7), C30 C36 1.500(7), C30 C31 1.552(7); C30 O8 Si2 126.5(3), O8 C30 C36 108.3(4), O8 C30 C31 109.3(4), C36 C30 C31 110.8(4), O9 C31 C30 119.1(5).

All the isomers involved in this study are depicted in Figure 1.15 with their configuration at C5', originating from that of compound **1.81**.

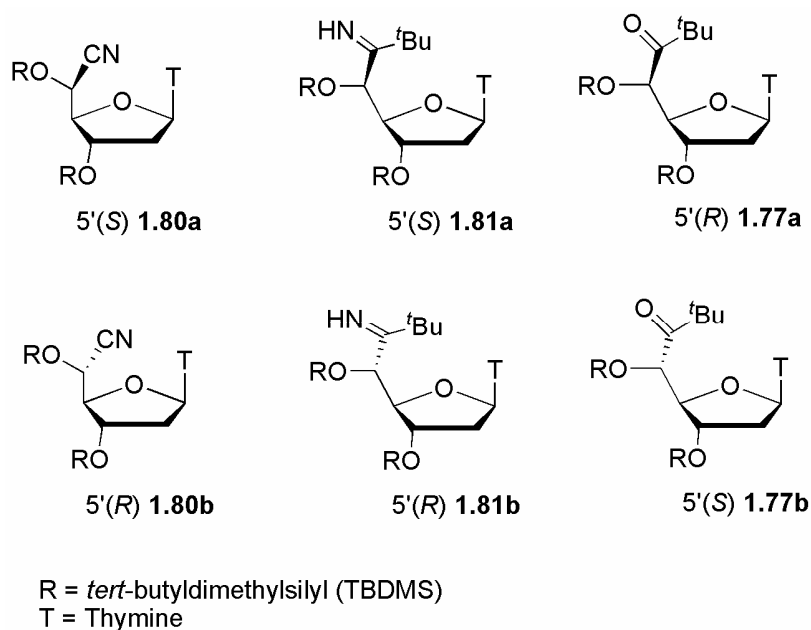
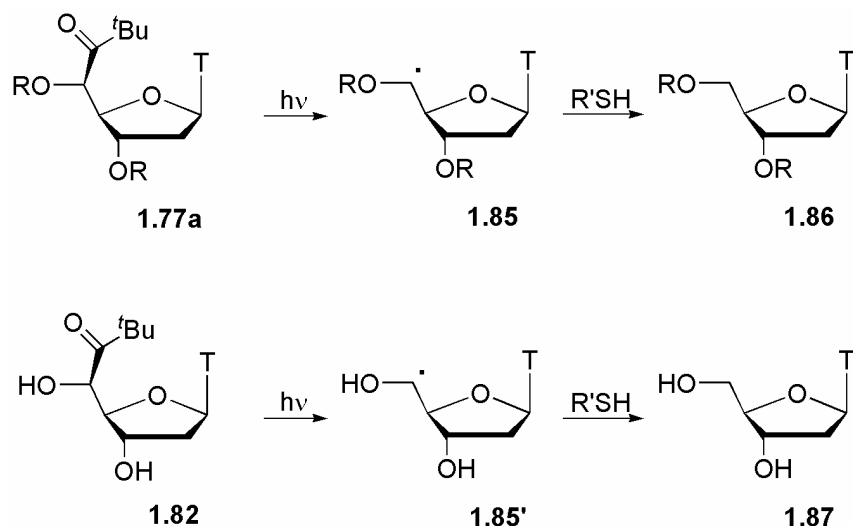


Figure 1.15. Configuration of the isomers of the cyanohydrines **1.80a** and **1.80b**, of the imines **1.81a** and **1.81b** and of the ketones **1.77a** and **1.77b**.

Photochemistry

Compounds **1.77a** and **1.82** were used as precursors of the C5' radical. The UV irradiation (1000 W, Xe-lamp) of the protected ketone **1.77a** was carried out in the presence of a hydrogen donor such as 1-butanethiol in MeCN. The photolysis of the unprotected ketone **1.82** was instead achieved in water using 2.5 mM glutathione (GSH) as H-donor. In each assays oxygen-free conditions were used. Both photolysis led quantitatively to the formation of thymidine **1.86** and **1.87**, respectively (Scheme 1.24). Figure 1.16 shows the analysis by reversed phase HPLC of aliquots taken during the photolysis of **1.77a** (0.12 mM in MeCN) in the presence of 1-butanethiol (2.5 mM) for 30 min. Under these conditions the half-life of **1.77a** was calculated to be $t_{1/2} = 6.6$ min. without any cyclisation product being observed. The resulting C5' radical **1.85** could be obtained either by *Norrish* Type I photocleavage or by initial formation of an acyl radical that decarbonylates with a rate constant in the range of 10^5 – 10^6 s⁻¹.^[104] The thiol (2.5 mM, physiological concentration of GSH) is able to trap the C5' radical, thus preventing it from subsequent reactions, such as the intramolecular attack onto the C6–C5 double bond of thymine.^[78]



Scheme 1.24. Generation of C5' radical from photolysis of **1.77a** and **1.82**. R'SH = BuSH for **1.77a** and GSH for **1.82**. T = thymine.

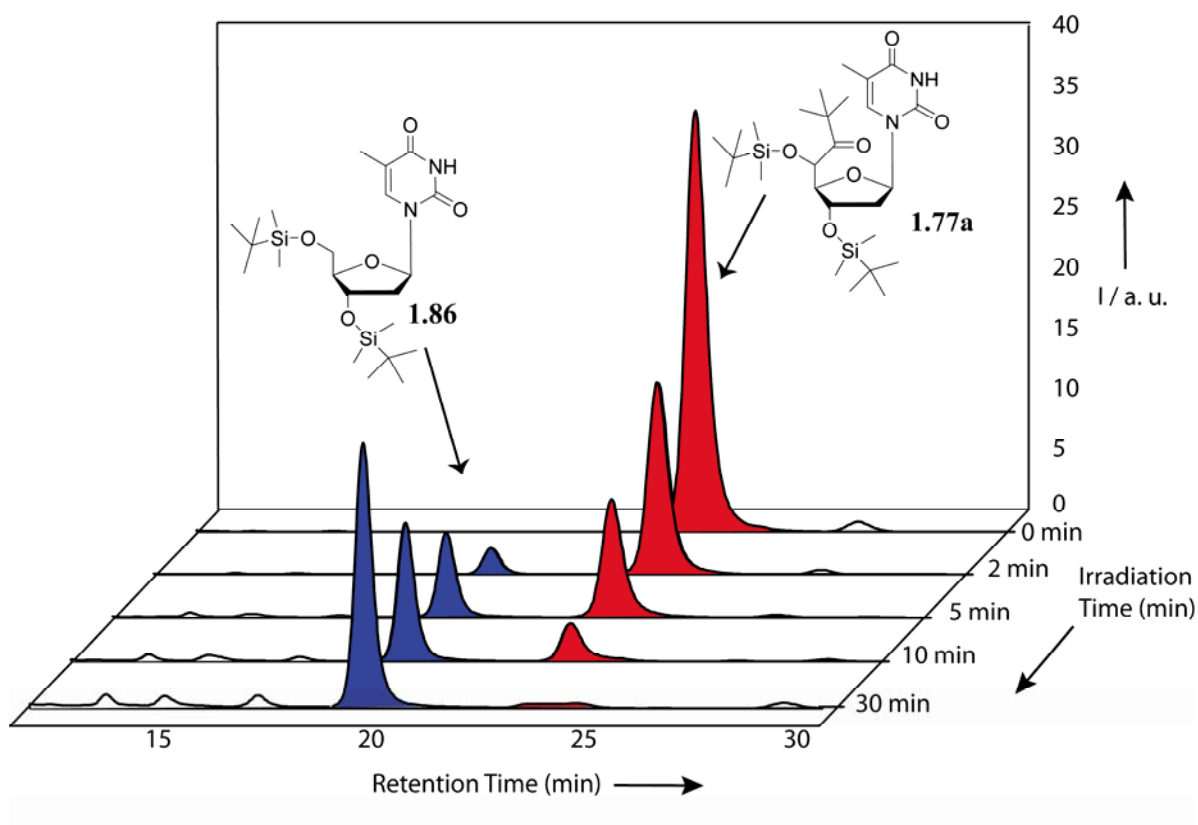


Figure 1.16. Time-dependent HPLC chromatogram showing the disappearance of **1.77a** (red peaks) and the formation of **1.86** (blue peaks) during photolysis (normalized peaks).

Conclusion

A new synthetic route for the preparation of (5'*R*)-*tert*-butyl ketones **1.77** and **1.78** was disclosed. These results demonstrate that their photolysis selectively affords the corresponding C5' radical. The nature of the base plays an important role in the fate of the C5' radical. In the presence of a physiological concentration of alkanethiol, the thymidin-5'-yl radical is efficiently reduced, whereas the 2'-deoxyguanosin-5'-yl radical adds intramolecularly to the C8–N7 double bond of the guanine moiety with a rate constant of ca. $1 \times 10^6 \text{ s}^{-1}$ (data not shown),^[55] nearly an order of magnitude faster than the analogous 2'-deoxyadenosin-5'-yl radical.^[25]

These findings furnish a molecular basis for forthcoming experiments involving the incorporation of these photolabile precursors in oligonucleotides and their application in mechanistic studies of DNA damage. The concentration of oxygen and thiol determine the reaction pathways of the C5' radical, which are (i) 6-*exo-trig* cyclisation, (ii) repair reaction by hydrogen abstraction from glutathione, (iii) trapping by oxygen to give the corresponding peroxy radical. These reaction pathways can eventually be evaluated in relation to restricted conformations of dsDNA. The photo-stability of the imine **1.81a** and its capability to hydrolyze in acidic media to the photo-labile ketone **1.77a** pave the way for applying this transformation in biotechnological applications.^[32,105,106] The imine could be used as an anti cancer drug which is activated only in acidic media (i.e. tumor cells). A subsequent UV-treatment would affect only the ketone generated *in situ* from the hydrolysis of the imine. Thus, the active form of the drug would be present only into the cancer cells. The radical species formed after homolysis of the ketone would then damage and eventually destroy selectively the DNA of the tumor cells.

1.3 Conclusions

Nucleoside-model studies for the comprehension of the generation and fate of C5' radicals and associated radicals have been achieved and are described in Chapter 1.

It was possible to synthesise selective thermolabile and photolabile precursors for the *pseudo*-C4' radical (section 1.2.1) and for the C5' radical (section 1.2.3). An alternative way to generate C5' radicals has been explored using a silyl-radical addition to an aldehyde allowing the access to bio-relevant DNA lesions (section 1.2.2). The cyclisation rate constant was also determined using a radical clock reaction.

The synthetic steps required in this work have been achieved in good yields. In addition new synthetic strategies have been applied here, such as the efficient photolytic deprotection of TTMSS and the C-C bond formation in the cyclisation reaction. The mechanistic aspect of the radical reaction, strictly connected with DNA damage mechanisms, has been disclosed for the models used in this work. Kinetic parameters were also taken in account. Specifically, a rate constant for the cyclisation reaction to cyclo-dhT in organic solvents was estimated for the first time.

The data collected with these models represent the starting point for the investigation of C5' radicals in single and dsDNA. The incorporation of nucleoside models by automated or enzymatic DNA synthesis is aimed to such an enquiry and will be facilitated by these studies on the nucleoside level.

2 Electron Transfer Through DNA

2.1 Introduction

The possibility that the π -stacked base pairs of DNA, with an average stacking distance of 3.4 Å might function as a one-dimensional conductor or molecular wire was first advanced by *Eley* and *Spivey*^[107] shortly after *Watson* and *Crick* deduced the double-helical structure of DNA.^[1] Interest in the wire-like behaviour of DNA was kindled in the early 1990s by a series of reports by *Barton* suggesting that ultrafast, photoinitiated charge transfer (CT) between intercalated electron donors and acceptors could occur over long distances in DNA.^[108,109] These reports stimulated experimental studies of the photoinitiated CT processes in DNA as well as the theoretical interpretation of the obtained data. DNA CT has since been the subject of great interest.^[110-113] The process is in fact involved, among others, in the complex pathway that gives rise to oxidative DNA damage formation. CT is also implicated in the reductive repair of certain DNA lesions where it plays a key role in the enzymatic maintenance of the genome.

Oxidative electron transfer

Scientific attention was first focused at the positive charge migration or hole transfer (HT) in DNA. The research interest was sparked by the biological implications of HT.^[114] Single electron oxidation of DNA yields a guanine radical cation ($G^{\bullet+}$) in close vicinity to the initial oxidation site. The radical cation mainly localises at guanine (G) because this nucleobase has the lowest oxidation potential.^[115,116] γ -Radiolysis studies^[117,118] and investigations of defined electron acceptor DNA systems have revealed, over the past decade, that $G^{\bullet+}$ participates in long range (~ 200 Å) charge transfer processes.^[119-122] It was found that an adjacent G in the DNA duplex is able to donate an electron to the initial $G^{\bullet+}$ site. The sequential electron transfer between G-bases allows rapid transfer of the positive charge in DNA. The charge virtually hops through DNA by using G-bases as stepping stones (Fig.2.1).^[111,123]

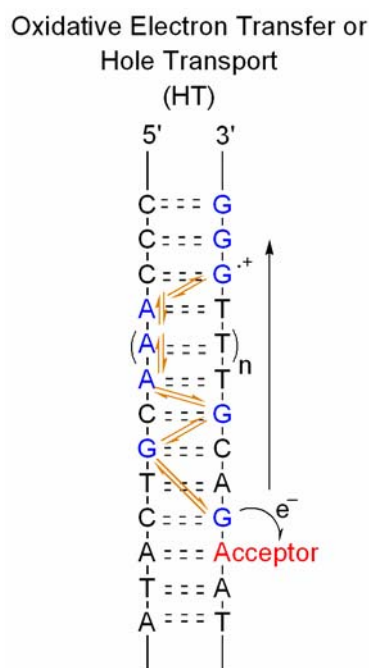


Figure 2.1 Oxidative electron transfer or hole transport in DNA. The acceptor is the site of oxidation of the DNA. The charge hops through G or A bases in a sequence-dependent fashion. The final electron donor is a GG or GGG site, where the radical cation is trapped by water or oxygen.

However the involvement of adenine (A) in the HT was found to be also significant. In the absence of G in the sequence, the adenines (so-called A-tracts)^[124] bridge the gap between the electron donor and the acceptor. In the case of HT the final electron donor is mainly a GG or GGG site which provides the electron for the G⁺. These G-rich tracts have in fact an even lower oxidation potential than isolated G. Thus formally the positive charge moves from G⁺ to GG sequence. Here the charge is eventually trapped by water or oxygen. The trapping reactions at such sites are favoured over the trapping in the isolated G, thus increasing the probability to form a lesion.^[123]

At short distances, typically <10 Å (1-3 bps), the relative efficiency of HT was observed to decrease exponentially, whereas at longer distances (4-16 bps) the process depends only weakly on the distance. This fact was attributed to a change of the mechanism from tunnelling (or superexchange) at short distances to multistep hole hopping at longer distances (Figure 2.2).^[123] Every single step of the latter mechanism can be referred to a single superexchange transfer.

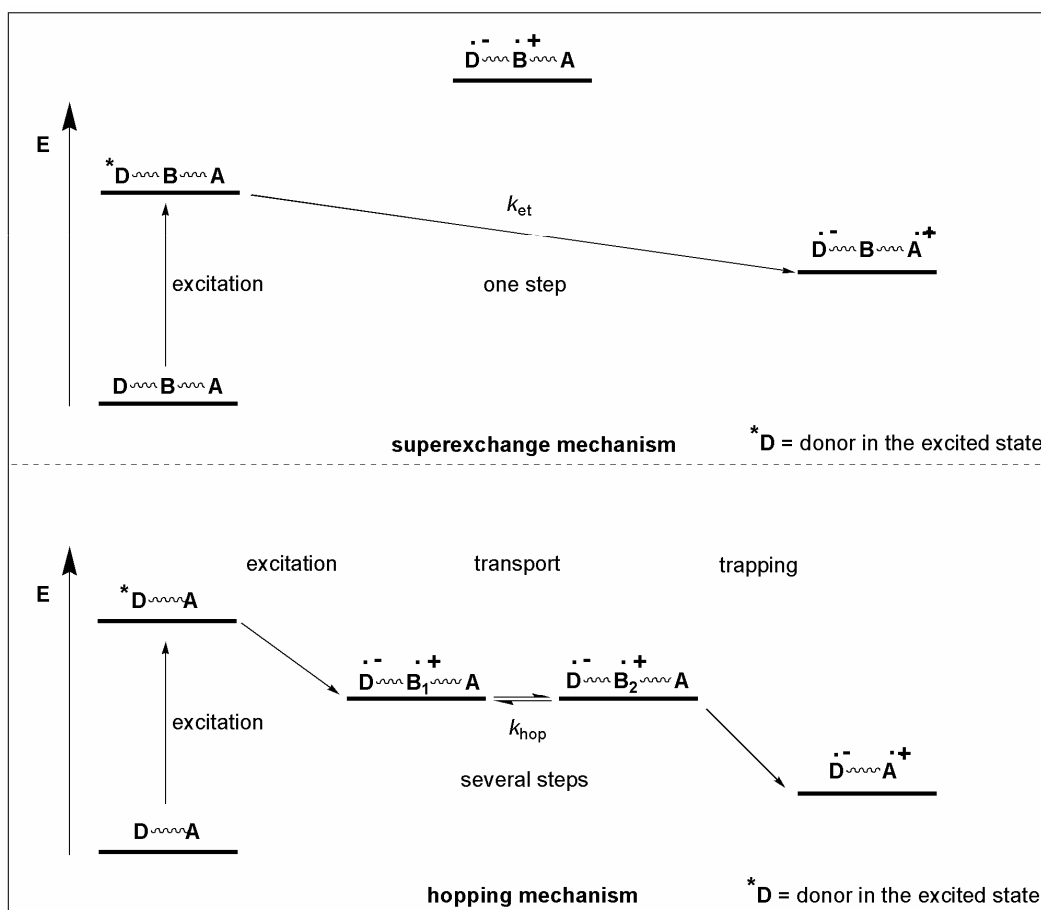


Figure 2.2 Superexchange (top) and hopping mechanism (bottom) of DNA mediated hole transfer and transport, respectively. D = donor, A = acceptor, B = base.^[34]

These two different mechanisms are represented by the corresponding equations, the *Marcus-Levich-Jortner* equation (eq. 2.1) for the superexchange mechanism^[125-132] and eq. 2.2 for the hopping mechanism.^[112,133]

$$k_{\text{et}} = k_0 e^{-\beta \Delta r} \quad (\text{eq. 2.1})$$

$$k_{\text{hop}} \approx \tau^{-1} N^\eta \quad (\text{eq. 2.2})$$

In eq. 2.1, the electron transfer rate k_{et} , depends exponentially on the distance r between the donor and the acceptor. The β -value in eq. 2.1 represents the crucial parameter to describe the distance dependence of CT in DNA. It depends on the nature of the bases between the donor and the acceptor. Values of β determined for HT in DNA can be found in a wide range from $\beta < 0.1 \text{ \AA}^{-1}$ to $\beta = 1.5 \text{ \AA}^{-1}$.^[134-137] On average, short-range HT rates are reported to be $k_{\text{et}} = 10^9\text{-}10^{12} \text{ s}^{-1}$, with β -values of $0.6\text{-}0.8 \text{ \AA}^{-1}$.

At very small β -values ($\leq 0.1 \text{ \AA}^{-1}$) the electron transfer process shows a shallow distance dependence and it can be described by eq. 2.2, in which N is the number of hopping steps and η ($1 < \eta < 2$) represents the influence of the medium. The rate for a single hopping step from G to GG was determined to be $k_{\text{hop}} = 10^6 - 10^8 \text{ s}^{-1}$,^[138] with the lower limit of $k_{\text{hop}} = 10^6 \text{ s}^{-1}$ measured over 50 \AA through the base stack.^[139] On the other hand, the rate of A-hopping has been determined to be $k_{\text{hop}} = 10^{10} \text{ s}^{-1}$. Consequently, once the G^{*+} oxidizes A (endothermic reaction)^[111] the charge is transferred rapidly along the adjacent adenines until it is trapped by a GGG unit. The A-hopping proceeds more efficiently than G-hopping since the charge is more slowly trapped by water or oxygen. The transfer through A-tracts is therefore almost distance independent.^[140-143] The differences between transfer through G and A bases have been explained by taking the proton transfer in the oxidized bases into account. Specifically, the G^{*+} can be protonated by one of the protons of the cytosine forming the *Watson-Crick* hydrogen bonds in the G:C bp. In theory the proton transfer process can occur on a time scale comparable to the charge transfer reaction. Thus, the intra-base pair proton transfer can influence the CT efficiency due to the separation of the radical and the positive charge.^[144] The pK_a value of G^{*+} (~ 3.9) is very similar compared to dC (4.5),^[145] thus the reversible protonation of G^{*+} interferes with the CT. On the other hand, protonation of adenosine radical cation (A^{*+}) by thymidine (T) is not favoured ($A^{*+} pK_a = 1$, T $pK_a = -5$)^[145] allowing the A^{*+} to transfer the charge to the next A or G with higher efficiency. These complex interrelations make the HT a base-sequence dependent process.

Although this hopping process is now well established, particularly due to the fundamental contributions by *Barton*,^[119] *Giese*,^[120] *Lewis*,^[146] *Schuster*^[147] and *Wasielewski*,^[148] the mechanistic details of the long range hole hopping process are still under intensive investigation and certain observations are still controversially debated.^[149-152] All researchers in the field, however, agree that the G^{*+} reacts with water or oxygen to give oxidative DNA lesions, which are mutagenic *in vivo* and responsible for cell death.^[153] These oxidative lesions require efficient cellular DNA repair in order to avoid the harmful effects of oxidative DNA damage.^[154]

Reductive electron transfer

Although over the last years the knowledge about oxidative hole transfer and its biological consequences significantly improved,^[108,121,122,148,155] much less is known about the transfer of excess electrons - negative charges - through DNA (excess electron transfer, EET) as depicted in Figure 2.3.^[146,156] When an electron donor injects electrons into a duplex, negative charges move to an acceptor site in DNA.^[157] Evidences for this process were reported since the last decade and they are believed to be a possible basis for the development of DNA as a charge transport medium^[158,159] in nano-electronic devices.^[160,161]

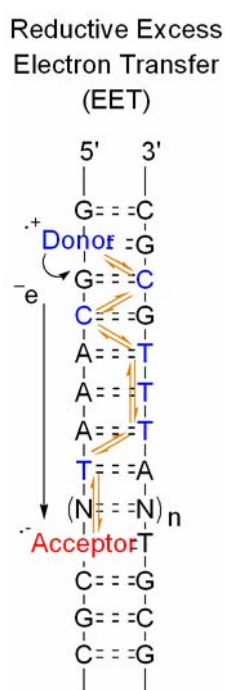


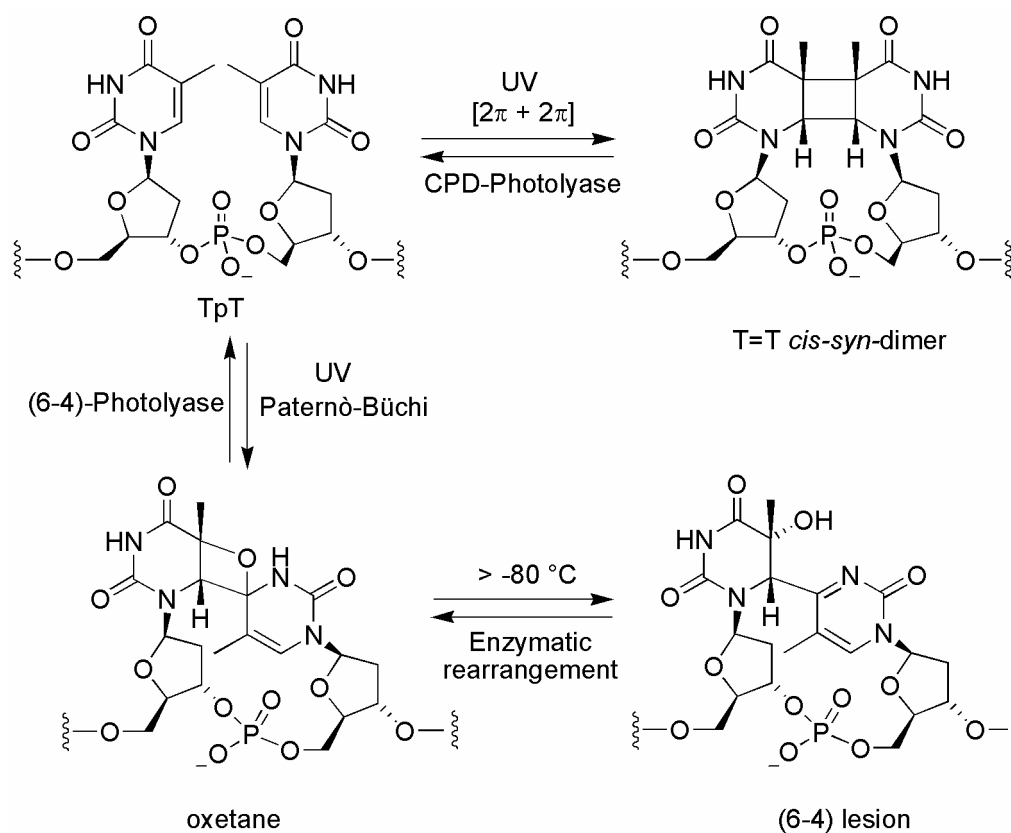
Figure 2.3 Reductive transfer of an excess electron through DNA.

Strong efforts are under way to create DNA-based nanoelectronic materials with self-organizing properties.^[162-165] The long-term goal is that such a novel material may self assemble into complex conductive nano-wire networks with computing or diagnostic potential.^[166,167] These latter functions also rely on the superb ability of DNA to assemble into predictable and complex structures.^[168,169] In this context, the question of how electrons travel through DNA is of fundamental importance.^[170] Moreover, a very similar event is used by certain DNA repair enzymes, which use a flavin adenine dinucleotide (FAD) cofactor to inject an electron into DNA, starting an electron transfer process.^[171-175] A deeper understanding of

flavin induced electron transfer events in DNA is consequently not only informative in respect to the question of how DNA mediates EET but may also allow to gain fundamental insights into some of the nature's most important DNA repair pathways. Investigations on how charges move through DNA and studies of how the electron transfer can be accelerated^[176] and controlled is, in consequence, an active field of research.^[177]

Flavin as electron donor in nature

Electron injection into DNA is probably achieved by nature since millions of years. Presumably since life exists exposed to sunlight, enzymes called DNA photolyase or (6-4) photolyase^[173,178,179] are used by many organisms to repair genotoxic UV induced lesions.^[180,181] UV irradiation of cells induces the formation of cyclobutane-pyrimidine dimers (CPD) by a photochemical $[2\pi+2\pi]$ cycloaddition of adjacent pyrimidines in the double strand (Scheme 2.1).^[182] The (6-4) photolesions are formed by a Paternò-Büchi reaction between two pyrimidine bases to give an oxetane which decomposes to the final lesion (Scheme 2.1).



Scheme 2.1 UV light induced formation and enzymatic repair of cyclobutane-pyrimidine dimer (CPD lesion) and (6-4) photolesions.^[175]

The lesions are enzymatically repaired (split reaction) by electron injection from a light excited, reduced and deprotonated flavin adenine dinucleotide coenzyme (FADH^*) inside the protein. A crystal structure of a photolyase bound to a CPD-like DNA lesion after *in situ* repair was recently reported (Figure 2.4).^[179]

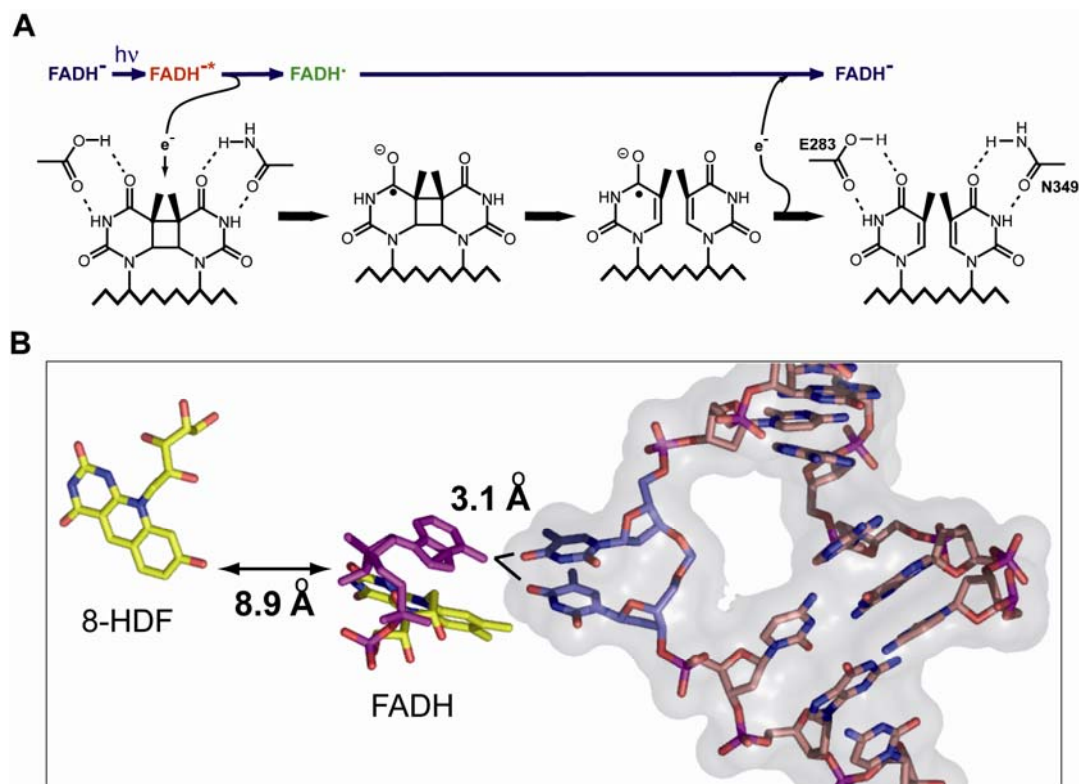
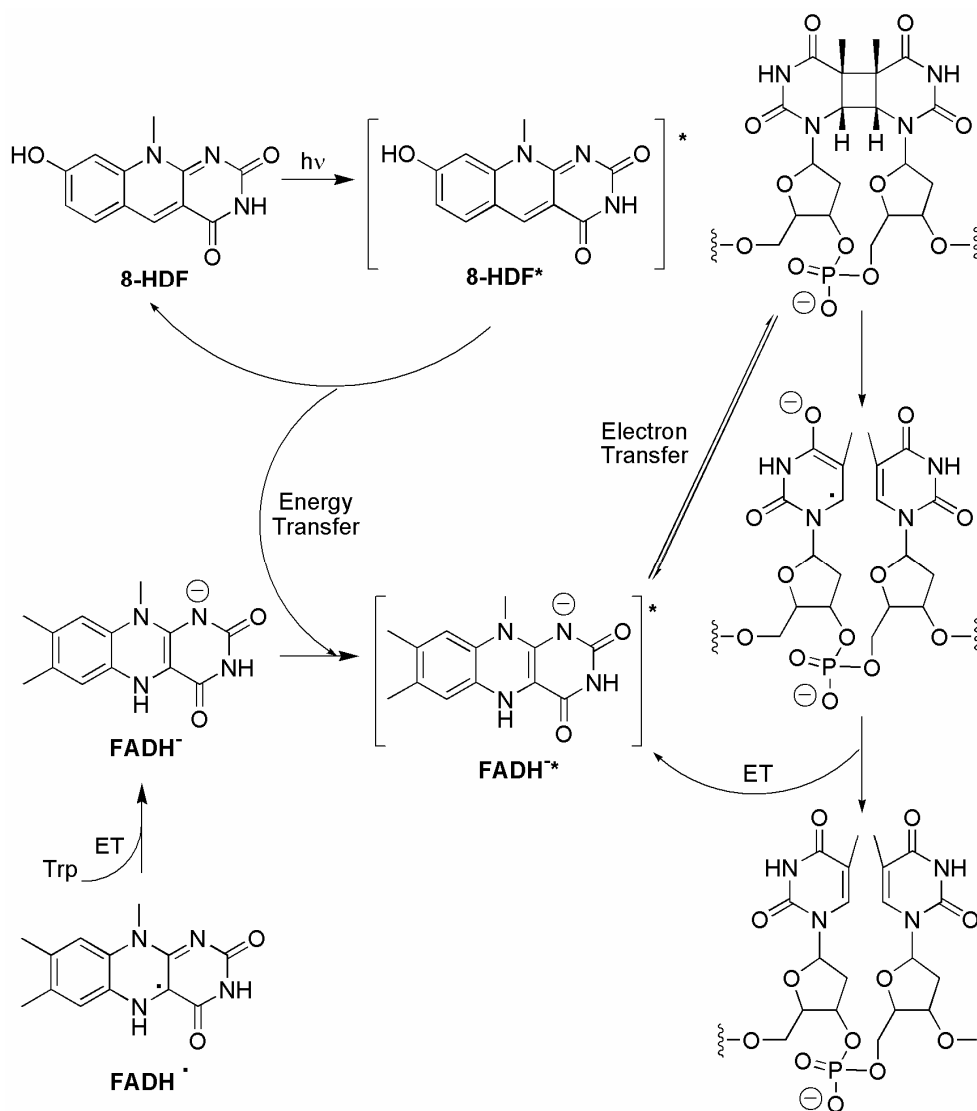


Figure 2.4 (A) Mechanism of blue light-mediated repair of CPD lesion by DNA photolyase (enzyme active site). (B) The active site of the co-crystal structure of a photolyase (*A. nidulans*) complexed with a DNA substrate at 1.8 Å resolution. The CPD lesion just after the cleavage is highlighted in blue, the cofactors in yellow and the adenine moiety of the FAD in purple.^[179]

The crystal structure (1.8 Å resolution) shows, among other features, how the thymine dimer (T=T dimer) is specifically recognised in the active site by being completely flipped out of the duplex DNA. After substrate binding, photon absorption by an antenna pigment (8-hydroxy-5-deazaflavin, 8-HDF) triggers the transfer of the excitation energy to the catalytic flavin adenine dinucleotide cofactor present in the reduced state (FADH⁻). The excited cofactor then transmits an electron to the T=T dimer to induce splitting of the cyclobutane ring. The resulting radical anion transfers the excess electron back to the FADH⁻ cofactor, closing the catalytic cycle. (Scheme 2.2).^[172]



Scheme 2.2 Mechanism of the repair of natural CPD lesions by DNA CPD-photolyase.^[175]

The postulated repair mechanism of CPD lesions is very similar to that of (6-4) lesions. The (6-4) photolyase repair enzymes are believed to rearrange the (6-4) lesion back to the oxetane which is also believed to be cleaved by single electron reduction. Again the electrons are supposed to come from a reduced, deprotonated and light excited flavin.

The electron transfer process from a light excited FADH^{-*} to a T=T dimer or a (6-4) lesion is a thermodynamically favorable process and was extensively investigated with model compounds.^[183-190] The reduction potential of the reduced and deprotonated FADH^{-*} in its photoexcited state is believed to be around $E_{\text{red}}^* = -2.6$ V against NHE.^[191-193] This value is negative enough to reduce three of the four nucleobases (dG may be an exception) including the T=T dimer as evident from the reduction potentials of the nucleobases listed in Table 2.1. The reduction potentials show that thymine and the T=T dimer are most easily reduced.

Table 2.1. Reduction potentials of some nucleobases.

Base	Reduction potentials in V		
	E(Red) ^a	E(Red) ^b	E(Red) ^c
dG	-2.76		
dA	-2.45		
dC	-2.23	-1.09	-2.1 (DMC)
dT	-2.14	-1.10	-2.1 (DMT)
U	-2.04	-1.05	-2.1 (DMU)
T=T			-2.2 (DMTD)

DMC = Dimethylcytosine, DMT = Dimethylthymine, DMU = Dimethyluracil, DMTD = Dimethylthymine-Dimer. [a] Polarographic potentials in DMF versus NHE.^[115] [b] Data from pulse radiolysis experiments in water at pH = 8.5 against NHE.^[194] [c] Data from fluorescence quenching experiments in acetonitrile against SCE.^[192,193]

Theoretical studies predict the adiabatic electron affinities for the neutral and anionic forms of the four 2'-deoxyribonucleosides in DNA.^[195] The results indicate that dT is the nucleoside with the highest electron affinity. Consequently, thymine can accept an electron more efficiently than the other nucleobases. These values are summarized in Figure 2.5 and they are uniformly greater than those of the corresponding isolated bases.^[195]

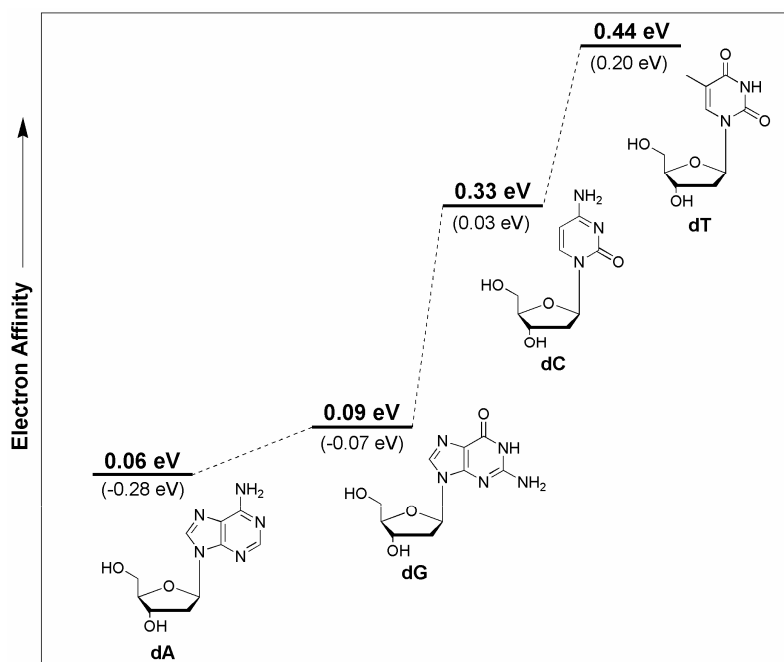


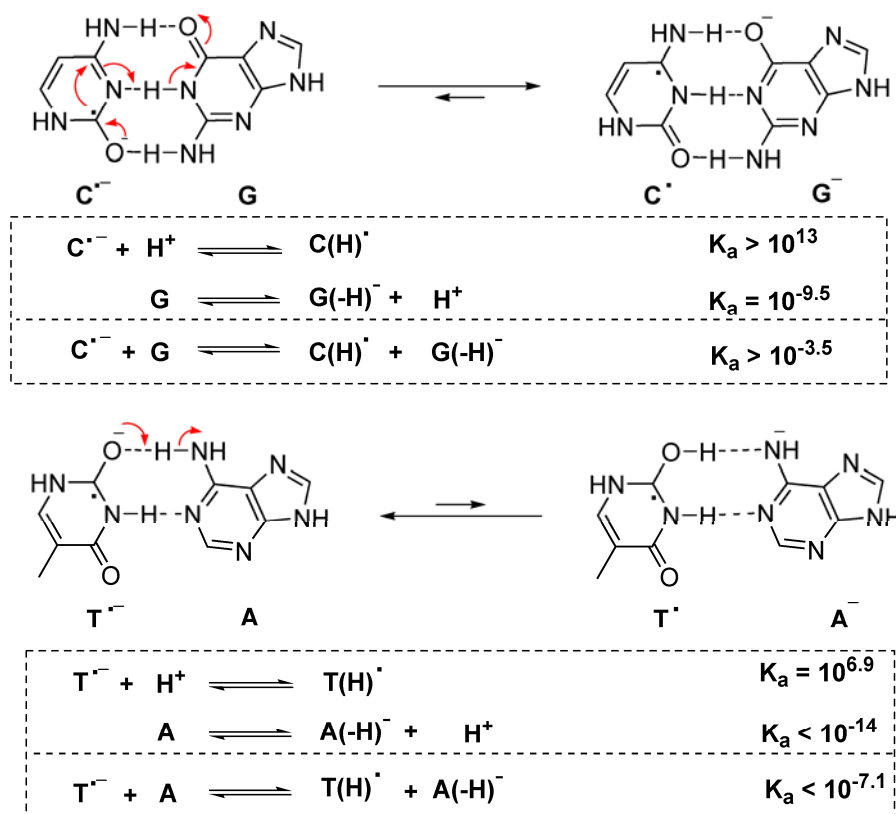
Figure 2.5 Predicted electron affinities for the nucleosides 2'-deoxyriboadenosine (dA), 2'-deoxyriboguanosine (dG), 2'-deoxyribocytidine (dC) and 2'-deoxyribothymidine (dT). In parenthesis the values for the isolated bases, adenine, guanine, cytosine and thymine.^[195]

In an aqueous environment the pK_a -values of the nucleobase radical anions need to be considered as well, because proton transfer will have a strong impact on the reduction and oxidation potentials. Table 2.2 lists the pK_a -values of some nucleobase.^[144]

Table 2.2. pK_a -values of the reduced nucleobases.^[144,196]

Equilibrium		pK_a
$T^{\cdot-}$	$\rightleftharpoons [T-H^+]^{\cdot-} + H^+$	6.9
TH^+	$\rightleftharpoons T + H^+$	-5
$A^{\cdot-}$	$\rightleftharpoons [A-H^+]^{\cdot-} + H^+$	>14
$C^{\cdot-}$	$\rightleftharpoons [C-H^+]^{\cdot-} + H^+$	13
CH^+	$\rightleftharpoons C + H^+$	4.3
$G^{\cdot-}$	$\rightleftharpoons [G-H^+]^{\cdot-} + H^+$	9.5

The pK_a of the thymine radical anion is close to 7. Protonation of the cytosine radical anion ($pK_a = 13$), however, is strongly exothermic (Scheme 2.3). An excess electron deposited on a cytosine may therefore trigger rapid protonation of the radical anion $C^{\cdot-}$ to give the neutral dC radical, $C(H)^{\cdot}$. This can trap the excess electron on cytosines and disrupt any excess electron transfer through the duplex.



Scheme 2.3 Proton dissociation constant in GC and AT bp's.^[144,196]

In summary, the data indicate that a reduced and deprotonated flavin, if light excited, is able to inject an electron into a DNA double strand regardless of the sequence context. This electron can be eventually transferred through the DNA strand. If it encounters a cyclobutane pyrimidine dimer lesion it should induce ring opening. The excess electron may also travel over C:G base pairs, but it has also larger chance to get trapped by cytosine radical anion protonation. Alternatively it can trigger a base decomposition process leading to the formation of reductive DNA lesions, such as 5,6-dihydrodT, with concomitant consumption of the excess electron.

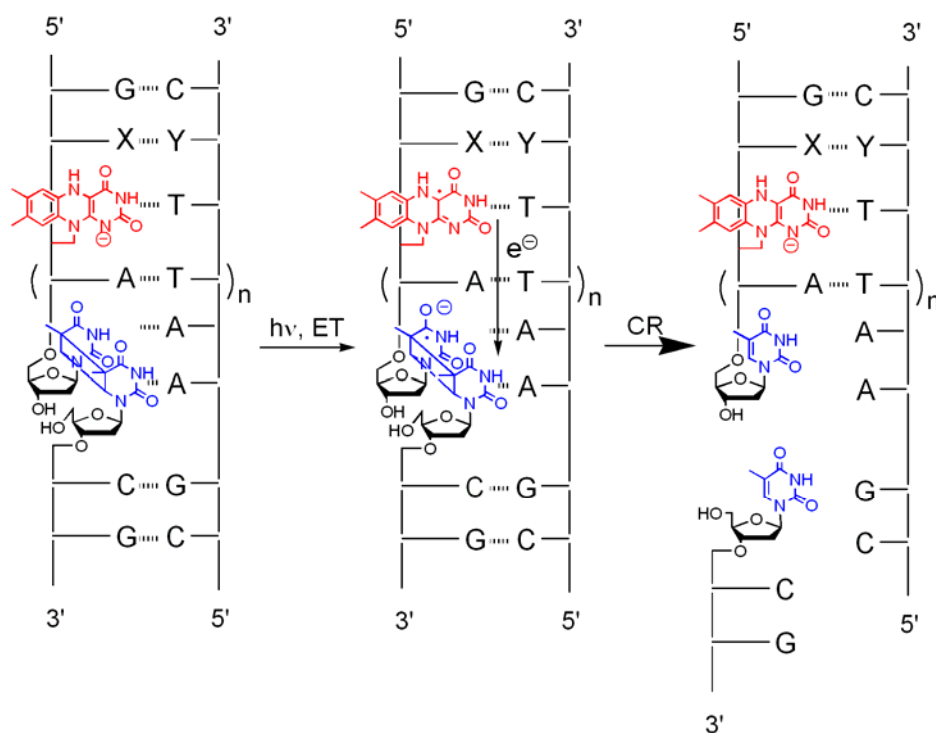
Excess electron transfer in DNA initiated by the flavin

In recent years the knowledge about EET has broadened fundamentally due to studies performed with a large range of different model systems that allowed detailed mechanistic investigations. The data were obtained with direct radiolysis studies of (i) DNA, (ii) DNA modified with intercalators^[197], (iii) pyrene-modified oligonucleotides^[198] in combination with short time spectroscopy^[199] and (iv) studies with defined donor-DNA-acceptor systems. The system employed by *Rokita* utilises an aromatic amine as the electron donor and a 5-Br-2'-deoxyuridine (BrdU) as the electron acceptor. Upon irradiation and subsequent electron transfer a cascade of reactions ultimately yields an alkaline sensitive site (see also Scheme 1.3, Chapter 1). The latter eventually gives rise to a measurable strand break after hot piperidine treatment.^[33]

The following sections present an overview, based on recent reviews,^[200,201] of the studies of EET conducted with the flavin electron injector. Important electron transfer features are covered in this introduction such as the distance and the sequence dependence of the process as well as the direction of the charge transfer in DNA. The flavin-based electron transfer was mostly carried out in the research group of *Carell* and it is very relevant for the work presented in *Results and Discussion* of Chapter 2.

Distance dependence

The first defined model system used to study excess electron transfer in DNA possessed a flavin electron donor and a T=T dimer acceptor. This dimer cleaves spontaneously after single electron reduction.^[202] In order to investigate over which distances an excess electron may be able to travel in DNA a series of experiments was conducted. Oligonucleotides containing a special T=T dimer and a flavin donor were synthesised.^[203] The T=T dimer building block possesses an open backbone inducing an easily detectable strand break after single electron reduction (Scheme 2.4).



Scheme 2.4 Sequence of events occurring upon irradiation of DNA modified with a flavin electron donor and a T=T dimer electron acceptor with an open backbone.^[203]

A series of such DNAs was prepared to evaluate the distance dependence of the process. In these double strands, the distance between the flavin donor and the dimer acceptor was systematically increased from 3.4 Å to about 30 Å using additional A:T base pairs between the redox partners. Since efficient repair (splitting) of the dimer was observed, even in the longer double strands, the experiments showed that an excess electron can travel over a distance of at least 30 Å.^[203] The rather small decrease of the repair efficiency with increasing distance gives rise to some important mechanistic conclusions. The excess electron does not travel directly from the flavin to the dimer by a *Marcus* type mechanism, but hops over the intermediate A:T base pairs, which function as temporary charge carriers. The results reported by the authors were in good agreement with data previously obtained by other research groups using γ -radiolysis and EPR experiments.^[197,204,205]

Other different systems were provided taking advantage of a similar model for the EET study. Among them the synthesis of DNA hairpin structures which increases the stability of the system in which two unnatural structure-disturbing modifications (the donor and the acceptor) are present. Hairpin-shaped oligonucleotides are DNA strands, which possess a self-complementary stem and a loop region called the “head” of the hairpin.^[206-208] DNA hairpins

are stably folded oligonucleotides with a sharp, concentration independent melting point. Therefore DNA hairpins are reliable models for EET studies.

Carell and co-workers prepared a series of DNA hairpins in which the distance between the flavin donor **1** and the dimer acceptor **2** was again systematically (6.8 Å to 17 Å) increased (Figure 2.6). The DNA hairpins contained the modified flavin molecule **1** as a cap in the loop region. The DNA hairpins contained the modified flavin molecule **1** as a cap in the loop region.^[209] They consequently possessed only one helix disturbing unit, the dimer, inside the DNA duplex region. This was considered to be an advantage because two disturbing units are most likely hindering the DNA to adopt a B-type double helix conformation between the donor and the acceptor.

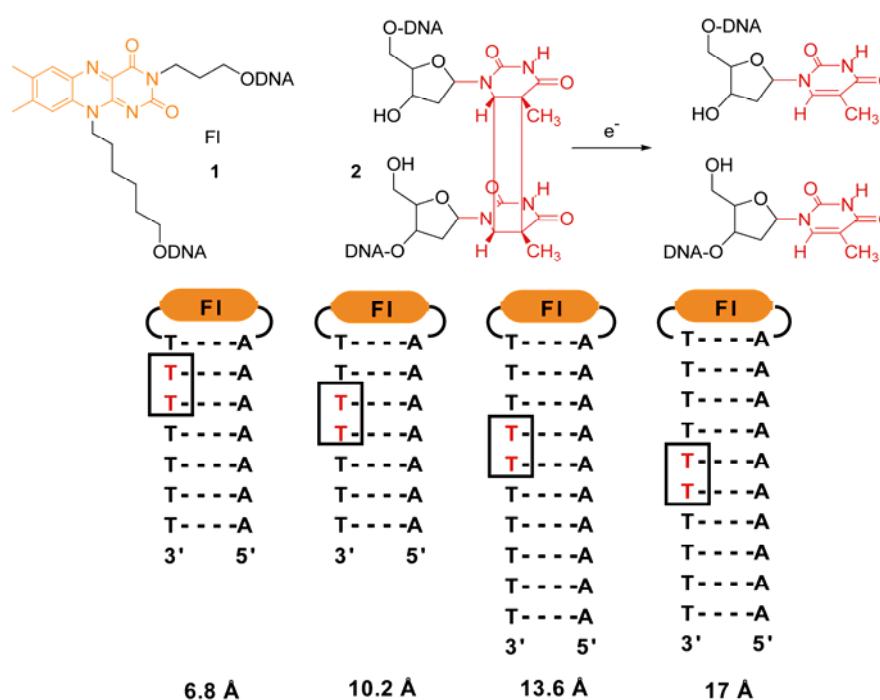


Figure 2.6 Depiction of the DNA hairpins used to study the distance dependence of excess electron transfer. FI = Flavin **1**, red T T = cyclobutane-thymidine dimer **2**.^[209]

The data collected show that dimer cleavage proceeds efficiently in all hairpins depicted in Figure 2.6. Excess electron transfer decreases with increasing distance from 2 % repair per minute at 5°C to about 0.1 % repair per minute in the longest hairpin. The distance between the two redox partners increases in these hairpins from 6.8 Å to about 17 Å. Consequently, the distance dependence is shallow and hence not in agreement with a *Marcus* type behavior, thus supporting the hopping model. Overall, however, the distance dependence of the EET is more pronounced than hole transfer, which is in good agreement with short time spectroscopic studies and with data from *Rokita* and co-workers.^[33,146,156]

Specifically, *Marcus* type electron transfer is exponentially distance dependent as reported in eq. 2.1, described previously.

$$k_{\text{et}} = k_0 e^{-\beta\Delta r} \quad (\text{eq. 2.1})$$

For DNA, β -values between 0.7 \AA^{-1} and 1.2 \AA^{-1} were determined earlier.^[120,210] These β values predict that the repair yield should drop by a factor of about 8 with every additional base pair introduced between the dimer and the flavin. Transferring this data to the EET studies, a repair yield of only 0.004% per minute should be expected for the longest hairpin in Figure 2.6. This predicted value is, however, one to two orders of magnitude lower than the value measured by the authors. A plot of the yields obtained with these hairpins ($\ln y$) against the distance Δr (Figure 2.7, inset) provided a β -value of about 0.3 \AA^{-1} at 5°C and at 0°C . This is in contrast to the expected β -value of about 0.7 \AA^{-1} . These data can not be explained by a direct *Marcus* type electron transfer model.

In the hopping model, in contrast, the electron is not directly transferred but uses intermediate charge carriers to hop from the donor to the acceptor. In the hopping scenario, the transfer efficiency is much less distance dependent. With $\ln(k_{\text{ET}}) = -\eta \ln(N)$ (eq. 2.2), the transfer rate is proportional to the number of hopping steps (N).^[210] The proportionality factor η should be around 2 if the electron moves in a random walk-like process.^[112,210] Under the assumption that the electron uses the T bases in every A:T base pair as stepping stones, the authors plotted the measured cleavage yields per minute $\ln(y)$ against $\ln(N)$ (Figure 2.7). This plot provided an η -value close to 2 in agreement with the hopping model.^[33,203]

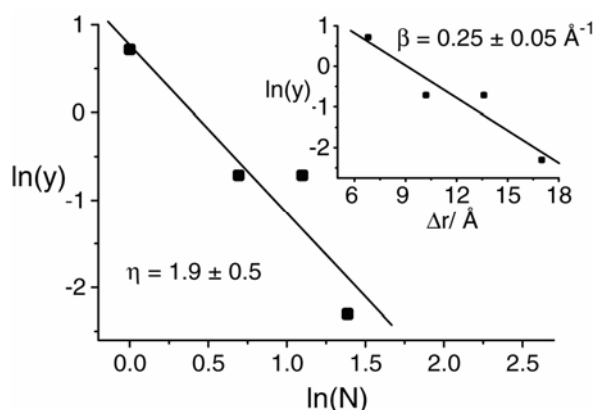
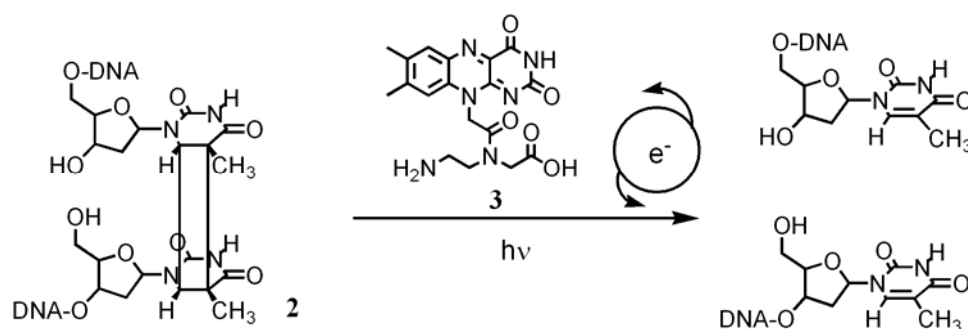


Figure 2.7 Plots of the data obtained with the hairpins reported in fig. 2.6 using the *Marcus* model [$\ln(y)$ against Δr] and the hopping model ($\ln(y)$ against $\ln(N)$).^[209]

Transfer direction

Controversial results about the direction of the electron transfer in DNA were obtained by different research groups.^[211,212] If the electrons move in a random walk like hopping process, it would be expected that the excess electron travels along a DNA duplex in both directions (5'→3' versus 3'→5') with the same efficiency. This hypothesis was probed with a series of PNA:DNA^[213] double strands, which contain the flavin **3** electron donor in the PNA strand and the dimer **2** in the DNA counterstrand (Scheme 2.5).^[212,214]



Scheme 2.5 T=T dimer cycloreversion operated by flavin **3** used in the experiments with DNA:PNA hybrids.

The measured cleavage yields obtained from the authors after irradiation of the DNA:PNA hybrids show that the dimer cleavage proceeds efficiently in all investigated double strands even over the rather large distance of about 24 Å.^[212] In agreement with previous results, the dimer cleavage is not very distance dependent even in these intermolecular cases. In fact, the distance dependence in these DNA:PNA hybrids influences the EET process by only a factor of 2, which can be considered almost negligible. Comparing the cleavage data obtained with PNA:DNA hybrids in which the electron transfer proceeds in the 5'→3' direction with the hybrids in which the electron transfer proceeds in the 3'→5' direction, no significant difference in repair yield was observed. These data led to the conclusion that the repair of a T=T dimer even over rather large distances of 24 Å is independent of the electron transfer direction. This result nicely supports the idea that EET in duplexes is a thermally activated random walk-like process in which the electrons hop along the DNA duplex without showing any directional preference. Nevertheless this observation strongly contrasts with the data reported by *Ito and Rokita*.^[33,211,215] Using a *N, N, N', N'*-tetramethyl-1,5-diaminonaphthalene as photoexcitable electron donor and BrdU as electron trap, these authors reported a strong influence of the process on the electron transfer direction. Comparing nearly identical

sequences, a more efficient EET was observed in the 3'→5' direction. The complementary process HT favours migration in the opposite direction (5'→3'),^[216] but this process also involves electron migration in the 3' to 5' direction. An asymmetry in the highest occupied molecular orbital (HOMO) overlap of nucleobases acting as charge carriers has been proposed as an explanation for the directionality of HT.^[216] An equivalent suggestion based on the lowest unoccupied molecular orbital (LUMO) overlap has been proposed for EET.^[211]

The controversial results obtained by *Carell* on the one side and by *Ito* and *Rokita* on the other side can be ascribed to the different models used to study the EET in DNA. The transfer direction as well other features of EET such as the sequence dependence can be drastically influenced by the donor and/or the electron trap used in such models.

Sequence dependence

The question how the sequence influences the excess electron transfer process was initially controversial as well. The outcome of the experiments was again dependent on the system used to study this phenomena.^[211,217,218] A sequence study carried out with a series of DNA hairpins was reported by *Carell* and co-workers.^[217] Taking advantage of the well established synthesis, irradiation and analysis methods developed in the previous works, the authors investigated whether the base sequence between the donor and the acceptor influences the T=T dimer repairing yield. To this end another series of flavin **1** capped hairpins containing the T=T dimer **2** with an open backbone was synthesised. The distance between the donor and the acceptor in such hairpins ranged between 13.6 Å and 17.0 Å (Figure 2.8). This rather large separation ensured that the electron transfer has to proceed by charge hopping and not by direct transfer.^[112,210]

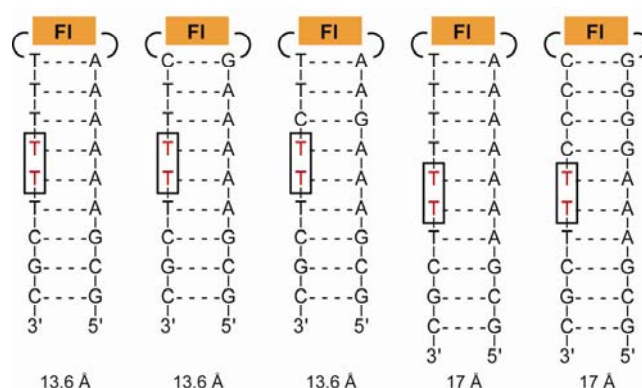


Figure 2.8 Depiction of the DNA hairpins used to study the sequence dependence of the excess electron transfer. Fl = Flavin **1**, red T T = cyclobutane-thymidine dimer **2**.^[217]

The T=T dimer cleavage by EET again proceeded highly efficiently in all hairpins described. The data presented by the authors clearly indicates that the sequence between the flavin and the T=T dimer does not influence the dimer splitting yield. Thus, the reductive cleavage of a T=T dimer in DNA hairpins is not sequence dependent over a distance of 17 Å. However, this conclusion is in contrast to the results reported by *Ito* and *Rokita*. Using the above mentioned diaminonaphthalene derivative as electron donor and BrdU as electron acceptor, it was demonstrated that the EET is less efficient through G:C bp sequences.^[33,219] The authors suggest that the radical anion C⁻ can be protonated with a rate constant that competes with the rate constant of the entire electron transfer process. The EET studies carried out by *Wagenknecht* and co-workers on the sequence dependence furnished very similar conclusions.^[218] The model used in the last case consists of phenothiazine-modified DNA containing BrdU as electron trap. Therefore, two different electron donors (diaminonaphthalene and phenothiazine derivatives) bearing different features show very similar EET performance in combination with the same electron acceptor (BrdU). In contrast, the combination of a flavin electron donor with a T=T dimer acceptor leads to divergent results, suggesting that the trap system might play a key role in the analysis of EET. A model that contains flavin as donor and BrdU as acceptor could elucidate this issue.

Repair pathway

Another crucial question associated with the excess electron transfer process is the exact repair pathway. Electrons can, as described in detail before, hop through the DNA using the pyrimidine bases as stepping stones. Alternatively it can be envisioned that charges diffuse along the double helix as solvated electrons (e_{aq}⁻).^[220]

In order to gain more insight into the excess electron transfer pathways *Carell* and co-workers prepared the series of DNA hairpins depicted in Figure 2.9.^[221] The hairpins again contained the flavin electron donor **1** as the cap structure, while in the stem region one of the two different oxetane units **4** or **5** is used as the electron acceptor. Oxetanes have the advantage that they cleave very rapidly and irreversibly after single electron reduction with well established rate constants between 10⁻⁷ s⁻¹ and 10⁻⁸ s⁻¹.^[27,183,188,190,222-228] Furthermore, oxetanes are believed to be natural substrates of the (6-4) photolyases^[171-173] in the generation and repair of (6-4) lesion, as already described (see also Scheme 2.1). The cleavage of oxetanes with various electron donors already served as a model to investigate the (6-4) photolyase mechanism of repair.^[189,190,226]

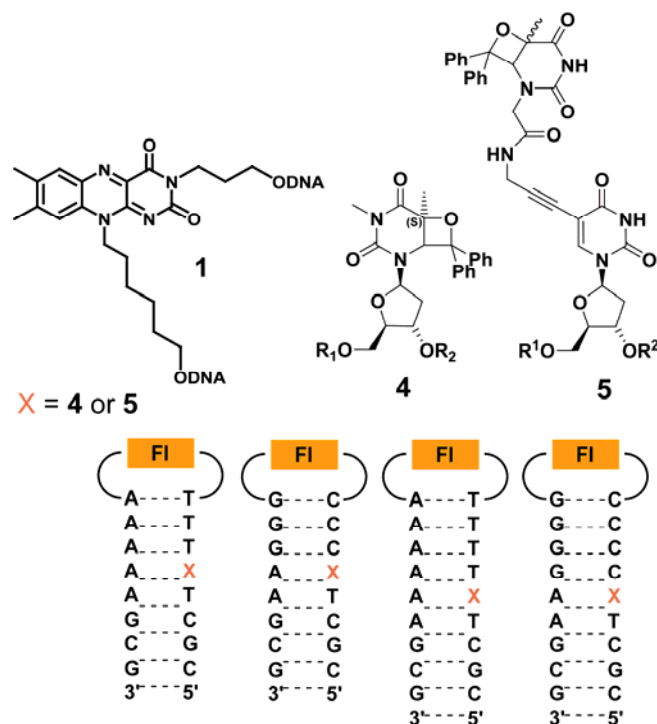
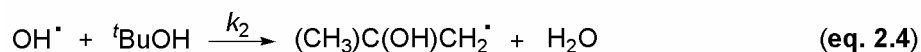


Figure 2.9 Hairpin sequence for the study of the electron transfer pathways in DNA. Fl = flavin **1**, X = **4** or **5**, the two oxetane acceptors used in the work.^[221]

The repair mechanism is assumed to involve single electron donation followed by cleavage of the oxetane intermediate. The hairpins in Figure 2.9 containing the oxetane **4** have the electron acceptor positioned close to the duplex. In contrast, the oxetane **5** is located outside the duplex. A semi-flexible propargylamide spacer places the electron acceptor at a distance of about 10 Å away from the nucleotide stack. Thus, the oxetane acceptor **5** points out of the major groove into the surrounding medium. The cleavage of oxetanes **4** and **5** after single electron reduction is followed by the release of benzophenone with formation of HPLC-detectable hairpins, which can be distinguished from the unreacted oxetane-containing hairpins. The design of such oxetane-containing models was aimed at investigating the electron pathways, from the donor to the acceptor. With such a system it was enquired if the surplus electron hops through the duplex using the bases as stepping stones, or if electrons travel externally along the DNA duplex as e_{aq}^- species, which could consequently cleave **5** as well. Although the electron trap positioned outside the duplex was efficiently repaired, one could exclude that the excess electrons move along the DNA as solvated species. This claim was based on control experiments carried out in presence of a well known quencher (N_2O) able to react promptly with any e_{aq}^- present in solution.

In N₂O-saturated solution (~ 0.02 M), e_{aq}⁻ are efficiently transformed in HO[•] radicals with a rate constant of $k_1 = 9.1 \times 10^9 \text{ M}^{-1} \text{ s}^{-1}$ (eq. 2.3).

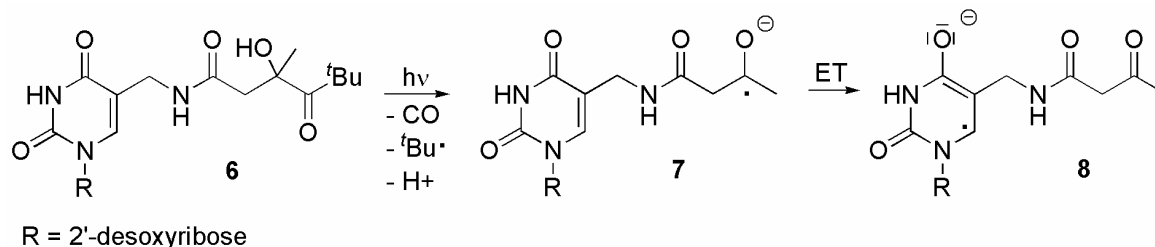


Subsequently, in the presence of a tertiary alcohol, HO[•] radicals are scavenged efficiently with a rate constant of $k_2 = 6.0 \times 10^8 \text{ M}^{-1} \text{ s}^{-1}$ (eq. 2.4).^[229]

Single electron donor

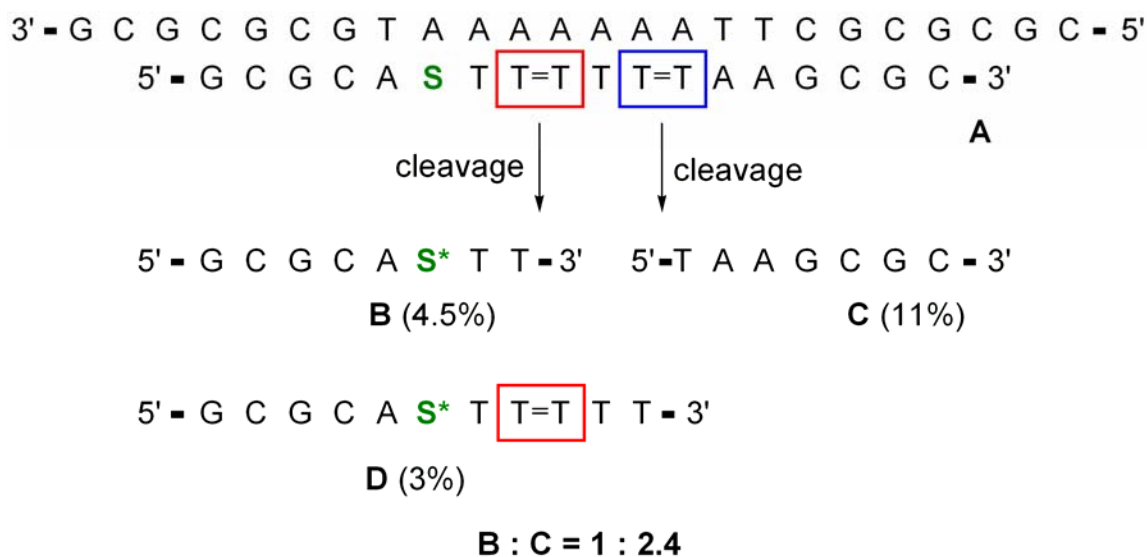
The cyclobutane reversion caused by the excess electron on the T=T dimer leads to one neutral thymidine and one thymidine radical anion. In principle, the excess electron can be either trapped or it can continue to proceed through the DNA duplex. In the latter case the excess electron can be detected by a second trap or, in terms of DNA lesion repair, it can cleave a second T=T dimer at another position. In that case a catalytic repair process, i.e. initiated by the electron injection from a DNA-photolyase could be assumed.

In order to investigate the fate of the injected electron, investigations were performed with the electron injector developed by *Giese* and co-workers.^[230] In contrast to the flavin electron injector, *Giese*'s single electron donor (SED) **6** transfers only a single extra electron into the DNA double strand upon irradiation. The basis for the new injector is the less negative redox potential of thymine^[115,194,231] compared to dialkylketone radical **7**.^[232] Thus, a ketyl radical anion (**8**) produced in close proximity to a thymine by a *Norrish* type I cleavage was used to prepare a single thymine radical anion inside a DNA duplex (Scheme 2.6).



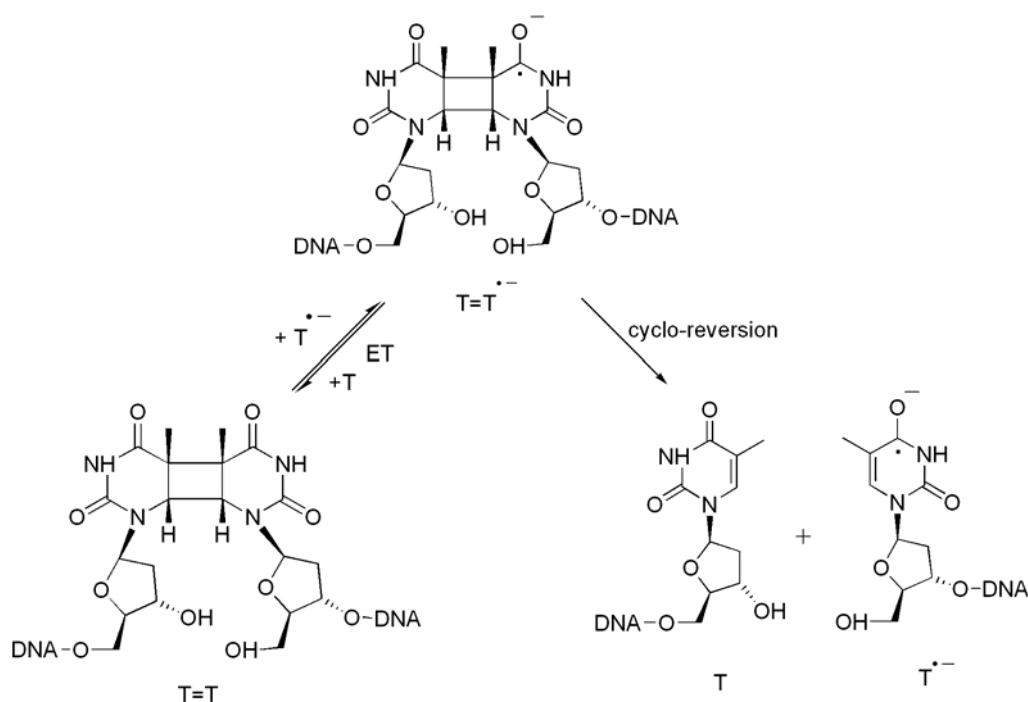
Scheme 2.6 Photolysis ($\lambda = 320 \text{ nm}$) of ketone **6** (SED) and generation of thymine radical anion **8** via the dialkylketone radical **7**, proven by ESR spectroscopy at 75K.^[230]

Interesting results were achieved by the irradiation ($\lambda = 320$ nm) of the double strand **A** in Scheme 2.7. One strand contains two T=T dimers in a row separated by a single A:T base pair. Upon irradiation of double strand **A**, cleavage at the proximal and in addition at the distal T=T dimer site was observed. This process leads to the shorter strands **B** and **C** in Scheme 2.7. Surprisingly, the cleavage yield at the distal site (**C** = 11 %) was more than two times higher than at the proximal site (**B** = 4.5 %).



Scheme 2.7 Experiments with two T=T dimers (in the red and blue squares) in a row per strand gave hints that the electron is not trapped at the first dimer. The single electron donor before (S) and after irradiation (S*) is depicted in green.^[230]

If an electron migrates to the distal thymine dimer only after the proximal dimer has been cleaved, the yield ratio **C/B** can not be larger than 1.0. The observed **C/B** ratio of 2.4 requires that a different mechanism must be involved in the electron transport to the distal T=T dimer. In this new hypothetical scenario the proximal T=T dimer is not readily cleaved, as confirmed by the detection of the cleavage product **D** (3%). In this strand the proximal T=T dimer is still intact, while the distal dimer was obviously cleaved. This result led the authors to the conclusion that the cleavage of the T=T dimer radical anion is as fast as or at least comparable with the overall electron transfer process. The electron can hop over the first T=T dimer without causing any cleavage. Thus, the transition state energy of the charge detection by the thymine dimer is at least as high as that of the electron transfer steps or, with other words, the charge transfer rate may be in the same range than the T=T dimer cleavage rate. Thus, dimer cleavage may be rate determining (Scheme 2.8).



Scheme 2.8 Competition between cleavage and electron transfer for T=T dimer radical anion **8**.^[230]

The cleavage rate of a T=T dimer in a duplex in absence of any photolyase is not well established, but data from *Falvey* point to a value of $k_{\text{split}} = 10^6 \text{ s}^{-1}$ for the reductive cleavage of a thymine-dimer model.^[193] If the electron transfer is faster than 10^6 s^{-1} the flavin-T=T dimer system is unable to detect any sequence differences, as this would in turn be the rate-determining step. *Ito* and *Rokita* used BrdU as electron acceptor.^[33,219] This acceptor system has a less negative redox potential than thymine or the T=T dimer.^[146] Therefore, the BrdU electron-detection system might be faster than the T=T dimer trap. This difference could explain why the assay used by *Ito* and *Rokita* is able to report, as aforementioned, the influence of the base sequence and of the electron transfer direction on the EET, while with the T=T dimer system these effects are not detectable. The EET through DNA is then sequence and distance independent within the time frame of the system, which may be defined by the dimer splitting rate. Recent studies on the T=T dimer at the nucleoside level suggest a k_{split} higher than 10^6 s^{-1} .^[233] But the k_{split} value inside a duplex DNA is not yet known. Using a faster electron acceptor, such as BrdU, in combination with the T=T dimer detection system may strengthen the results reported by *Giесе* and co-workers. Moreover, this proposed model containing two different acceptors (T=T dimer and BrdU) could be able to clarify the functionality of the T=T dimer as EET electron trap and, in principle, enable an estimation of k_{split} .

2.1.1 Aim of Chapter 2

Whereas hopping of electrons through DNA is now a generally accepted model, it remained to address the conflicting data about the sequence dependence, as well as the direction of electron transfer and the role of the electron acceptors used in this process. In summary, investigations of the electron transfer process using DNA modified with either arylamines,^[33,215,219] pyrenes or phenothiazines^[218,234] as electron donors and BrdU as electron acceptor pointed out that G:C bps, in contrast to A:T bps, reduce the efficiency of the excess electron transfer through the duplex. Studies with a flavin as electron donor and a T=T dimer as electron acceptor, in contrast, showed in contrast no sequence dependence.^[217] *Giese* and co-workers ascribed the divergent results to the rate of the T=T dimer cycloreversion, which might be too low to fully report the EET process.^[230] However new pulse radiolysis studies, carried out at the nucleoside level in solution, suggest a very fast and irreversible dimer opening close to the diffusion range ($> 10^{7-8} \text{ s}^{-1}$).^[233] This value would be in contrast to the observation described in the previous paragraph and reported in *Giese's* work. These and other open questions are the subject of the *Results and Discussion* of Chapter 2 as summarised as follows.

- Different electron acceptors (i.e. BrdU) were planned be used in combination with the widely employed flavin donor, allowing a systematic study of the function of electron traps in the EET.
- A sequence dependence study of the EET was planned to be undertaken in order to disclose the capacity of the flavin-containing system to fully report the process.
- The single electron donor developed by *Giese* was intended to be used in combination with the T=T dimer and BrdU for a more in-depth investigation of the dimer splitting process.
- A parallel study was planned to be achieved, using the flavin in order to compare the two electron donors and evaluate the role of their redox potentials in the EET process.
- A new model for DNA-based nano-wire applications will be described and tested.

The first two points have been achieved in collaboration with *Sascha Breeger* (from the *Carell* group).

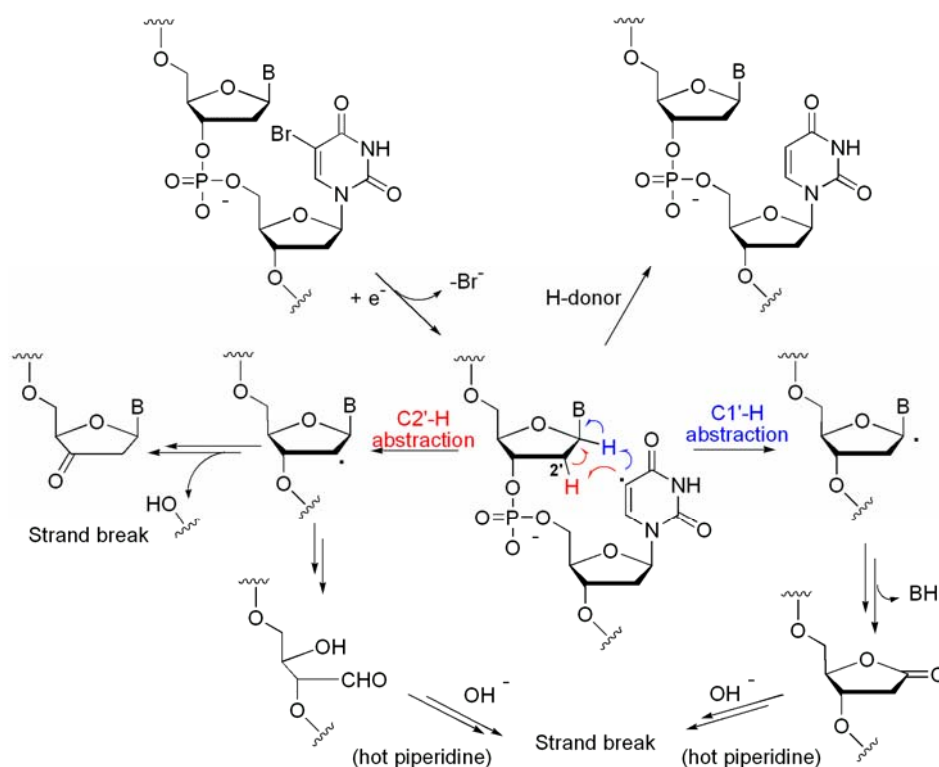
Before the results are presented, a short introduction about the electron acceptors features used in this work is necessary. The driving forces for the selection of such molecules as electron traps in the EET process are here described.

Electron acceptors: BrdU

Replacement of thymidine in DNA by BrdU has long been known to enhance photosensitivity with respect to DNA-protein-mediated photo-cross-linking,^[235] single- and double-strand breaks^[236] and creation of alkali-labile sites.^[237] In addition, the effect of a BrdU substitution in DNA is well known for a long time.^[238] This residue is nearly isosteric to thymidine and typically pairs with adenosine when incorporated into DNA, although occasional mispairing with guanine contributes to its mutagenic effect.^[239,240] The nature of the photolability of BrdU was intensively studied and is described now as a process that involves three main steps: acceptance of an electron, elimination of a bromine anion and generation of an intermediate uridinyl radical. The fate of this radical depends on specific reaction conditions, the local structural and solvent environment.^[237,241]

Saito and co-workers reported a highly efficient reaction at 5'-A^{Br}U-3' sequences vs. 5'-G^{Br}U-3' in a series of direct oligonucleotide irradiation experiments (BrU = BrdU).^[236] Further investigations carried out by the research group of *Greenberg* indicated that halide elimination may compete with charge migration and recombination.^[242] The mechanism of degradation of BrdU-containing ODNs upon UV irradiation (302 nm) was already reported in Scheme 1.3 of Chapter 1.

The uridine-5-yl radical, generated after debromination of the photoexcited BrdU / dA couple or after single electron reduction, abstracts hydrogen from the vicinal sugar moiety, specifically from the position C1' and/or C2'. The carbon centered radicals so formed undergo a succession of rearrangement and elimination reactions yielding alkaline labile intermediates and eventually to strand breaks (Scheme 2.9). In the presence of a hydrogen donor (H-donor) the uridine-5-yl radical eventually gives rise to the 2'-deoxyuridine (dU) after H-abstraction. The C1' and C2' radical chemistry has previously been described in more detail in Chapter 1.



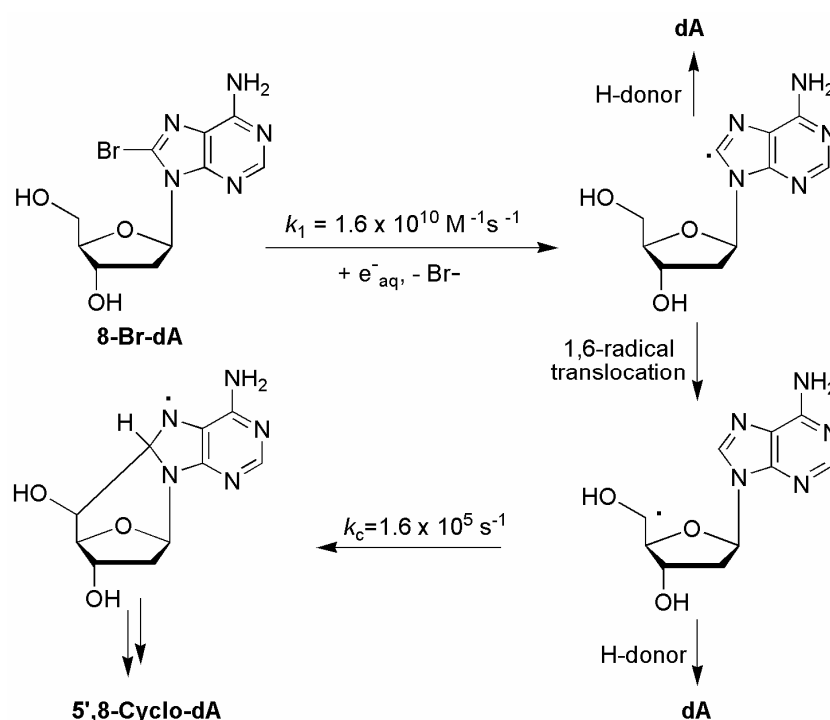
Scheme 2.9 Pathways of degradation of BrdU-containing oligonucleotides upon single electron injection.

All the halogenated pyrimidines are expected to exhibit higher electron affinities than their natural counterparts,^[156,243] and all have been observed to capture an electron during nanosecond pulse radiolysis.^[244] Specifically, the radical anion of BrdU is highly transient and decomposes with a half-life of 1.7 ns.^[244] The adiabatic electron affinity was calculated using the density functional theory (DFT). For solvated 5-Br-uracil (no sugar unit) it is in the order of 2.44 eV while 2.02 eV were determined for the natural uracil.^[245] Thus, BrdU is expected to be more easily reduced than dU (or dT).

As already mentioned, BrdU was efficiently used in excess electron transfer studies by *Rokita* and *Ito* in ODNs containing a *N, N, N', N'*-tetramethyl-1,5-diaminonaphthalene (TMDN) as electron donor.^[33,219] The low energy excited state ($\lambda_{\text{max}} = 325 \text{ nm}$) of this strong reductant ($E^*_{\text{ox}} \approx -2.8 \text{ V vs SCE}$) enables a selective excitation of the chromophore without direct excitation of DNA bases.^[33] The reduction potential of the flavin used in the previously described EET experiments is reported to be very similar ($E^*_{\text{ox}} \approx -2.6 \text{ V vs SCE}$).^[191] All these factors persuaded to test BrdU as electron transfer acceptor in flavin-containing hairpin systems.

Electron acceptors: BrdA

The selection of 8-bromo-2'-deoxyadenosine (BrdA) as electron acceptor derives from numerous studies about this compound and the products of one-electron reduction. The above mentioned cyclonucleosides, illustrated in Chapter 1, are among these products. For example, in the case of the 5',8-cyclo-2'-deoxyadenosine (Cyda), the cyclisation was triggered by radiolytic or photolytic methods.^[25,26] Specifically, reactions occurring upon single electron reduction of BrdA were investigated. Using calculations (DFT-B3LYP), pulse radiolysis and product studies, *Chatgialoglu* and co-workers described kinetic and thermodynamic properties of this reaction, summarized in Scheme 2.10.^[25-27,53]



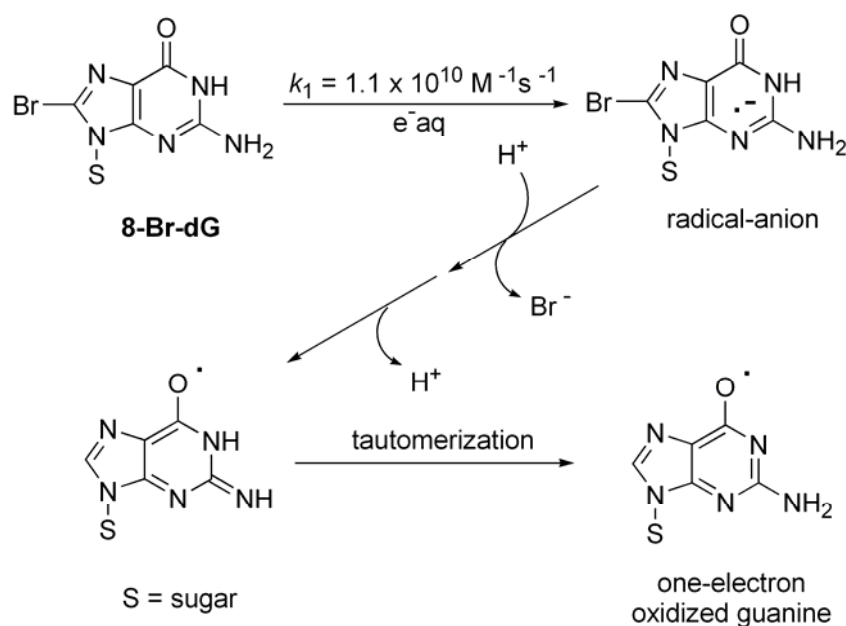
Scheme 2.10 Reaction of BrdA with solvated electrons. k_1 was determined by measuring the rate of the optical density decrease of e_{aq}^- at 720 nm ($\epsilon = 1.9 \times 10^4 \text{ M}^{-1} \text{ s}^{-1}$) as a function of nucleoside concentration.^[25-27,53]

Briefly, the rate constant for the reaction of solvated electrons (e_{aq}^-) with BrdA was determined by measuring the rate of the optical density decrease of e_{aq}^- at 720 nm ($\epsilon = 1.9 \times 10^4 \text{ M}^{-1} \text{ s}^{-1}$) as a function of nucleoside concentration. The bimolecular rate constant was found to be $k_1 = 1.6 \times 10^{10} \text{ M}^{-1} \text{ s}^{-1}$. Comparing the analogous reaction with the natural adenosine (dA, $k = 8.2 \times 10^9 \text{ M}^{-1} \text{ s}^{-1}$), the presence of bromine increases the rate constant of the reduction by a factor of 2.^[25]

With a rate constant of $k_1 = 1.6 \times 10^{10} \text{ M}^{-1} \text{ s}^{-1}$, BrdA was chosen as fast electron sink in the following EET studies. Moreover, BrdA it is also known not to affect the stability of duplex DNA adversely,^[246] whereas its use as electron acceptor in EET is unprecedented.

Electron acceptors: BrdG

8-bromo-2'-deoxyguanosine (BrdG), like BrdU and BrdA, reacts comparably fast with electrons.^[247] For this reason it has been selected as electron acceptor in these EET studies as well. As already mentioned in Chapter 1, the one-electron reduction of BrdG and the ribose analogue 8-bromo-guanosine (BrG) does not follow the same pathway as BrdA. The reduced adduct undergoes protonation at C8 and tautomerization to afford the one-electron oxidised 2'-deoxyribo-guanosine or riboguanosine (Scheme 2.11).^[53,54,248] Nevertheless, BrdG reacts with solvated electrons very fast. A rate constant of $k_1 = 1.1 \times 10^{10} \text{ M}^{-1} \text{ s}^{-1}$ was determined for the reaction of BrdG with e^-_{aq} by measuring the rate of the optical density decrease of e^-_{aq} as a function of the concentration of the nucleoside added.^[53]



Scheme 2.11 Reaction of BrdG with solvated electrons. Pathway of one-electron oxidised guanine formation. k_1 was determined as for BrdA.^[54]

BrdG was also used as electron acceptor in EET investigations in G-quadruplex^[249] and in double stranded DNA.^[247]

The choice of BrdG as an electron acceptor in the following studies was driven by the necessity to have a larger variety of acceptors. Furthermore, the reduction of Br-purines in a duplex can yield important information for the cyclo-purine generation pathway in DNA.

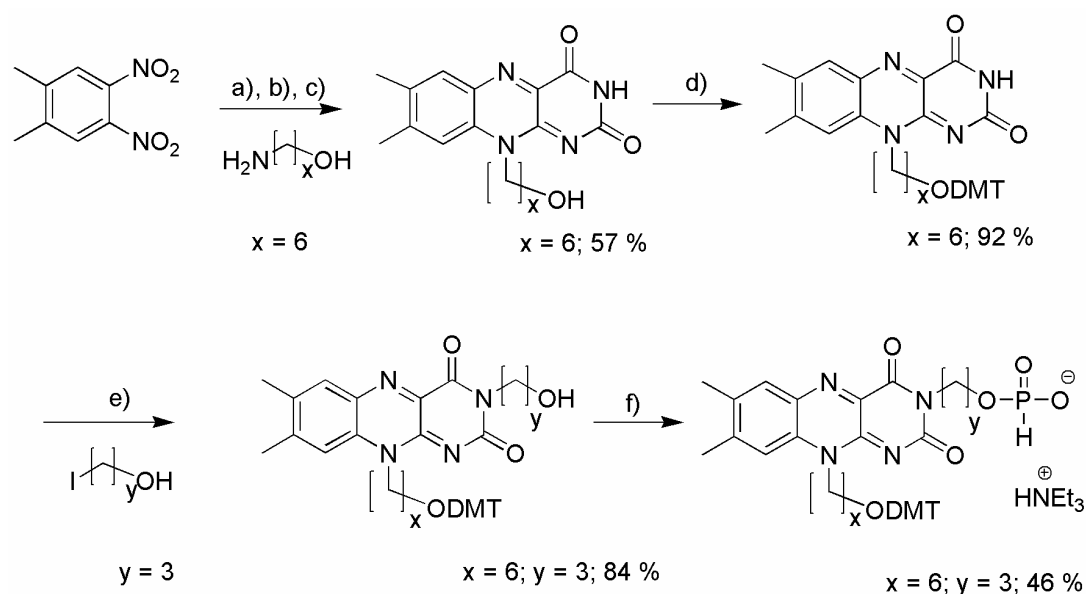
In summary, the bimolecular rates of the reaction of a solvated electron with all three selected electron acceptors (BrdA, BrdG and BrdU) are known, and they are in the diffusion controlled regime^[250] with about $1-2 \times 10^{10} \text{ M}^{-1} \text{ s}^{-1}$.^[25,53,251] The reduction is followed by a prompt release of Br^- .^[25,54,237,244] The flavin donor that will supply the electrons in the Br-nucleosides containing models has a reduction potential of $E^*_{\text{ox}} \approx -2.6 \text{ V}$ vs SCE.^[191] Thus, the redox-properties of the selected Br-acceptors have to be taken into account. Although not all of the redox potential of the Br-substituted bases are known, it can be roughly assumed, based on the reduction potentials of the unmodified nucleobases, that they follow the order $\text{BrdU} > \text{BrdA} > \text{BrdG}$. Thus, BrdU is the easiest to reduce, followed by BrdA and BrdG. The redox potentials E° of the nucleobases are reported as T = 1.7 V, C = 1.6 V, A = 1.4 V, G = 1.3 V vs NHE,^[115] whereas their rate constants (dT, dC, dA and dG) with solvated electrons are all in the diffusion controlled region of $0.6-1.8 \times 10^{10} \text{ M}^{-1} \text{ s}^{-1}$.^[252] BrdU is reported to be 40-50 mV easier to reduce than dT.^[253] Thereby, BrdU, BrdA and BrdG possess the correct features for an applications as electron acceptors in combination with the flavin electron donor.

2.2 Results and Discussion

2.2.1 Flavin / Br-nucleoside model systems

Synthesis of the flavin donor

The flavin used in the following EET studies is introduced during the solid phase oligonucleotide synthesis as *H*-phosphonate because flavin phosphoramidites were found to be efficiently oxidized under aerobic conditions.^[254,255] The synthesis of the *H*-phosphonate flavine **1** was achieved according to the previous work,^[256] as depicted in Scheme 2.12 and will not be discussed in detail in this thesis. The synthesis started with the reaction between the dimethyldinitrobenzene and 1-amino-hexan-6-ol. The nitro group of the product was subsequently hydrogenated and the resulting amine was added, without prior isolation, to a solution containing alloxan and boric acid in acetic acid. The standard dimethoxytrityl protection of the free alcohol was followed by the alkylation at *N*(3) with 1-iodopropan-3-ol, using Cs₂CO₃ as base in DMF. The final conversion of the hydroxyl group into the *H*-phosphonate gave the flavin *H*-phosphonate, ready for the incorporation into oligonucleotides.

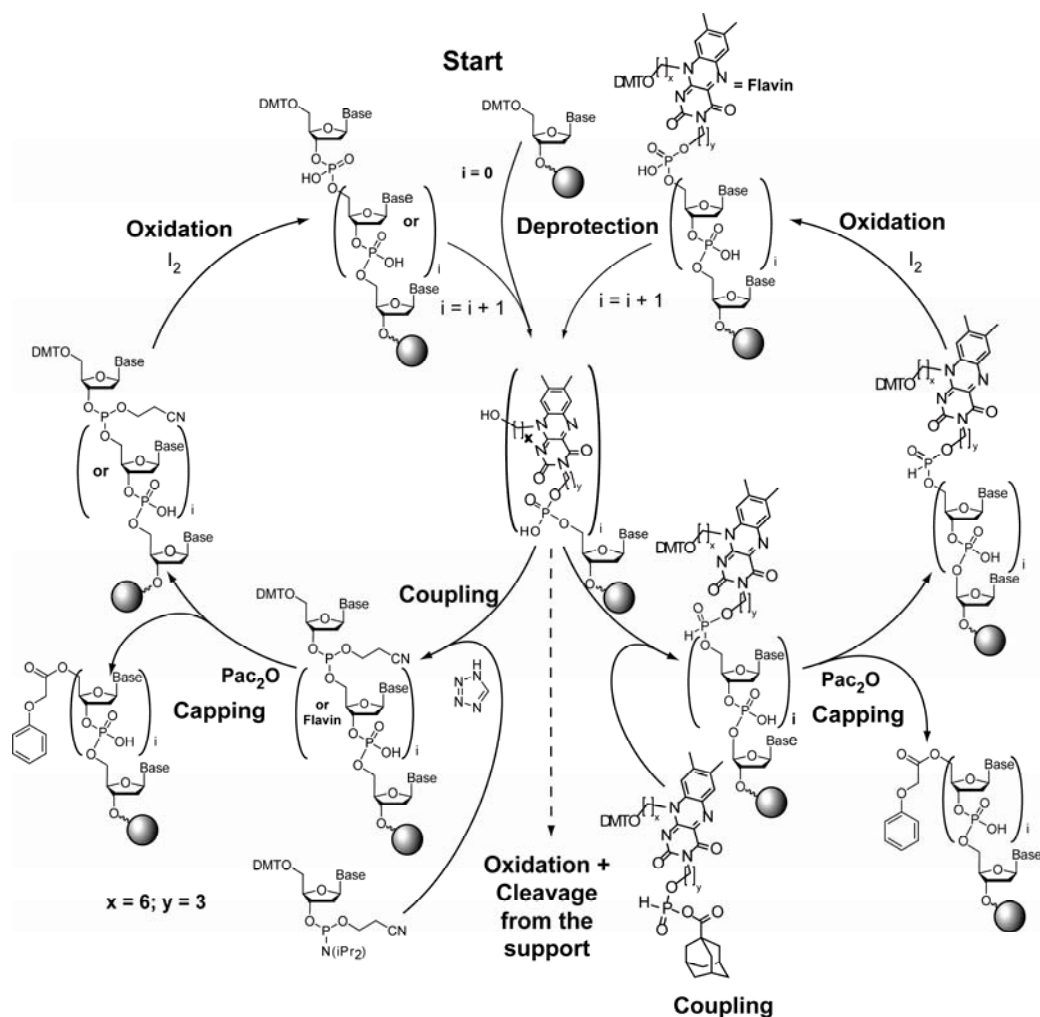


a) pyridine, 19 h reflux; b) H₂, Pd/C; c) HOAc, B(OH)₃, alloxan, r.t.; d) DMTrCl, pyridine, r.t. 92%; e) Cs₂CO₃, DMF, 16 h, 84%; f) PCl₃, triazole, N-methylmorpholine, 46%.

Scheme 2.12 Synthesis of the light-triggered flavin electron injector as *H*-phosphonate salt.^[256]

Synthesis of flavin-containing ODNs

The synthesis of the oligonucleotides containing the flavin *H*-phosphonate was performed on an Expedite 8900 DNA synthesizer using a mixed phosphoramidite/ *H*-phosphonate/ phosphoramidite coupling protocol (Scheme 2.13).^[256] This unusual protocol is required because flavin phosphoramidites were found, in previous works, to be efficiently oxidized under aerobic conditions.^[254,255] The synthesis of the flavin ODNs therefore started with standard phosphoramidite chemistry. After cleavage of the DMT-protecting group from the nucleotide that is prior to the flavin, the synthesizer was programmed to pump simultaneously the flavin *H*-phosphonate and adamantoyl acid chloride, the *H*-phosphonate activator. Coupling time of the flavin building block was extended to about 10 min (2 min for standard phosphoramidite chemistry). After coupling of the flavin, the oxidation of the *H*-phosphonate to the phosphate was achieved using iodine (I₂) in H₂O / MeCN / lutidine. For a full oxidation an additional oxidation step was necessary at the end of the synthesis using I₂ in MeCN and *N*-methylmorpholine in H₂O as first oxidation solution and I₂ in MeCN and NEt₃ in H₂O as the second one. The DNA synthesis continued with phosphoramidite chemistry, even in the presence of the unprotected phosphate. Cleavage of the DNA from the solid support and of all nucleobase protecting groups requires, at the end of the synthesis, the treatment of the solid support with a solution made up of NH_{3(aq)} (28 %)/EtOH 3:1 (v/v) at 20°C for 16-20 h. In the presence of Br-nucleotides, incorporated in the oligos from the commercially available phosphoramidite derivatives, the final deprotection step needs to be ethanol free, in order to avoid the nucleophilic substitution of the bromine. Thus, NH_{3(aq)} (28 %) is added to the solid support for 20-24 h, before filtration and evaporation of the solvents. All the oligonucleotides were subsequently purified by reversed phase (RP) HPLC, on a C18 Nucleosil reversed phase column, or by ion exchange chromatography, on a Nucleogel SAX column. After fraction collection, they were characterized by RP HPLC, MALDI-Tof or ESI FT-ICR mass spectroscopy, UV-melting point studies and circular dichroism (CD) spectroscopy. Quantification was generally achieved by UV-spectroscopy of the synthesised ODNs.^[202,257] More details about the analytic methods and results are reported in the *Experimental Part* (Chapter 4).



Scheme 2.13 DNA synthesis cycle using a mixed phosphoramidite / *H*-phosphonate / phosphoramidite coupling protocol.

Single strand test-oligonucleotides

The first attempt to test the validity of the new donor-acceptor couples was achieved by the synthesis of two simple single strands. In these test-oligos the electron donor (flavin) and electron acceptor (BrdA and BrdG respectively) are next to each other (**T1** and **T2** in Figure 2.10). This design was aimed at disclosing the ability of the flavin to reduce the selected acceptors. The distance from the flavin to the brominated base is minimal and the oligonucleotide in solution is probably in a random coil conformation. Thus, the expected electron transfer can be addressed to be in the superexchange regime. Nevertheless, these single strands were needed to adjust the irradiation conditions and to set up the appropriate analysis of the products.

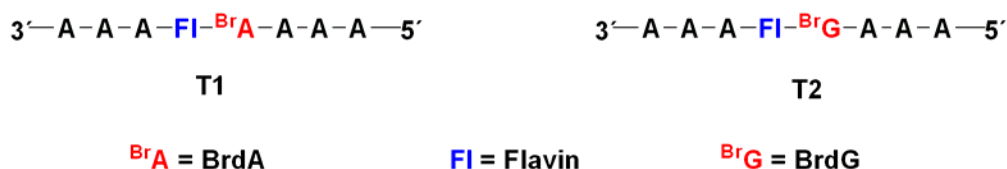


Figure 2.10 Sequence of the two single strand oligonucleotides **T1** and **T2** used as test-probes.

The purified strands **T1** and **T2** were irradiated separately to induce the electron injection by the flavin. To this end they were separately dissolved in irradiation buffer (150 mM NaCl, 10 mM Tris-HCl, pH = 7.4) to a final concentration of $[\text{DNA}] = 20 \mu\text{M}$. The solutions were filled into 1 mL fluorescence cuvettes stoppered with a rubber septum. Argon was then bubbled through the solvent for typically 20 min in order to establish anaerobic conditions. Subsequently, a basic 9.8 mM sodium dithionite solution ($\text{Na}_2\text{S}_2\text{O}_4$, pH = 8) was added to reduce the flavin to the required strong electron donor. Argon was bubbled through the solutions for additional 10 min and finally the solutions were irradiated with a 1000 W xenon lamp equipped with a cooled (10°C) cut-off ($\lambda = 340 \text{ nm}$) filter. A continuous low flow of argon was maintained during the whole irradiation experiment to ensure the homogeneity of the solutions as well as anaerobic conditions. During the irradiation, small aliquots ($20 \mu\text{L}$) were removed from the assay solutions and shaken for 10 min in the dark exposed to air to reoxidise the flavin. The samples were finally analysed by RP HPLC. Figure 2.11 shows the HPLC chromatograms of these first two irradiation experiments.

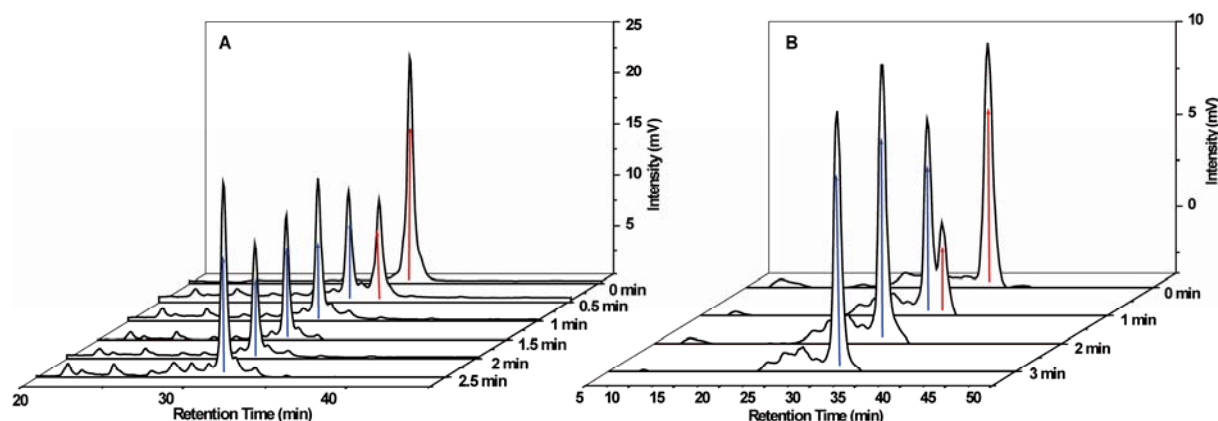


Figure 2.11 HPLC chromatograms of the irradiation experiments of (A) the test single strand **T1** containing Fl-BrdA and (B) the test single strand **T2** containing Fl-BrdG. The parent strand peaks are highlighted with red-lines while the peaks of the debrominated strand have blue-lines.

Interestingly, already after 1 min of irradiation the single strand **T1** containing the BrdA-trap was fully debrominated whereas the strand **T2** with the BrdG-trap could be debrominated to only 70 % in the same time range (Figure 2.11). The analysis of the starting materials ($t = 0$) and of the final products of **T1** and **T2** ($t = 5$ min and 10 min respectively) was achieved by MALDI-ToF mass spectrometry. The spectra, reported in Figure 2.12, are in a good agreement with the calculated molecular weights. In both cases the debrominated strands (**T1**-Br and **T2**-Br) are the only products formed upon irradiation (in blue, Figure 2.12 A and B respectively). Control experiments established that in absence of dithionite or light no debromination is observed. Consequently, an electron transfer occurs exclusively from the light excited, deprotonated and reduced flavin to the Br-nucleotide traps.

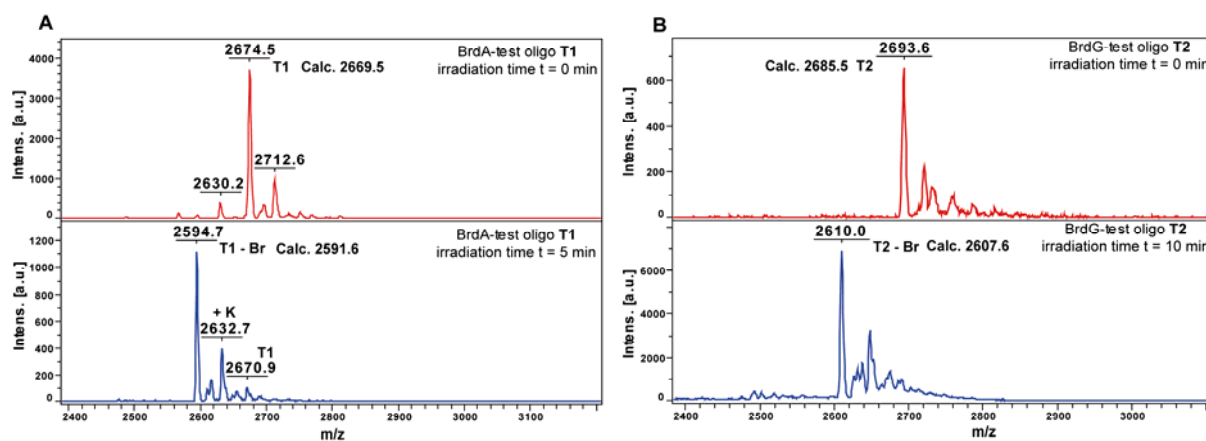


Figure 2.12 MALDI-ToF mass analysis of (A) **T1** before (red) and after (blue) 5 min of irradiation and (B) **T2** before (red) and after (blue) 10 min of irradiation.

This positive result was further confirmed by irradiation of two longer single strands, **T3** and **T4** depicted in Figure 2.13. The irradiation experiments were carried out under the same conditions as previously described. Again the samples removed from the assays were analysed by RP HPLC. However, a clear separation of the peaks was not possible in those cases.

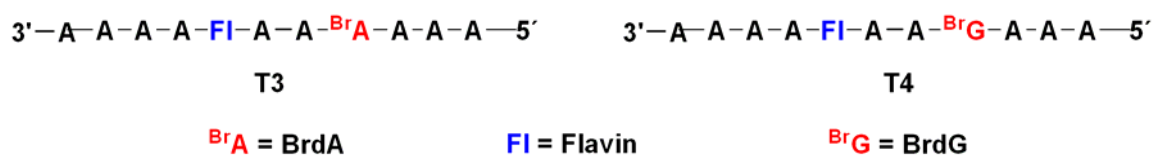


Figure 2.13 Sequence of two single strand oligonucleotides **T3** and **T4** used as test-probes.

The HPLC chromatogram series reported in Figure 2.14 refers to the irradiation of **T4**, which represents the longest oligo with which it was still possible to, at least partially, separate the brominated from the debrominated strand by HPLC. It became clear at this point that, for further investigations, longer oligonucleotides had to be analysed with a different method.

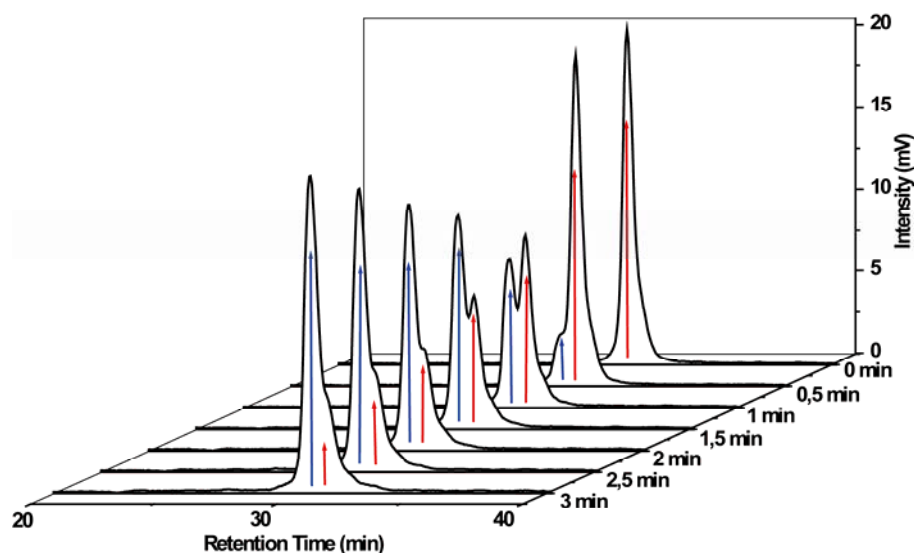


Figure 2.14 HPLC chromatogram series of the BrdG-containing single strand **T4**. The peaks are highlighted with red (parent strand) and blue (debrominated strand) arrows.

Although the quantification of the debrominated **T4** strand was not optimal by HPLC analysis, it was possible to integrate the peaks and plot them versus the irradiation time. The corresponding points describe the curve depicted in Figure 2.15. The slope of this curve through the zero point gives rise to the debromination yield per time of irradiation (so-called **Y**, in $\% \text{ min}^{-1}$). This value can be correlated to the efficiency of the electron transfer process from the flavin donor to the BrdG acceptor. Although the **Y** does not correspond to the absolute rate of electron transfer, it gives a relative estimation of how the electron moves through the DNA. Modulating, i.e., the sequence or the distance between the donor and the acceptor and comparing their resulting **Y** values it is possible to deduce some important features of the EET process, such as the sequence or the distance dependence as described in the introduction.

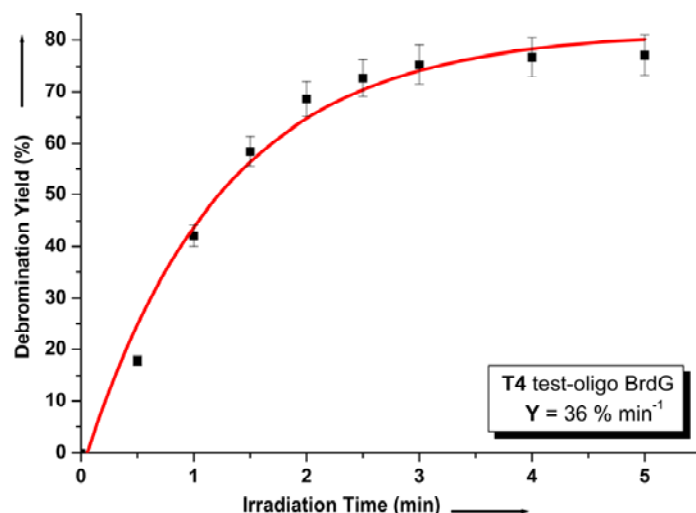


Figure 2.15 Debromination rate relative to the irradiation of **T4**. The amount of debrominated strand was plotted versus the irradiation time. Y = debromination yield per time of irradiation.

In contrast to the ambiguous HPLC, the MALDI-ToF mass analysis allowed for a better interpretation. The sample removed from the irradiation assay after 5 min showed the peaks (without and with counter-cations) corresponding to the debrominated **T4** (B in Figure 2.16, blue peaks). Also the analysis of the irradiation of **T3** gave similar results. The sample removed from the assay after 5 min clearly showed the peaks corresponding to the debrominated **T3**, in which BrdA is converted to dA.

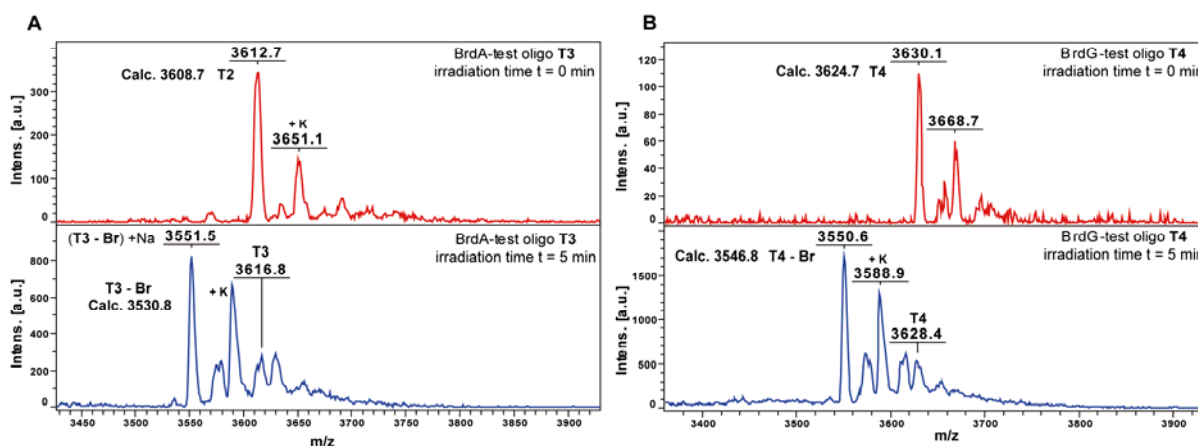


Figure 2.16 MALDI-ToF mass analysis of (A) **T3** before (red) and after (blue) 5 min of irradiation, (B) **T4** before (red) and after (blue) 5 min of irradiation.

Although these first experiments were limited to test the feasibility to synthesize and analyse oligonucleotides containing both flavin and a Br-nucleotide, they highlighted some

main features: (i) the light excited, deprotonated and reduced flavin is able to transfer electrons to both BdA and BrdG acceptors; (ii) the process is, for short oligos, very efficient; (iii) the analysis of the chemical transformation (debromination) occurring upon electron transfer shows that the process is a clean conversion (i.e., no alkaline digestion); (iv) in contrast to the mass analysis, the HPLC analysis of the irradiated samples is limited to short oligos, since the loss of bromine in a large DNA fragment does not allow a full separation of the product from the parent strand.

Hairpins containing a flavin donor and a BrdU acceptor

The next point was to prepare more complex oligonucleotides, which would allow a more profound investigation of the EET process. To this end the hairpin **1a** in Figure 2.17 was prepared using the same oligonucleotide synthesis mixed-protocol previously described. This hairpin contains the flavin electron donor in the loop region and the BrdU acceptor in the stem region. This structure resembles the flavin-containing hairpins of the EET studies described in the introduction.^[217]

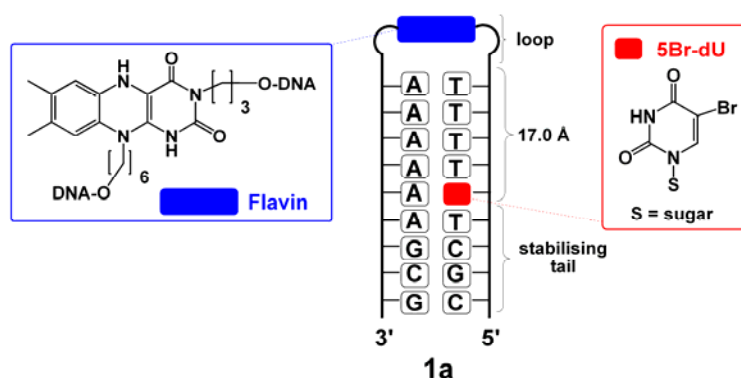


Figure 2.17 Sequence of hairpin **1a** and structures of the flavin-donor and the BrdU-acceptor.

The hairpin was designed to ensure that the electron transfer proceeds through a hopping mechanism where the intermediate base pairs function as charge carriers.^[112,210] Four A:T base pairs between the flavin donor and the BrdU acceptor were used to this end, affording a distance of about 17 Å. Moreover, the tail of the hairpin is G:C rich in order to enhance the stability of the duplex part. After the automated solid phase synthesis, the deprotection from the solid support was achieved using mild conditions ($\text{NH}_3(\text{aq})$ (28 %), 24 h) as already described for the test-oligos. The HPLC purification yielded a clean hairpin as reported in Figure 2.18, where the chromatograms of **1a** are depicted before and after the purification.

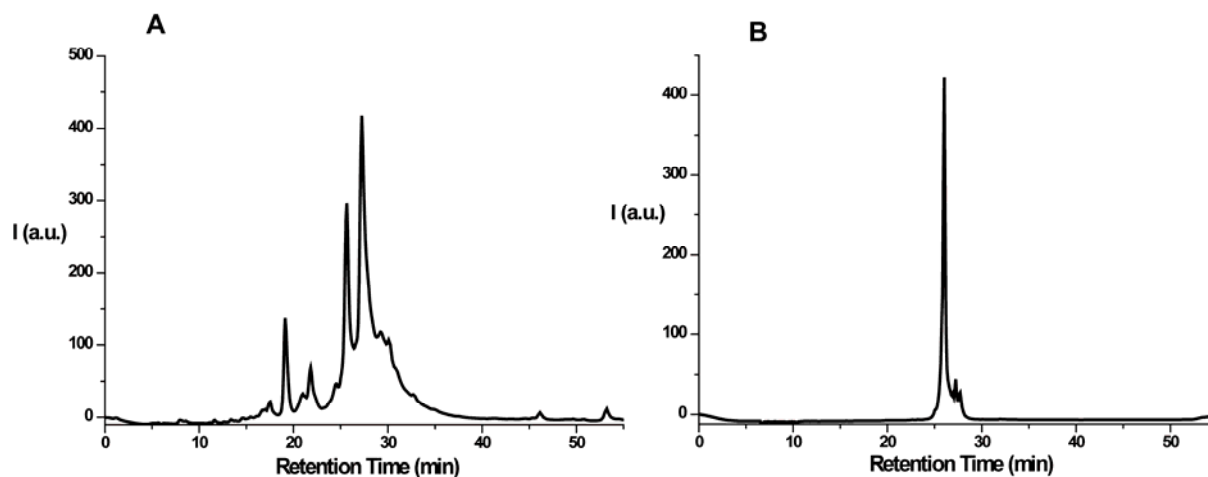


Figure 2.18 Analytical HPLC chromatograms of hairpin **1a** after solid phase synthesis (A) and after HPLC purification (B).

Further analyses were needed in order to evaluate the stability and the conformation of the hairpin in solution. To this end the hairpin **1a** was dissolved in the appropriate buffers (see *Experimental Part* for buffer compositions) and analysed by UV and CD spectroscopy. The melting point resulting from the thermal denaturation monitored by UV spectroscopy at 260 nm was found to be very high ($> 74\text{ }^{\circ}\text{C}$) indicating a relatively undisturbed duplex structure (Figure 2.19, A). On the other hand, the CD spectrum shows bands at ca. 280 nm (maximum) and at ca. 250 nm (minimum), typical for a B-DNA conformation (Figure 2.19, B).^[258]

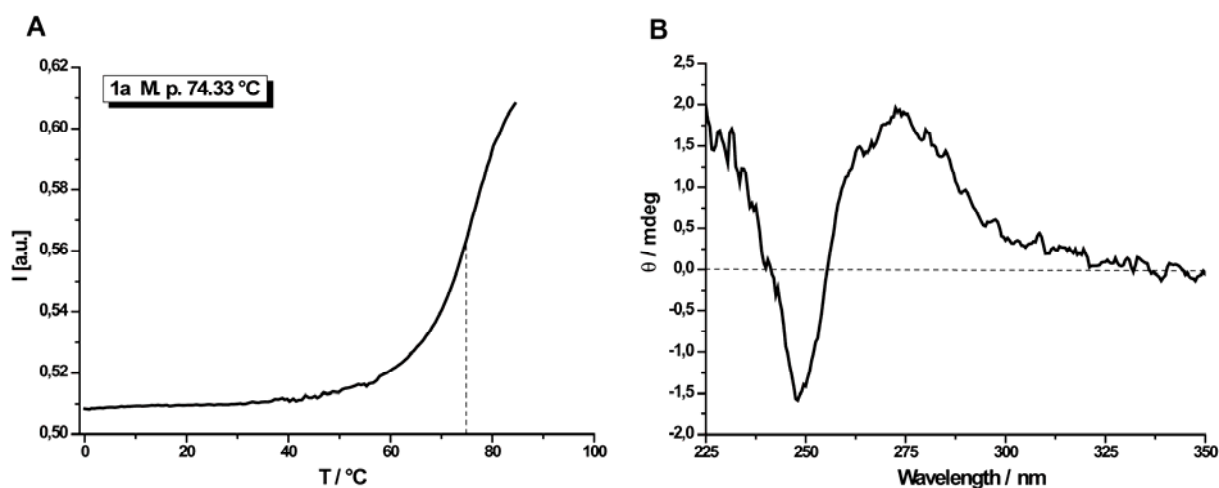


Figure 2.19 UV melting curve (A) and CD spectrum (B) for the purified hairpin **1a**.

Finally the MALDI-Tof mass spectrometry confirmed the nature of **1a** with a mass of 6040 Dalton ($M + Na$), which is in a good agreement with the calculated mass of 6021 Dalton (Figure 2.20).

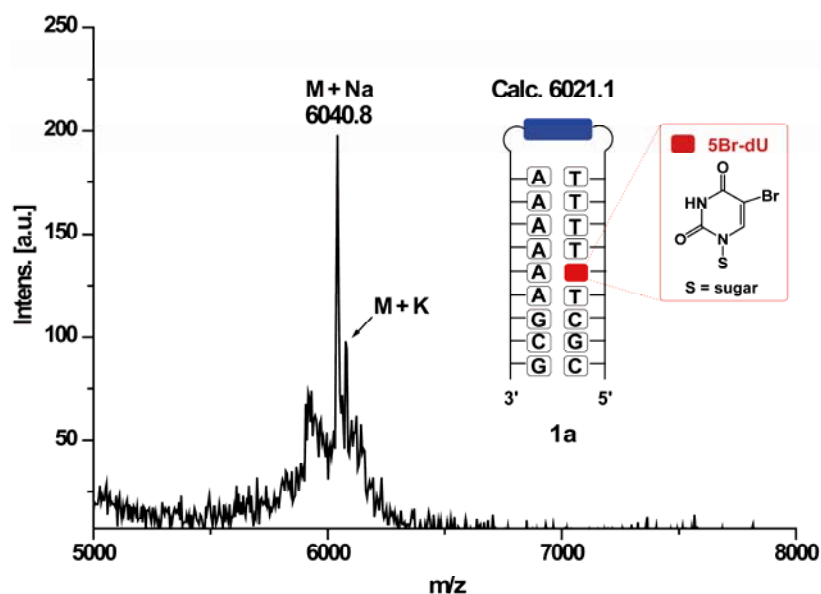


Figure 2.20 MALDI-Tof spectrum of the purified hairpin **1a**.

Hairpins containing a flavin donor and BrdU, BrdA or BrdG acceptors

Based on the positive results obtained with the hairpin **1a**, three series of five flavin-containing hairpins were prepared. They contained the usual light dependent flavin electron injector placed in the loop region of the hairpin and one of the three electron acceptors selected for this work (BrdU = series a, BrdA = series b and BrdG = series c) positioned in the stem region at a distance of about 17 Å to the flavin. While the tail is maintained in every hairpin, the region between the donor and the acceptor was systematically changed in order to study the sequence effects on the EET and the influence of different bps on the trapping efficiency. In Figure 2.21 the hairpin sequences are depicted together with the structure and the position of the electron traps used. The hairpins type-1 (**1a**, **1b** and **1c**, Figure 2.21, B) contained a homo-A:T stretch between the flavin donor and the Br-nucleotide acceptors (BrdU, BrdA and BrdG respectively). In hairpins type-2 and type-4 one of the A:T bps was replaced by a G:C bp at different positions. Finally, in hairpins type-3 and type-5 two of the A:T bps were replaced by two G:C bps at different positions. During the hairpin design it was also intended to compare the EET efficiency through homologous sequences, such as hairpins type-2 and type-4 and hairpins type-3 and type-5. This design was aimed at

evaluating how the G:C bp position in the sequence would affect the efficiency of the EET process.

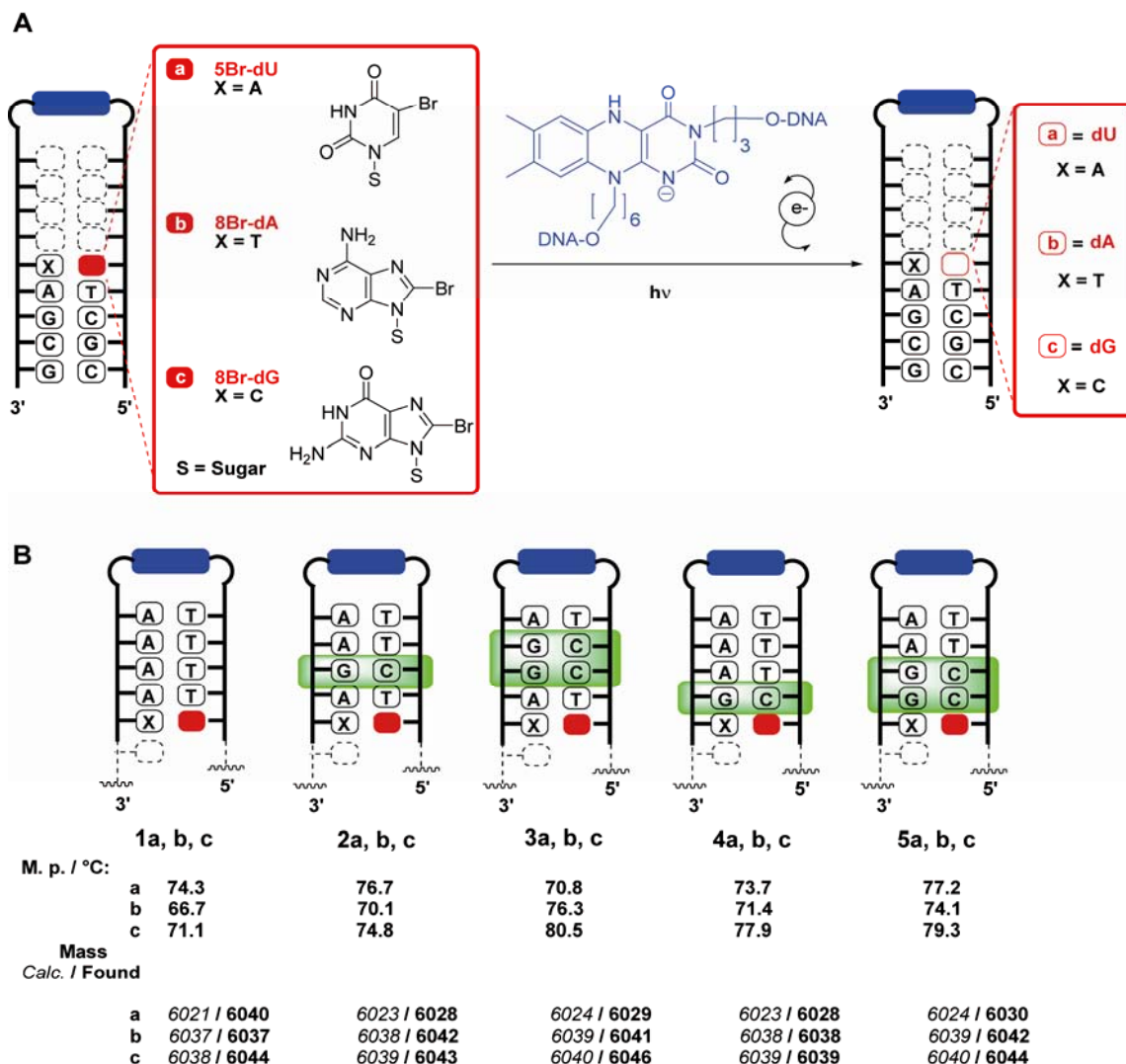


Figure 2.21 DNA hairpin models 1-5. (A) Blue rectangles represent the flavin electron donor in the reduced and deprotonated form. The red squares represent the three different electron traps: a = BrdU. b = BrdA. c = BrdG. The trap counter bases are indicated as X. (B) Sequences of hairpins 1-5 for the three series (a, b and c). In blue and red the flavin and the traps, respectively. Highlighted in green are the number and the position of G:C bps. Melting points and calculated (italic) and found (bold) masses of the hairpins.

All 15 hairpins depicted in Figure 2.21 were synthesised, purified and characterised by the same procedures as used for the previous hairpin **1a**. All of them show melting points significantly above room temperature (Figure 2.21). The MALDI-Tof mass analyses are in good agreement with the calculated values as reported in the lower part of Figure 2.21. In addition, the circular dichroism measurements of all the hairpins show positive bands around

280 nm and negatives bands around 250 nm, consistent with the formation of a B-DNA structure in solution in all cases (Figure 2.22).

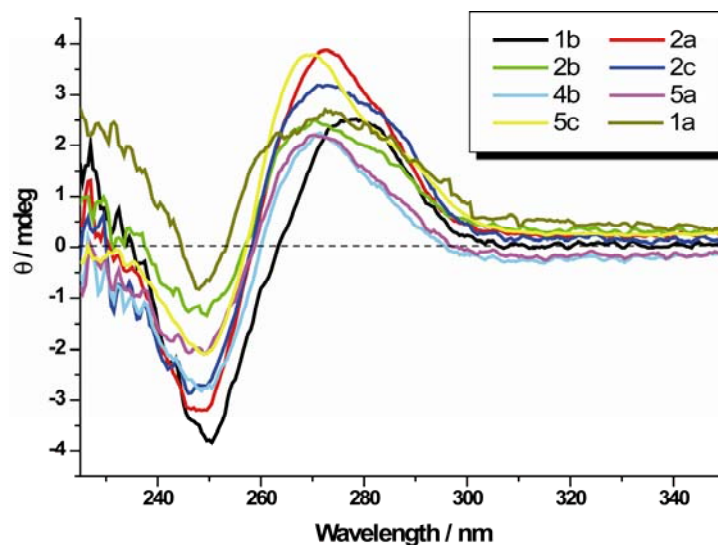
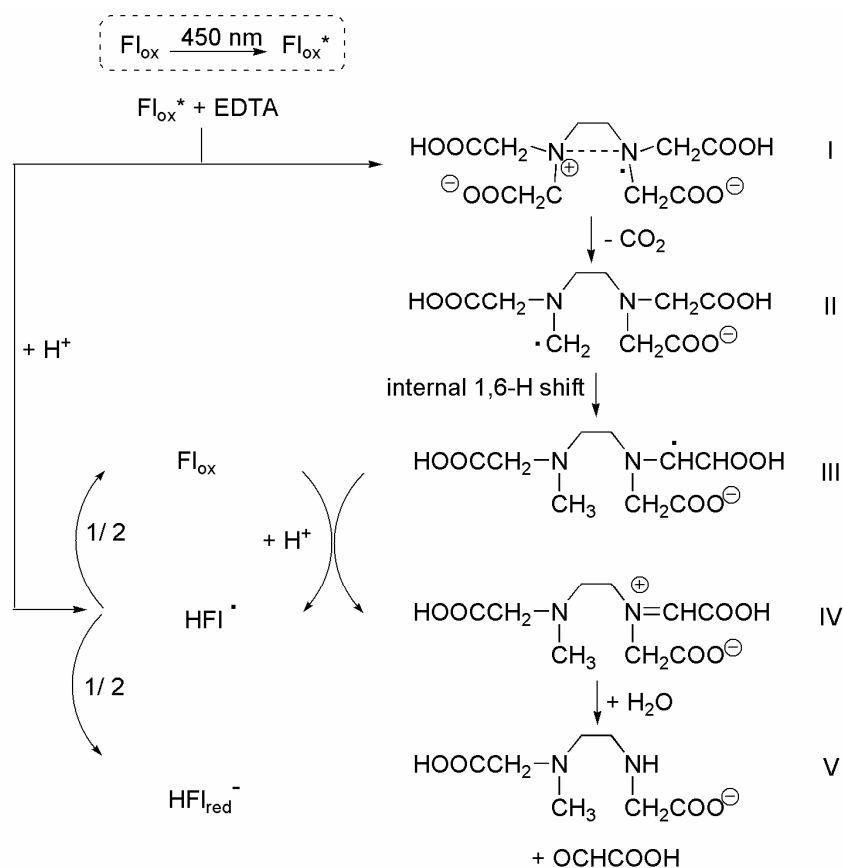


Figure 2.22 Selection of CD spectra from the hairpins used in this work.

Reduction of the flavin

As already described, in order to have a strong electron donor it is necessary to light-excite the reduced and deprotonated flavin. The flavin was reduced with dithionite ($\text{Na}_2\text{S}_2\text{O}_4$) in previous studies and in the aforementioned test-oligos.^[203,209,256] However, it was observed in the first experiments carried out with the test-oligos and the hairpins of Figure 2.21 that dithionite reduction inhibits the EET process at longer than 5 min irradiation times, confirming previous data reported by *Ito* and *Rokita*.^[219] Although a clear explanation for this inhibition was not object of extensive inspection, it might be ascribed to some kind of radical reaction initiated by $\text{S}_2\text{O}_4^{\bullet-}$ or $\text{SO}_2^{\bullet-}$ formed upon irradiation of $\text{Na}_2\text{S}_2\text{O}_4$,^[259,260] which possess a maximum absorption at 330 nm. Adducts between SO_2 and tertiary amines have also been observed,^[261] as well as the formation of H_2 from the irradiation of aqueous dithionite solutions.^[262] In order to achieve the flavin reduction in a more stable and consistent medium, a sodium salt of the ethylenediaminetetraacetic acid (EDTA) was used during the photoreduction process.^[263]

The principle of EDTA-photoreduction was clarified by flash photolysis studies more than 20 years ago.^[263] It consists of several steps, depicted in Scheme 2.14, starting from the photo-excitation of the flavin in its oxidised form, Fl_{ox} , with blue light (450 nm).



Scheme 2.14 Mechanism of EDTA-mediated flavin photo-reduction.^[263]

The excited oxidised flavin Fl_{ox}^* receives an electron from the EDTA salt (step I, Scheme 2.14). The EDTA radical undergoes an irreversible decarboxylation (step II) followed by an internal 1,6-hydrogen shift (step III). These fast processes change the redox properties of the radical making a further donation of an electron possible (step IV). The acceptor of the second electron is the Fl_{ox} which is regenerated by disproportionation of the flavosemiquinone HF1^{\cdot} , generated in the primary one-electron transfer process. From the disproportionation of the flavosemiquinone HF1^{\cdot} , the reduced flavin $\text{HF1}_{\text{red}}^-$ is also generated. Thus, two electron equivalents are transferred from the EDTA to the flavin in the overall reaction to yield the reduced flavin. The whole process is very efficient and can afford the reduced and deprotonated (for $\text{pH} > 6.7$) flavin within a few seconds.

In a typical irradiation experiment EDTA (20 mM) was added to a DNA-hairpin solution ($[\text{DNA}] = 20 \mu\text{M}$, 10 mM Tris-HCl ($\text{pH} = 7.4$) 150 mM NaCl) and irradiated in fluorescence cuvettes under anaerobic conditions for 1 min with white light to photoreduce the flavin. The photoreduction can be monitored by fluorescence spectroscopy following the quenching of the emission band at $\lambda_{\text{em}} = 520 \text{ nm}$ ($\lambda_{\text{ex}} = 366 \text{ nm}$). A more simple monitoring of the

photoreduction is achieved by visual inspection of the mixture containing the hairpins, which turns from yellow colour (flavin in the oxidised form) to colourless (flavin in the reduced state). After photoreduction, the samples were further irradiated with a 1000 W Xe-lamp, equipped with a 10 °C cooled 340 nm cut-off filter, as previously described. For the analysis, 10 μ L samples were removed from the assay solution after defined time intervals, aerated for 10 min, desalted and analysed by capillary electrophoresis as described in the next section.

Although the initial Y values determined using dithionite are very similar to that obtained using EDTA, the latter reduction method allows the establishment of a stable, fully reduced flavin-hairpin system for > 1h. In Figure 2.23 an example of irradiation data using dithionite as the chemical flavin-reductant (blue points) or EDTA as photo-reductant (red points) is reported. In the graphic the points represent the percentage of debrominated hairpin formed upon irradiation under anaerobic conditions. The results in Figure 2.23 confirm that for the first 5 min of irradiation the debromination yields increase with the same efficiency for both reduction systems. The blue (dithionite) and the red (EDTA) points significantly diverge for irradiation times > 5 min. The presence of dithionite clearly inhibits the debromination process at higher irradiation times. The EDTA-containing assay allows longer irradiations.

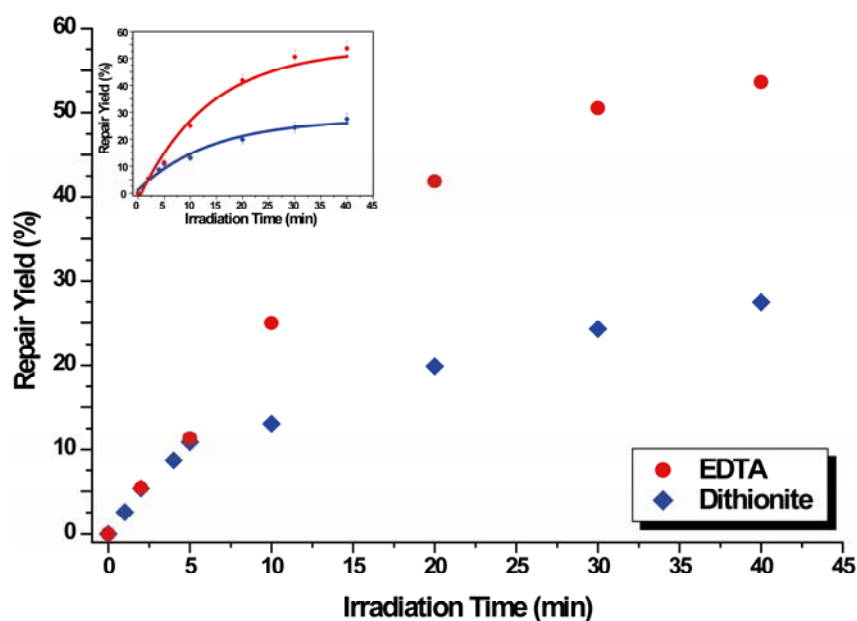


Figure 2.23 Example of irradiation analysis after dithionite-based chemical- (blue) or EDTA-based photo-reduction (red) of the flavin-containing hairpin **1b**. The inset shows a first order exponential fitting to the points.

Capillary electrophoresis

As already mentioned, the analysis of the data by HPLC was not appropriate for the long hairpins used in this study. The capillary gel-electrophoresis (CE) analysis was found to be a good alternative. With this technique some nanoliters of the sample are introduced via an electrokinetic injection into a 30 cm fused silica capillary filled with 6 % polyacrylamide gel in 0.1 M Tris-borate buffer and 2 mM EDTA at pH = 8.4. The very small amount of sample used for the CE analysis allows, when needed, to inject several times the same mixture. Subsequently, for the separation of the mixture, a voltage is applied at the ends of the capillary, typically 9 kV for 40-50 min. This method allows the separation of very small volumes of sample-mixtures. Additionally, the separation power of the CE is based on the different mobility of the compounds present in the mixture. The mobility as a function of the molecular weight, the applied electric field and polymer concentration into the capillary is a peculiar feature of every molecule. This CE properties permitted a full analysis of all the hairpins (**1-5**)**a**, **b** and **c**, before and after irradiation. An example of a CE analysis of an irradiation experiment performed with the hairpin **1a** is given in Fig. 2.24.

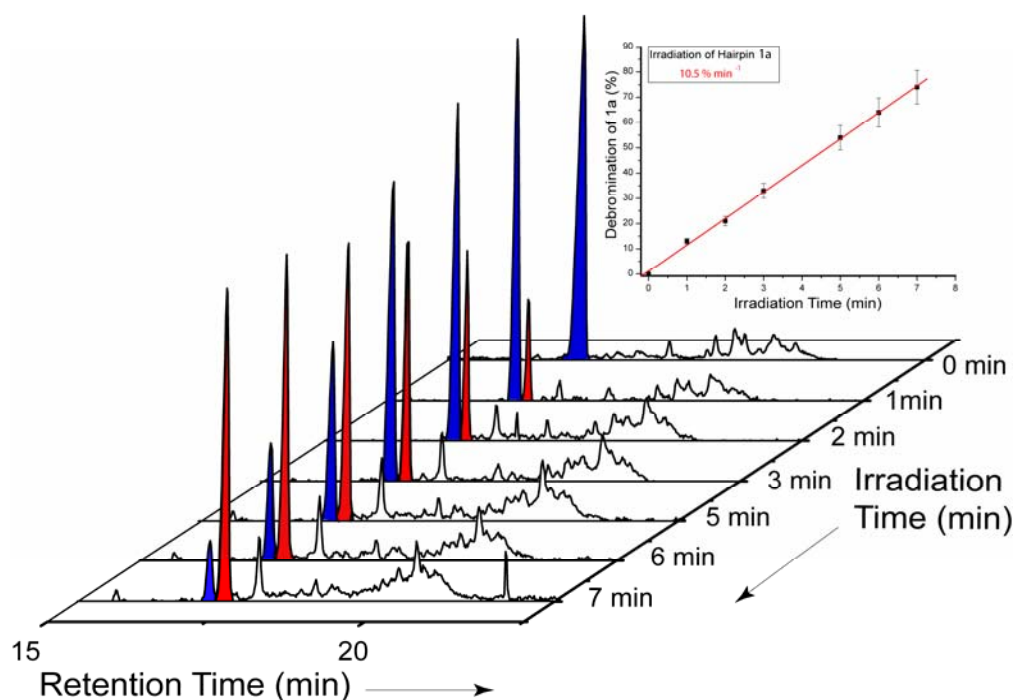


Figure 2.24 Irradiation of hairpin **1a**. Time-dependent debromination of the acceptor inside hairpin **1a**. The parent and the debrominated strand are highlighted in blue and red, respectively. The inset shows the debromination rate ($Y = 10.5\%$ per min) calculated by peak area integration and linear approximation of the data.

In the past, the evaluation of excess electron transfer through DNA with BrdU was performed by observing the strand cleavage induced by hot alkaline treatment before the electrophoretic gel analysis. The alkaline labile site is in this case localised next to the original BrdU trap. The neutral dU radical, generated after one-electron capture, is responsible for such alkaline site formation, as previously described.^[242] Capillary electrophoresis in contrast allowed the direct detection of the loss of Br⁻ anion within the intact 19-mer hairpins after electron capture, as evident from Figure 2.24. CE analysis in the study of EET through DNA is unprecedented and has many advantages compared to the commonly used gel electrophoresis. The gel electrophoresis analysis of the irradiated and alkaline digested strands, reported in early studies,^[33,218,219] was not able to fully report the chemical transformations upon irradiation of the hairpins used in this work. Two main problems prevent the use of the latter analytical technique in the present studies. The first concerns the nature of the strands. Hairpins with a flavin-loop are largely shifted in the gel, making the rationalization of the data difficult. A second but even more important problem concerns the products formed upon irradiation. In the present experimental conditions the main product of the irradiation is the debrominated hairpin, in which the bromine of the acceptors is replaced by a hydrogen (BrdU → dU). These hairpins, not including any unnatural bases, are obviously not sensitive to the hot alkaline treatment. This means that strand break and the subsequent DNA fragmentation will not occur with loss of information.

Analysis of the products

In order to confirm the nature of the products derived from the electron transfer process, MALDI-Tof analyses were carried out. Due to the low amount of sample injected in the CE capillary, the same samples used for CE analysis could also be analysed by MALDI-Tof mass spectroscopy. The resulting molecular weights are in a good agreement with the calculated values for the brominated and debrominated strands. A representative example is reported in Figure 2.25, where the hairpin **1a** is analysed before and after the irradiation. It is worthwhile noting that EET through hairpin **1a** induces a complete debromination of the strand within the first 10-15 min (75 % after 7 min, Figure 2.24). After 20 min of irradiation, no other main peaks were detected by MALDI-Tof beside the peak corresponding to the debrominated hairpin (**1a** -Br). This is in sharp contrasts with previous data reporting the formation of an alkaline labile site, generally an abasic site, generated from BrdU after one-electron capture. The reason of such a difference between the present results and the previously reported data

using BrdU as electron acceptor^[33,218,219] can probably be attributed to the media used for the assay.

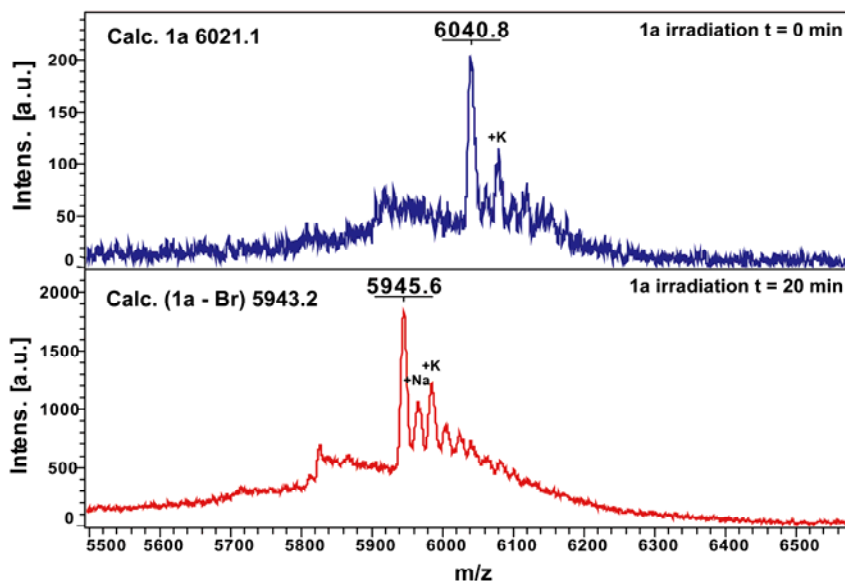
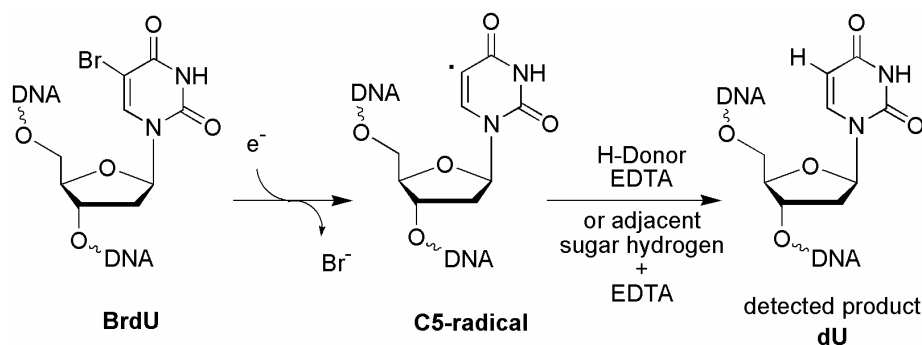


Figure 2.25 Comparison of the MALDI-ToF spectra of hairpin **1a** before (blue) and after 20 min of irradiation (red).

The hydrogen atom needed for the reduction of the nucleobase radicals formed upon one-electron capture is quite likely to be donated by the EDTA present in the solution. With these results a new scenario can be described in which the neutral radical generated from the debromination of the Br-nucleoside acceptors does not generate an alkine labile site.

One-electron reduction of BrdU

In the case of BrdU, the neutral radical probably abstracts a hydrogen atom from the EDTA present in high concentration in the solution (Scheme 2.15).

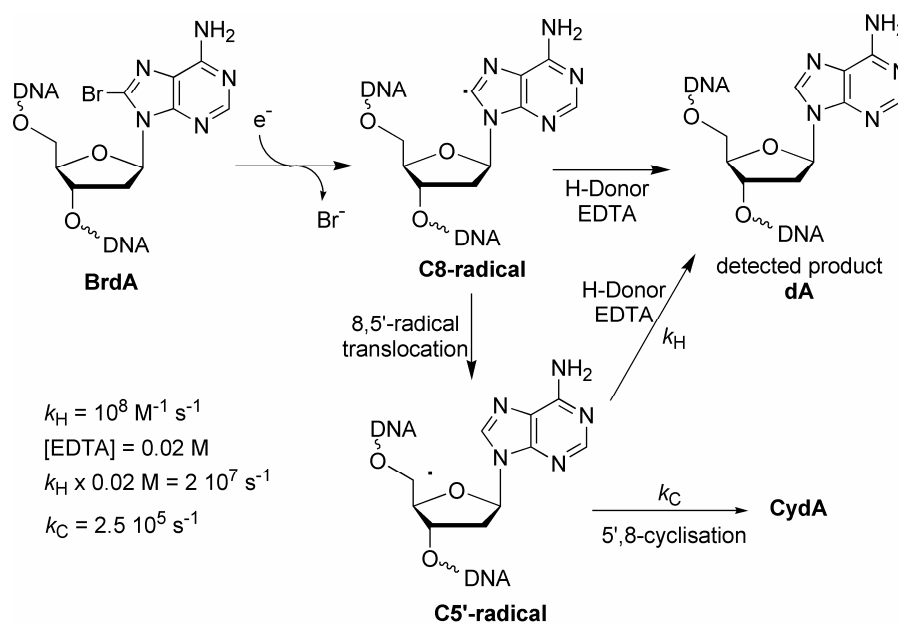


Scheme 2.15 Generation of uridin-C5-yl radical and its reduction by hydrogen abstraction from EDTA.

As an alternative, hydrogen abstraction is possible from adjacent sugar moieties as described in Chapter 1 and in Scheme 2.9 (pag. 26). Nevertheless, also in this case it is possible to assume a subsequent hydrogen abstraction from the reducing medium (EDTA). A small part of sugar-radicals that diverge from this pathway are probably responsible for a small percentage (< 10%) of hairpin degradation. Degradation products were in fact detected by CE analysis, but only for the BrdU-containing hairpins.

One-electron reduction of BrdA

In the case of the BrdA acceptor the neutral C8 radical can mainly react via two different pathways. A direct hydrogen abstraction from EDTA yields the detected natural dA,^[27] whereas an intramolecular hydrogen abstraction (or radical translocation) gives rise to the C5' radical (Scheme 2.16)^[25-27,78]. The latter radical translocation can be strongly affected by the DNA steric demand.



Scheme 2.16 Generation of adenosine-C8-yl radical and the two possible pathways for the formation of the detected 2'-deoxyadenosine, dA. The formation of 5',8-cyclo-2'-deoxyadenosine (CydA) is not favoured by the kinetic data in which $k_C < k_H$.

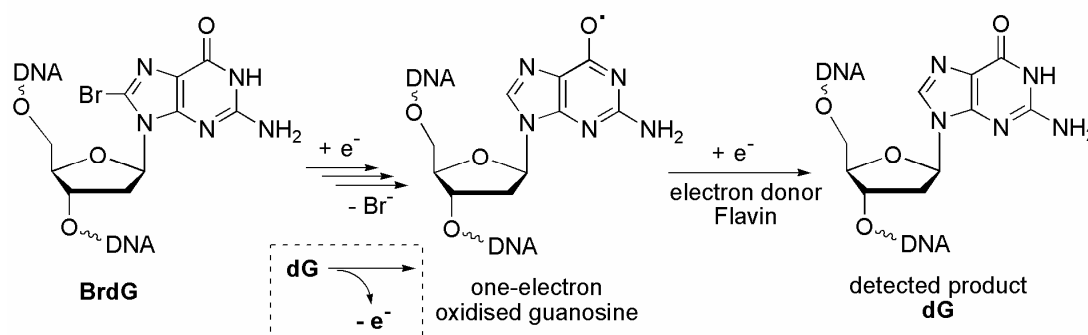
If generated, the C5' radical could attack the N7-C8 double bond in the above mentioned cyclisation reaction with a rate constant of $k_C = 2.5 \cdot 10^5 \text{ s}^{-1}$ at the nucleoside level.^[26] On the other hand, the rate constant for the reaction of the C5' radical with EDTA to give the natural nucleobase is unknown, but expected to be in the order of $k_H = 10^8 \text{ M}^{-1} \text{ s}^{-1}$. Since during the irradiation experiments the EDTA concentration is relatively high (20 mM), the H-abstraction could be favoured and the cyclisation process does not take place. The analysis carried out by

MALDI-Tof is not able to reveal the presence of the 5',8-cyclo-dA inside the irradiated hairpin since only two mass units distinguish the cyclo compound from the natural dA. However, also the LC-MS analysis of the enzymatic total digestion of irradiated mixtures did not show any cyclic compound. The formation of the C5' radical by radical translocation, verified at the nucleoside level,^[25,26] has probably a minor effect in the DNA environment. The geometric organisation of the nucleotides inside the DNA structure may interfere with such *intra*-molecular hydrogen abstraction reaction, favouring alternative pathways for the C5' radical.

The source and position of the hydrogen (C8 or C5') in the acceptor nucleobase might reveal important mechanistic features. Experiments carried out in deuterated media, followed by total digestion and mass analysis, could not clarify this point. In an alternative approach to solve the problem, the use of reducing media should be avoided in order to avoid the reduction of the radical. Therefore, a different electron donor is required to this end.

One-electron reduction of BrdG

When BrdG is reduced by the addition of one electron, elimination, protonation and tautomerization may occur as already described in Scheme 2.11. (pag. 28)^[53,54] The resulting neutral radical chemically corresponds to the one-electron oxidised and deprotonated dG (Scheme 2.17). This radical requires an electron to generate the reduced form, the natural dG. In the hairpin-systems used in this work, the flavin injects electrons constantly upon irradiation, providing the electrons necessary to reduce the one-electron oxidised dG[•] to the natural dG.



Scheme 2.17 Generation of one-electron reduced BrdG corresponding to the one-electron oxidised dG (dashed box) and the detected reduction product, dG.

Data collection

The data of all 15 hairpins (1-5)a, b and c were collected in the same way as described for hairpin 1a. In summary, the samples removed from the irradiation assay were shaken in the dark in presence of air and subsequently desalted. The latter step was required in order to have a clean electrokinetic injection, in which charged species, such as DNA molecules, move to the capillary driven by an applied voltage difference (typically 10 kV for 2 sec). Thus, the presence of large amounts of salts in solution interferes with the electroinjection. After CE separation, the peaks were integrated using the instrument software and the percentages of debrominated product hairpins were obtained. Plotting these percentages *versus* the corresponding irradiation time gave rise to a series of points which describe the progression of the debromination as a function of the reaction time. Thus, the value Y describes the rate of debromination that is strictly connected with the efficiency of the EET process. The case of hairpin 1a is reported in Figure 2.26, many other examples can be found in the *Experimental Part*, Chapter 4.

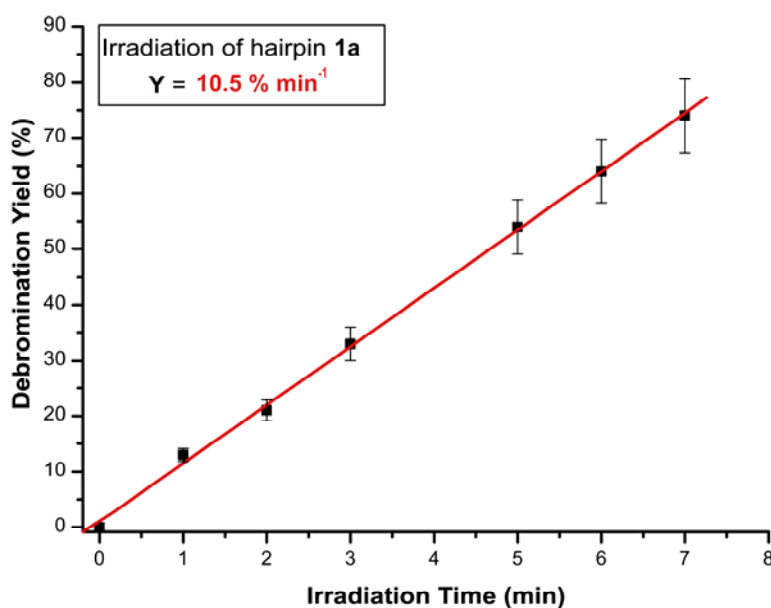


Figure 2.26 Plot and fitting of a linear progression of the debromination yields, obtained by CE peak integration, versus the corresponding irradiation time. The slope of the line gives rise to the debromination rate, Y , in % per min.

The Y values obtained for all 15 hairpins (1-5)a, b and c, are depicted as bar graphs in Figure 2.27. The cylinders related to the debromination rate of the hairpins containing BrdU (series a) are depicted in blue, whereas in red and in green the BrdA- (series b) and

BrdG-containing (series c) hairpins are presented, respectively. They show the time-dependent formation of the debrominated 19-mer hairpins as average values obtained from at least three independent experiments for each hairpin.

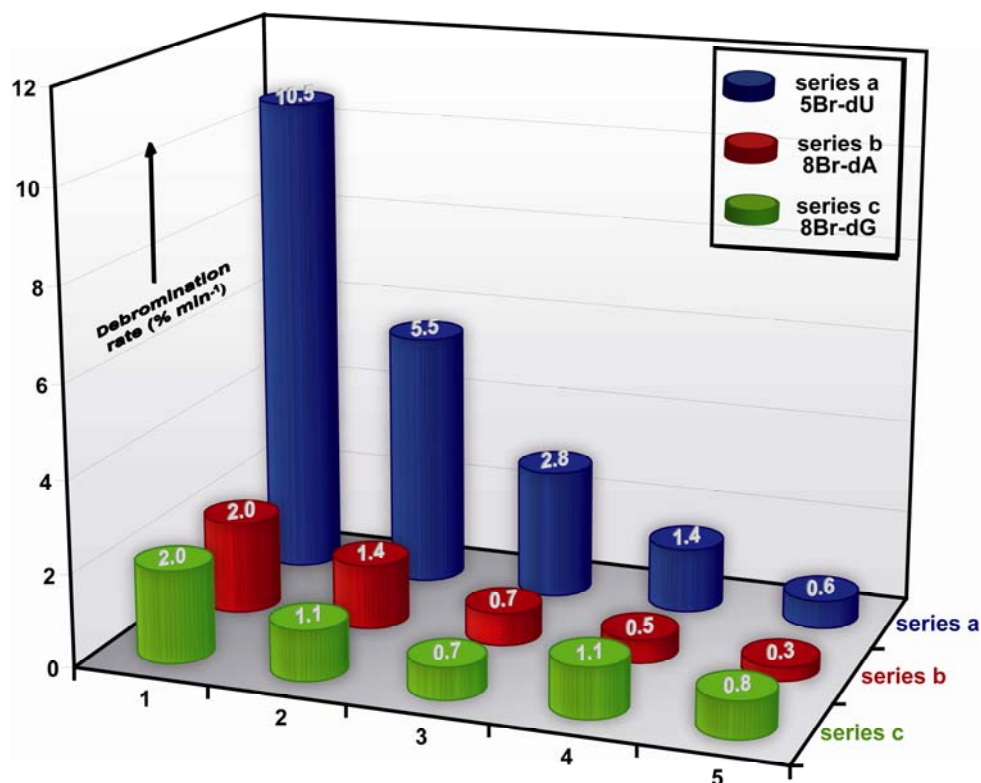


Figure 2.27 Graphic bars for the debromination rates of the hairpins (1-5) a, b, c. The three different series are highlighted in blue (series a, BrdU), red (series b, BrdA) and green (series c, BrdG). The calculated repair rates are given as % of debrominated hairpin formed per minute. Analyses were performed by CE of at least three independent measurements per hairpin. The calculation was carried out by peak area integration of the data up to 5 min of irradiation time followed by linear approximation of the data (for an example see Figure 2.26).

The cylinders in Figure 2.27 give a first idea how large the difference between the three electron acceptors used in this work is. Considering that analogous sequences were exploited for each acceptor, the shown differences are remarkable.

In Figure 2.28 the numeric values of the debromination rate (Y in % min⁻¹) along with the sequences of the analysed hairpins are reported. The errors are calculated as standard deviations of three separate measurements per hairpin.

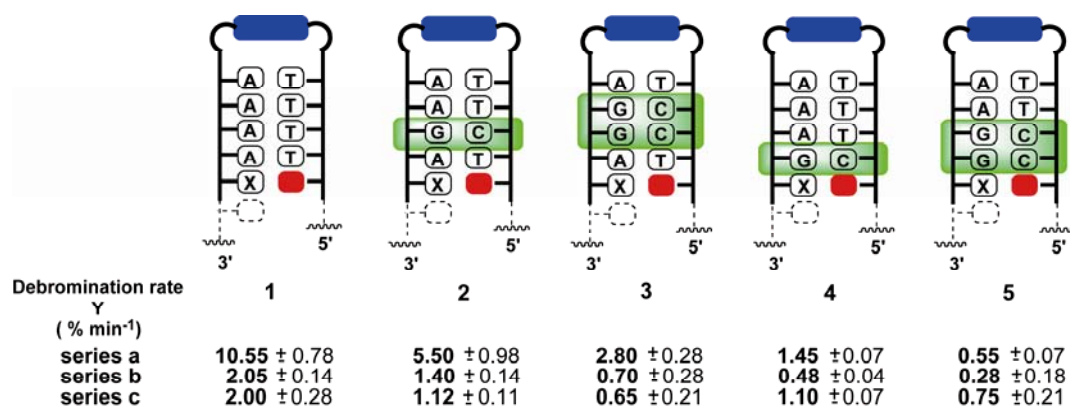


Figure 2.28 Debromination rate values (Y , % min⁻¹) for series a, b and c of hairpins type-1-5 and depiction of the sequence between the donor and the acceptor. The complete 19-mer sequence is reported in Figure 2.21.

Strength of the acceptor

First of all, it is worth to notice how the nature of the acceptor influences the debromination yield and therefore the EET process analysis. The hairpin series type-1 possesses just A:T base pairs between the flavin donor and the Br-nucleotide acceptor. The data show that the debromination rates strongly depend on the kind of the acceptor used in the system. The fastest debromination is observed with BrdU ($Y-1a = 10.5$ % min⁻¹) followed by BrdA ($Y-1b = 2.0$ % min⁻¹) and BrdG ($Y-1c = 2.0$ % min⁻¹). This trend reflects the ease of reduction of these acceptors, but not their one-electron reduction rate constants. The latter are, in fact, all within the diffusion controlled regime, that is $1-2 \times 10^{10} \text{ M}^{-1} \text{ s}^{-1}$.^[25,53,251] This experimental evidence indicates how the redox properties of the species involved in the EET play a major role in the efficiency of the process. Moreover, the differences shown by the traps indicate that the reduction of the acceptor can indeed be the rate determining step. Thus, in the process of electron migration through DNA, which involves electron injection, migration and capture, the latter step might determine the final efficiency of the whole process. Similar conclusions were previously suggested by *Giese* and co-workers,^[230] but, to date, the present work is the first systematic study of how different electron traps influence the EET.

Base sequence dependence

Another very important point concerns the base-sequence dependence of the electron transfer. This feature was studied with the hairpins type-2 and type-3, where one or two A:T base pairs are replaced by G:C base pairs (Figure 2.29). The three different electron acceptors react to these changes in a similar way. For the BrdU acceptor strands **2a** ($Y-2a = 5.5 \% \text{ min}^{-1}$) and **3a** ($Y-3a = 2.8 \% \text{ min}^{-1}$) it could be observed that the Y value drops down by 50 % with every G:C base pair. These data are in agreement with previous studies conducted with the same electron acceptor, but with other donors, as already mentioned.^[33,218,219] It was therefore possible to detect a clear EET sequence dependence in flavin-containing systems for the first time. This observation confirms that in flavin-T=T dimer systems the acceptor and not the electron hopping process may determine the results.

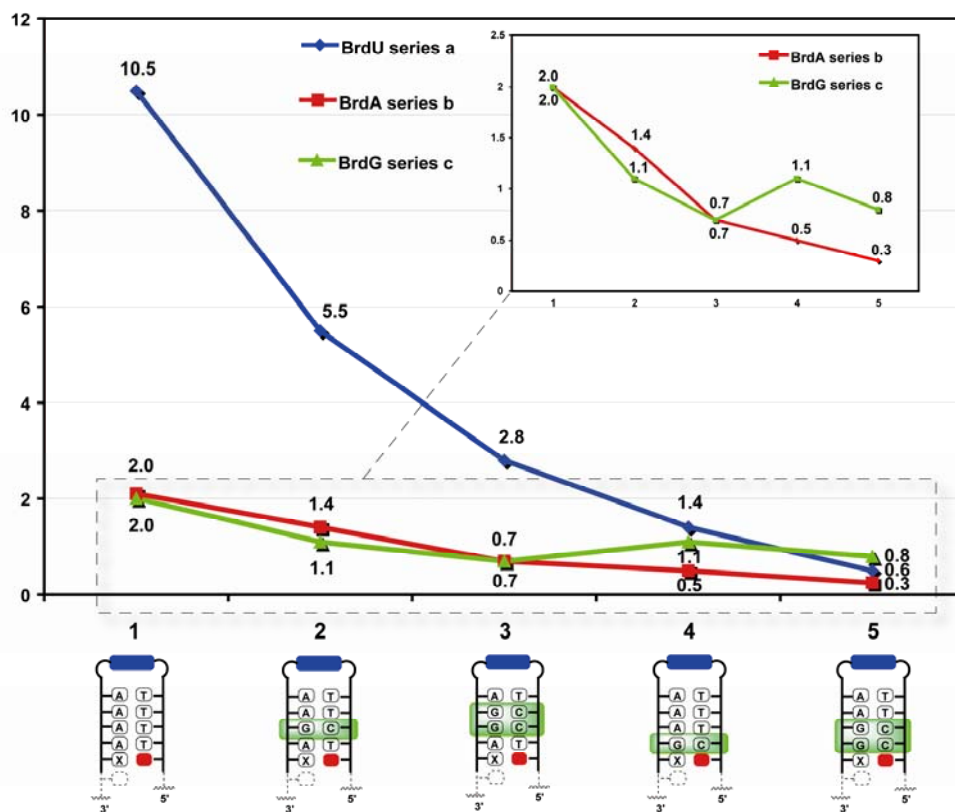


Figure 2.29 Planar profile of the debromination rates. Trends of the EET sequence dependence for the 15 hairpins. The three coloured lines correspond to the three series (a, b and c). The five hairpin sequences used are depicted at the bottom of the Figure. The numbers on the points are the Y values in $\% \text{ min}^{-1}$. The inset shows an enlargement for the series b (BrdA) and c (BrdG).

For the purine acceptors BrdA (series b) and BrdG (series c) the data lead to similar conclusions. The Y values of **2b** and **3b** ($Y-2b = 1.4 \% \text{ min}^{-1}$ and $Y-3b = 0.7 \% \text{ min}^{-1}$) and of **2c** and **3c** ($Y-2c = 1.1 \% \text{ min}^{-1}$ and $Y-3c = 0.6 \% \text{ min}^{-1}$) indicate that the EET efficiency drops by 50 % for the second G:C bp added to the sequence. This trend is maintained also in the case of homo-A:T sequences. Thus, hairpins type-**1** compared with hairpins type-**2** show an almost doubled debromination efficiency ($Y-1a-b-c \approx 2Y-2a-b-c$), although the absolute Y values of series b (BrdA) and series c (BrdG) are more than 4 times lower than for the corresponding BrdU-containing sequences (series a).

G:C bp position-effect

Very important is the unprecedented observation that the position of the G:C bps in the sequence significantly influence the efficiency of the process. Surprisingly, this position-effect seems to be even more important than the number of G:C bps for the EET efficiency. If either one G:C bp or both G:C bps are shifted in a position so that they directly stack on top of the acceptor, dramatic Y reductions are observed. In the hairpins of series a (BrdU), Y values drop from $Y-1a = 10.5 \% \text{ min}^{-1}$ to about $Y-4a = 1.4 \% \text{ min}^{-1}$ with one G:C bp and again to $Y-5a = 0.6 \% \text{ min}^{-1}$ with two G:C bps. The same was observed when BrdA was used as acceptor, although the reduction of the Y values were much less pronounced in these cases (series b). It is worth to note that the aforementioned G:C position-effect could not be observed when BrdG was used as electron acceptor (series c). The inset in Figure 2.29 shows the Y values of the hairpins of series b (BrdA, in red) and of series c (BrdG, in green). The red line decreases from $Y-1b = 2.0 \% \text{ min}^{-1}$ to $Y-5b = 0.3 \% \text{ min}^{-1}$, showing a clear G:C position-effect when $Y-2b$ and $Y-4b$ or $Y-3b$ and $Y-5b$ are compared. The green line (series c, BrdG, Figure 2.29) instead shows a discontinuous trend. The first three points follow the same tendency of the red line with a decrease of about 50 % for every G:C bp added. The last two points rather show an enhancement of the Y values. In these cases there is no influence of the G:C position-effect on the Y values as clearly evident when $Y-2c$ and $Y-4c$ or $Y-3c$ and $Y-5c$ are compared. Indeed, their values are almost identical. Thus, the replacement of A:T bps with G:C bps reduces the Y values, but the G:C position does not affect this reduction when BrdG is the trap.

Interstrand vs intrastrand EET

The last point considered in these flavin-based EET studies concerns the influence of the interstrand vs intrastrand electron transfer. All the previous hairpins used up to this point, were designed in order to have the pyrimidine bases (carrying the negative charge) in the 3'→5' direction from the flavin donor in the same strand (Figure 2.30, left side Scheme). This choice was aimed at using the most efficient negative charge propagation pathway. In order to investigate the interstrand vs intrastrand dependence the hairpin **1a_{inv}** was prepared and irradiated following the same procedures as the previous hairpins. This hairpin was designed to have the same sequence of hairpin **1a**, but in **1a_{inv}** an A:T bp was converted into a T:A bp (Figure 2.30, highlighted in orange). This change ensures that, if the changed base pair is involved in the hopping process, the electron transfer through the A:T bp thymidine will proceed in the counter strand (Figure 2.30, right side Scheme).

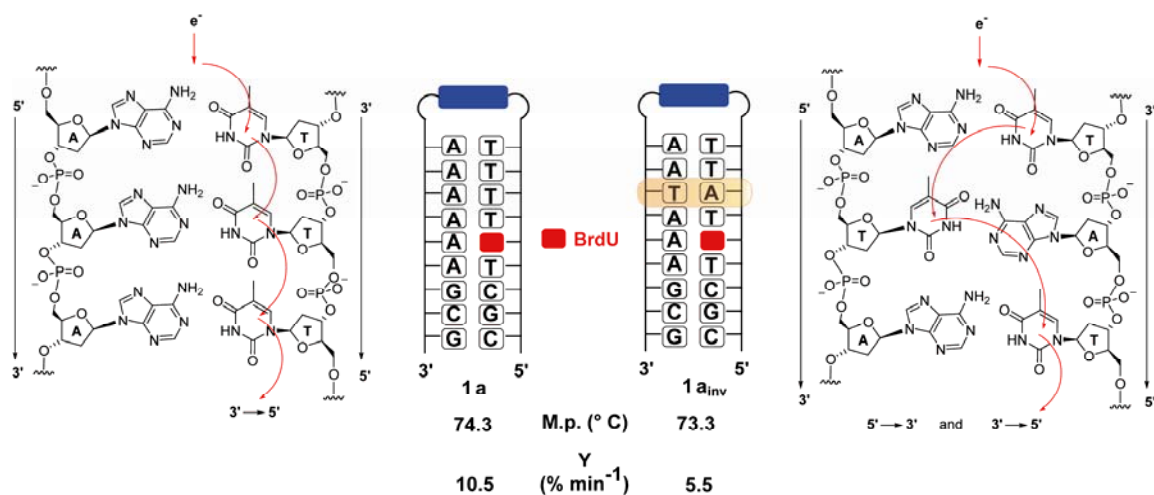


Figure 2.30 Electron transfer interstrand vs intrastrand dependence. In the hairpin **1a_{inv}** an A:T bp is replaced by a T:A bp (highlighted in orange). Melting points (M. p.) and debromination rates (**Y**) are reported at the bottom. On the left and right side a schematic representation of EET through dTs for intrastrand and for interstrand transfer respectively is reported.

The melting points of **1a** and **1a_{inv}** were almost identical, thus the alteration in the sequence of the second hairpin does not influence the stability of the duplex. Surprisingly, in the second hairpin (**1a_{inv}**) the rate of debromination **Y** compared to **1a** was almost halved (Figure 2.30). This single data reveals an important feature of the EET, namely the dependence of the process on the transfer pathway even in flavin-containing systems. A quantification of this effect is also possible and can be compared with the effect of a G:C bp in the sequence.

Conclusions

Three different Br-nucleotides were used as electron acceptors for EET investigations in hairpins containing a flavin donor. From these studies it is now clear, that a G:C bp between the donor and the acceptor reduces the excess electron transfer efficiency approximately by a factor of two. The reason for such a decrease can be ascribed to the partial protonation of the cytosine radical anions $C^{\bullet-}$, generating neutral radicals $C(H)^{\bullet}$, which are unable to transfer the charge further on. This process is in accordance with the cytosine pK_a as already described and was previously suggested (see *Introduction*). However, the base sequence dependence is only fully reported with very efficient acceptors such as BrdU and, to a smaller extent, BrdA. Weaker electron acceptors provide systems with a rate determining electron capture step unable to fully report the process. This is the case for the T=T dimer, as *Giese* and co-workers already described, or the BrdG investigated in this work. The latter seems to lie on the border between strong and weak electron acceptors, where a strong acceptor is able to fully report every modification on the electron transport efficiency of the system. Such divergence between electron acceptors with almost the same one-electron reduction rate constants is probably ascribed to the redox property differences. The efficiency of the traps reflects the ease of one-electron reduction of the the traps. In fact, BrdU is the most efficient and BrdG the last in the reduction potential scale.

More important is the unprecedented observation that the position of G:C base pairs between the donor and the acceptor strongly influences the efficiency of the process. Although every G:C bp reduces the EET efficiency by about 50 %, the position of a single G:C bp in proximity to the trap can decrease the efficiency by more than 85 %. This effect is not observed when BrdG is the electron acceptor, underscoring the role of the trap in the EET efficiency. In order to measure the G:C position-effect, a fast electron trap is required, while a slower trap, such as BrdG, seems to represent the rate determining step of the process. Theoretical studies have suggested that the electron affinity of halouracil residues may depend on their neighboring base pairs and local conformation of the DNA.^[243] Thus, another reason to explain the detected G:C position-effect could again be a modulation of the redox potential of the acceptors by the stacking environment. These results are similar compared to what was observed in the hole transfer process (HT), where stacking of guanines renders the oxidation of nucleobases more efficient.

2.2.2 SED: Single electron donor and multiple acceptors

To further investigate the EET through DNA, it was chosen to initiate the process by the injection of one single electron per strand. Taking advantage of the one-electron injector developed by *Giese* and co-workers,^[230] a series of experiments were designed in order to further clarify the acceptor role in the EET mechanism. The previous results obtained with two T=T dimers in a row opened a new scenario for the repair pathway of this UV-lesion and required a deeper investigation. Furthermore, the availability of very efficient alternative electron acceptors such as BrdU and BrdA represent the appropriate tools for such an enquiry.

DNA duplexes and hairpins containing one electron donor and two different electron acceptors in a row were synthesised. The incorporation of the single electron donor (SED) in the DNA duplexes, developed by *Giese*, ensures the donation of only a single electron into the base-stack of the DNA. A first electron acceptor (T=T dimer) was followed by a second trap (BrdU). The latter was selected for this study due to the higher electron affinity shown in the previously reported experiments. Flavin-capped hairpins, containing two electron acceptors in a row, were synthesised as well. The design of these hairpins was aimed at comparing the electron transfer process initiated by one electron in the SED-containing duplexes with the process in which the flavin ensures a continuous electron injection into the base-stack.

Synthesis of the SED

The synthesis of the single electron donor, reported here only briefly, was achieved following the procedure reported in the PhD-Theses of *Barbara Carl* and of *Thomas Carl* from the *Giese* group (University of Basel, Switzerland).^[264,265]

The pivaloyl acid **8**, which represents the photo-labile radical precursor, was coupled to an amino-modified thymidine **3** for the subsequent incorporation into the oligonucleotide. The compounds **3** and **8** in Figure 2.31 are the building-blocks for the convergent synthesis of the SED.

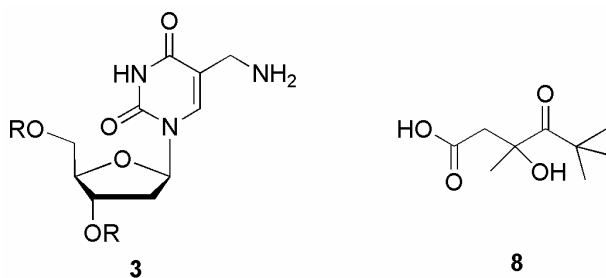
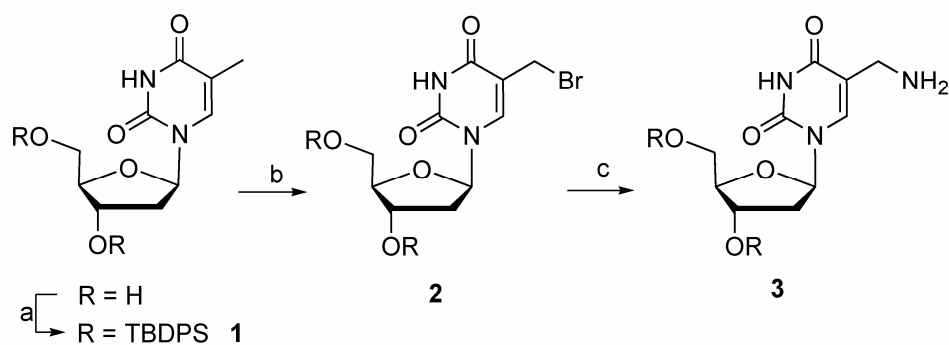


Figure 2.31 Thymidine and pivaloyl building blocks for the synthesis of SED.

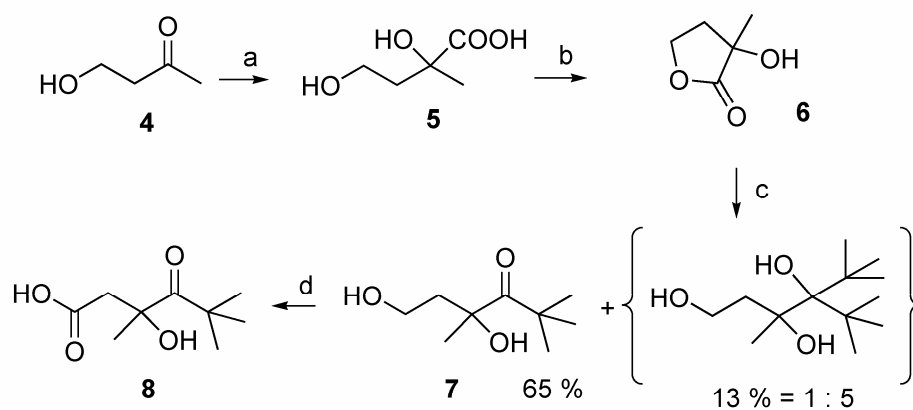
The synthesis starts from the TBDPS-protected thymidine **1**, which was brominated by the addition of a bromine-radical generated from the photolysis of *N*-bromosuccinimide (NBS) in CCl_4 . A silica gel purification leads to the brominated compound **2** with good yields. The amination step was achieved using DMF saturated with ammonia in the presence of a base. The amino-thymidine **3** was isolated pure after silica gel purification with a yield of 52 % (Scheme 2.18).



TBDPS = *tert*-butyl-di-phenylsilyl. a) TBDPSCI, Imidazole, DMF, r.t., 12 h, 96%.
 b) NBS, CCl_4 , $h\nu$ (254 nm), 30 min, 60%. c) NH_3 , DIA, DMF, r.t., 24 h, 52%.

Scheme 2.18 Synthesis of the amino-thymidine **3**.

The synthesis of the pivaloyl acid **8** required some challenging steps due to the high polarity of the products and reagents involved. Specifically, the extraction of the acid **5** from the water phase was performed by a liquid-liquid extraction over 48 h. The resulting dark oil was dehydrated in an dessiccator over NaOH under reduced pressure conditions. The lactone **6** was purified by distillation (132 °C, 10 mbar) with 55 % yield for these first steps from alcohol **4**. The addition of *tert*-Butyl lithium at -100 °C gave a 5:1 mixture of mono- and bis-adducts, which was used for the next oxidation reaction to the acid **8** without separation of the products (Scheme 2.19).

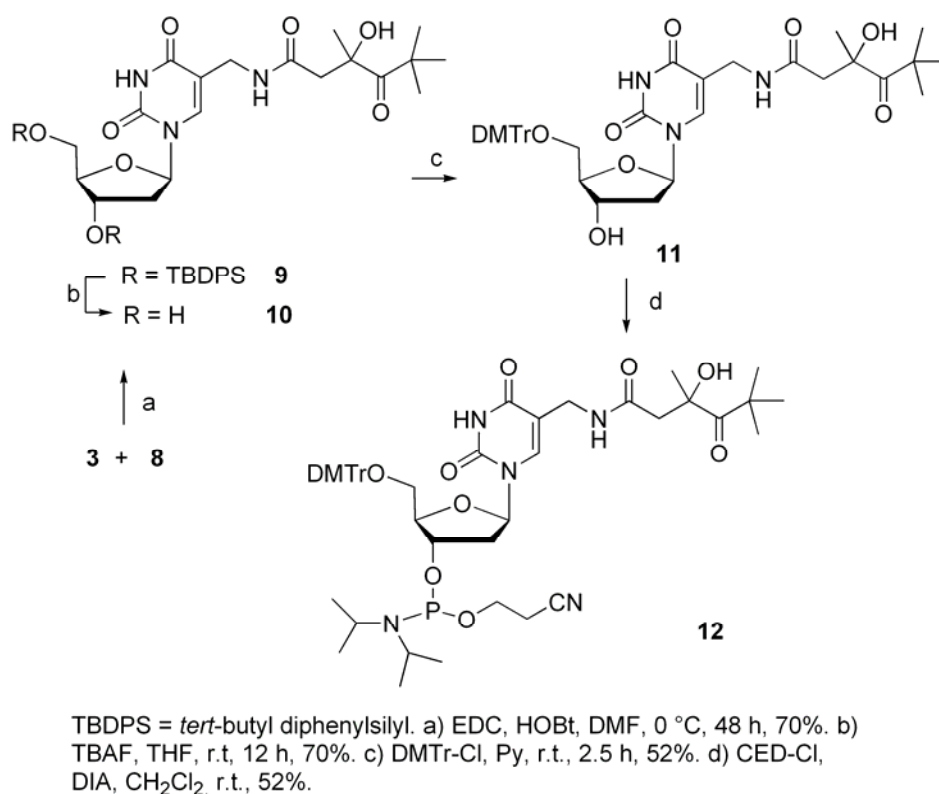


a) 1. NaHSO₃, KCN, H₂O, r.t. 2. HCl conc. b) NaOH, 55 % over 3 steps. c) *t*BuLi, Et₂O, from -100 °C to -40 °C, 79 %. d) TEMPO, NaOCl, NaClO₂, MeCN, pH 6.8-Buffer, 35 °C, 82 %.

Scheme 2.19 Synthesis of the pivaloyl acid **8**.

The coupling step between the modified amino-thymidine **3** and the pivaloyl acid **8** was achieved by a standard amino-acid coupling procedure with a yield generally higher than 70 %. The subsequent total deprotection of the alcohol moieties in 3' and 5' positions was carried out efficiently with tetrabutylammoniumfluoride (TBAF) in THF for 12 h. The 3'-*O*-dimethoxytrityl protection was achieved in dry piperidine using the standard dimethoxytrityl chloride (DMTr-Cl) procedure. The subsequent synthesis of the 5'-phosphoramidite was finally performed using 2-cyanoethoxy-*N,N*-diisopropylaminochlorophosphoramidite (CED-Cl) leading to the building block **12**, ready for the automated phosphoramidite DNA synthesis (Scheme 2.20).

For the detailed experimental part of this multi-step synthesis the reader is referred to the original works of *B. Carl* and of *T. Carl*.^[264,265]



Scheme 2.20 Synthesis of the 3'-DMT, 5'-CED-phosphoramidite SED **12**.

Synthesis of ODNs containing the SED

The electron injector **12** was used for the automated synthesis of the oligonucleotide **S1** containing two other modifications (Figure 2.32). The phosphoramidite **12** was dissolved in dry dichloromethane (DMC) for the automated synthesis instead of the standard dry acetonitrile (MeCN) because of solubility problems. Again, the commercially available BrdU phosphoramidite was used. The T=T dimer acceptor, prepared by *Claudia Gräf* (*Carell* group) possesses an open back bone that allows a fast analysis of the dimer cleavage process, as described in the *Introduction*. The T=T dimer phosphoramidite was incorporated into the ODNs with the open back bone protected as a cyclic silyl ether, as previously reported.^[203,209] The only modification of the previous procedure concerns the final cleavage of these ODNs from the solid support. The presence of BrdU forces to use mild cleavage conditions (NH_{3(aq)} (28 %) in the absence of ethanol). In this case, the deprotection of the silyl protecting group present in the T=T dimer proceeded much slower. Thus, a mild cleavage over five days at 24 °C was necessary to fully remove the T=T dimer silyl group.

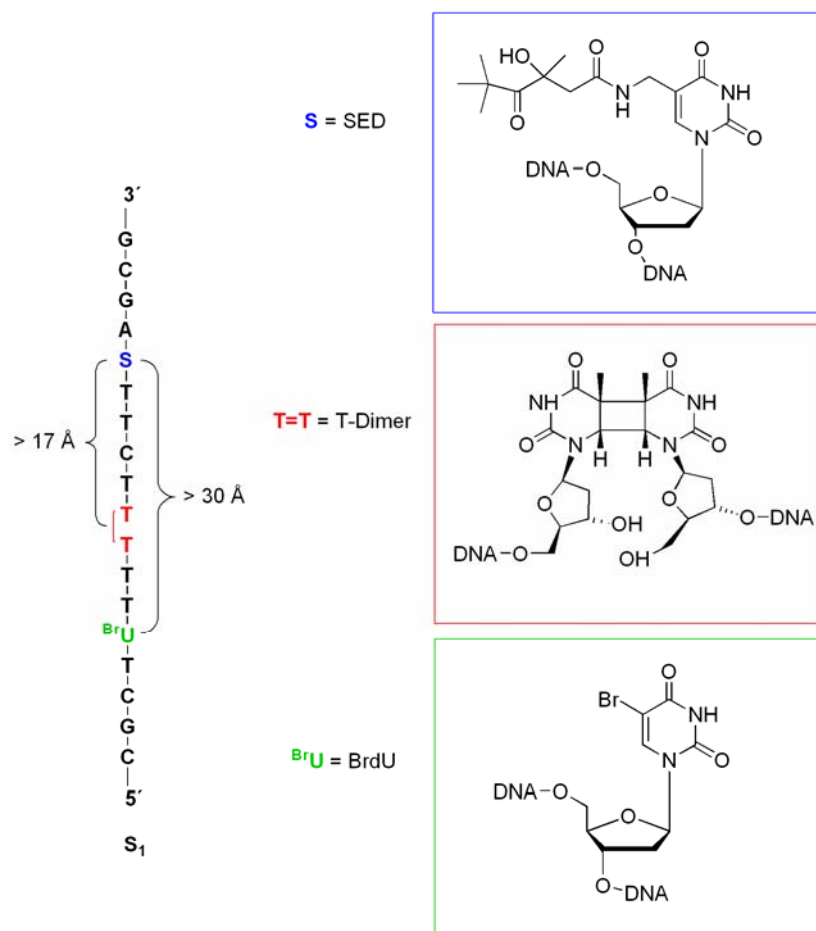


Figure 2.32 Oligonucleotide containing the SED as injector system. On the right side of the Figure the structures of the single electron injector (S), the first electron acceptor (T=T) and the second acceptor (BrdU) are depicted.

The distance of 17 Å between the SED donor and the first acceptor (T=T dimer), calculated for the 4 bps in an ideal B-DNA, ensures that the electron transfer proceeds through a hopping mechanism.^[123] A dC was also placed among the dTs of the first 4 bases after the donor. The second electron acceptor (BrdU), positioned two bases after the T=T dimer, is 30.6 Å away from the SED donor. Also this distance is calculated for an ideal B-DNA conformation with a bp stacking distance of 3.4 Å. Moreover, in the double strand the BrdU is positioned one complete turn of the helix away from the SED donor. This unusually large distance requires a really efficient EET process to cover the distance between the donor and the acceptor. This necessitated the selection of the very efficient BrdU as second electron acceptor.

The purification of **S1** was achieved by RP HPLC and the characterisation by MALDI-ToF mass analysis and UV-visible spectroscopy. In Figure 2.33 the HPLC chromatograms before and after purification of the strand are reported.

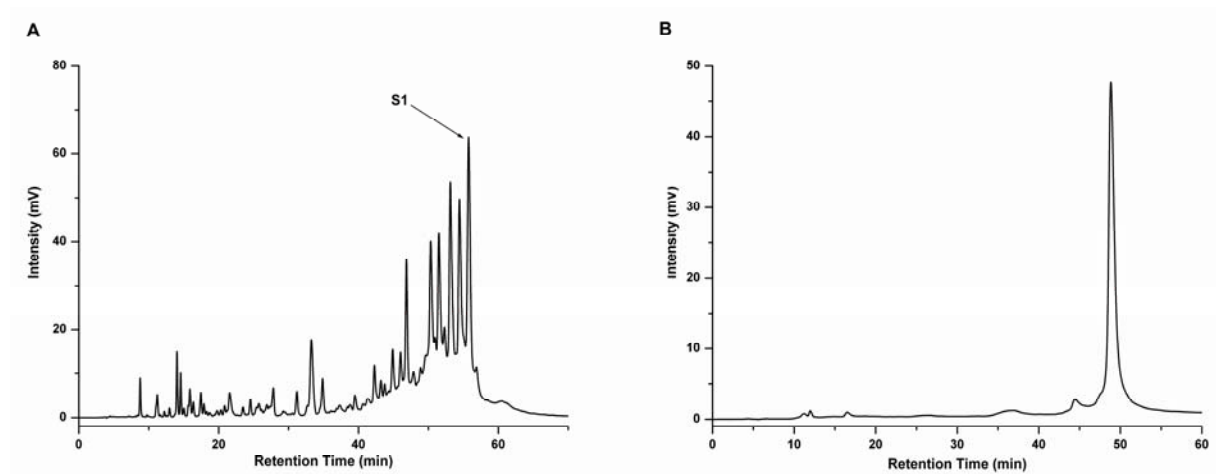


Figure 2.33 RP HPLC chromatograms of the single strand **S1** before (A) and after HPLC purification (B).

The mass analysis of the purified strand **S1** shows a neat peak in good agreement with the calculated mass (Figure 2.34).

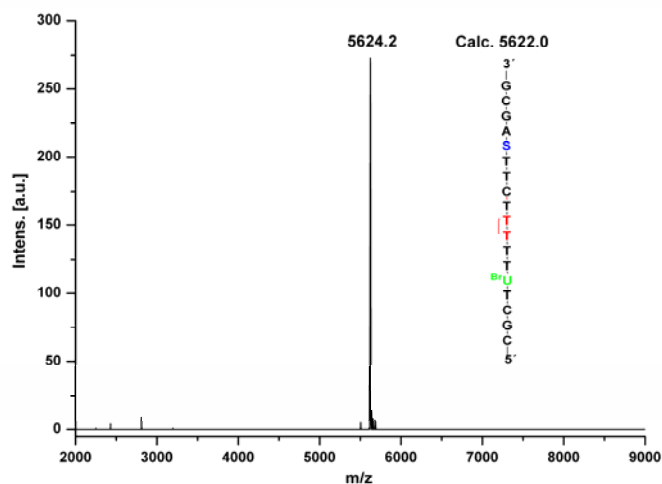


Figure 2.34 MALDI-ToF spectrum of **S1** as single strand after RP HPLC purification and desalting.

The purified oligonucleotide **S1** was hybridised with a full length matching counter strand (**S1-cs**). After UV calculation of the concentration, a 1:1.3 mixture of **S1** and **S1-cs** in buffer

(see *Experimental Part* for details) was hydridised. Subsequently the solution was analysed by CD spectroscopy in order to explore the ability of the oligo **S1** containing three modifications to form a double strand (ds**S1**) in the B-DNA conformation. Indeed, the CD spectrum of the ds**S1** showed the typical positive band around 280 nm and the negative band around 250 nm consistent with the formation of a B-DNA helix (Figure 2.35).^[258]

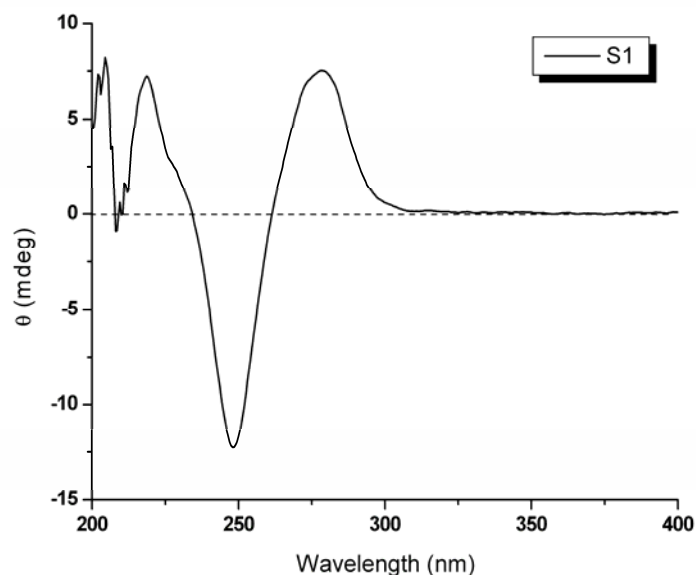


Figure 2.35 CD spectrum of ds**S1**.

Irradiation experiments

The irradiation at 320 nm of SED-containing ds**S1** initiates, as mentioned in the *Introduction*, a cascade of homolysis, charge translocation and deprotonation enabling the final electron injection into the DNA base stack. This process is initiated by a *Norrish* type I photolysis of the *tert*-butyl α -hydroxy ketone of the SED moiety. The product of such a photolysis after one-electron injection is the dicarbonyl-SED depicted in Figure 2.36.

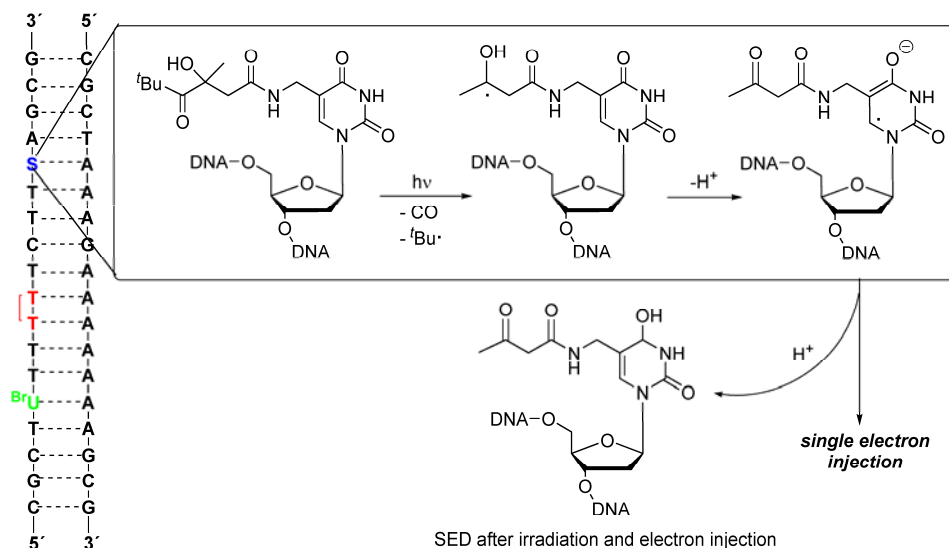


Figure 2.36 Mechanism of photoinitiation of the electron transfer through the irradiation of SED-containing DNA. The photolysis of the injector and the subsequent charge transfer irreversibly transform the SED donor into an inactive dicarbonyl.

The irradiation experiments of ds**S1** for EET studies were accomplished under anaerobic conditions using a 1000 W Xe-lamp equipped with a cooled (10 °C) 320 nm cut-off filter. Quartz cuvettes sealed with a rubber septum to allow sampling were used as reaction vessels. Different concentrations of DNA have been tested ($[DNA] = 3\text{--}30\ \mu\text{M}$ in 0.01 M Tris, pH = 7.4, 0.15 M NaCl). For the analysis, 10 μL (CE) or 20 μL (HPLC) samples were removed during the irradiation from the assay solution after defined time intervals, desalted and analysed by CE or RP HPLC.

HPLC analysis

In Figure 2.37 the HPLC chromatograms of a typical irradiation experiment are reported. The chromatograms of ds**S1** before (black) and after 40 min (red) of irradiation are overlaid in order to detect the newly formed peaks.

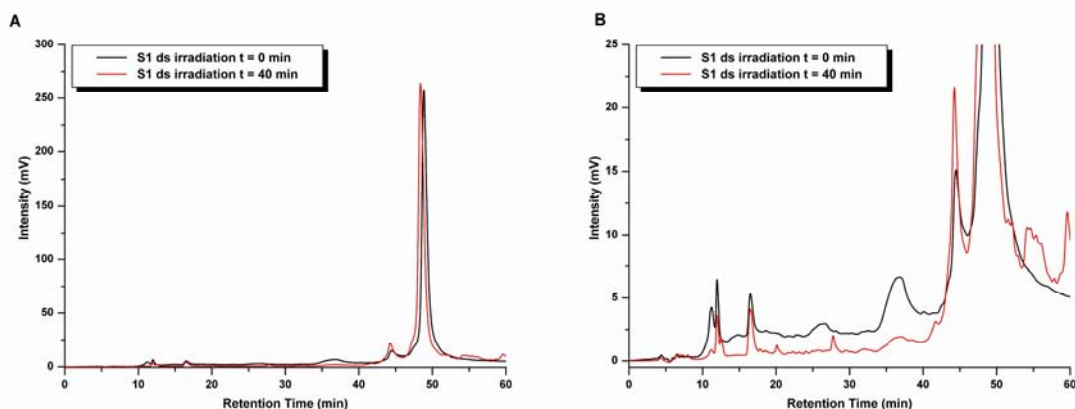


Figure 2.37 Comparison between the dsS1 HPLC chromatograms before (black line) and after irradiation (red line). In **A** the full scale chromatogram, in **B** the enlargement of the low intensity signals. There are no relevant differences between the two chromatograms.

As can be seen from the enlargement B in Figure 2.37, it was not possible to determine the presence of new peaks after the irradiation of dsS1 using HPLC chromatography. Although the chromatogram in red (after irradiation) does not perfectly match with the black trace (before irradiation), it is possible to ascribe every red peak one of the original dsS1 DNA.

CE analysis

An alternative analytic method was required in this case as well, even though, small fragments are supposed to be cleaved off during irradiation.

The samples removed from the irradiation assay were analysed by capillary electrophoresis, after an additional step to remove the excess salt, as described above. The resulting electrophoretic chromatograms are reported as a time-dependent series in Figure 2.38. It is worth to note that the retention time is not a reliable parameter in the CE analysis. In fact, the mobilities of the analytes are the deciding values of the CE, but it is common use to report the analysis in a HPLC-like form. Moreover, a minor limitation of the CE analytic method is the gel inside the capillary that must be exchanged every 5-7 runs. Consequently, the homogeneity of the resulting retention time of the peaks can be affected.

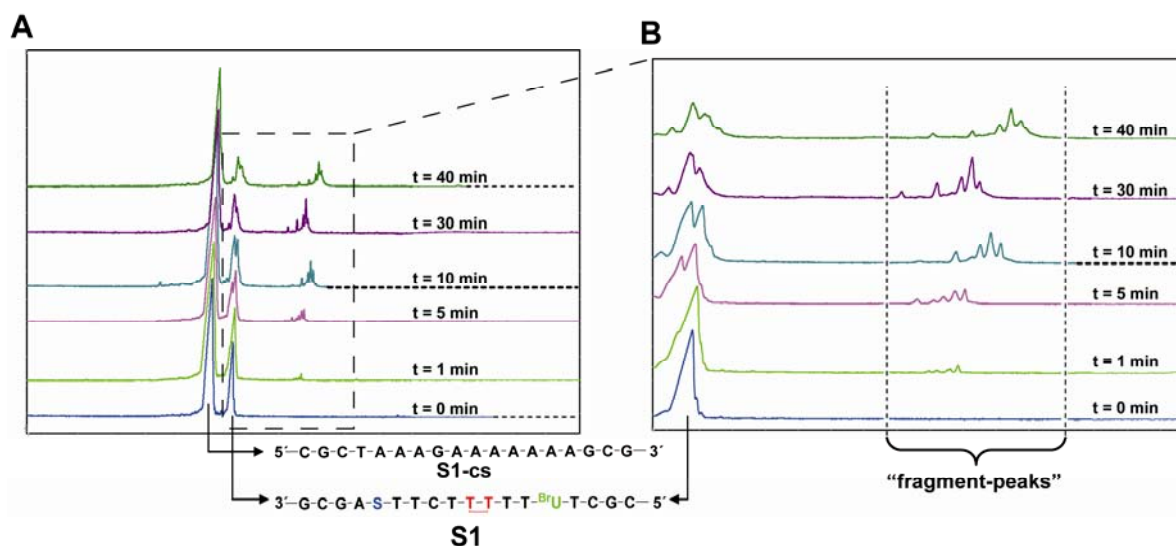


Figure 2.38 CE chromatogram series from $t = 0$ min to 40 min of ds**S1** irradiation as full scale in **A** and enlargement in **B**.

The two main peaks in **A** of Figure 2.38 at the irradiation time of $t = 0$ are the single strand **S1** and its counter strand (**S1-cs**, in excess). During the irradiation only the **S1** peak is consumed to generate other peaks, as evident from the enlargement (**B** in Fig. 2.38). After 5 min of irradiation the **S1** peak gives rise of a second peak with a similar retention time. Simultaneously new “fragments” are formed. The latter are 4-5 peaks, increasing size in the 10 min and 30 min chromatograms. For a longer irradiation time of 40 min the original **S1** peak became a broad signal where it is not possible anymore to clearly distinguish individual peaks. The “fragment-peaks” at 40 min of irradiation are broadened as well. Although the detection of new peaks arising from the irradiation was possible by CE analysis, the nature of these peaks still remains unclear.

Mass spectrometry

In Figure 2.39 the expected fragments deriving from the irradiation of ds**S1** are depicted. The corresponding calculated masses are listed underneath the double strand. Fragment 7, for example, corresponds to the original **S1** after photolysis of the labile SED moiety, thus the mass of **S1** minus the mass of a $t\text{BuCO}(+\text{H})$ group was calculated.

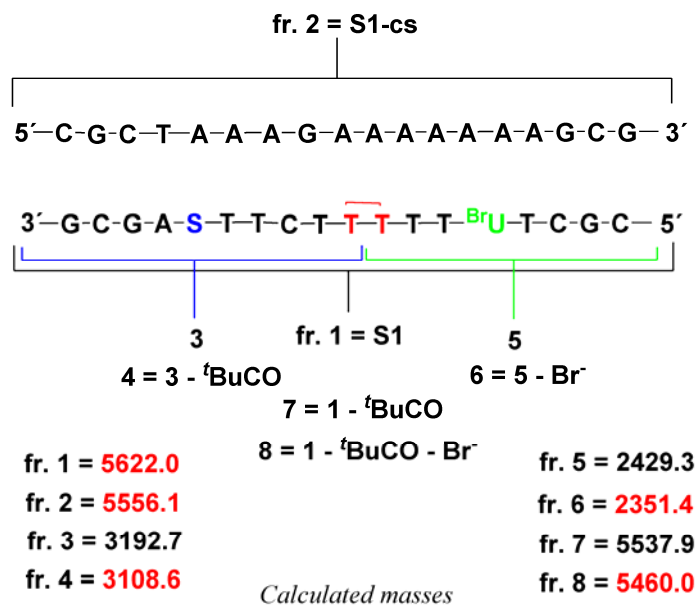


Figure 2.39 Calculation of the fragment masses deriving from the irradiation of dsS1. The masses in red are the fragments clearly detected by MALDI-Tof analysis (see below).

The mass analysis performed by MALDI-Tof is reported in Figure 2.40. The S1 single strand mass (A, blue) is compared with the mass of dsS1 (B, red). The latter is much less defined than the first due to the presence of salts necessary for the hybridisation with the S1-cs and for the irradiation of dsS1. These salts were not completely removed even after a desalting step. The third mass spectrum (C, green) corresponds to the sample removed from the irradiation assay after 40 min. It shows the presence of at least three new peaks and two of them are small fragments of S1. Although the intensity of such peaks is not very high, they are clearly visible in the subsequent enlargement (Figure 2.40 and 2.41). Moreover, the long S1 oligo was designed to ensure the electron transfer through a hopping mechanism and only one electron is injected per strand. Thus, very low yields in the fragmentation products are expected.

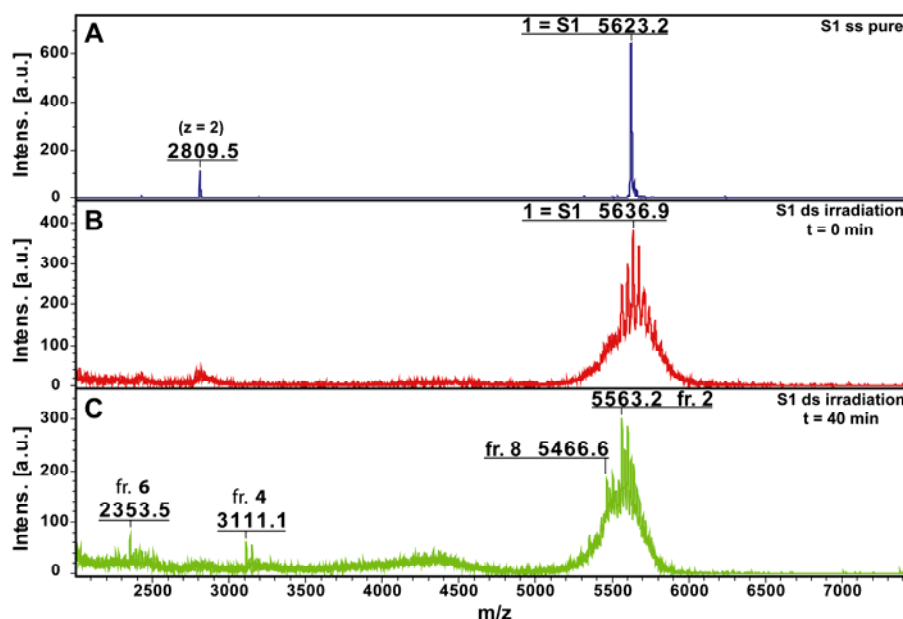


Figure 2.40 MALDI-ToF spectrum of (A) S1 as single strand; (B) dsS1 in the irradiation buffer at irradiation time $t = 0$ min; (C) dsS1 in the irradiation buffer at irradiation time $t = 40$ min. The peaks labelled as fr. 6, fr. 4 and fr. 8 represent the fragments 6, 4 and 8 reported in Figure 2.39.

In order to envisage clearly the above-mentioned peaks, an enlargement between 2200 and 3400 m/z of the MALDI-ToF spectrum series is reported in Figure 2.41. The green spectrum (after irradiation, C, Figure 2.41) clearly shows the presence of two main peaks (a third one for a K^+ -salt adduct) that are not present in the red spectrum (before irradiation, Figure 2.41, B). The calculated mass for the fragment 6 (Calc. 2351.4 Da, fr. 6) is in excellent agreement (2353.5 m/z) with one of these peaks. The second main peak has a mass of 3111.1 m/z which, most likely, corresponds to the fragment 4 (Calc. 3108.6 Da, fr. 4). From the enlargement in Figure 2.41 it is also possible to observe a small peak which might be associated to fragment 5 (Calc. 2429.3 Da, found 2430.3 m/z , fr. 5).

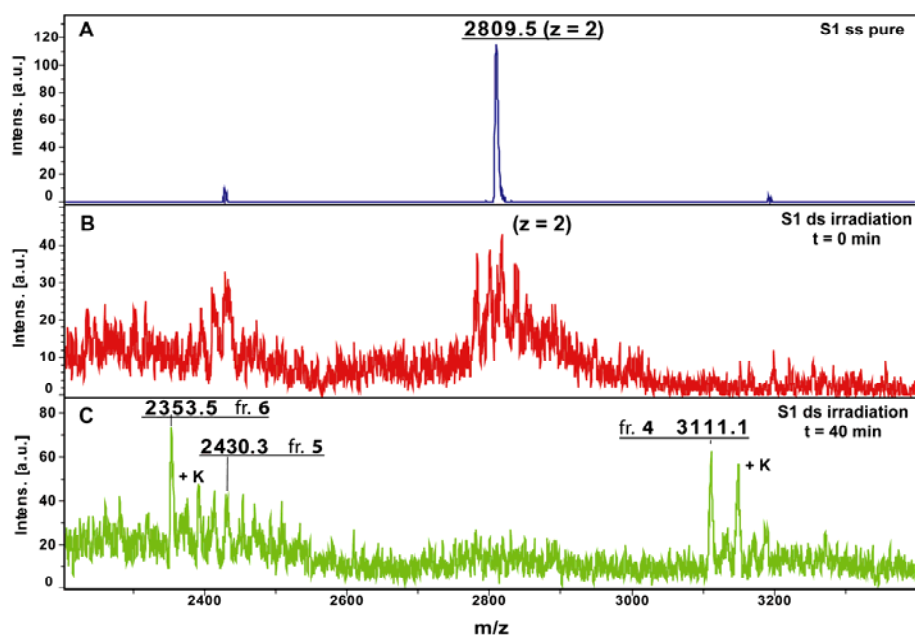
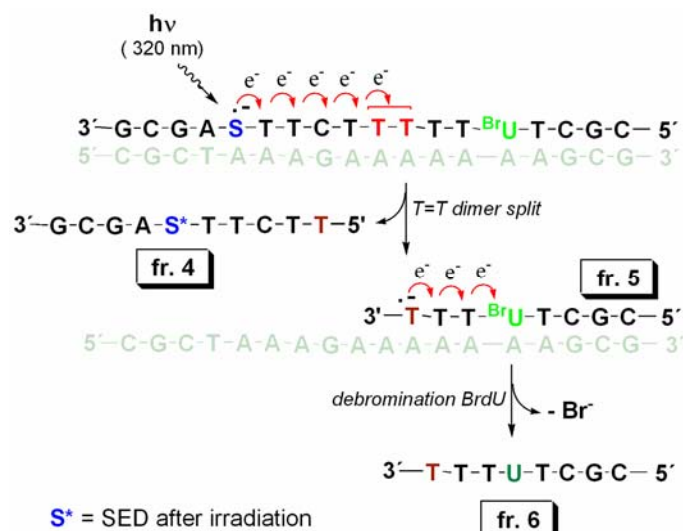


Figure 2.41 MALDI-ToF spectrum as enlargement between 2200 and 3400 m/z . (A) **S1** as pure single strand; (B) **dsS1** in the irradiation buffer at irradiation time $t = 0$ min; (C) **dsS1** in the irradiation buffer at irradiation $t = 40$ min.

Such a fragmentation of **S1** occurring upon irradiation is in contrast with the final conclusions reported by *Giese* and co-workers.^[230] The presence of fr. **4** and fr. **6** in the irradiation mixture can be explained by the sequence of events described in Scheme 2.21. A single electron is injected from the SED donor in the base pairs stack upon irradiation. The electron hops through the DNA using thymidines and one cytidine base present in the sequence and reaches the T=T dimer. The latter undergoes a cyclo reversion causing the strand to break under formation of fr. **4**. The charge (radical anion) partially remains localised on the thymidine of this fragment and partially on the other thymidine. In the first case fr. **5** will also be a product of the irradiation. In the second case the electron transfer proceeds to BrdU, where the fast release of the bromo anion (Br^-) stops the electron transfer process and yields fr. **6**.

It is worth to note the large distance between the SED donor and the second acceptor BrdU ($> 30 \text{ \AA}$). The presence of the debrominated fr. **6** in the irradiation mixture confirms the low distance dependence of the EET and proves the catalytic properties to the single injected electron. Thus, one electron is able to hop through a mixed sequence and reacts with two electron traps located more than 30 \AA away from the injection site.



Scheme 2.21 Irradiation of dsS1 and formation of fr. 4 by a T=T dimer cycloreversion and fr. 6 by subsequent debromination. The formation of fr. 5 is possible when the charge remains on the first T of the opened T=T dimer. The counter strand cs of S1 is depicted in light green colour and corresponds to S1-cs of the MALDI-ToF spectrum reported in Figure 2.42.

The enlargement of Figure 2.40 in the mass region between 5300 and 5900 m/z is reported in Figure 2.42. Also in this case the peaks resulting from the irradiation of dsS1 are depicted in green (C), while the original DNA is in red (B).

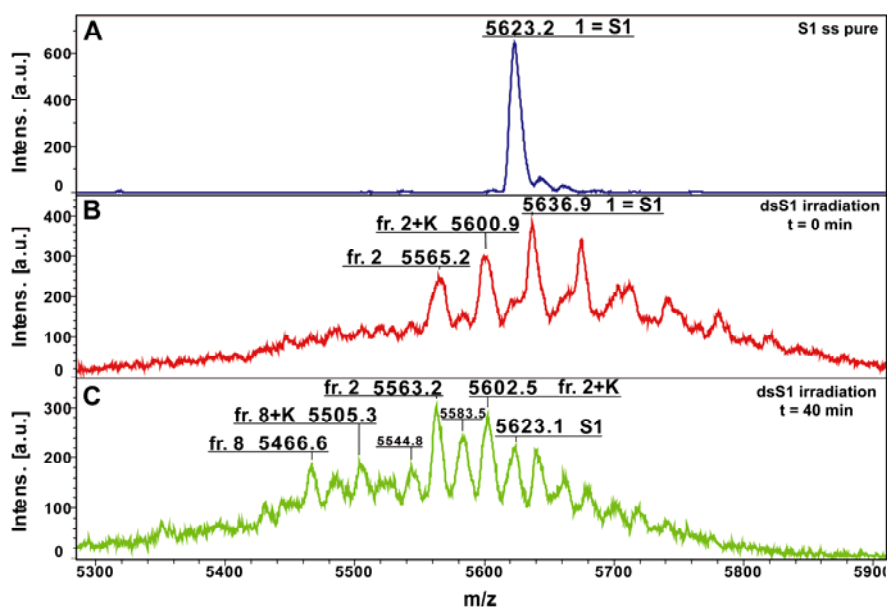
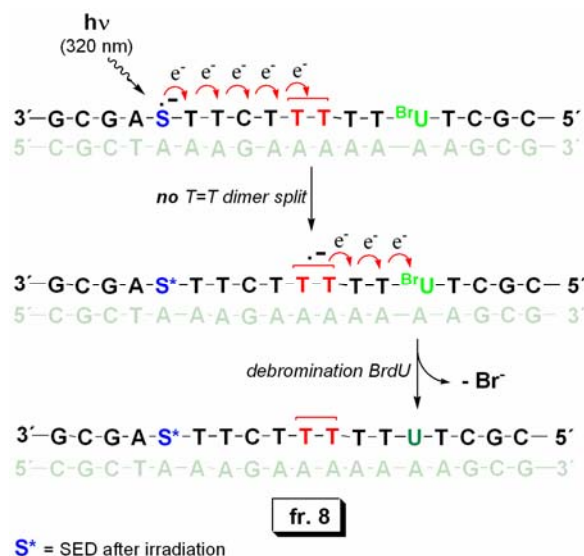


Figure 2.42 MALDI-ToF spectrum as enlargement between 5300 and 5900 m/z . (A) S1 as single strand; (B) dsS1 in the irradiation buffer at irradiation time $t = 0$ min; (C) dsS1 in the irradiation buffer at irradiation time $t = 40$ min.

The main peaks detectable in the mass analysis of the irradiated mixture in Figure 2.42 are the counter strand (fr. **2**, 5563.2 m/z with the sodium (5583.5 m/z) and potassium (5602.5 m/z) adducts), the **S1** peak (5623.1 m/z) and the peaks corresponding to fr. **8** and its potassium adduct at 5466.6 m/z and 5505.3 m/z , respectively (Figure 2.42, C). The presence of the latter peaks (fr. **8**) supports the partially rate determining T=T dimer cyclo reversion mechanism suggested by *Giесе* and co-workers.^[230] A schematic representation of the possible pathway involved in the formation of fr. **8** is depicted in Scheme 2.22.



Scheme 2.22 Schematic representation of the formation of fr. **8** by the single electron injection. The **S1** counter strand **cs** is depicted in light green colour and corresponds to fr. **2** of the MALDI-ToF spectrum reported in Figure 2.42.

Also in this case the process starts with the injection of a single electron into the base stack of the duplex. The electron transfer proceeds via the hopping mechanism along the four base pairs separating the donor from the T=T dimer. The resulting T=T radical anion can undergo a cyclo reversion with formation of the fragments in Figure 2.41 or can transfer the charge to the following base pair. The latter pathway is responsible for the formation of fr. **8**, since BrdU releases a Br⁻ anion very rapidly and in an irreversible way. In this case, one electron injected into the duplex by SED reaches the BrdU trap located a full helix turn away from the site of injection, using also the T=T dimer as a stepping stone. This observation is again in agreement with the previous study,^[230] confirming that the T=T dimer cleavage can be the rate determining step in the EET investigations, in which it is used as electron acceptor. Thus, the rate of the T=T cyclo reversion is smaller or comparable to the rate of the electron transfer in DNA.

HPLC and mass analysis

In order to confirm these results an irradiation experiment was carried out with a solution containing a high concentration (30 μM) of dsS1. Proceeding as in the previous experiments, the solution was degassed with argon for 30 min and irradiated with the same apparatus previously described. Only two samples, at time $t = 0$ min and $t = 40$ min were taken. Both samples were used for the RP HPLC analysis and the resulting fractions were collected. The fractions were concentrated and analyzed by MALDI-ToF mass spectrometry. A fraction of the irradiated sample corresponding to the HPLC peak with the retention time at 41 min shows the mass of fr. 6, deriving from the T=T dimer cleavage followed by the debromination of BrdU (Figure 2.43).

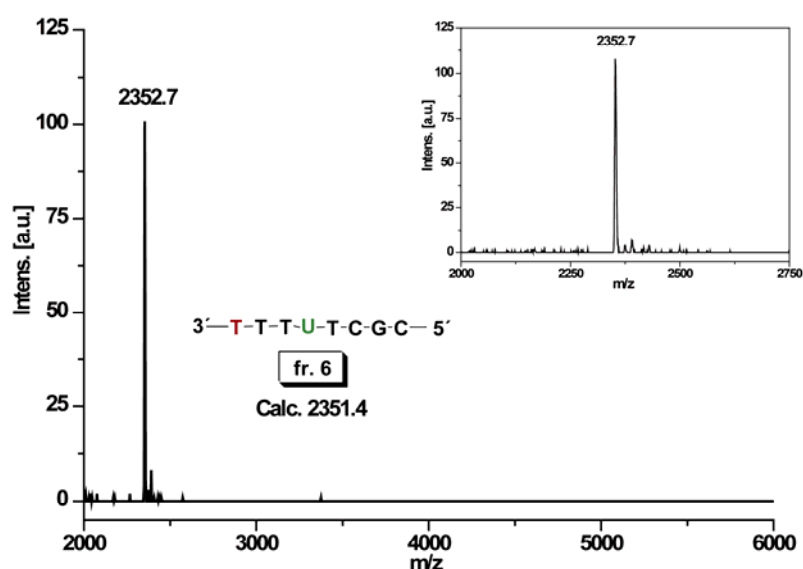


Figure 2.43 Analysis of the 41 min fraction (HPLC) by MALDI-ToF spectroscopy. The inset shows the enlargement of the spectrum between m/z 2000 and 2750.

The isolation of this peak validates the previous MALDI-ToF mass analysis of the irradiation mixture in which the same peak was detected as a weak signal. Thus, the above-mentioned fragmentation pathways are confirmed by the combination of HPLC and mass analysis as well.

Synthesis and irradiation of flavin-hairpin containing two electron acceptors

In order to gather insight into the pathways involved in the mechanism of T=T dimer repair, the SED donor was replaced by the flavin donor. A new flavin-capped hairpin was

prepared. This hairpin possesses an identical sequence between the donor and the two acceptors previously used in **S1**. The same flavin donor already described and used in this work was incorporated in a sequence containing the T=T dimer as first acceptor and BrdU as second one. Also in this case the synthesis was achieved by a mixed phosphoramidite/H-phosphonate protocol as previously described, followed by a mild deprotection step ($\text{NH}_3(\text{aq})$, 28 %, 5 days). The hairpin **F1** is an analogue of the ds**S1** where the single electron donor is replaced by a donor able to provide a continuous electron flow upon irradiation (Figure 2.44).

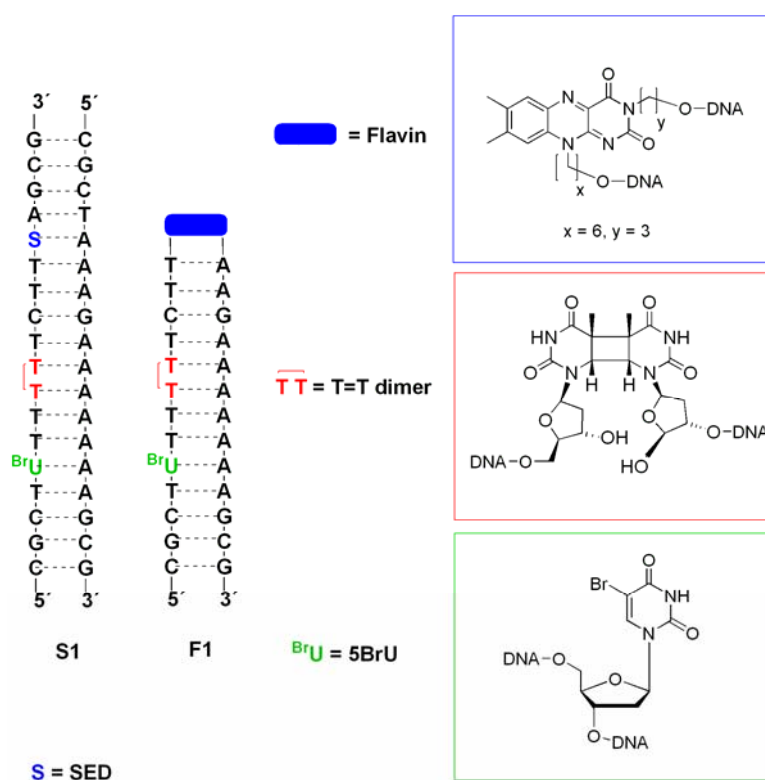


Figure 2.44 The flavin-capped hairpin **F1** containing two electron acceptors together with the ds**S1** previously described. The sequence starting from the donors is identical with that of ds**S1** in which SED is the donor.

The irradiation of hairpin **F1** was accomplished in a quartz cuvette, with a 1000 W Xe-lamp as previously described for hairpins (1-5)**a**, **b**, **c**. The EDTA-photoreduction, the subsequent irradiation at 340 nm and the sampling through the rubber septum were performed in the standard conditions of this work. The MALDI-ToF mass analysis of the samples before and after irradiation are reported in Figure 2.45.

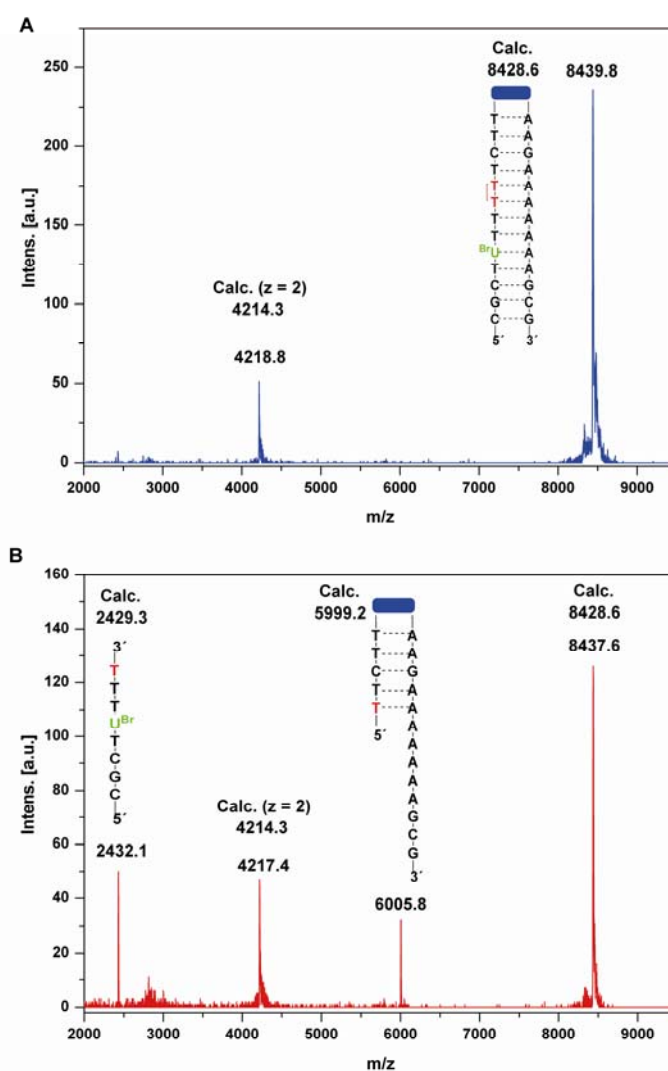


Figure 2.45 MALDI-ToF spectrum of **F1** before (A) and after 15 min of irradiation (B).

The mass analysis shows that a sample of **F1** (Figure 2.45, A) generates a set of fragments upon irradiation (Figure 2.45, B). In both cases, before and after irradiation, it is possible to detect the doubly charged **F1** hairpin (4217 m/z , $z = 2$) along with the mass of **F1** (8437 m/z). After irradiation two new peaks are formed. The first, with a value of 6005 m/z can be assigned to a fragment (carrying the flavin) in which the T=T dimer underwent the cyclo reversion, resulting in the strand break. The second peak, with a value of 2432 m/z , is in good agreement with the small fragment generated after T=T dimer splitting (Calc. 2429 Da) containing the second acceptor. Surprisingly, in this fragment the second electron trap remains integral. Therefore, the electrons injected by the flavin do not reach the BrdU trap. This result strongly contrasts the previous results obtained with the SED.

Conclusions and outlook

In this section 2.2.2 the use of a single electron donor (SED) was alternated with the use of the flavin donor in systems containing two electron acceptors in a row. The results obtained upon irradiation of the SED-containing duplex are in agreement with the data observed in a previous work.^[230] Moreover, a long distance EET, initiated by a single electron donation event, was proven. On the other hand, the results observed upon irradiation of a flavin-containing hairpin, provide an astonishing result. The chemistry that is triggered by a charge in DNA depends on how the charge was initially injected at least in systems in which the charge is detected not too far away from the donor. In excited state systems, the injected electron has to fight against the efficient charge recombination process, which seems to limit and bias charge propagation. If, however, ground state chemistry is employed to inject the charge, no recombination trap is present. In this case, the charge can move freely. Excess electrons injected by such a system can trigger more than one reaction, establishing a catalytic electron, and they can hop over acceptors if their triggering mechanism is slower than the hopping step. A side reaction involving the direct photo-reduction of BrdU was detected in control experiments. The amount of such side reaction was quantified to be around 1 % and 5 % during the irradiation at 320 nm. These experimental evidences support the choice of different single electron donors, which may be irradiated at higher wavelengths. A clear explanation of this data however requires a deeper investigation using, for example, competitive reactions occurring at two acceptors located at the same distance from the donor. An accurate design of such systems should allow to investigate important information concerning the T=T dimer splitting mechanism and the rate. Some examples are depicted in Figure 2.46. The hairpins **F2**, **F3**, **F4** and **F5** could eventually elucidate the influence of the direction ($3' \rightarrow 5'$ vs $5' \rightarrow 3'$) in the EET process as well while the fluorescein tag would increase the detection power of the fragments formed upon irradiation.

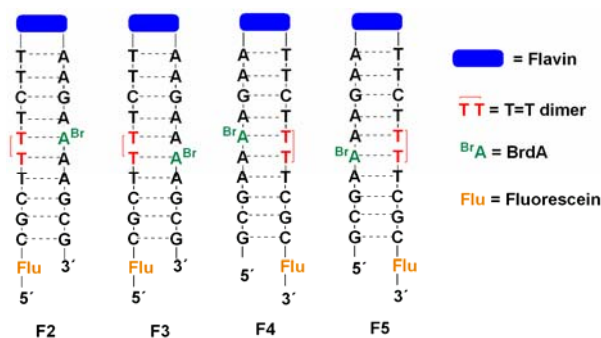


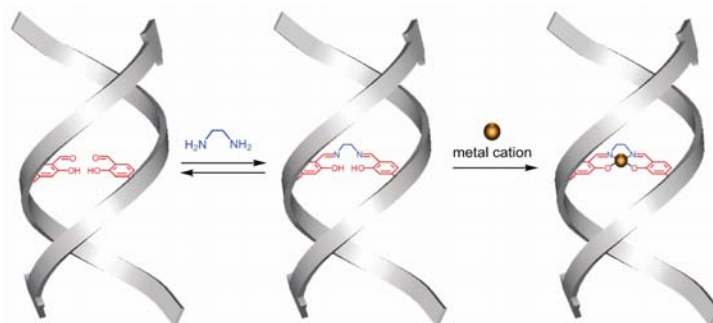
Figure 2.46 Depiction of flavin-capped hairpins **F3**, **F4**, **F5** and **F6**.

2.2.3 M-MEET: Metal-Mediated Excess Electron Transfer

Introduction

Nanoscaled structures, such as molecular wires, may take advantage of the unique self-organisation properties of the DNA.^[169] Nevertheless, the lack of electrical conductivity of natural DNA limits its use as molecular wire.^[161,266,267] This limitation can be overcome by DNA metallisation, which might increase the conductivity and potentially be fine-tuned.^[268] Nonetheless, random external DNA metallisation techniques disrupt the extraordinary DNA properties preventing reversible self-assembling features.^[268] The improvements achieved in selective DNA metallisation,^[269] in concert with the development of methods for conductivity investigation,^[270] may allow in the future the design of DNA-inspired molecular wires.

Recently *Carell* and co-workers^[271,272] and the group of *Shionoya*^[273,274] reported a controlled assembly of metallised DNA in which one or more natural base pairs are replaced by nucleosides carrying flat metal complexes. This new concept, called metal-base pair, is not more than few years old.^[275,276] A graphical example showing a salen metal complex inside the DNA duplex is depicted in Scheme 2.23.^[271]



Scheme 2.23 Assembly of a DNA strand in which the replacement of natural base pairs by a metal-base pair gives rise of an internally metal complexing DNA. Two salicylic aldehydes form a salen ligand in the presence of ethylenediamine. The addition of an appropriate metal cation forms the salen metal complex.^[271]

Up to ten metals atoms were lined up by the DNA self-assembling scaffold.^[277] Selective metal complexation could be achieved as well. Different metal ions, such as copper(II) and mercury(II) ions have been arranged in a programmable fashion using the salen complex and a mismatched T-T site. (Figure 2.47).^[278] The latter is known since the 1960s to be able to complex Hg^{2+} .^[279,280]

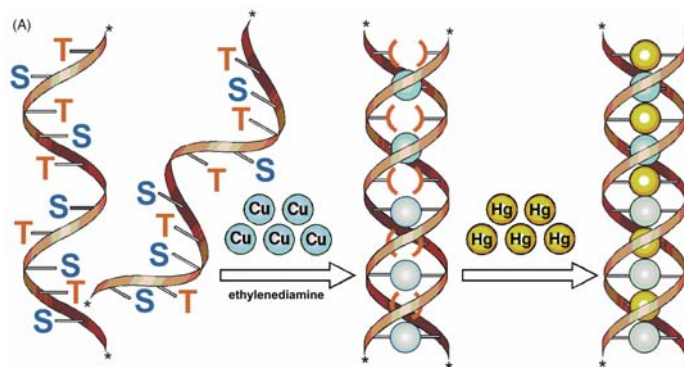


Figure 2.47 Alternating assembly of 5 Cu^{2+} and 5 Hg^{2+} into the DNA base-stack. T = thymidine; S = salicylic aldehyde.^[278]

Although magnetic properties have been recognised in DNA containing five metal-base pair in a row,^[273] this DNA-inspired bio-inorganic materials need a deeper investigation. In collaboration with *Clever*, a new system to explore the excess electron transfer (EET) was designed and the electron transfer in such metal-derivatised DNA need to be measured.

Taking advantage of the systems developed within the *Carell* group,^[35,271] a series of DNA hairpins containing the light dependent flavin electron donor and the fast electron acceptor BrdU were designed. A salen-metal complex between the donor and the electron acceptor was introduced during the oligonucleotide solid phase synthesis in order to establish the influence of one metal in the electron transfer process.

The design of hairpins **H1**, **H2** and **H3** in Figure 2.48 was aimed at exploring the electron transfer through the salen-metal complexes in the context of mixed sequences. The effect of only one metal per DNA was investigated in this proof of concept study, in which only the nature of the metal and the irradiation conditions were systematically changed.

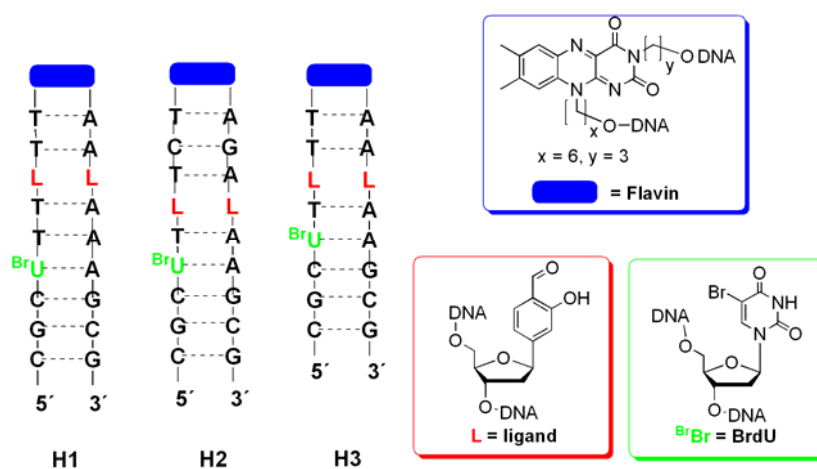


Figure 2.48 Hairpins **H1**, **H2** and **H3** and their modifications.

Synthesis and characterisation of the hairpins

The synthesis of hairpins **H1**, **H2** and **H3** was accomplished using a mixed phosphoramidite/ H-phosphonate/ phosphoramidite protocol applied in a standard automated oligonucleotide synthesis.^[256] An additional ligand deprotection step was needed at the end of the synthesis as previously described.^[271,272] High-resolution mass spectrometry was used to characterize the hairpins. The internal metal complexes are formed, as extensively described,^[271,272] by addition of ethylenediamine, followed by the addition of a salt of the metal in question. Hairpins before (**HX**, with X = 1, 2 and 3) and after addition of ethylenediamine (**HX-en**, with X = 1, 2 and 3; **en** = ethylenediamine) and after addition of metal (**HX-M**, with X = 1,2 and 3; M = metal cation) are described in the following text. Examples of high resolution mass analysis are reported for the hairpin **H1**. More spectra are included in the *Experimental Part*, Chapter 4.

The analysis of metal-containing oligonucleotides is best performed using electron spray ionisation (ESI) high resolution mass spectrometry technique. Attempts to use the MALDI-Tof mass analysis, as in the previous sections, failed due to the lability of the complexed metal towards the laser ionisation method.

In Figure 2.49 the ESI spectrum of the hairpin **H1** after RP HPLC purification is reported. A list of the calculated molecular weights of the ion patterns on the top of the Figure accompanies each of the following ESI spectrums.

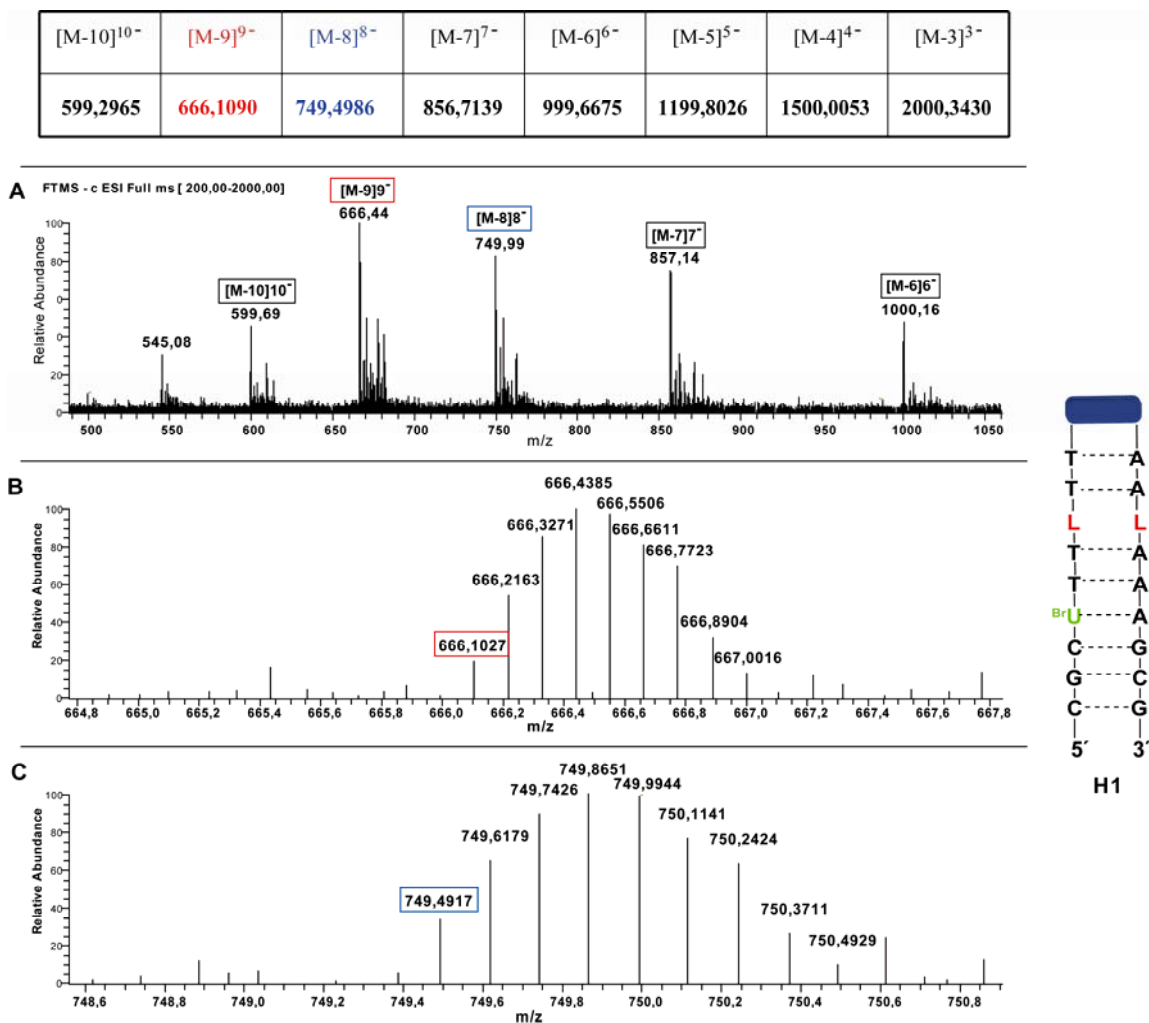


Figure 2.49 High resolution ESI mass spectrum of **H1**. (A) spectrum between m/z 500 and 1050; (B) spectrum between m/z 664 and 667 for the $[M-9]^{9-}$ peak and (C) spectrum between m/z 748 and 750 for the $[M-8]^{8-}$ peak.

The ion patterns found in this analysis are in excellent agreement with the calculated molecular weights. Thus, the synthesis of **H1**, containing four modifications, was effectively achieved. Similar mass analyses were performed for the other hairpins with equally clear results.

Synthesis of metal-containing hairpins

Samples of the purified hairpins were used for the complexation with different metals. This base-metal formation was achieved, as previously described, through the addition of ethylenediamine followed by the metal salt. Hairpins containing Cu^{2+} , for example, were formed by addition of CuSO_4 , the hairpins containing Mn^{3+} were generated by addition of

MnSO₄ (and spontaneous oxidation to Mn³⁺ occurs successive to the salen-complexation). Also other metal cations (Fe³⁺, VO²⁺) were incorporated into hairpins **H1**, **H2** and **H3** (Figure 2.50). Thus, the capability of two salicylic aldehyde ligands developed by *Clever* to complex a large assortment of metals is also highly efficient in the presence of other modifications.

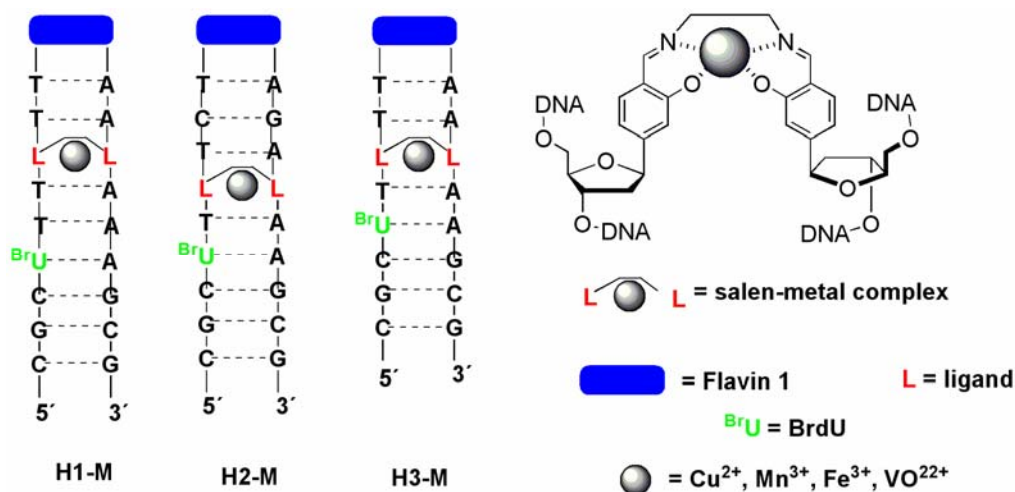


Figure 2.50 Hairpins **H1-M**, **H2-M** and **H3-M** along with the salen-metal complex and the metal cations used in this work.

In the following Figure 2.51 the ESI spectrum of **H1-Cu** is reported, whereas the spectrum of **H1-Mn** is included in the *Experimental Section*. Also in these cases the formation of the desired product is confirmed by the agreement between the calculated and the found molecular weights. Two of the ion patterns are enlarged and reproduced below the full spectrum for a better visualisation of the data.

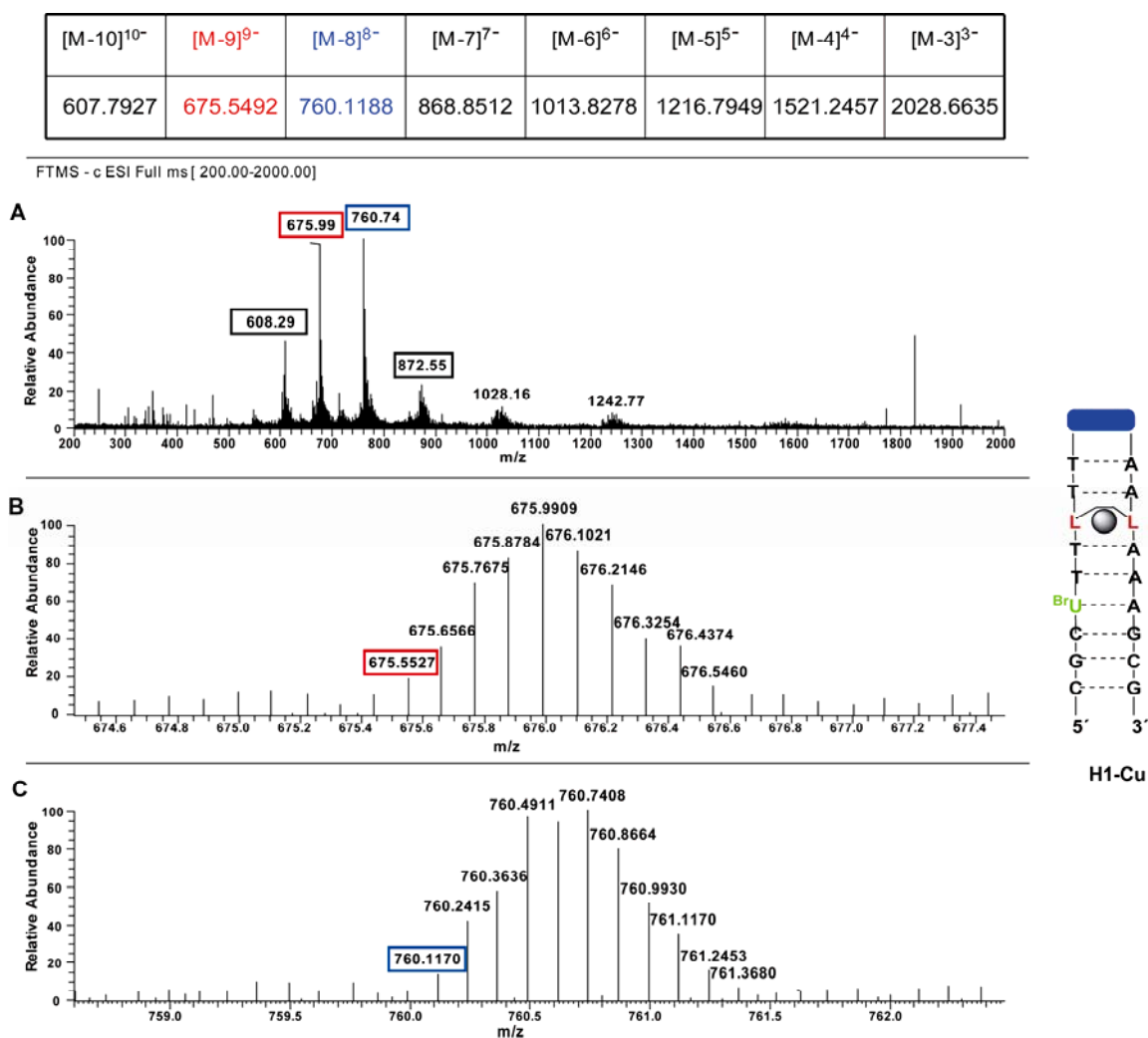


Figure 2.51 High resolution mass spectrum of **H1** after addition of **en** and Cu^{2+} (**H1-Cu**). (A) spectrum between m/z 200 and 2000; (B) spectrum between m/z 674 and 677 for the $[\text{M}-9]^{9-}$ peak and (C) spectrum between m/z 758 and 763 for the $[\text{M}-8]^{8-}$ peak.

Irradiation of metal containing hairpins

The irradiation experiments were carried out under anaerobic conditions, as previously reported in this work.^[35] However, the analysis of irradiated hairpins was now accomplished by using high-resolution mass spectrometry. The irradiation of **H1**, was performed under several conditions. As control experiment the hairpin **H1** was irradiated before the addition of ethylenediamine and the metal. Surprisingly, after 20 min of irradiation, it was possible to observe the corresponding debrominated hairpin (**H1**-Br) as the expected product of the electron transfer process initiated by injection of an electron from the irradiated flavin (Figure 2.52). As control, the experiment was repeated in absence of any reductant to prevent the electron injection. The flavin, in fact, injects electrons into the hairpin base pairs stack in

the deprotonated, reduced and light-excited state. In the control experiment the debrominated product was not observed. This data validates the assumption that efficient electron transfer between the flavin-donor and the BrdU acceptor is possible also through a mismatch as established by the salicylic aldehydes.

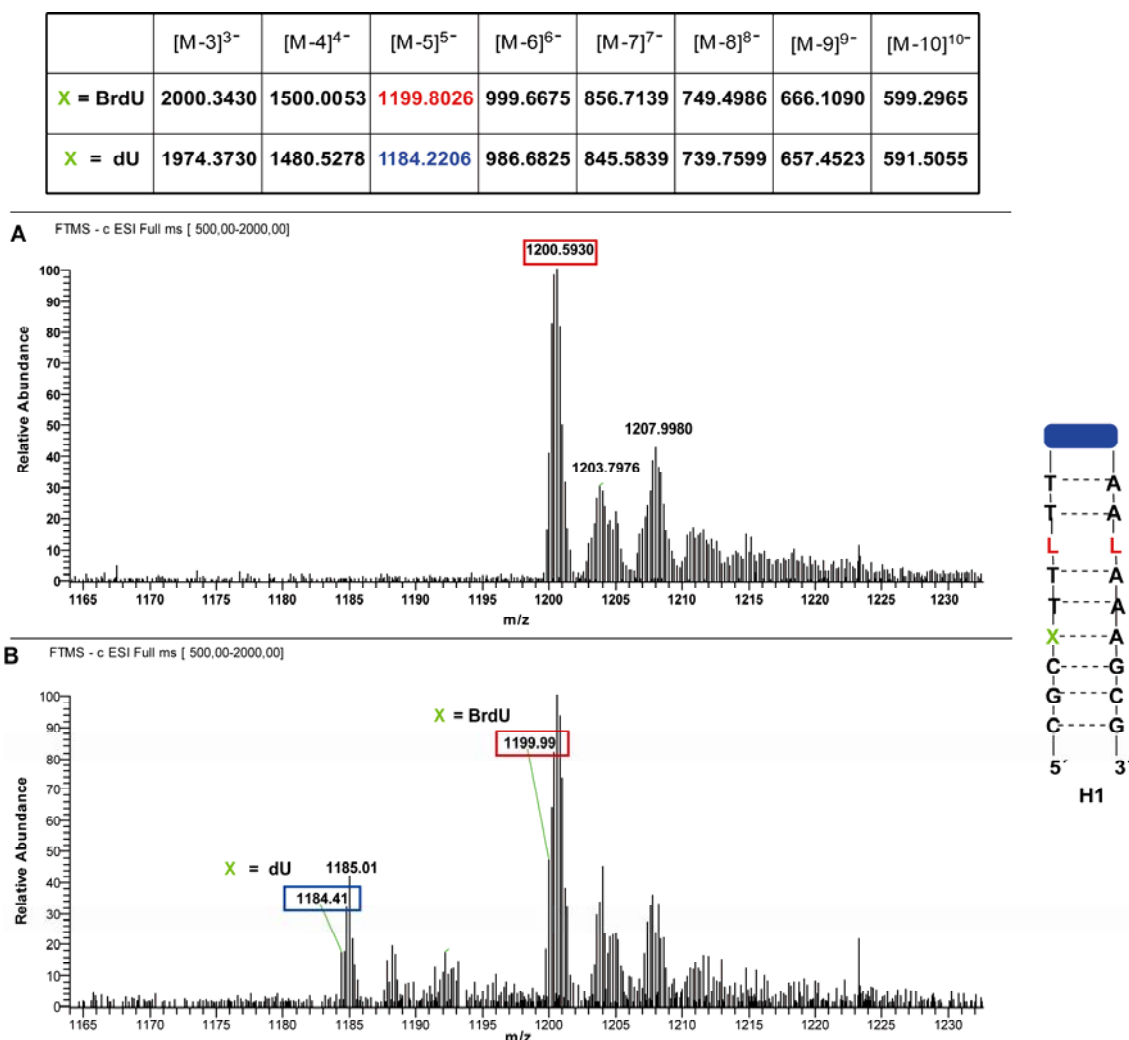


Figure 2.52 High resolution mass spectrum of **H1** before (A) and after (B) irradiation. The [M-5]⁵⁻ peak is highlighted in red for the parent strand and in blue for the debrominated strand.

To further investigate the control experiment, **en** was added to a fresh solution containing **H1**. The addition of **en** to the hairpins is reversible, forming iminic bonds with the two salicylic aldehydes present in the sequence and slightly increasing the melting point and the stability of the formed duplex.^[271] The irradiation of **H1** in presence of 10 equivalents of **en** (**H1-en**) yielded again a debrominated hairpin, detected by ESI mass analysis (Figure 2.53).

The data show that the salen ligand being formed upon addition of **en**, remains intact in both the parent (**H1-en**) and the debrominated hairpin (**H1-en**–Br).

	[M-3] ³⁻	[M-4] ⁴⁻	[M-5] ⁵⁻	[M-6] ⁶⁻	[M-7] ⁷⁻	[M-8] ⁸⁻	[M-9] ⁹⁻	[M-10] ¹⁰⁻
X = BrdU	2000.3430	1500.0053	1199.8026	999.6675	856.7139	749.4986	666.1090	599.2965
X = dU	1974.3730	1480.5278	1184.2206	986.6825	845.5839	739.7599	657.4523	591.5055

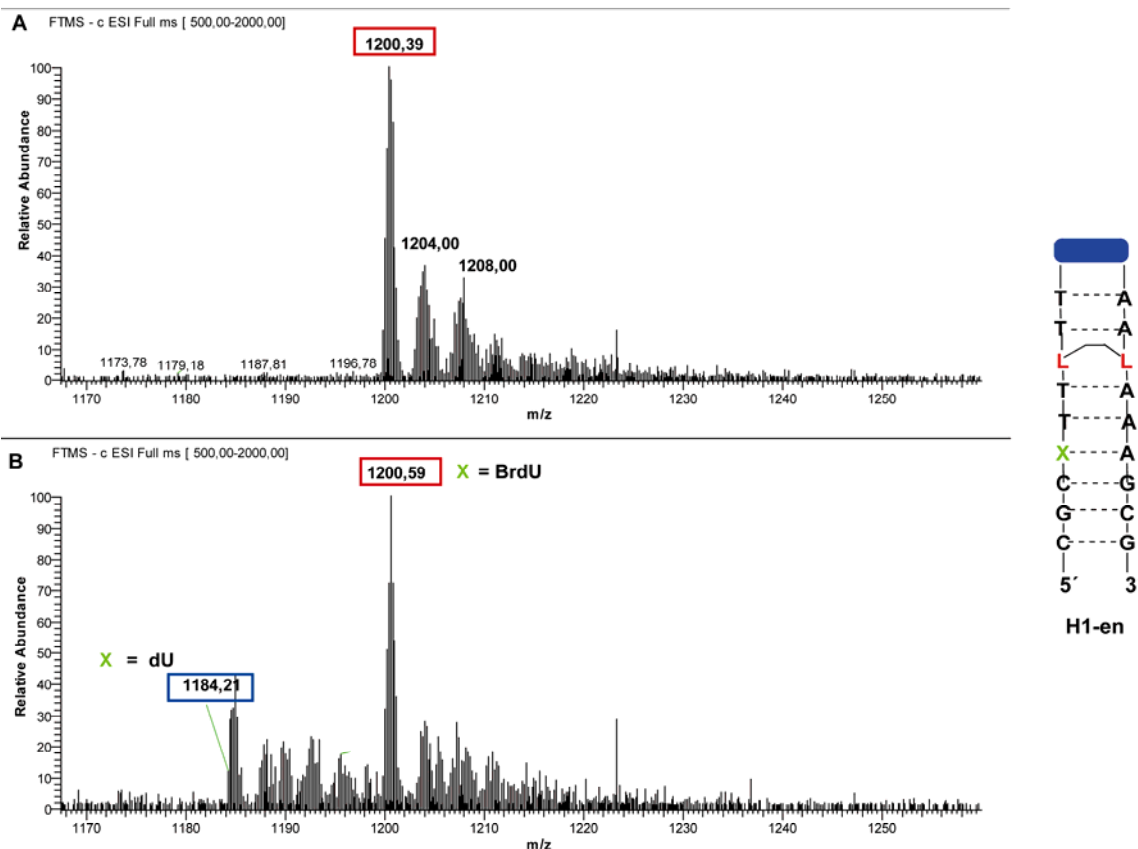


Figure 2.53 High resolution mass spectrum of **H1** after addition of ethylenediamine, (**H1-en**) before (A) and after (B) irradiation. The [M-5]⁵⁻ peak is highlighted in red for the parent strand and in blue for the debrominated strand.

The salen-metal complex was finally formed inside the hairpin **H1** following the previous works, by adding 10 equivalents of **en** and 5 equivalents of CuSO₄. The stability of the formed hairpin **H1-Cu**, was improved as evident from the increased melting point due to the new coordination bonds formed.

The irradiation was carried out under the same photoreaction conditions of the control experiments and the analysis was achieved again by ESI mass spectrometry (Figure 2.54). Although the presence of Cu²⁺ inside the the duplex appears to influence the amount of by-products deriving from the irradiation, it was possible to clearly identified the ion patterns

of the debrominated hairpin (**H1-Cu** -Br). This data is the first proof of the concept that the electron transfer can hop through a base-metal stack. Thus a metal-mediated excess electron transfer (M-MEET) is observed here for the first time.

However, ion patterns in which the mass of Cu^{2+} was not any more included in the hairpin structure were also found. These peaks correspond to the parent hairpin (**H1-Cu** - Cu^{2+}) and to the debrominated hairpin in two forms: with **en** inside (**H1-Cu** -Br - Cu^{2+}) and without **en** (**H1** -Br - Cu^{2+} -**en**).

	[M-3] ³⁻	[M-4] ⁴⁻	[M-5] ⁵⁻	[M-6] ⁶⁻	[M-7] ⁷⁻	[M-8] ⁸⁻	[M-9] ⁹⁻	[M-10] ¹⁰⁻
X = BrdU	2028.6635	1521.2457	1216.7949	1013.8278	868.8512	760.1188	675.5492	607.7927
X = dU	2002.6935	1501.7682	1201.2129	1000.8428	857.7212	750.3801	666.8925	607.7927

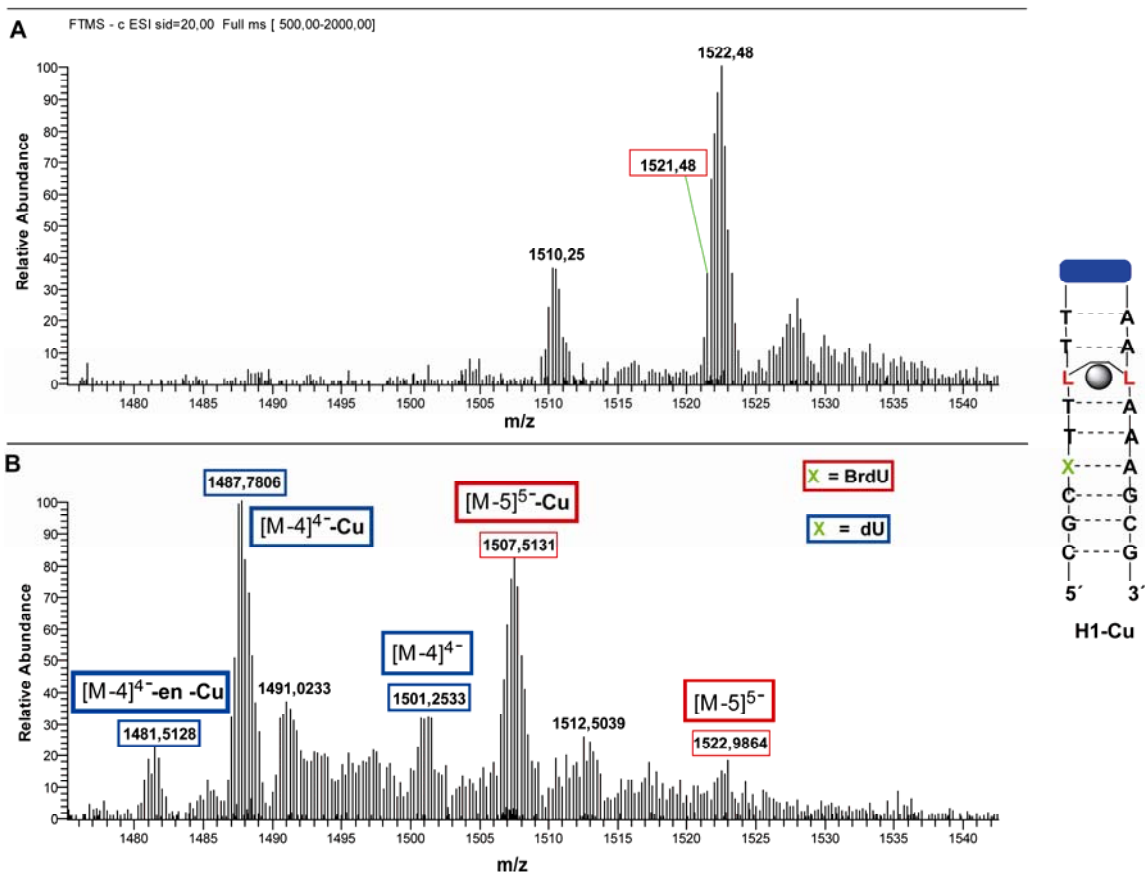


Figure 2.54 High resolution mass spectrum of **H1** after addition of ethylenediamine, Cu^{2+} (**H1-Cu**) and before (A) and after (B) irradiation. The $[\text{M}-4]^{4-}$ peaks are highlighted in red for the parent strand and in blue for the debrominated strand.

The partial release of Cu^{2+} was only observed after the irradiation experiments. The 1000 W Xe-lamp used for the photoreaction was filtered by a cooled 340 nm cut-off glass filter in order to excite the reduced and deprotonated flavin, without any excitation of the

nucleobases. Nevertheless, a maximum absorption peak at 360 nm is known to be typical for Cu^{2+} -salen complex $\pi \rightarrow \pi_1^*$ transitions.^[272] Therefore, the excitation of the Cu^{2+} -salen complex could explain the loss of the metal from the complex. Such a limitation can be overcome by using different metals in the salen-complex.

The question how efficient the electron transfer proceeds through the Cu^{2+} -base pair must be addressed in a different way, in which the photo-electron injection event does not interfere with the metal-complex. Many injectors are known in literature as for example the above-mentioned diaminonaphthalene (TMDN, $E_{\text{ox}}^* \approx -2.8$ V vs SCE; $\lambda_{\text{max}} = 325$ nm) used in excess electron transfer studies,^[33,211,215] or the previously reported single electron donor (SED, $\lambda_{\text{max}} = 320$ nm).

The investigation of the physical properties of DNA containing metal-base pairs can surely take advantage from EET studies carried out with covalently bound electron injectors and acceptors.

2.3 Conclusions

The Br-nucleosides used in the first part of Chapter 2 revealed many details of the excess electron transfer process, such as the base sequence and direction dependence and the influence of different acceptors on the charge transfer efficiency. It was also possible to establish, for the first time, a strong influence of the G:C bp position on the trap efficiency. The capillary electrophoresis technique was applied successfully for the first time in an EET study. Furthermore the Br-nucleoside system assay can represent an alternative and convenient method to investigate the fate of the *in situ* generated radicals. Specifically, BrdU can be used to explore the C1' and C2' radical formation and fate within a duplex, without the involvement of a direct UV irradiation. BrdA represents a valid precursor of C8 radicals that, at the nucleosides level, undergo a cascade of reactions yielding cycloadenosine lesions. It is not yet well established if the C8 radical can evolve analogously when generated inside a duplex. Finally, BrdG as shown to act as a one-electron oxidised guanine precursor. This behaviour is of great importance for the investigation of oxidative damage in DNA. An appropriately designed assay, containing for example SED and BrdG, might provide an important tool for the selective generation of oxidative lesions and their study.

In the second part of Chapter the effect of one electron injected into DNA was studied. Two electron acceptors in a row were used. The data corresponds with that of a similar model from *Giese*. Moreover, when a flavin is used as donor an astonishing result is obtained. The chemistry that is triggered by a charge in DNA depends on how the charge was initially injected. In excited state systems, the charge recombination process seems to limit the charge propagation. If, however, ground state chemistry is employed to inject the charge, no recombination trap is present. In this case, the charge can move freely. Excess electrons injected by such a system can trigger more than one reaction.

In the last part a new DNA-based device was developed and tested in this work. The so-called M-MEET represents the first step towards a real application of the recently developed DNA metal complexation method.

3 Molecular Beacons for DNA-Photography. Selective Detection of a Target

3.1 Introduction

There is a great need in the medical, scientific and non-scientific community for rapid and simple diagnostic assays able to detect biomaterials such as oligonucleotides (ODNs), DNA, RNA and proteins. The methodologies available today are possible thanks to expensive equipment and technologies and they are mostly suited for specialised users. In the case of DNA detection, the polymerase chain reaction^[281] (PCR) or comparable target-amplification methods are still the most widely used and well known for their reliability and sensitivity (5-10 DNA molecules). In some cases these methods exhibit short-comings in terms of specificity and require an expensive multi-component assay. Direct detection methods were developed recently using complex technologies such as fluorescent, chemoluminescent, electrochemical, radioactive processes, using partially sophisticated materials such as micro-arrays and nano-particles.^[189,282-287] Although these new assays can detect selected ODNs in the pico-, femto- and even atto-molar range, their application requires a specific scientific background, thus limiting the method to highly specialised laboratories. A novel approach to detect DNA and RNA without any specific scientific background would be a landmark in the desire to extend these kinds of diagnostics to a large variety of applications. Such a method should cover the fields of human in vitro diagnostics such as testing for infectious diseases and bioterrorism agents or testing for oncological applications.

The work reported in Chapter 3 was aimed at developing an easy to use method for all these fields without the involvement of sophisticated and expensive instrumentation. In order to achieve this goal the final method should not require the use of a specialised laboratory.

A very basic chemical laboratory, accessible even for non-specialised users, is a dark room for photographic development. Such rooms can be set up rapidly and are widely available even after the advent of digital photography. In order to run a dark room a profound scientific knowledge is not required even though the chemistry behind the photographic process is relatively complex and involves chemicals and materials such as silver halides and different dyes. It can be assumed that one of the most simple and small chemical labs ever commercialised was the Polaroid[®] camera. The technology described herein is inspired by such techniques. Based on the black-and-white (b/w) photographic process we developed a novel method for the direct detection of DNA with high sensitivity levels of 300 attomoles.^[288] However, several steps of this technology are still to be optimised. This new

application based on the very old idea of photography could be able to satisfy the needs outlined above.

Photography

The irradiation of a photo paper or of an emulsion containing silver halide crystals generates Ag_4 nuclei as latent images.^[289] These clusters are selectively enlarged by the subsequent reductive development process. This development step can be seen as the amplification of the original signal, the latent image, by a factor of more than 10^{11} .^[289] The sensitivity of such emulsions or papers is called *intrinsic sensitivity* and is limited to wavelengths absorbed by the silver halide. The process called *spectral sensitisation* adds sensitivity to longer wavelengths of the visible spectrum. This requires the addition of dyes called *spectral sensitizers* to the emulsion grains.^[290] Cyanine, merocyanine and pinacyanol dyes constitute the majority of spectral sensitizers employed thus far, though many other molecules were used in photography before the cyanines were recognised as the best class of dyes for this application.^[291]

DNA-Photography

Taking advantage of the working principle of b/w photography, a facile method for highly sensitive DNA detection was realised and called DNA-photography (DP) by the *Carell* group.^[288] An application of the DP method to detect DNA as possible in many fields even for non-specialised users. There is no need for a professional laboratory. This working principle is illustrated in Figure 3.1.

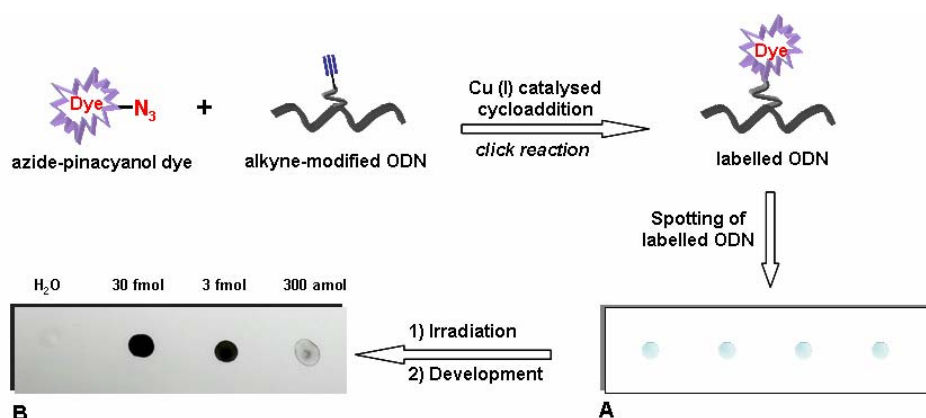


Figure 3.1 Schematic representation of the envisaged DNA detection method using the methods of black and white photography. A) commercial photopaper loaded with different concentrations of the labelled ODN. Graphical representation. B) photopaper after irradiation and development. Visual detection of the labelled ODN at three different concentrations. Spotted 1 μ L (x 4) (scanner reproduction).

A series of ODNs and dsDNA were labelled with one or more pinacyanol dyes. The labelling was achieved, as reported recently, using the ability to modify oligonucleotides with the help of the Cu (I) catalysed azide/alkyne cycloaddition (click chemistry).^[292-296] The building blocks for the synthesis of the pinacyanol labelled ODNs are depicted in Figure 3.2.

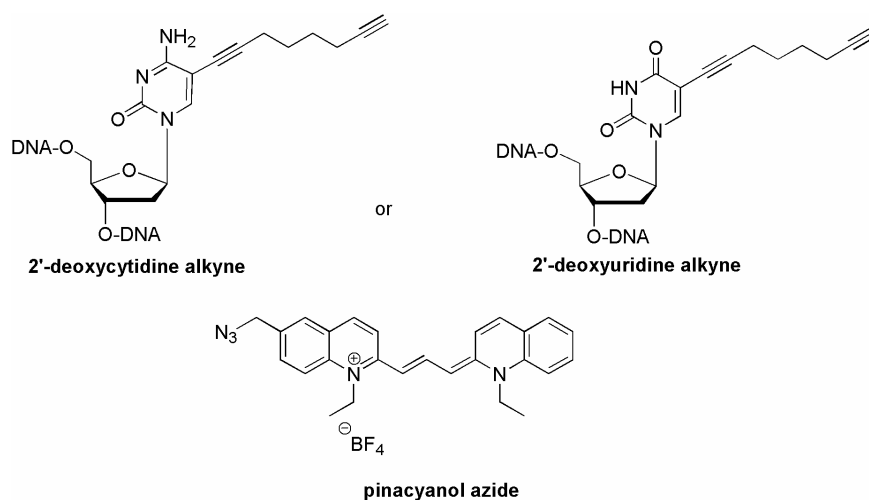


Figure 3.2 Building blocks used for the synthesis of ODN 1-3.^[288]

The solutions containing such ODNs were individually spotted on commercially available photographic paper (Ilfospeed RC Deluxe, Ilford) lacking any *spectral sensitiser*. The irradiation and the standard development of the photo paper allowed the detection of the labelled DNA in picomolar sensitivities (300 attomoles, Figure 3.3). These preliminary results, together with the work presented here, are part of a publication.^[288]

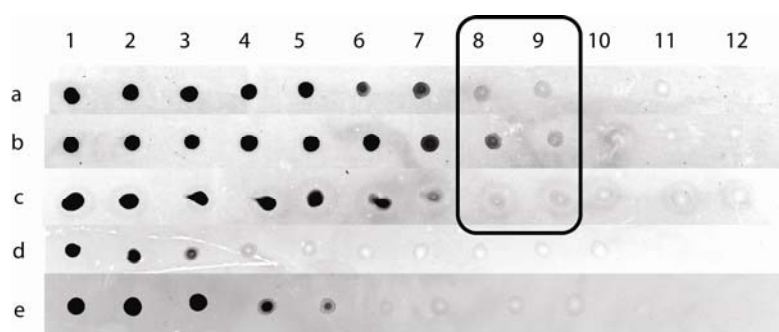


Figure 3.3 Photo strips with sensitizer-modified ODNs: (a) ODN-1; (b) ODN-2; (c) ODN-3; (d) Cy5-ODN; (e) Cy3-ODN. Amounts of DNA (1 μ L each): 1: 10 pmol, 2: 1 pmol, 3: 300 fmol, 4: 100 fmol, 5: 30 fmol, 6: 10 fmol, 7: 3 fmol, 8: 1 fmol, 9: 300 amol, 10: 100 amol, 11: 30 amol, 12: H₂O. The black box shows the detection limit.^[288]

Molecular Beacons in DNA-Photography

The astonishing result achieved using the new straightforward detection method DP encouraged a deeper investigation. A specific DP application was designed that allows the detection of a selected DNA sequence. There are many techniques suitable for this purpose, but not all of them are compatible with the principle of b/w photography and with the intent to keep this method as simple as possible. Many of these methods involve the highly selective hybridisation step between the target (ODN, DNA or RNA) and the probe. One of these techniques, extensively documented in literature, uses modified ODNs called molecular beacons (MBs).^[297] These compounds (Figure 3.4) are single-stranded oligonucleotide hybridization probes able to form a stem-and-loop structure (hairpin). The loop contains a probe sequence that is complementary to the target sequence. The stem is formed by the annealing of complementary arm sequences that are located on either side of the probe sequence. A fluorophore (or *reporter*) is covalently linked to the end of one arm and a quencher is covalently linked to the end of the other arm. Molecular beacons do not fluoresce when they are free in solution. However, when they hybridise to the target nucleic acid strand containing a complementary sequence, they undergo a conformational change that enables them to fluoresce brightly.

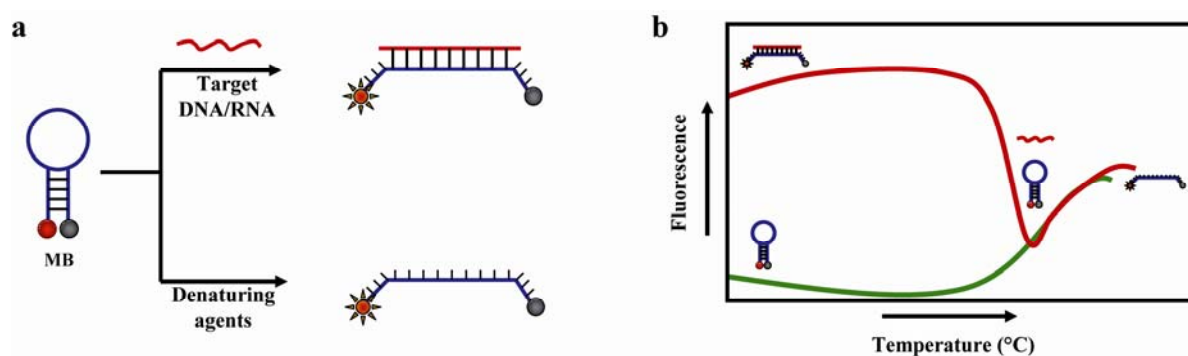


Figure 3.4 MB working principle. a) Two different pathways to denature the hairpin structure of MBs, by a target annealed to the loop region of the hairpin (top) and by temperature, denaturing reagents or ssDNA binding proteins (bottom). b) a typical temperature denaturation monitored by fluorescence spectroscopy of a MB in its open (red line) and closed (green line) conformation.

Some fluorophores used for these probes are the same dyes used in the b/w photography as *spectral sensitizers*.^[298] The MB working principle takes advantage of the fluorescence resonance energy transfer (FRET) process between the two dyes covalently bound at the ends

of the MB. In the absence of targets, the probe does not fluoresce, because the stem places the fluorophore closely to the nonfluorescent quencher. Thus the dyes transfer the excitation energy to the quencher by FRET, eliminating the ability of the fluorophore to fluoresce. When the probe encounters a target molecule, it forms a probe-target hybrid that is longer and more stable than the stem hybrid. The rigidity and length of the probe-target hybrid precludes the simultaneous existence of the stem hybrid. Consequently, the MB undergoes a spontaneous conformational reorganization that forces the stem hybrid to dissociate and the fluorophore and the quencher to move away from each other, restoring fluorescence (Figure 3.4).

This class of oligonucleotides carrying a *spectral sensitizer* and a quencher could be the perfect candidate to set up a DP-based application. In the following work a clear correlation between fluorescence measurements of MBs and the signals detected using the DP detection method was verified (Figure 3.5). This technique was then called *Molecular Beacon DNA Photography* (MBDP).

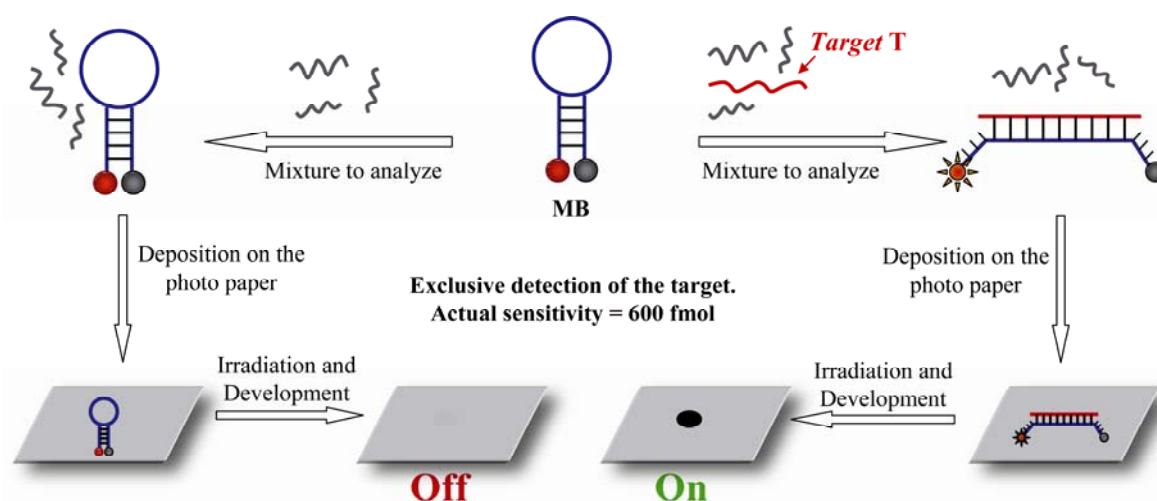


Figure 3.5 Schematic representation of the DNA-photography working principle based on MBs, MBDP. Only the *mixture to analyze*, in which **MB** is annealed with the target **T** gives a positive signal as a black spot on the photo paper. The closed form of **MB** gives no signal on the photo paper.

3.2 Results and Discussion

Materials and Methods

To prove the MBDP concept and its validity an ODN sequence associated with the *Yersinia pestis* bacteria (5'-AGCCACGCCTCAAGGG-3') was chosen as the *Target (T)*. This bacteria causes the infectious disease *plague* in animals and humans, which is of current importance.^[299,300] Specifically, a molecular beacon was designed that binds to amplicons generated from the 16S rRNA genes of *Y. pestis*. Commercially available MBs were purchased and called **MBX** (**X** = 1 - 4, Figure 3.6). They all possess the same sequence, 5'-Dye-CGCTGCCCCCTTGAGGCGTGGCTGCAGCG-Quencher-3', in which the underlined bases form the stem region of the MB. The loop region of **MBX** has a sequence complementary to the 16mer ODN gene of *Y. pestis*, **T**. The non-modified 16 mer ODN **T'** in Figure 3.6 was designed to be complementary with **T** and to trap it when required by competitive hybridisation. The commercially available **Cy3-ODN** was used as reference ODN. The complete sequences are reported in Figure 3.6 along with the dyes used and their absorption and emission wavelengths.

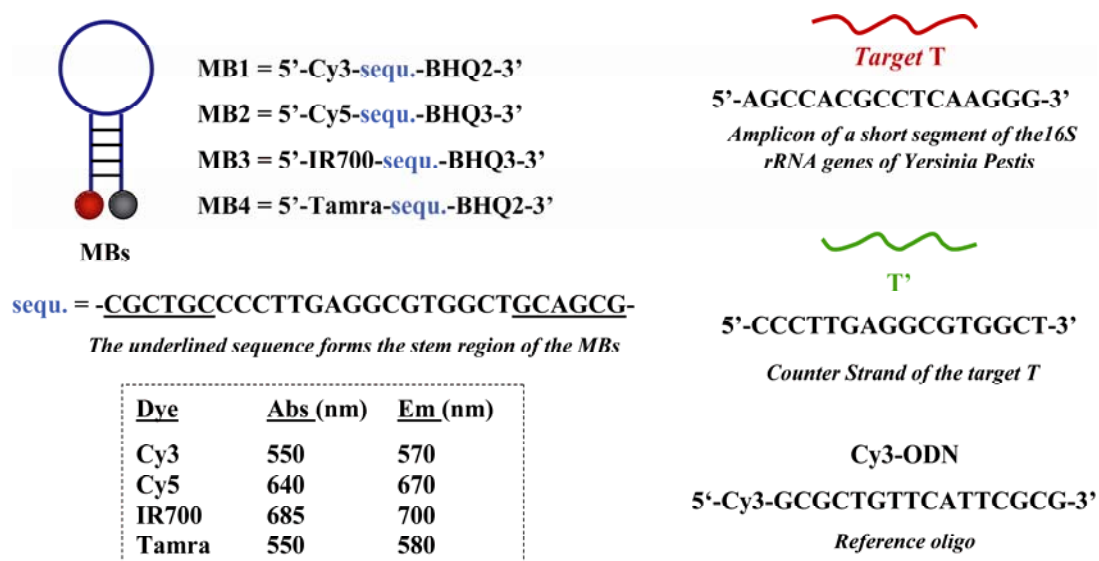


Figure 3.6 Graphical representation of **MBX** (**X** = 1 - 4), **T**, **T'** and **Cy3-ODN** along with their sequences. On the bottom-left side the absorption and emission wavelengths of the dyes used in this work are listed.

Selection of a reporter / quencher couple

Many dyes have been reported in literature in conjunction with MBs. The widespread use of MB probes is also due to the large variety of dyes and quenchers able to accomplish, i.e., multiplex detection of different target sequences. Some of these dyes are used, as free molecules, as *spectral sensitizers* in photography because of their capacity of being adsorbed into the photo paper transferring energy to the silver halide crystals. In order to link the MB detection method with the DP, four different reporters were tested. The dye/quencher couples were selected on the basis of the relative quenching efficiency (i.e. Cy3/BHQ2 or Cy5/BHQ3).^[298] For such tests the same MB target sequence for *Y. pestis* strand **T** was used. Always following the same procedure, four different MBs, **MB1**, **MB2**, **MB3** and **MB4**, were first analysed by fluorescence spectrometry before being tested on the photo paper. In Figure 3.7 the chemical structures of the dyes and the quenchers tested in this work are depicted.

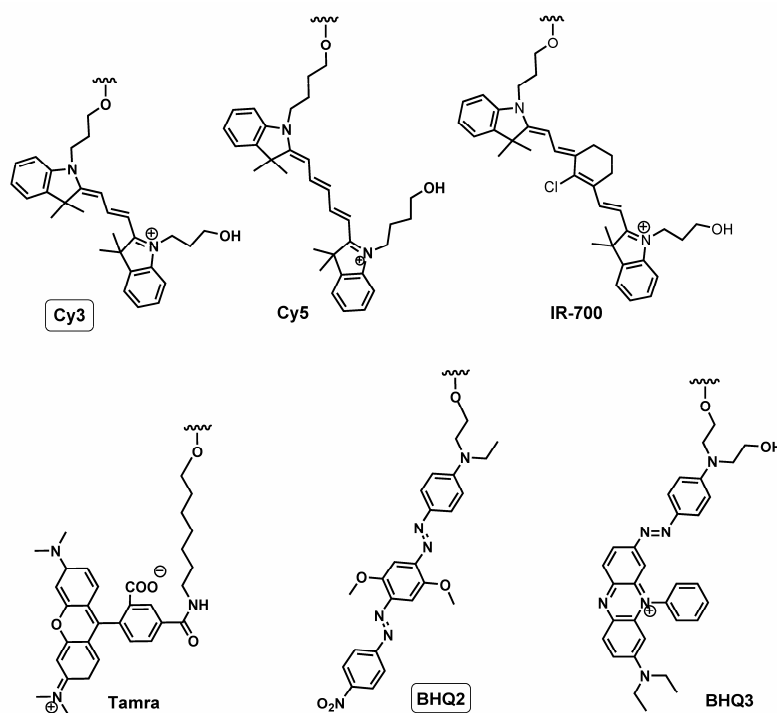


Figure 3.7 Chemical structures of the dyes (Cy3, Cy5, IR-700 and Tamra) and the quenchers (BHQ2 and BHQ3) used in the MB experiments.

After irradiation with the appropriate wavelength, only **MB1** containing Cy3 and BHQ2 showed positive results in the DNA-photography experiments.

The cyanine dyes, such as the Cy3 (in **MB1** and **Cy3-ODN**, Figure 3.6), are the dyes of choice in commercial photography. Covalently linked to the 5'-end, Cy3 is the reporter in

MB1. The black hole quencher (BHQ2), linked to the 3'-end of the same hairpin, establish a good quenching efficiency of 97 %.^[298]

The ability of **MB1** to identify its target was first tested using a fluorescence spectrometer. **MB1** hybridises with an excess of **T** in the presence of a salt concentration over 5 mM. Different hybridisation buffers and salts were tested as mentioned above using different concentrations to obtain the best result with the minimal salt concentration in solution. The salt concentration indeed influences the sensitisation process of the photo paper. Furthermore, the nature of the salt and its anion were shown to play a major role for MBDP sensitivity whereas **MB1** hybridisation properties were influenced only slightly. The fluorescence behaviour of **MB1** was generally consistent with the data reported in literature.^[301] In Figure 3.8 an example of fluorescence analysis of **MB1** is reported.

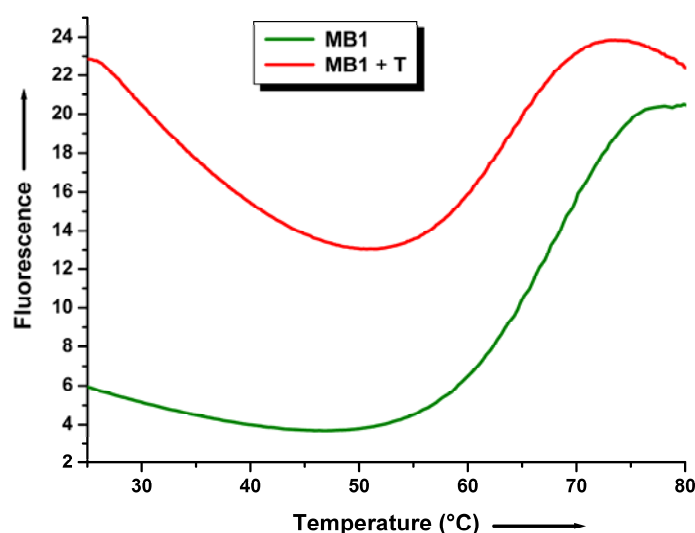


Figure 3.8 Fluorescence spectrometer measurements (emission at 570 nm). Green curve: **MB1** 0.2 μM (from 25 $^{\circ}\text{C}$ to 85 $^{\circ}\text{C}$). Red curve: after the addition of 1.2 μM of **T** to the same solution. Crude data.

Photographic experiments

In a typical MBDP experiment 1 μL of the solution to analyse is placed on the photo paper. The evaporation of the solvent and the penetration of the sample into the resin protecting coat of the paper can be achieved slowly at room temperature (30-60 minutes) or quickly (1-5 minutes) at higher temperatures. In the latter method the loaded photo paper is placed on a warm surface (30-40 $^{\circ}\text{C}$). Higher temperatures can damage the photo paper. The latter method seems to improve the adsorption of the sample into the photo paper as highlighted by the

slightly enhanced sensitivity. It is worth noting that only the dye adsorbed to the silver halide surface is effective as sensitizer.^[291]

Once the 1 μL drops are adsorbed onto the photo paper, the irradiation is performed with white light through a 550 nm cut-off filter and a 2 times “density” filter (0.5 OD). The development of the photo paper was achieved using standard and commercially available solutions as described in *Experimental Part* (Chapter 4). The complete procedure is performed in a dark room. The only instrumentation needed for experiments not included in a standard dark room consisted of a micro-pipette for the sample deposition.

Detection of 10 picomoles of target T

In a preliminary experiment a solution of 1 μM **MB1** in a solution containing Tris-HCl (pH 8, 10 mM) and MgCl_2 (1 mM) was prepared. To one batch of this solution was added a large excess of **T** (10 μM). Both mixtures and a solution containing only **T** (10 μM , 10 mM Tris-HCl pH 8, 1 mM MgCl_2) were warmed up to 80 $^\circ\text{C}$ for 5 minutes and then cooled down slowly (hybridisation procedure). All the samples were analysed by fluorescence spectrometry and in parallel with the new MBDP technique. The latter simply consists of spotting 1 μL of each of the three solutions, plus a reference solution containing only the hybridisation buffers, on the commercially available photo paper as described before.

The results of this first experiment are shown in Figure 3.9. Under these non-optimised conditions it is already possible to distinguish between the *closed* form of **MB1** (1 μL of 1 μM sol. = 1 pmol) in spot 3 and the *open* form in which **MB1** is annealed with **T** (1 μL of 10 μM sol. = 10 pmol) in spot 4 (Figure 3.9, a' and b'). Although spot 3 gives a weak positive signal as well, this is due to the high concentration used in this first experiment and to the non-quantitative quenching of the dye. There is indeed a residual fluorescence signal of **MB1** in its *closed* form (detectable also by fluorescence spectroscopy) even at low temperatures (previous Figure 3.8). Spots 1 and 5 are the references and their white colour (false negative) is in contrast with spot 2 relative to the target **T** (1 μL of 10 μM sol. = 10 pmol) in which the sensitiser (dye) is missing. It is reasonable to conclude that the white aspect of the reference spots is due to the so called salt-effect, namely the interaction of chloride anions present in the reference solution (10 mM Tris-HCl pH 8, 1 mM MgCl_2) with the silver cations of the photo paper. Indeed using these conditions (high Cl^- conc.) when the concentration of any Cy3-labelled ODN is below 0.05 μM it is possible to detect a negative white signal. Above this concentration the spectral sensitisation of the paper due to the dye of the labelled ODN

outperforms the negative effect of the salts. Unlabelled ODNs give weak false positive results (dark spots) for concentrations higher than 50 mM (50 nmol per microliter). In the light of this experimental evidence it is possible to explain spot 2 relative to the solution of the target **T**. It does not appear white as the blank because of the presence of an ODN in high a concentration.

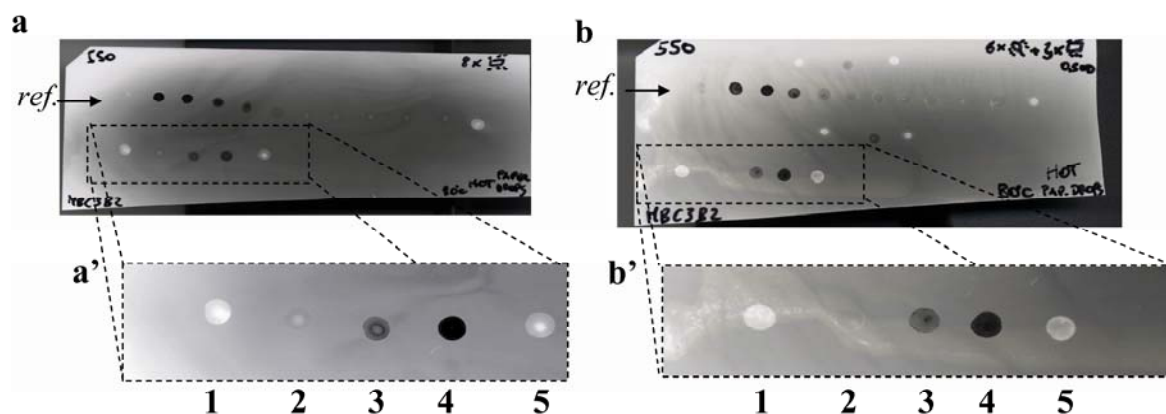


Figure 3.9 Scanner reproduction of two typical photo-experiments. In **a** and **b** in the lane *ref.* a Cy3-labelled ODN (**Cy3-ODN**) is spotted in a dilution series from 10 μ M to 100 fM. In **a'** and in **b'** the enlargements relative to the MBDP experiments are reported. Spots **1** and **5** = hybridisation buffer; spot **2** = 10 μ M **T**; spot **3** = 1 μ M **MB1**; spot **4** = **MB1** + **T** (1:10).

With such an easy experiment it was verified that the molecular beacon principle is applicable for the DNA-photography technique detecting 10 picomoles of **T**. Afterward different conditions were investigated to improve the signal / background ratio and many other parameters in order to extend the applicability of this method to the detection of sub-picomoles ($< 10^{-12}$ moles) of target.

Screening of different hybridisation buffers

Various buffers and salts were tested in order to achieve the hybridisation of **MB1** with **T** with a minimal salt-effect on the photo paper. A list of selected buffers used for this purpose is reported here.

B = 1 M Tris-HCl pH 8, 100 mM $MgCl_2$

B1 = 1 M Tris-HCl pH 8, 400 mM $MgCl_2$, 150 mM KCl

B2 = 900 mM NaCl, 90 mM Na-Citrate

B3 = 1 M KH_2PO_4

B4 = 1 M Na-Formate

B5 = 1M Na-Acetate

B6 = 1M *tri*-Na-Citrate

B7 = 1M Na-tetraborate

B8 = 1M K_2CO_3

None of these buffers improved the performances already achieved using the salt composition of buffer **B** for the MBDP application although many of them showed good hybridisation properties monitored by fluorescence (Figure 3.10). Some examples of photographic experiments are reported in lane A (Figure 3.11).

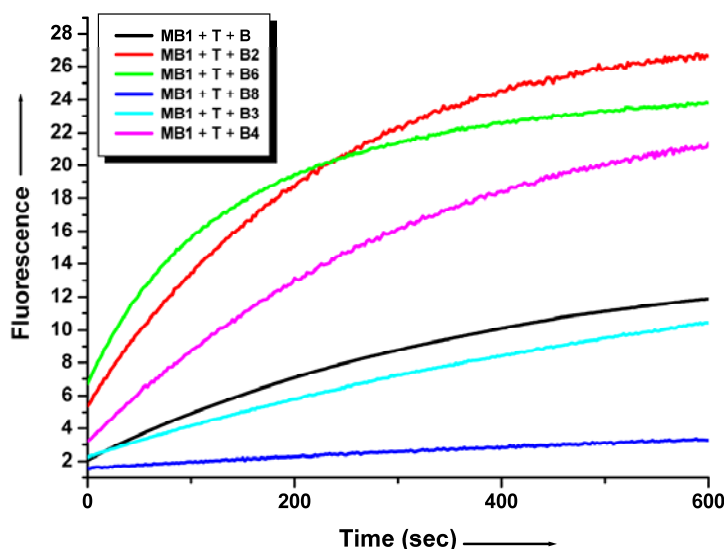


Figure 3.10 Fluorescence emission time acquisitions at 570 nm of the addition of 1.2 μM of **T** to solutions containing 0.2 μM of **MB1** and different hybridisation buffers in different colours.

Lane B in Figure 3.11 is the reference **Cy3-ODN**. Here this ODN is simply dissolved in water and is spotted in a dilution series from 10 μM to 100 fM. To investigate the salt-effect a concentration of 0.2 μM **MB1** was used and only a 3-fold excess of **T** was added (lane A, Figure 3.11). This small excess of **T** is enough for an efficient hybridisation as shown in A3 and A4 (Figure 3.11) and as confirmed by fluorescence monitoring. Interestingly, when *tri*-Na-Citrate (**H6**) or KH_2PO_4 (**H3**) were used as hybridisation salts, the corresponding spots in A6 and A7, respectively, appeared to be quenched, but no white spot was noticeable.

	1	2	3	4	5	6	7	8	9	10	11	12
A	H ₂ O	T	MB1*	(MB1+T)* 1:3	T**	(MB1+T)**	(MB1+T)***	H ₂ O**				
B	C3 10µM	C3 1µM	C3 100nM	C3 30nM	C3 10nM	C3 3nM	C3 1nM	C3 100pM	C3 10pM	C3 1pM	C3 100fM	H ₂ O
C	H ₂ O	B1	B2	B3	B4	B5	B6	B8	B6 conc.	(MB1+T)#		

[MB1] = 0.2 mM C3 = Cy3-ODN * = [B]/400 ** = [B6]/400 *** = [B3]/100 + [B6]/200 # = [B3]/200

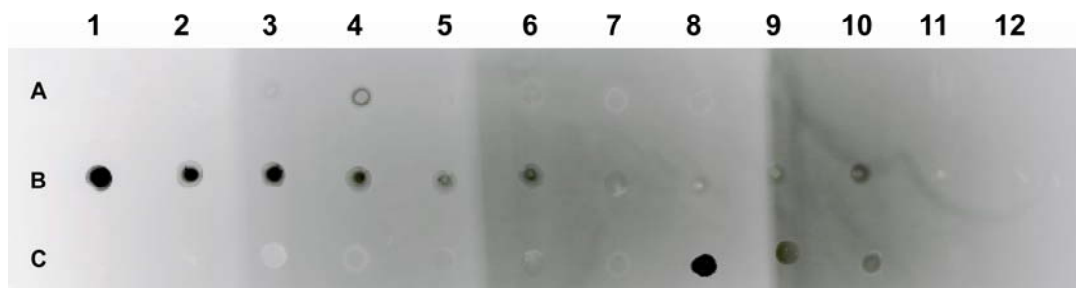


Figure 3.11 Scanner reproduction of the buffer screening photo paper. The samples used are listed in the table.

In lane C of Figure 3.11, solutions containing only water and the buffers are spotted in the same concentration used for the hybridisation experiments. It is worth noting that only the Cl⁻-containing salts give a white spot on the photo paper supporting the assumption that Cl⁻ anions strongly interact with the Ag⁺ cations of the paper. Moreover, some of the buffers sensitised the photo paper even in the absence of any dye. In some cases it was even possible to detect a positive result as for K₂CO₃ (**B8**) in C8 and for a concentrated solution of *tri*-Na-Citrate (**B6**) in C9 of Figure 3.11. As a conclusion, the nature of the salts employed in these experiments and their concentration can strongly influence the sensitivity of the method.

Detection of 600 femtomoles of target T

In spot A4 of Figure 3.11 a clear detection of 600 fmol of **T** by the hybridisation with 200 fmol of **MB1** was reported. In Figure 3.12 the **MB1** concentration was decreased to 0.1 µM (100 fmol per µL) in order to test the minimum amount of “reporter” able to sensitise the photo paper. **T** was used in a 6-fold excess and the buffer concentration was decreased to 5 mM of Tris-HCl pH 8 and 0.5 mM of MgCl₂. Under such experimental conditions it was still possible to detect the target **T** present in spot 4 in a concentration of 0.6 µM, when added to the **MB1** (0.1 µM). Thus, the direct detection of 600 fmol of **T** was achieved using 100 fmol of **MB1** and a commercial, standard photo paper. Spots 7 and 8 were used here as

references. They contained the commercially available **Cy3-ODN** in the concentrations of 1 μM and 0.1 μM , respectively (5 mM Tris-HCl pH 8 and 0.5 mM MgCl_2).

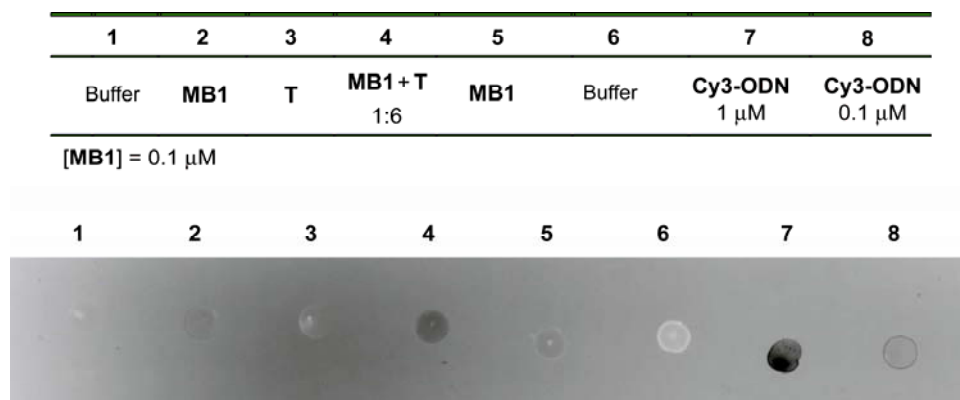


Figure 3.12 Direct detection of 600 fmol of **T** in 1 μL sample containing 100 fmol of **MB1** (spot 4). At these concentrations **MB1** gives no signal on the photo paper. Buffer = 5 mM of Tris-HCl pH 8 and 0.5 mM of MgCl_2 . Irradiation wavelength > 570 nm (cut-off filter), standard development.

Control experiment

The sensitisation of the photo paper by an adsorbed dye gives rise to a black spot as shown in the previous Figures. In the case of a molecular beacon, a quencher such as BHQ2 is able to inhibit the sensitisation process initiated by a dye such as Cy3. The addition of a sequence complementary to the loop region of the MB results again in the sensitisation of the photo paper, visualised by a black spot formation (after irradiation and development). In order to verify the MB principle associated with the photographic sensitisation, a control experiment was carried out in which **T** was added to **MB1**, removed by **T'** addition and re-added to the **MB1**. This sequence of additions was monitored by fluorescence spectroscopy, while the mixture was spotted onto the photo paper at each step. The interpretation of the low intensity spots in this on-off experiment was fully confirmed by the parallel use of the fluorescence spectrometer. This lack of resolution on the photo paper was ascribed to the low concentration of the samples and to the above-mentioned salt-effect. Once the **MB1** was annealed with its target **T** (spot 4 in Figure 3.13) it was possible to “switch off” the signal generated by the addition of the counter strand **T'** in excess (spot 5). This strand hybridises with **T** in competition with **MB1**. The **T/T'** hybridisation will be favoured over the **T/MB1** hybridisation by the large excess of **T'** used and by thermodynamic factors (**MB1** can form a

stable hairpin). In spot 6 the fluorescence of the mixture in the fluorescence spectrometer and the spot on the photo paper were restored again by the addition of **T**. The unlabelled DNA formed by **T/T'** hybridisation gave a negative spot on the photo paper (spot 7), even for high concentrations of 1.2 μM used here.

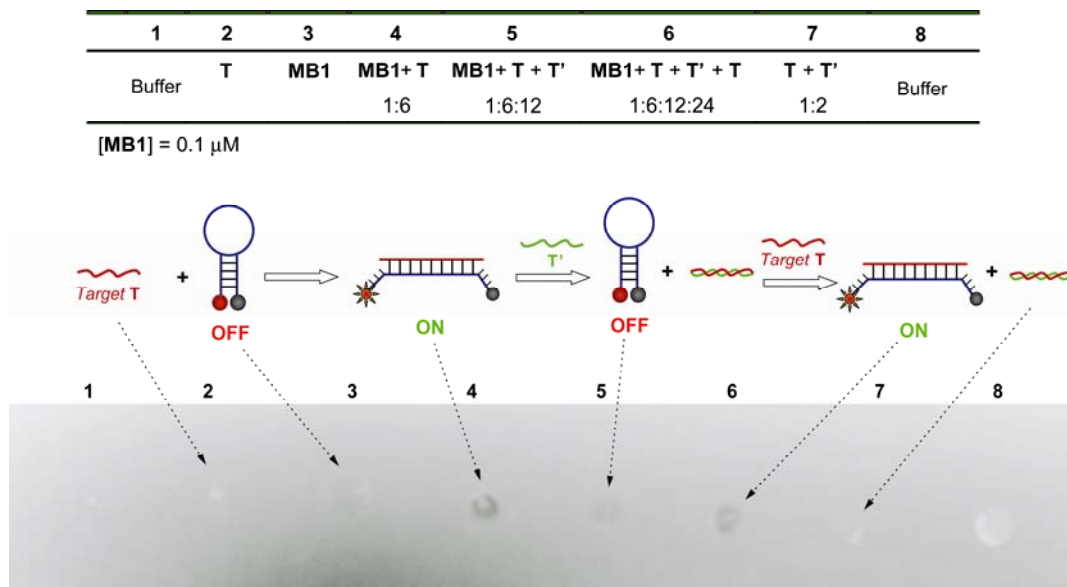


Figure 3.13 Scanner reproduction of the photo paper after development. $[\text{MB1}] = 0.1 \mu\text{M}$; $[\text{T}] = 0.6 \mu\text{M}$ (6-fold excess). **T'** = (5'-CCCTTGAGGCGTGGCT-3') counter strand of **T**. Buffer = 5 mM of Tris-HCl pH 8 and 0.5 mM of MgCl_2 . Irradiation wavelength > 570 nm (cut-off filter), standard development.

Detection in presence of genomic DNA

In order to prove the feasibility of the MBDP to detect a target in samples, such as a gene in a complex mixture, a simplified experiment was designed. The experiment was aimed to prove if the detection of a target was possible in the presence of genomic DNA (**gDNA**). The target **T** and the molecular beacon **MB1** were used as first test for a better evaluation in comparison with the aforementioned collected data. The clear detection of 600 fmol of *Y. pestis* gene (**T**) was achieved in a complex mixture by adding **gDNA** to the buffer solution (5 mM Tris-HCl pH 8 and 0.5 mM MgCl_2) containing 0.2 μM **MB1** and 0.6 μM **T**. The genomic DNA was previously fragmented by sonication. The majority of the resulting fragments ranged from less than 0.5 kb to up to 2 kb (1 kb = 1000 bases). The extraction and the digestion of **gDNA** were performed by *Melanie Maul* of the *Carell* group. More details are reported in the *Experimental Section*. The concentration of **gDNA** in the following experiments ranged between 9 (Figure 3.14) and 30 ng/ μL (Figure 3.15).

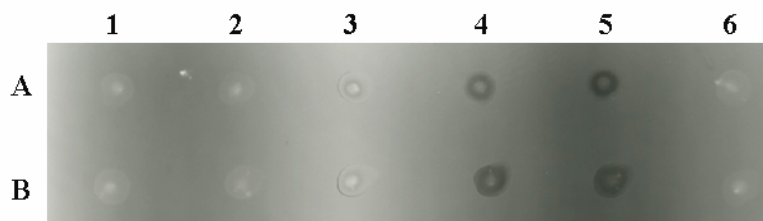


Figure 3.14 Lane A: photopaper loaded with 1 μL of 1) buffer (5 mM Tris-HCl pH 8 and 0.5 mM MgCl_2); 2) **T** 0.6 μM in buffer; 3) **MB1** 0.2 μM in buffer; 4) and 5) two different batches of **MB1** 0.2 μM plus **T** 0.6 μM in buffer; 6) as in spot 1. Lane B: the photopaper was loaded with 1 μL of 1) buffer (5 mM Tris-HCl pH 8 and 0.5 mM MgCl_2) plus 9 ng/ μL of **gDNA**; 2) **T** 0.6 μM plus 9 ng/ μL of **gDNA** in buffer; 3) **MB1** 0.2 μM plus 9 ng/ μL of **gDNA** in buffer; 4) and 5) two different batches of **MB1** 0.2 μM plus **T** 0.6 μM plus 9 ng/ μL of **gDNA** in buffer; 6) as in spot 1. Irradiation wavelength > 570 nm (cut-off filter), standard development.

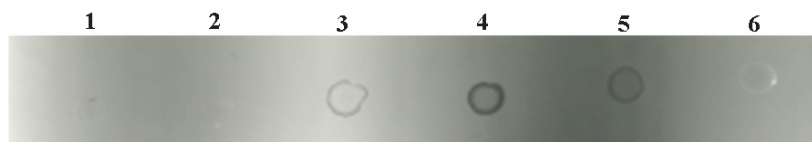


Figure 3.15 Photopaper loaded with 1 μL of 1) buffer (5 mM Tris-HCl pH 8 and 0.5 mM MgCl_2) plus 30 ng/ μL of **gDNA**; 2) **T** 0.6 μM plus 30 ng/ μL of **gDNA** in buffer; 3) **MB1** 0.2 μM plus 30 ng/ μL of **gDNA** in buffer; 4) and 5) two different batches of **MB1** 0.2 μM plus **T** 0.6 μM plus 30 ng/ μL of **gDNA** in buffer; 6) as in spot 1. Irradiation wavelength > 570 nm (cut-off filter), standard development.

For higher concentrations of **gDNA** false positive signals were detected (Figure 3.16). For a comparison, the concentration of 0.6 μM **T** corresponds to 3 ng/ μL of **T** in solution.

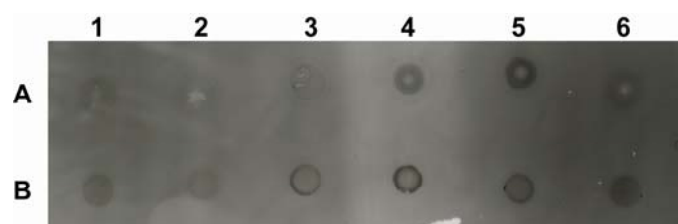


Figure 3.16 Photopaper loaded with 1 μL of (for both lane A and B). 1) buffer (5 mM Tris-HCl pH 8 and 0.5 mM MgCl_2) plus **gDNA**; 2) **T** 0.6 μM plus **gDNA** in buffer; 3) **MB1** 0.2 μM plus **gDNA** in buffer; 4) and 5) two different batches of **MB1** 0.2 μM plus **T** 0.6 μM plus **gDNA** in buffer; 6) as in spot 1. In lane A [**gDNA**] = 50 ng/ μL ; in lane B [**gDNA**] = 80 ng/ μL . Irradiation wavelength > 570 nm (cut-off filter), standard development.

3.3 Conclusions and Outlooks

A novel method to detect ODNs/DNA was established using the principle of black and white photography. Picomolar sensitivity levels could be achieved without extensive optimisation. A technique suitable for practical applications of this new method was established based on the highly specific hybridisation properties of DNA. Preliminary experiments showed that this technique is easy to use and inexpensive although astonishing results could already be achieved with it. So far the detection limit using the above-mentioned commercial photo paper and the conditions reported here is 600 femtomoles of target **T** per 1 μL of solution analysed.

It is easy to believe that the so-called MBDP could be the base technology to develop new assays and new transportable instrumentation for the *in situ* detection of a large variety of biomolecules. In the introduction the “Polaroid[®]” camera was cited as one of the less complex chemical laboratory ever commercialised. A similar device (a *camera*) could be used for a MBDP application in which a built-in sampler deposits the analytes on the photo paper.

Different targets can be detected using different MBs at the same time since the specificity of these probes is well established in literature.^[302] MBs are indeed applied in single nucleotide polymorphism (SNP) studies and in multiplex detection of different targets as well.^[303] Reported modification of the MBs structure as in the locked nucleic acid based MBs (LNA-MBs)^[304] or of the dye / quencher couples as for MBs with superquenchers^[305] or with gold-quenchers^[303] make these MBs the perfect candidates for many applications.

4 Experimental Section

General

All solvents were of the quality puriss. p. a., or purum. Purum solvents were distilled prior to use. The commercially available reagents were purchased from Sigma-Aldrich, ACROS or Lancaster and used without further purification. Analytical thin-layer chromatography (TLC) was carried out using aluminum-based plates Silica 60 F₂₅₄ from Merck. Plates were visualized under UV-light ($\lambda = 254$ nm) or by staining with anisaldehyde solution or with 2,4-dinitrophenylhydrazine solution in ethanol. Flash chromatography was carried out using Merck Silica 60 (230-400 mesh) with N₂ overpressure. Samples were applied as saturated solutions in an appropriate solvent. ¹H-NMR spectra were recorded on Bruker DRX 200 (200 MHz), AMX 300 (300 MHz), ARX 300 (300 MHz), AMX 400 (400 MHz), AMX 500 (500 MHz), AMX 600 (600 MHz), Varian Oxford 200 (200 MHz) and Varian XL 400 (400 MHz) spectrometers. The chemical shifts were referenced to (CH₃)₂CO ($\delta = 2.05$ ppm) in (CD₃)₂CO-d₆, DMSO ($\delta = 2.50$ ppm) in DMSO-d₆ and CHCl₃ ($\delta = 7.26$ ppm) in CDCl₃. ¹³C-NMR spectra were recorded on Bruker ARX 200 (50 MHz), AMX 300 (75 MHz), ARX 300 (75 MHz), AMX 500 (125 MHz), AMX 600 (150 MHz) and Varian XL 400 (100 MHz) spectrometers. The chemical shifts were referenced to (CH₃)₂CO ($\delta = 30.83$ ppm) in (CD₃)₂CO-d₆ and CHCl₃ ($\delta = 77.00$ ppm) in CDCl₃. Standard pulse sequences were employed for ¹H, ¹H and ¹H, ¹³C correlation studies. Mass spectra and high-resolution mass spectra were measured on Finnegan TSQ 7000, Finnegan MAT 95S, Finnegan MAT 95Q, Finnegan MAT 90 (FAB), Finnegan LTQ-FT, PE Sciex Q-Star Pulsar and Bruker Autoflex II (MALDI-TOF). Irradiation Experiments were achieved using a 1000-W Xe Lamp (254 nm). Fluorescence cuvettes stoppered with a rubber septum and cooled at 10°C during irradiation were used as reactors. The solutions were bubbled with Argon before (30 min) and during irradiation in order to establish anaerobic conditions. Analytical HPLC was performed with Merck-Hitachi systems equipped with L7420 UV-Vis and L-7455 DAD detectors. Analytical separations were performed with a *CC 250/4 Nucleosil 120-3 C8* column with a isocratic flow (MeCN/H₂O 80:20).

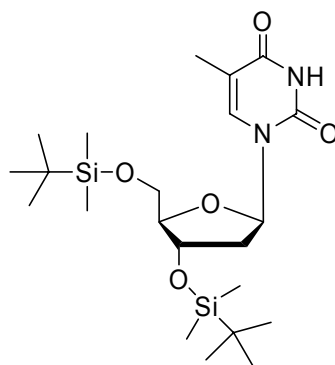
4.1 Nucleoside models for the study of C5'-radicals fate associated with oxidative damage of DNA

NMR spectra were recorded with a Varian 400 instrument using Me₄Si as an internal standard. HPLC analyses were performed with a Waters X-Terra C18 MS instrument equipped with a C18 column and a diode array detector. Mass spectra were recorded with a VG 7070E instrument using electron spray ionisation both in positive (ES+) and negative (ES-) ionization..

4.1.1 Formation and fate of the *pseudo* C4'-radical

Thymidine and thymine were commercially available. Thymidinoic acid **1.65**^[306] and the reduced product **1.64**^[307] were identified by comparison with spectral data reported in the literature. The *tert*-butylacetal **1.63a** was characterized by NMR and MS spectral analysis. The methylacetal **1.63b** was not separated as a pure compound; its characterization came from ¹H NMR and MS spectral analysis of a mixture of **1.63b** and **1.66**.

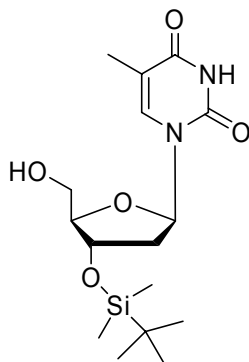
3',5'-*O*-(*tert*-Butyldimethylsilyl)thymidine **1.58**^[308]



Following the procedure of Ogilvie^[309], thymidine (1.00 g, 4.10 mmol) was dissolved in a 1:1 mixture of dry THF/DMF (15 mL), then imidazole (1.10 g, 16.50 mmol), AgNO₃ (1.55 g, 9.10 mmol) and *tert*-butyldimethylsilyl chloride (TBDMSCl, 1.40 g, 9.10 mmol) were added, in this order, under nitrogen atmosphere and the mixture was stirred at room temperature for 3h. The reaction mixture was filtered, diluted with ethyl acetate (20 mL), washed with several portions of water, dried over MgSO₄ and concentrated under reduced pressure. The resulting residue was chromatographed on silica gel column by gradual elution with ethyl

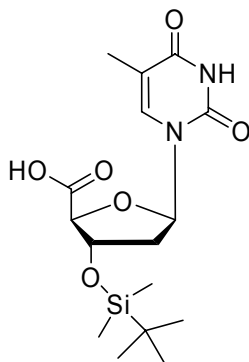
acetate/hexane mixture (up to 20% ethyl acetate). 3',5'-*O*-(*tert*-Butyldimethylsilyl)thymidine was obtained as a white solid (1.90 g, 4.05 mmol).

3'-*O*-(*tert*-Butyldimethylsilyl)thymidine **1.59**^[310]



Following the procedure of White^[311] pyridinium *p*-toluenesulphonate (PPTS; 4.10 g, 16.20 mmol) was added to a solution of 3',5'-*O*-(*tert*-butyldimethylsilyl) thymidine **1.58** (1.90 g, 4.05 mmol) in methanol (30 mL). The resulting mixture was stirred at room temperature until t.l.c. showed disappearance of starting material (16-20 h), then the solvent was evaporated under reduced pressure. The residue was dissolved in ethyl acetate (10 mL), washed with several portions of water, dried over MgSO₄ and concentrated under reduced pressure. Crude 3'-*O*-(*tert*-butyldimethylsilyl) thymidine **1.59** was obtained as a white solid (1.00 g, 2.80 mmol) and reacted without further purification.

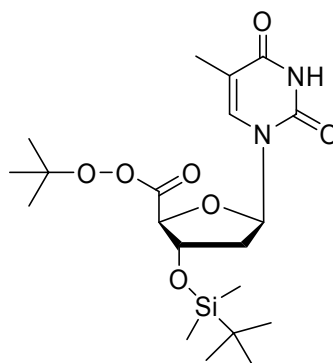
3'-*O*-(*tert*-Butyldimethylsilyl)-5'-carboxythymidinoic acid **1.60**^[312]



Following the procedure of Piancatelli et al.^[70] tetramethylpiperidinium-*N*-oxide (TEMPO; 0.10 g, 0.60 mmol) and bis-acetoxyiodobenzene (BAIB; 2.15 g, 6.70 mmol) were added to a solution of 3'-*O*-(*tert*-butyldimethylsilyl) thymidine **1.59** (1.00 g, 2.80 mmol) in 1:1

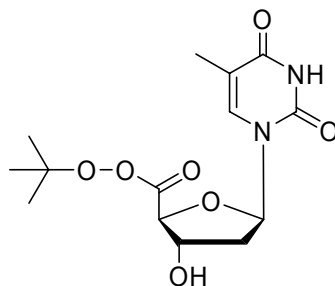
MeCN/H₂O (20 mL). After stirring at room temperature for 2 h, the reaction mixture was diluted with ethyl acetate (10 mL), washed with several portions of water, dried over MgSO₄ and concentrated under reduced pressure. The resulting residue was chromatographed on silica gel column by gradual elution with ethyl acetate/hexane mixture (up to 40% ethyl acetate). 3'-*O*-(*tert*-Butyldimethylsilyl)-5'-carboxythymidinoic acid **1.60** was obtained as a white solid (1.00 g, 2.75 mmol).

3'-*O*-*tert*-Butyldimethylsilylthymidine-5'-carboxylic acid *tert*-butyl perester **1.61**



Carbonyldiimidazole (CDI; 0.45 g, 2.75 mmol) was added to a solution of 3'-*O*-(*tert*-butyldimethylsilyl)-5'-carboxy thymidinoic acid **1.60** (1.00 g, 2.75 mmol) in dry THF (20 mL). The solution was stirred at room temperature for 1 h under nitrogen atmosphere, then cooled at 0°-5°C (ice bath) and *tert*-butyl hydroperoxide (*t*-BuOOH; 5M solution in decane; 1.20 mL, 6.05 mmol) was added dropwise. The reaction mixture was stirred for 20 minutes, then diluted with diethyl ether (20 mL), washed with several portions of cold brine, dried over MgSO₄ and concentrated under reduced pressure. The oily residue was chromatographed on florisil column by gradual elution with diethyl ether/hexane mixture (up to 70% ether). The title product **1.61** was obtained as a white solid (1.10 g, 2.50 mmol).

[δ_{H} (CDCl₃) 9.2 (1H, br s, disappeared on D₂O shake; NH), 8.0 (1H, s, H6), 6.57 (1H, dd, $J_1 = 9.5$, $J_2 = 4.8$ Hz, H1'), 4.54 (1H, d, $J = 4.0$ Hz, H3'), 4.43 (1H, s, H4'), 2.29 (1H, A part of an ABX system, $J_{\text{AB}} = 13.0$ Hz, $J_{\text{AX}} = 4.8$ Hz, H2''), 2.04 (1H, B part of an ABXY system, $J_{\text{AB}} = 13.0$ Hz, $J_{\text{BX}} = 9.5$ Hz, $J_{\text{BY}} = 4.0$ Hz, H2'), 1.93 (3H, s, CH₃), 1.35 (9H, s, *t*-BuO), 0.9 (9H, s, *t*-BuSi), 0.12 (3H, s, CH₃Si), 0.11 (3H, s, CH₃Si); δ_{C} (CDCl₃) 0.00 (CH₃Si), 0.03 (CH₃Si), 17.57 (CH₃), 22.96 (q), 30.60 (CH₃), 31.03 (CH₃), 44.40 (CH₂), 80.84 (CH), 87.93 (CH), 89.63 (q), 91.33 (CH), 116.63 (q), 140.86 (CH), 115.87 (q), 168.83 (q), 174.02 (q); MS (ES⁻) m/z 441 (M-1)⁻, MS(ES⁺) m/z 465 (M + Na)⁺]

Thymidine-5'-carboxylic acid *tert*-Butyl perester 1.55

To a solution of 3'-*O-tert*-butyldimethylsilylthymidine-5'-carboxylic acid *tert*-butyl perester **1.61** (1.10 g, 2.50 mmol) in dry THF (10 mL) tetrabutylammonium fluoride (TBAF; 1M solution in THF, 2.75 mL, 2.75 mmol) was added dropwise at 0°-5°C (ice bath) under nitrogen atmosphere. The reaction mixture was stirred for 30 min, then cold brine (5 mL) was added. The resulting mixture was extracted with diethyl ether (5 x 10 mL), the organic phase washed with cold brine (5 mL), dried over MgSO₄ and concentrated under reduced pressure to give the *tert*-butyl perester of 5'-carboxythymidinoic acid **1.55** as a white solid (0.40 g, 1.25 mmol).

[m.p. 85-86° C; δ_{H} (CDCl₃) 9.1 (1H, br s, NH), 8.0 (1H, s, H6), 6.6 (1H, dd, $J_1 = 8.5$, $J_2 = 4.5$ Hz, H1'), 4.65 (1H, d, $J = 4.0$ Hz, H3'), 4.6 (1H, s, H4'), 2.5 (1H, A part of an ABX system, $J_{\text{AB}} = 13.0$ Hz, $J_{\text{AX}} = 4.5$ Hz, H2''), 2.1 (1H, B part of an ABXY system, $J_{\text{AB}} = 13.0$ Hz, $J_{\text{BX}} = 8.5$ Hz, $J_{\text{BY}} = 4.0$ Hz, H2'), 1.95 (3H, s, CH₃), 1.4 (9H, s, *t*-Bu); δ_{C} (DMSO) 15.57 (CH₃), 28.90 (CH₃), 53.16 (CH₂), 68.94 (q), 74.34 (CH), 84.76 (CH), 86.09 (CH), 110.47 (q), 136.51 (CH), 151.21 (q), 164.30 (q), 169.39 (q); MS(ES⁻) m/z 327 (M-1)⁻; UV $\lambda_{\text{max}} = 266$ nm]. The perester **1.55** was found to be stable for several days at -14 °C in the solid state, whereas it underwent smooth decomposition in solution [$t_{1/2}$ (*t*-BuOH, 30 °C) = 11 h; $t_{1/2}$ (MeOH, 20 °C) = 2 h]

Thermal decomposition of *tert*-Butyl perester of 5'-carboxythymidinoic acid (1.55)

General Procedure. A 1.5 mM solution of perester **1.55** (5 mL) in the appropriate solvent (THF, methanol, *tert*-butanol, 3:1 water/*tert*-butanol) in a sealed tube was bubbled with the appropriate gas (air, 10% oxygen, 1% oxygen or argon), then kept in a thermostatic bath a 85 °C for 1 h, unless otherwise stated. In all cases qualitative and quantitative analyses of reaction mixtures were performed by HPLC. When appropriate, reactions were repeated on

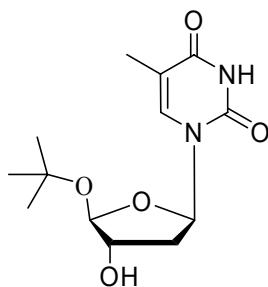
50 mL scale, the solvent eliminated under reduced pressure and the residue chromatographed on silica gel column by gradual elution with ethyl acetate/n-hexane.

Thermal decomposition of *tert*-Butyl perester **1.55** in THF

The reaction was carried out on analytical scale both in the absence and in the presence of thiophenol (4 μ L, 5 molar equiv). Yields of reaction products, determined by HPLC analysis, are given in Table, entries 1 and 2, respectively. Attempts to analyse reaction mixtures by GC/MS were unsuccessful: no peaks were detected.

[(*S*)-4-Hydroxy-(*S*)-5-*tert*-butoxytetrahydrofuran-(*R*)-2-yl]thymine **1.63a**

The reaction in the presence of thiophenol was carried out on preparative scale. Column chromatography separated pure samples of the reduced product **1.64**, the acid **1.65**, and **1.63a** as a white solid.



[δ_{H} (CDCl_3) 9.0 (1H, br s, NH), 7.7 (1H, s, H6), 6.65 (1H, t, $J = 7.0$ Hz, H1'), 5.3 (1H, s, H4'), 4.2 (1H, d, $J = 4.0$ Hz, H3'), 2.4 (1H, A part of an ABX system, $J_{\text{AB}} = 14.0$, $J_{\text{AX}} = 7.0$ Hz, H2''), 2.1 (1H, B part of an ABXY system, $J_{\text{AB}} = 14.0$, $J_{\text{BX}} = 7.0$ Hz, $J_{\text{BY}} = 4.0$ Hz H2'), 2.0 (3H, s, CH_3), 1.3 (9H, s, t-Bu); δ_{H} (DMSO) 11.2 (1H, br s, NH), 7.6 (1H, s, H6), 6.35 (1H, t, $J = 8.0$ Hz, H1'), 5.35 (1H, d, $J = 4$ Hz; collapsing to s upon irradiation at δ 4.0; H4'), 5.15 (1H, s; disappeared on D_2O shake; C3'-OH), 4.0 (1H, t, $J = 4.0$ Hz, H3'), 2.1 (1H, A part of an ABX system, $J_{\text{AB}} = 13.5$, $J_{\text{AX}} = 8.0$ Hz; collapsing to A part of an AB system, $J = 13.5$ Hz, upon irradiation at δ 6.35; H2''), 2.0 (1H, B part of an ABXY system, $J_{\text{AB}} = 13.5$, $J_{\text{BX}} = 8.0$ Hz, $J_{\text{BY}} = 4.0$ Hz; collapsing to B part of an ABX system upon irradiation at δ 6.35; H2'), 1.8 (3H, s, CH_3), 1.2 (9H, s, t-Bu); δ_{C} (DMSO) 13.05 (CH_3), 29.07 (CH_3), 37.85 (CH_2), 75.59 (q), 75.91 (CH), 85.46 (CH), 103.92 (CH), 110.26 (q), 137.02 (CH), 151.33 (q), 164.34 (q); MS(ES^+) m/z 307 ($\text{M} + \text{Na}$) $^+$; MS(ES^-) m/z 283 ($\text{M}-1$) $^-$; UV $\lambda_{\text{max}} = 266$ nm].

The reaction in the absence of thiophenol was repeated on analytical scale in deuterated d8-THF. HPLC analysis showed a peak with the same retention time of **1.64**, which was identified as the deuterated d-5. Compounds d-5 and **1.63a** were present in 2% and 14% yield, respectively.

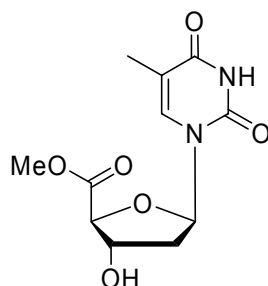
Thermal decomposition of *tert*-Butyl perester (**1.55**) in *tert*-butanol

The reaction was carried out on analytical scale both in the absence and in the presence of thiophenol (4 μ L, 5 molar equiv). Yields of reaction products are given in Table, entries 3 and 4, respectively. The reaction in the absence of thiophenol was carried out on preparative scale. Column chromatography separated the (4'S)-acetal **1.63a** as the main reaction product together with minor amounts of thymine 3.

Thermal decomposition of *tert*-Butyl perester (**1.55**) in methanol

The reaction was carried out on analytical scale both in the absence and in the presence of thiophenol (4 μ L, 5 molar equiv). In both HPLC analysis (Table, entries 5, 6) showed peaks due to thymine 3, *tert*-butylacetal **1.63a**, the reduced product **1.64**, and acid **1.65**, in addition to an unknown peak X. Both reactions were repeated on preparative scale both in the absence and in the presence of thiophenol. Column chromatography separated the product responsible for the peak X. In the reaction carried out in the presence of thiophenol the product X was identified as pure *methyl ester* **1.66**.^[313]

Thymidine-5'-carboxylic acid methyl ester **1.66**

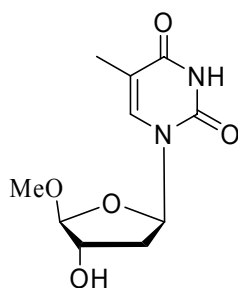


$[\delta_{\text{H}}$ (DMSO) 11.2 (1H, br s, NH), 7.95 (1H, s, H6), 6.34 (1H, dd, $J_1 = 9.2$, $J_2 = 5.2$ Hz, H1'), 5.85 (1H, d, $J = 3.2$ Hz, H4'), 4.45 (1H, broad signal; collapsing to doublet, $J = 5.0$ Hz, upon irradiation at δ 5.85, H3'), 3.75 (3H, s, OMe), 2.10 (1H, A part of an ABX system, $J_{\text{AB}} = 13.0$ Hz, $J_{\text{AX}} = 5.2$ Hz, H2''), 2.0 (1H, B part of an ABXY system, $J_{\text{AB}} = 13.0$ Hz, $J_{\text{BX}} = 9.2$

Hz, $J_{\text{BY}} = 5.0$ Hz, $\text{H}2'$), 1.77 (3H, s, CH_3); δ_{C} (DMSO) 13.12 (CH_3), 38.61 (CH_3), 52.98 (CH_2), 74.32 (CH), 84.99 (CH), 86.17 (CH), 110.26 (q), 136.78 (CH), 151.21 (q), 164.34 (q), 172.21 (q); MS(ES^-) m/z 269 ($\text{M} - 1$)⁻; MS(ES^+) m/z 293 ($\text{M} + \text{Na}$)⁺].

An independent experiment showed that perester **1.55** decomposed in methanol solution at room temperature to give the methyl ester **1.66** as the exclusive reaction product. In the reaction carried out in the absence of thiophenol the product X was found to be a 3:1 mixture of the methyl ester **1.66** and the methyl acetal **1.63b**, as indicated by ^1H NMR and MS spectral analysis.

[(4-Hydroxy-5-methoxytetrahydrofuran-2-yl)thymine 1.63b



δ_{H} (DMSO) 11.2 (1H, br s, NH), 7.22 (1H, s, H6), 6.45 (1H, t, $J = 7.5$ Hz, $\text{H}1'$), 5.44 (1H, d, $J = 3.2$ Hz, $\text{H}4'$), 4.38 (3H, s, OMe), 4.12 (1H, broad signal; collapsing to doublet, upon irradiation at δ 5.44, $\text{H}3'$), 2.0-2.15 (2H, multiplet, $\text{H}2'$), 1.77 (3H, s, CH_3); δ_{C} (DMSO) 13.15 (CH_3), 37.36 (CH_3), 55.07 (CH_2), 74.58 (CH), 85.63 (CH), 110.10 (CH), 110.97 (q), 136.22 (CH), 151.40 (q), 164.20 (q); MS(ES^-) m/z 241 ($\text{M} - 1$)⁻; MS(ES^+) m/z 242 (M)⁺, 265 ($\text{M} + \text{Na}$)⁺].

Thermal Decomposition of *tert*-Butyl perester (1.55) in 3:1 water/*tert*-butanol

The reaction was carried out on analytical scale both in the absence and in the presence of glutathione (2 or 5 molar equiv) under different oxygen concentration. Yields of reaction products are given in Table, entries 7-13.

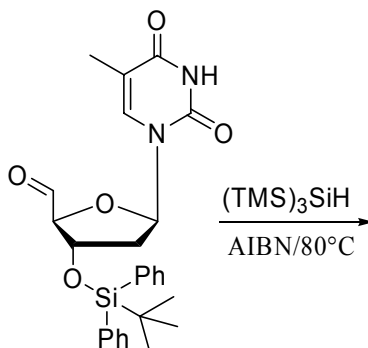
4.1.2 Radical Cyclization Approach to Cyclonucleosides

General: ^1H and ^{13}C NMR spectra were recorded on a Varian Mercury 400 spectrometer at 400 MHz and 100.6 MHz, respectively. Chemical shifts are expressed in ppm (δ) and coupling constants in Hertz (Hz). LC/MS analyses were performed on a Agilent 1100 HPLC system and a Esquire 3000 Plus Bruker mass spectrometer. LC analyses were performed on a Zorbax C8 column (4.6 \times 150 mm, 5 μm) with a linear gradient acetonitrile/water from 50:50 to 95:5 in 20 min at a flow rate 0.6 mL/min, detection at λ 260 nm. Column chromatography was performed by the method of Still using Merck 230-400 mesh ASTM silica gel 60. Analytical thin layer chromatography (TLC) was performed using Merck 60 F₂₅₄ 0.2 precoated silica gel plates, respectively. Compounds were visualized using ultraviolet light or by heating plates previously immersed in ammonium molybdate / ceric ammonium sulfate / sulfuric acid mixture. Solvents were freshly distilled prior to use. All other reagents were used as received.

Synthesis of 3'-*O*-*tert*-Butyldiphenylsilylthymidine 5'-carboxaldehyde (**1.70**)

Following the procedure of Angeloff et al.⁵ 3'-silylated thymidine (0.92 g, 2.6 mmol) and dicyclohexylcarbodiimide (2.14 g, 10.4 mmol) were dissolved in dry DMSO (10.0 mL). Then, a solution of dichloroacetic acid (112 mL, 1.32 mmol) in 1.5 mL of DMSO was added dropwise over 1 min with stirring at 0°C (ice bath). The reaction mixture was stirred at ambient temperature overnight. Ethyl acetate was added (8 mL), the mixture was cooled to about 5 °C, and oxalic acid (720 mg, 8 mmol) was added by little portions with stirring. Then, additional 8 mL of EtOAc were added, and cold mixture was stirred for 1 h. Precipitate of dicyclohexylurea was filtered off and washed with EtOAc (2 \times 8 mL). The organic solution was washed with aqueous sodium bicarbonate (2 \times 6 mL) and NaCl (6 mL), dried over sodium sulfate and evaporated to dryness. Aldehyde product **1.70** was precipitated from dichloromethane by pentane addition. Yield of the white powder: 650 mg (1.8 mmol, 70%).

Reaction of 5'-Carboxaldehyde **1.70** with (TMS)₃SiH

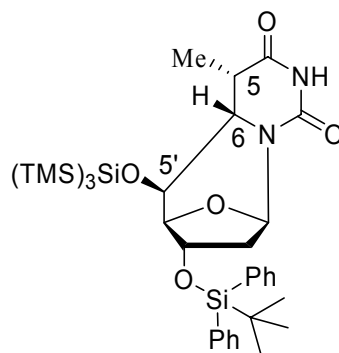


To a 0.01 M solution of aldehyde **1.70** (48 mg, 0.1 mmol), prepared following the reported procedure,^[90] in C₆H₅ (10 mL) were added AIBN (3 mg, 0.02 mmol) and (TMS)₃SiH (0.175 mL, 0.5 mmol). The solution was refluxed under argon atmosphere for 1 h. Analysis by LC/MS and ¹H NMR of the crude reaction mixture after evaporation of the solvent showed the formation of compounds **1.71a** and **1.71b** in 30:70 ratio and in 85% overall yield. Column chromatography on silica gel by gradient elution with *n*-hexane/ethyl acetate led to separation of the two compounds. The characterisation of this aldehyde is reported in literature.^[79]

Kinetic experiments

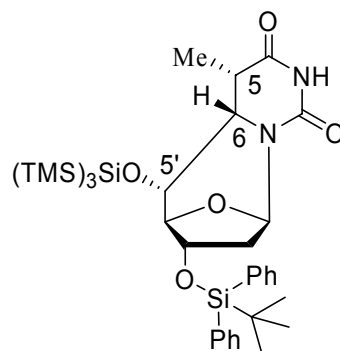
To a solution containing aldehyde **1.70** (0.1 mmol) in a particular solvent was added TTMSS (0.17 mL, 0.5 mmol) and the appropriate amount of BuSH. The reaction mixture was deoxygenate with argon for 30 minutes and than the appropriate initiator was added. Reactions at 25 °C were only partially deoxygenated (10 min) since the Et₃B requires oxygen (in trace) to generate Et·. Thermally activated reactions were initiated using (i) *tert*-butyl hyponitrite at 55 °C in benzene, (ii) AIBN at 80 °C in benzene, (iii) *tert*-butyl perbenzoate at 111 °C in toluene or (iv) di-*tert*-butyl peroxide at 142 °C in *o*-xylene. Solutions were refluxed for 1 h and analysed by ¹H-NMR spectroscopy and LC/MS. The integration of proton H-1' in the ¹H-NMR analysis, was taken in account to compare the amount of products in the reaction mixture. Specifically, the H-1' protons are at (i) **5.91 ppm** (d, *J*_{1',2'} = 6.0 Hz, 1H, H-1') for compound **1.71a**, (ii) 6.30 ppm (d, *J*_{1',2'} = 7.0 Hz, 1H, H-1') for compound **1.71b**, (iii) 6.38 ppm (dd, *J*_{1',2'} = 5.2, *J*_{1',2''} = 9 Hz, 1H, H-1') for compound **1.75** and (iv) 6.53 ppm (dd, *J*_{1',2'} = 5.3, *J*_{1',2''} = 9.1 Hz, 1H, H-1') for compound **1.70**.

(5'S,6S,5S)-O3'-(*tert*-Butyldiphenylsilyl)-O5'-[tris(trimethylsilyl)silyl]-5',6-cyclo-5,6-dihydrothymidine (1.71a)



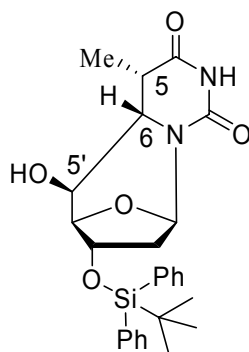
^1H NMR(400 MHz, CDCl_3): δ =7.25-7.80 (m, 10H, Ph), 7.2 (s, 1H, NH), 5.91 (d, $J_{1',2'} = 6.0$ Hz, 1H, H-1'), 4.67 (dd, $J_{2',3'} = 2$, $J_{2'',3'} = 7.0$ Hz, 1H, H-3'), 4.47 (d, $J_{4',5'} = 5.0$ Hz, 1H, H-4'), 3.58 (dd, $J_{4',5'} = 5.0$, $J_{5',6} = 9.2$ Hz, 1H, H-5'), 3.00 (dd, $J_{5,6} = 3.2$, $J_{5,6} = 9.2$ Hz, 1H, H-6), 2.73 (dq, $J_{5,6} = 3.2$, $J_{5,\text{Me}} = 7.2$ Hz, 1H, H-5), 2.27 (ddd, $J_{2',2''} = 14$, $J_{1',2'} = 6.0$, $J_{2',3'} = 2$ Hz, 1H, H-2'), 1.46 (dd, $J_{2',2''} = 14$, $J_{2'',3'} = 7.0$ Hz, 1H, H-2''), 1.22 (d, $J = 7.2$ Hz, 3H, Me), 1.05 (s, 9H, tBuSi), 0.15 (s, 27H, MeSi); NOE experiments: irradiation at δ =3.00 (H-6) caused enhancements of signals at δ =1.46 (H-2''), 2.73 (H-5, 9%) and 4.67 (H-3', 6%) whereas no enhancement of the signal at δ =3.58 (H-5') was found; irradiation at δ =3.58 (H-5') caused enhancements of signals at δ =4.47 (H-4', 8%) whereas no enhancement of the signal at δ =2.73 (H-5) was found; ^{13}C NMR(100.6 MHz, CDCl_3): δ =0.86 (Me), 11.68 (Me), 19.34 (q), 26.89 (Me), 36.25 (CH), 42.17 (CH_2), 54.79 (CH), 68.53 (CH), 71.64 (CH), 84.35 (CH), 86.65 (CH), 127.88 (CH), 128.16 (CH), 129.91 (CH), 130.15 (CH), 133.40 (q), 134.65 (q), 135.82 (CH), 135.91 (CH), 150.59 (CO), 172.43 (CO); MS (ESI): 749 (M + Na^+).

(5'R,6S,5S)-O3'-(*tert*-Butyldiphenylsilyl)-O5'-[tris(trimethylsilyl)silyl]-5',6-cyclo-5,6-dihydrothymidine (1.71b)



^1H NMR(400 MHz, CDCl_3): δ =7.4-7.70 (m, 10H, Ph), 7.1 (s, 1H, NH), 6.30 (d, $J_{1',2'} = 7.0$ Hz, 1H, H-1'), 4.55 (d, $J_{4',5'} = 2.0$ Hz, 1H, H-4'), 4.38 (dd, $J_{2',3'} = 2.5$, $J_{2'',3'} = 7.0$ Hz, 1H, H-3'), 3.18 (t, $J_{4',5'} = J_{5',6} = 2$ Hz, 1H, H-5'), 3.14 (dd, $J_{5,6} = 7.5$, $J_{5',6} = 2.0$ Hz, 1H, H-6), 2.64 (quintuplet, $J_{5,6} = J_{5,\text{Me}} = 7.5$ Hz, 1H, H-5), 2.07 (ABXY, $J_{\text{A,B}} = 14$, $J_{1',2'} = 7.0$, $J_{2',3'} = 2.5$ Hz, 1H, H-2'), 1.95 (ABX, $J_{\text{A,B}} = 14$, $J_{2'',3'} = 7.0$ Hz, 1H, H-2''), 1.14 (d, $J = 7.5$ Hz, 3H, Me), 1.05 (s, 9H, tBuSi). 0.15 (s, 27H, MeSi); NOE experiments: irradiation at δ =2.64 (H-5) caused enhancements of signals at δ =3.14 (H-6, 4%) and 1.14 (Me, 1.5%) whereas no enhancement of the signal at δ =3.18 (H-5'); Irradiation at δ =4.38 (H-3') caused enhancements of signals at δ =1.95 (H-2'', 2%), 3.18 (H-5', 5%), 3.14 (H-6, 6%), and 4.55 (H-4', 4%); ^{13}C NMR(100.6 MHz, CDCl_3): δ =0.94 (Me), 9.30 (Me), 19.28 (q), 26.92 (Me), 35.05 (CH), 40.14 (CH_2), 54.99 (CH), 69.40 (CH), 73.74 (CH), 85.22 (CH), 85.96 (CH), 128.07 (CH), 130.20 (CH), 133.33 (q), 133.86 (q), 136.04 (CH), 136.08 (CH), 154.05 (CO), 170.48 (CO); MS(ESI): 749 ($\text{M} + \text{Na}^+$).

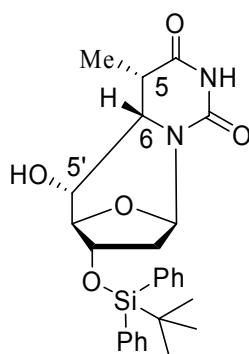
(5'S,6S,5S)-O3'-(tert-butylidiphenylsilyl)- 5',6-cyclo-5,6-dihydrothymidine (1.72a)



A 20 mM solution of **1.71a** (10 mg, 0.02 mmol) in a 8:3 $\text{CH}_2\text{Cl}_2/\text{MeOH}$ mixture (25 mL) was photolysed at λ 254 nm for 30 min to give quantitatively the O5'-desilylated compound **1.72a**.

^1H NMR(400 MHz, CDCl_3): $\delta=8.0$ (s, 1H, NH), 7.25-7.80 (m, 10H, Ph), 6.2 (d, $J_{1',2'}=6.0$ Hz, 1H, H-1'), 4.55 (dd, $J_{2',3'}=3.0$, $J_{2'',3''}=7.0$ Hz, 1H, H-3'), 4.18 (d, $J_{4',5'}=4.4$ Hz, 1H, H-4'), 3.67 (dd, $J_{4',5'}=4.4$, $J_{5',6}=9.3$ Hz, 1H, H-5'), 3.01 (dd, $J_{5,6}=3.6$, $J_{5',6}=9.3$ Hz, 1H, H-6), 2.75 (m, 1H, H-5), 2.31 (ddd, $J_{2',2''}=14.4$, $J_{1',2'}=6.0$, $J_{2',3'}=3.0$ Hz, 1H, H-2'), 2.12 (dd, $J_{2',2''}=14.4$, $J_{2'',3''}=7.0$ Hz, 1H, H-2''), 1.18 (d, $J=7.2$ Hz, 3H, Me), 1.05 (s, 9H, tBuSi); ^{13}C NMR(100.6 MHz, CDCl_3): $\delta=11.24$ (Me), 19.25 (q), 27.06 (Me), 36.00 (CH), 43.42 (CH_2), 53.75 (CH), 62.90 (CH), 69.97 (CH), 84.25 (CH), 86.20 (CH), 127.99 (CH), 128.05 (CH), 130.17 (CH), 130.19 (CH), 133.25 (q), 133.61 (q), 135.93 (CH), 151.18 (CO), 173.33 (CO); MS(ESI): 503 (M+23).

(5'R,6S,5S)-O3'-(*tert*-Butyldiphenylsilyl)- 5',6-cyclo-5,6-dihydrothymidine (1.72b)

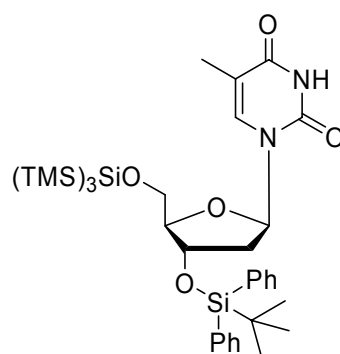


A 20 mM solution of **1.71b** (10 mg, 0.02 mmol) in a 8:3 $\text{CH}_2\text{Cl}_2/\text{MeOH}$ mixture (25 mL) was photolysed at λ 254 for 30 min to give quantitatively the O5'-desilylated compound **1.72b**.

^1H NMR(400 MHz, CDCl_3): $\delta=7.6$ (s, 1H, NH), 7.4-7.8 (m, 10H, Ph), 6.42 (d, $J_{1',2'}=6.0$ Hz, 1H, H-1'), 4.26 (dd, $J_{2',3'}=3.0$, $J_{2'',3''}=6.5$ Hz, 1H, H-3'), 4.24 (d, $J_{4',5'}=2.4$ Hz, 1H, H-4'), 3.20 (dd, $J_{5',6}=1.5$, $J_{5,6}=7.5$ Hz, 1H, H-6), 2.96 (bs collapsing to d upon irradiation at $\delta=3.2$, $J_{4',5'}=2.4$ Hz, 1H, H-5'), 2.88 (bs, 1H, OH), 2.70 (quintuplet, $J_{5,6}=J_{5,\text{CH}_3}=7.5$ Hz, 1H, H-5), 2.34 (A part of an ABXY system, $J_{\text{AB}}=14.5$, $J_{1',2'}=6.0$, $J_{2',3'}=3.0$ Hz, 1H, H-2'), 2.30 (B part of an ABX system, $J_{\text{AB}}=14.5$, $J_{2'',3''}=6.5$ Hz, 1H, H-2''), 1.18 (d, $J=7.2$ Hz, 3H, Me), 1.05 (s, 9H, tBuSi); ^{13}C NMR(100.6 MHz, CDCl_3): $\delta=9.16$ (Me), 19.25 (q), 27.04 (Me),

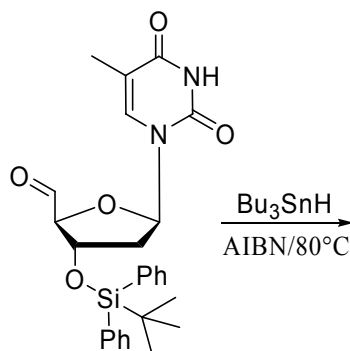
34.99 (CH), 39.78 (CH₂), 54.80 (CH), 65.56 (CH), 73.22 (CH), 85.52 (CH), 87.52 (CH), 128.12 (CH), 128.18 (CH), 128.21 (CH), 130.31 (CH), 133.52 (q), 136.12 (CH), 154.95 (CO), 171.51 (CO). MS(ESI): 503 (M+23)].

***O*3'-(*tert*-Butyldiphenylsilyl)-*O*5'-[tris(trimethylsilyl)silyl]thymidine (**1.75**)**



To a 0.01 M solution of the aldehyde **1.70** (48 mg, 0.1 mmol) in C₆H₅ (10 mL) were added AIBN (3 mg, 0.02 mmol), (TMS)₃SiH (0.175 mL, 0.5 mmol) and thiophenol (0.1 mL, 1.0 mmol). The solution was refluxed under argon atmosphere for 1 h. ¹H NMR analysis of the reaction mixture showed the presence of compound **1.75** in 95% yield. Column chromatography led to separation of a pure sample.

¹H NMR(400 MHz, CDCl₃): δ=8.0 (s, 1H, H-6), 7.3-7.70 (m, 10H, Ph), 7.2 (s, 1H, NH), 6.38 (dd, J_{1',2'} = 5.2, J_{1',2''} = 9 Hz, 1H, H-1'), 4.35 (d, J_{2'',3'} = 5.0, 1H, H-3'), 4.08 (bs, 1H, H-4'), 3.63 (dd, J_{5',5''} = 11, J_{4',5'} = 2 Hz, 1H, H-5'), 3.32 (dd, J_{5',5''} = 11, J_{4',5''} = 2 Hz, 1H, H-5''), 2.16 (dd, J_{2',2''} = 14, J_{1',2'} = 5.2 Hz, 1H, H-2'), 1.68 (ddd, J_{2',2''} = 14, J_{1',2''} = 9, J_{2'',3'} = 5.0 Hz, 1H, H-2''), 1.87 (s, 3H, Me), 1.05 (s, 9H, tBuSi), 0.15 (s, 27H, MeSi); ¹³C NMR(100.6 MHz, CDCl₃): δ=0.39 (3(CH₃)₃Si), 0.65 (q), 12.62 (CH₃), 26.89 ((CH₃)₃CSi), 41.16 (C2'), 68.01 (C5'), 74.05 (C3'), 84.90 (C1'), 87.90 (C4'), 110.64 (C5), 127.91 (CH), 133.19 (q), 133.31 (q), 135.19 (C6), 135.66 (CH), 135.70 (CH), 150.01 (q), 163.53 (q); MS(ESI): 749 (M + Na⁺).

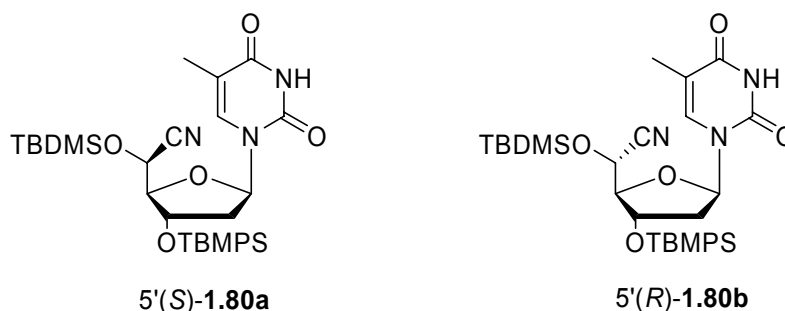
Reaction of 5'-Carboxaldehyde **1.70 with Bu₃SnH^[79]**

To a 0.01 M solution of aldehyde **1.70** (150 mg, 0.3 mmol) in C₆H₅ (30 mL), AIBN (0.06 mmol) and Bu₃SnH (0.6 mmol) were added. The solution was refluxed under argon atmosphere for 2 h.

The crude reaction mixture after evaporation was eluted on a silica gel column by n-hexane/ethyl acetate from 90:10 to 0:100 to eliminate tin by-products. ¹H NMR analysis of the residue after evaporation of the solvent showed the formation of three diastereoisomeric cyclisation products in a ratio **1.72a**/**1.72b**/(5'S,5R,6S)^[5]=65:20:15 and in 80% overall yield.

4.1.3 Independent Generation of C5'-Nucleosidyl Radicals in Thymidine

(5'*R*) and (5'*S*)-5'-Cyano-3',5'-di-*O*-(*tert*-butyldimethylsilyl)thymidine (**1.80a**, **1.80b**)

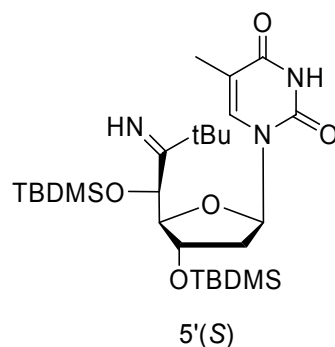


A solution of aldehyde **3** (600 mg, 1.70 mmol) in dry THF (6.0 mL) was added slowly to a mixture of LiOEt (85 μ L of 1M in THF, 0.085 mmol) and TBDMS-CN (311 mg, 2.20 mmol) in dry THF (4.0 mL) at 0°C (ice-bath) under N₂ atmosphere. The reaction mixture was stirred at room temperature until all the starting material was consumed (30-50 min). After work-up (EtOAc/water/brine) the organic layer was dried over Na₂SO₄ and concentrated. The resulting yellow oil was purified on silica (from 20% to 30% of EtOAc in *i*-Hexane) leading to two main fractions: a major isomer, 5'-cyano-thymidine **1.80a** (376 mg, 0.76 mmol, 45 %) and a minor isomer, 5'-cyano-thymidine **1.80b** (308 mg, 0.62 mmol, 37%) both as white foam for a total yield of 82% of pure compounds.

¹H NMR (400 MHz, CDCl₃), **isomer 1.80a**: δ = 8.30 (s, 1H, NH), 7.46 (d, 1H, H6, J_{6-Me} = 1.3 Hz), 6.45 (dd, 1H, H1', $J_{1'-2'a}$ = 9.3 Hz, $J_{1'-2'b}$ = 5.6 Hz), 4.64 (d, 1H, H5', $J_{5'-4'}$ = 4.0 Hz), 4.54 (dt, 1H, H3', $J_{3'-2'b}$ = 5.2 Hz, $J_{3'-4'}$ = 1.4 Hz), 4.02 (dd, 1H, H4', $J_{4'-5'}$ = 4.0 Hz, $J_{4'-3'}$ = 1.4 Hz), 2.25-2.13 (m, 2H, H2'), 1.93 (d, 3H, CH₃-5, J_{Me-6} = 1.2 Hz), 0.94 (s, 9H, ^{*t*}BuSi), 0.90 (s, 9H, ^{*t*}BuSi), 0.24 (s, 3H, CH₃Si), 0.20 (s, 3H, CH₃Si), 0.11 (s, 3H, CH₃Si) 0.10 ppm (s, 3H, CH₃Si). **isomer 1.80b**: δ = 8.13 (s, 1H, H3 (NH)), 7.25 (d, 1H, H6, J_{6-Me} = 1.3 Hz), 6.27 (dd, 1H, H1', $J_{1'-2'a}$ = 8.2 Hz, $J_{1'-2'b}$ = 6.0 Hz), 4.65 (d, 1H, H5', $J_{5'-4'}$ = 3.4 Hz), 4.48 (dt, 1H, H3', $J_{3'-2'b}$ = 6.1 Hz, $J_{3'-4'}$ = 3.1 Hz), 4.02 (dd, 1H, H4', $J_{4'-5'}$ = 3.3 Hz, $J_{4'-3'}$ = 3.3 Hz), 2.29-2.23 (ddd, 1H, H2_b', $J_{2'b-2'a}$ = 13.4 Hz, $J_{2'b-1'}$ = 6.0 Hz, $J_{2'b-3'}$ = 2.9 Hz), 2.19-2.12 (m, 1H, H2_b', $J_{2'a-2'b}$ = 13.4 Hz, $J_{2'a-1'}$ = 8.1 Hz), 1.93 (d, 3H, CH₃-5, J_{Me-6} = 1.2 Hz), 0.96 (s, 9H, ^{*t*}Bu-Si),

0.91 (s, 9H, ^tBu-Si), 0.26 (s, 3H, CH₃-Si), 0.20 (s, 3H, CH₃-Si), 0.14 (s, 3H, CH₃-Si) 0.13 ppm (s, 3H, CH₃-Si). ¹³C NMR (100.6 MHz, CDCl₃), **isomer 1.80a**: δ = 163.15 (C), 150.21 (C), 135.03 (CH), 118.66 (C), 111.66 (C), 87.26 (CH), 84.59 (CH), 72.31 (CH), 62.25 (CH), 40.15 (CH₂), 25.66 (CH₃), 25.59 (CH₃), 18.25 (C), 17.88 (C), 12.50 (CH₃), -4.58 (CH₃), -4.80 (CH₃), -5.23 (CH₃), -5.32 ppm (CH₃). **isomer 1.80b**: δ = 163.05 (C), 149.89 (C), 135.39 (CH), 117.67 (C), 111.39 (C), 87.46 (CH), 85.52 (CH), 71.23 (CH), 62.76 (CH), 39.93 (CH₂), 25.65 (CH₃), 25.62 (CH₃), 18.17 (C), 17.84 (C), 12.41 (CH₃), -4.62 (CH₃), -4.82 (CH₃), -5.00 (CH₃), -5.08 ppm (CH₃). **FT-MS isomer 1.80a**, calc.: M = 495.2585, (+ c ESI), found 496.2630 [M + H]⁺; (- c ESI), 530.2384 [M + Cl]⁻. **FT-MS isomer 1.80b** calc.: M = 495.2585, (+ c ESI), found 496.2661 [M + H]⁺; (- c ESI), 494.2509 [M - H]⁻, 530.2276 [M + Cl]⁻. **R_f 1.80a** (EtOAc / *i*-Hex 2:3) = 0.58. **R_f 1.80b** (EtOAc / *i*-Hex 2:3) = 0.68.

(5'*S*)-3',5'-di-*O*-(*tert*-Butyldimethylsilyl)-5'-(2,2-dimethylpropanimidoyl) thymidine 1.81a

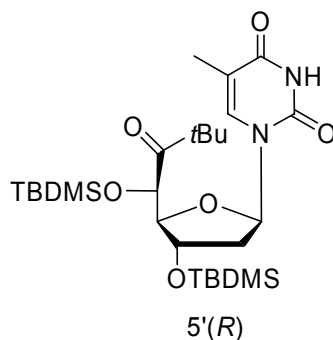


To a solution of **1.80a** (300 mg, 0.60 mmol) in THF (12 mL) at -78 °C was slowly added *tert*-BuLi 1.5 M (1.5 mL, 2.4 mmol). After 2 minutes of vigorous stirring at -78 °C the reaction was quenched by water addition and let warm up to room temperature. The mixture was diluted with EtOAc and the organic phases were then washed with water until neutrality and finally with brine. Anydrification on MgCl₂ and subsequent rotary evaporation of the solvent lead to 144 mg (0.27 mmol, 43%) of yellow oil. Analyzed as crude product.

¹H NMR (400 MHz, acetone-d₆): δ = 9.99 (s, 1H, NH), 7.51 (bs, 1H, H6), 6.28 (dd, 1H, H1', J₁ = 8.9, J₂ = 5.5 Hz), 4.78 (d, 1H, H5', J = 1.5 Hz), 4.53 (d, 1H, H3', J = 5.5 Hz), 4.21 (bs, 1H, H4'), 2.25-2.11 (m, 2H, H2'), 1.90 (d, 3H, CH₃-5, J = 1.1 Hz), 1.25 (s, 9H, ^tBu-CO), 1.02 (s, 9H, ^tBu-Si), 0.94 (s, 9H, ^tBu-Si), 0.24 (s, 3H, CH₃-Si), 0.18 (s, 3H, CH₃-Si), 0.17 (s, 3H,

CH₃-Si), 0.10 ppm (s, 3H, CH₃-Si). ¹³C NMR (100.5 MHz, acetone-d₆): δ = 185.82 (q, C=NH), 165.51 (C), 152.03 (C), 136.54 (CH), 112.00 (C), 89.29 (CH), 86.04 (CH), 73.11 (CH), 70.16 (CH), 42.46 (CH₂), 39.85 (C), 30.23 (CH₃), 27.38 (CH₃), 27.14 (CH₃), 19.88 (C), 19.56 (C), 13.70 (CH₃), -3.28 (CH₃), -3.50 (CH₃), -3.56 (CH₃), -3.64 ppm (CH₃). FT-MS calc.: M = 553.3367, (+ c ESI), found 554.3420 [M + H]⁺; (- c ESI), 589.2969 [M + Cl]⁻. R_f (EtOAc / *i*-Hex 2:3) = 0.36.

(5'*R*)-3',5'-di-*O*-(*tert*-Butyldimethylsilyl)-5'-(*tert*-butylcarbonyl)thymidine 1.77a

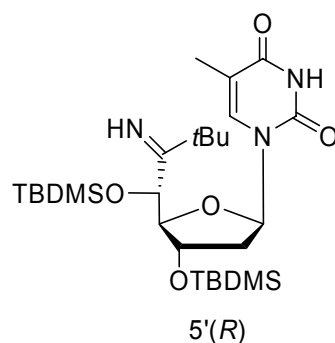


10 mL of an acidic solution (THF/H₂O/2N HCl, 40:20:1) were added to the imine **1.81a** (100 mg, 0.20 mmol) and the mixture was stirred for 3 h at r. t.. The phases were then separated after dilution with 10 mL of EtOAc and the organic layer was washed with water until neutrality and finally with brine. Anydrification on MgCl₂ and subsequent rotary evaporation of the solvent yielded an orange oil. Purification on silica gel (from 1 to 3% of MeOH in CHCl₃) provided the *tert*-butyl ketone **1.77a** as a yellow oil (98 mg, 0.18 mmol, 88%).

¹H NMR (400 MHz, acetone-d₆): δ = 9.89 (s, 1H, NH), 7.85 (d, 1H, H6, *J* = 1.2 Hz), 6.30 (dd, 1H, H1', *J*₁ = 9.1, *J*₂ = 5.4 Hz), 5.17 (d, 1H, H5', *J* = 2.4 Hz), 4.61 (d, 1H, H3', *J* = 4.8 Hz), 4.57 (d, 1H, H4', *J* = 2.2 Hz), 2.29-2.14 (m, 2H, H2'), 1.93 (d, 3H, CH₃-5, *J* = 1.1 Hz), 1.24 (s, 9H, ^tBu-CO), 0.96 (s, 9H, ^tBu-Si), 0.95 (s, 9H, ^tBu-Si), 0.18 (s, 3H, CH₃-Si), 0.17 (s, 3H, CH₃-Si), 0.15 (s, 3H, CH₃-Si), 0.11 ppm (s, 3H, CH₃-Si). ¹H NMR (600 MHz, CDCl₃): δ = 8.12 (s, 1H, H3 (NH)), 7.85 (bs, 1H, H6), 6.32 (dd, 1H, H1', *J*_{1'-2'a} = 9.0 Hz, *J*_{1'-2'b} = 5.4 Hz), 4.86 (d, 1H, H5', *J*_{5'-4'} = 2.0 Hz), 4.47 (d, 1H, H3', *J*_{3'-2'b} = 5.0 Hz), 4.44 (d, 1H, H4', *J* = 1.5 Hz), 2.25 (dd, 1H, H2b', *J*_{2b'-2'a} = 12.8 Hz, *J*_{2b'-1'} = 5.4 Hz), 2.02 (bs, 3H, CH₃-5), 2.00-1.98 (m, 1H, H2a', *J*_{2'a-2'b} = 12.9 Hz, *J*_{2'a-1'} = 9.0 Hz, *J*_{2'a-3'} = 4.9 Hz), 1.23 (s, 9H, ^tBu-CO), 0.92

(s, 9H, ^tBu-Si), 0.91 (s, 9H, ^tBu-Si), 0.11 (s, 6H, (CH₃)₂-Si), 0.10 (s, 3H, CH₃-Si), 0.02 ppm (s, 3H, CH₃-Si). ¹³C NMR (150.8 MHz, CDCl₃): δ = 210.57 (C), 163.72 (C), 150.13 (C), 136.49 (CH), 110.75 (C), 88.14 (CH), 86.07 (CH), 75.17 (CH), 74.76 (CH), 43.07 (C), 41.52 (CH₂), 27.52 (CH₃), 25.80 (CH₃), 25.77 (CH₃), 18.42 (C), 18.13 (C), 12.43 (CH₃), -4.48 (CH₃), -4.58 (CH₃), -4.78 (CH₃), -5.48 ppm (CH₃). FT-MS calc.: M = 554.3207, (+ c ESI), found 555.3277 [M + H]⁺; (- c ESI), 553.3208 [M - H]⁻. UV λ_{max} = 264 nm; ε₂₆₀ = 1049 ± 64 M⁻¹cm⁻¹. R_f (EtOAc / *i*-Hex 2:3) = 0.78.

(5'*R*)-3',5'-di-*O*-(*tert*-Butyldimethylsilyl)-5'-(2,2-dimethylpropanimidoyl) thymidine 1.81b

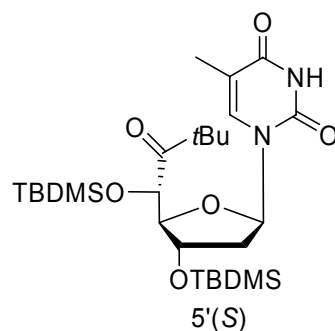


To a solution of **1.80b** (300 mg, 0.60 mmol) in THF (12 mL) at -78 °C was slowly added *tert*-BuLi 1.5 M (1.5 mL, 2.4 mmol). After 2 minutes of vigorous stirring at -78 °C the reaction was quenched by water addition and was left to warm up to r.t.. The mixture was diluted with EtOAc and the organic phases were then washed with water until neutrality and finally with brine. Anydrification on MgCl₂ and subsequent rotary evaporation of the solvent led to 125 mg (0.22 mmol, 38%) of yellow oil. Analyzed as crude product.

¹H NMR (400 MHz, acetone-d₆): δ = 10.06 (s, 1H, NH), 7.34 (bs, 1H, H6), 6.21 (bdd, 1H, H1', *J* = 7.2), 4.73 (d, 1H, H5', *J* = 1.4 Hz), 4.61 (m, 1H, H3'), 4.04 (dd, 1H, H4', *J*₁ = 3.4 Hz, *J*₂ = 1.3 Hz), 2.21-2.16 (m, 2H, H2'), 1.86 (bs, 3H, CH₃-5), 1.27 (s, 9H, ^tBu-CO), 1.00 (s, 9H, ^tBu-Si), 0.88 (s, 9H, ^tBu-Si), 0.14 (s, 3H, CH₃-Si), 0.10 (s, 3H, CH₃-Si), 0.07 (s, 3H, CH₃-Si), 0.03 ppm (s, 3H, CH₃-Si). ¹³C NMR (100.5 MHz, acetone-d₆): δ = 187.17 (q, C=NH), 164.99 (C), 156.93 (C), 137.05 (CH), 111.89 (C), 89.30 (CH), 88.20 (CH), 75.89 (CH), 70.54 (CH), 49.09 (CH₂), 40.14 (C), 30.58 (CH₃), 27.37 (CH₃), 27.18 (CH₃), 19.77 (C), 19.26 (C),

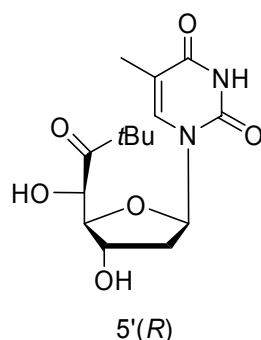
13.47 (CH₃), -2.22 (CH₃), -3.16 (CH₃), -3.38 (CH₃), -3.61 ppm (CH₃). **MS** calc.: M = 553.3367, (FTMS + c ESI), found 554.3431 [M + H]⁺. **R_f** (EtOAc / *i*-Hex 2:3) = 0.34.

(5'S)-3',5'-di-O-(*tert*-Butyldimethylsilyl)-5'-(*tert*-butylcarbonyl)thymidine 1.77b



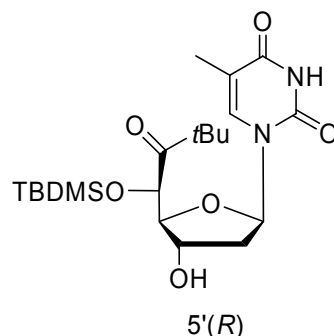
10 mL of CDCl₃ were added to the oil of the crude product containing **1.81b** (100 mg, 0.20 mmol) and the solution was stirred for 30 minutes at room temperature. The reaction was followed by ¹H-NMR. The hydrolysis of **1.81b** to **1.77b** was complete in 30 minutes. Longer time stirring of this solution led to the degradation of the product of reaction with the replacement of the NMR-peaks of **1.77b** by many unknown peaks. The CDCl₃ was removed by rotary evaporation followed by high vacuum and the obtained yellow oil (78 mg, 70%) was dissolved in acetone-d₆ for NMR characterization.

¹H NMR (400 MHz, acetone-d₆): δ = 10.03 (s, 1H, NH), 7.32 (s, 1H, H6), 6.27 (bdd, 1H, H1', *J* = 7.3), 5.00 (d, 1H, H5', *J*_{5',4'} = 2.5 Hz), 4.72 (m, 1H, H3'), 4.13 (bt, 1H, H4', *J* = 2.5 Hz), 2.15 (m, 2H, H2'), 1.85 (bs, 3H, CH₃-5), 1.25 (s, 9H, ^tBu-CO), 0.97 (s, 9H, ^tBu-Si), 0.89 (s, 9H, ^tBu-Si), 0.13 (s, 3H, CH₃-Si), 0.12 (s, 3H, CH₃-Si), 0.09 (s, 3H, CH₃-Si), 0.08 ppm (s, 3H, CH₃-Si). **¹³C NMR** (150.8 MHz, acetone-d₆): δ = 214.39 (C), 152.41 (C), 147.23 (C), 136.95 (CH), 111.94 (C), 88.68 (CH), 85.18 (CH), 76.66 (CH), 72.17 (CH), 45.34 (C), 41.82 (CH₂), 28.61 (CH₃), 27.38 (CH₃), 27.16 (CH₃), 19.88 (C), 19.36 (C), 13.51 (CH₃), -3.15 (CH₃), -3.21 (CH₃), -3.32 (CH₃), -3.51 ppm (CH₃). **FT-MS** calc.: M = 554.3207, (+ c ESI), found 557.3068 [M + Na]⁺; (- c ESI), 589.2945 [M + Cl]⁻. **R_f** (EtOAc / *i*-Hex 2:3) = 0.76.

(5'R)-5'-(*tert*-Butylcarbonyl)thymidine 1.82

To a solution of 3',5'(*R*)-TBDMS-ketone **1.77a** (170 mg, 0.3 mmol) in MeOH (10 mL) was added a solution of TBAF 1 M in THF (1 mL, 1.0 mmol). The mixture was refluxed for 5 hours and then stirred at r.t. for 24 hours. MeOH was then removed by reduced pressure and the crude product was purified on silica gel (EtOAc in *i*-Hexane from 30 to 90%). A white foam (61 mg, 0.19 mmol, 60 %) was isolated from the fractions and identified as 3',5'-OH ketone **1.82** by NMR and mass analysis. A less polar fraction was collected leading to 10 mg (7,3 % from the bis-protected ketone) of white powder analyzed by NMR and mass and identified as 3'-OH, 5'-TBDMS ketone **7**.

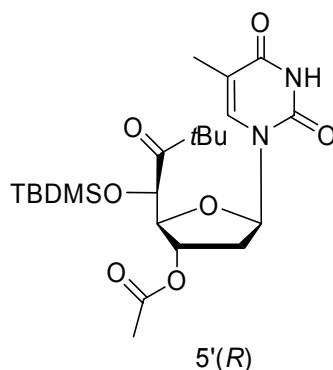
¹H NMR (600 MHz, CDCl₃) δ = 8.93 (bs, 1H, H3 (NH)), 7.36 (bs, 1H, H6), 6.26 (dd, 1H, H1', $J_{1'-2'a} = 7.5$ Hz, $J_{1'-2'b} = 6.2$ Hz), 4.77 (d, 1H, H5', $J = 1.6$ Hz), 4.72 (dt, 1H, H3', $J = 5.7$ Hz, $J = 2.7$ Hz), 4.46 (m, 1H, H4'), 2.37-2.34 (ddd, 1H, H2b', $J_{2b'-2'a} = 13.5$ Hz, $J_{2'b-1'} = 5.9$ Hz, $J = 2.9$ Hz), 2.23-2.18 (m, 1H, H2a', $J_{2'a-2'b} = 13.7$ Hz, $J_{2'a-1'} = 7.2$ Hz), 1.96 (bs, 3H, CH₃-5), 1.27 ppm (s, 9H, ^{*t*}Bu-CO). **¹³C NMR** (150.8 MHz, CDCl₃) δ = 214.10 (q, C5''), 163.71 (C), 150.37 (C), 135.48 (CH, C6), 111.22 (q, C5), 86.26 (CH, C4'), 85.38 (CH, C1'), 73.32 (CH, C5'), 72.49 (CH, C3'), 42.92 (q, C6''), 40.63 (CH₂, C2'), 27.08 (CH₃, C6''-^{*t*}Bu), 12.57 ppm (CH₃, C5-Me). **FT-MS** calc.: $M = 326.1478$, (- c ESI) found 325.1409 [$M - H$]⁻. **R_f** (EtOAc / *i*-Hex 1:1) = 0.11.

(5'R)-5'-O-(tert-Butyldimethylsilyl)-5'-(tert-butylcarbonyl)thymidine 1.83

An independent synthesis of **1.83** was achieved as follows: 170 mg (0.3 mmol) of ketone **1.77a** were dissolved in THF (10 mL) and TBAF (1M in THF, 1 mL, 1.0 mmol) was added to this mixture at low temperature (-15°C) and stirred for 24 hours at -15°C. Under these conditions the relative yields after purification on silica gel (EtOAc in *i*-Hexane from 30 to 90%) of **1.82** and **1.83** were 10% and 55% respectively.

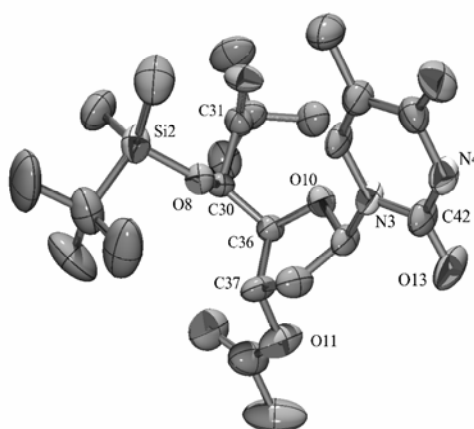
¹H NMR (600 MHz, DMSO-*d*₆): δ = 11.27 (s, 1H, H3 (NH)), 7.80 (bs, 1H, H6), 6.12 (dd, 1H, H1', $J_1 = 8.5$ Hz, $J_2 = 5.4$ Hz), 5.07 (d, 1H, H5', $J = 2.2$ Hz), 4.41 (bs, 1H, H3'), 4.30 (d, 1H, H4', $J = 4.8$ Hz), 2.15 (dd, 1H, H2', $J_1 = 13.2$ Hz, $J_2 = 5.7$ Hz), 1.93 (ddd, 1H, H2', $J_1 = 13.8$ Hz, $J_2 = 8.9$ Hz, $J_3 = 5.4$ Hz), 1.83 (bs, 3H, CH₃-5), 1.16 (s, 9H, ^{*t*}Bu-CO), 0.87 (s, 9H, ^{*t*}Bu-Si), 0.04 (s, 3H, CH₃-Si), 0.03 ppm (s, 3H, CH₃-Si). **¹³C NMR** (150.8 MHz, DMSO-*d*₆): δ = 210.81 (C), 163.25 (C), 149.70 (C), 135.38 (CH), 108.48 (C), 86.56 (CH, C4'), 84.69 (CH, C1'), 74.32 (CH, C5'), 71.90 (CH, C3'), 42.17 (CH₂, C2'), 26.56 (CH₃), 25.13 (CH₃), 17.48 (C), 11.80 (CH₃), -5.33 (CH₃), -5.91 ppm (CH₃). **FT-MS** calc.: $M = 440.2343$, (+ c ESI), found 441.2396 [M + H]⁺, 463.2217 [M + Na]⁺, (- c ESI) found 475.2078 [M + Cl]⁻. **R_f** (EtOAc / *i*-Hex 1:1) = 0.50.

Synthesis of (5'*R*)-3'-*O*-Acetyl-5'-*O*-(*tert*-butyldimethylsilyl)-5'-(*tert*-butylcarbonyl)thymidine **1.84**



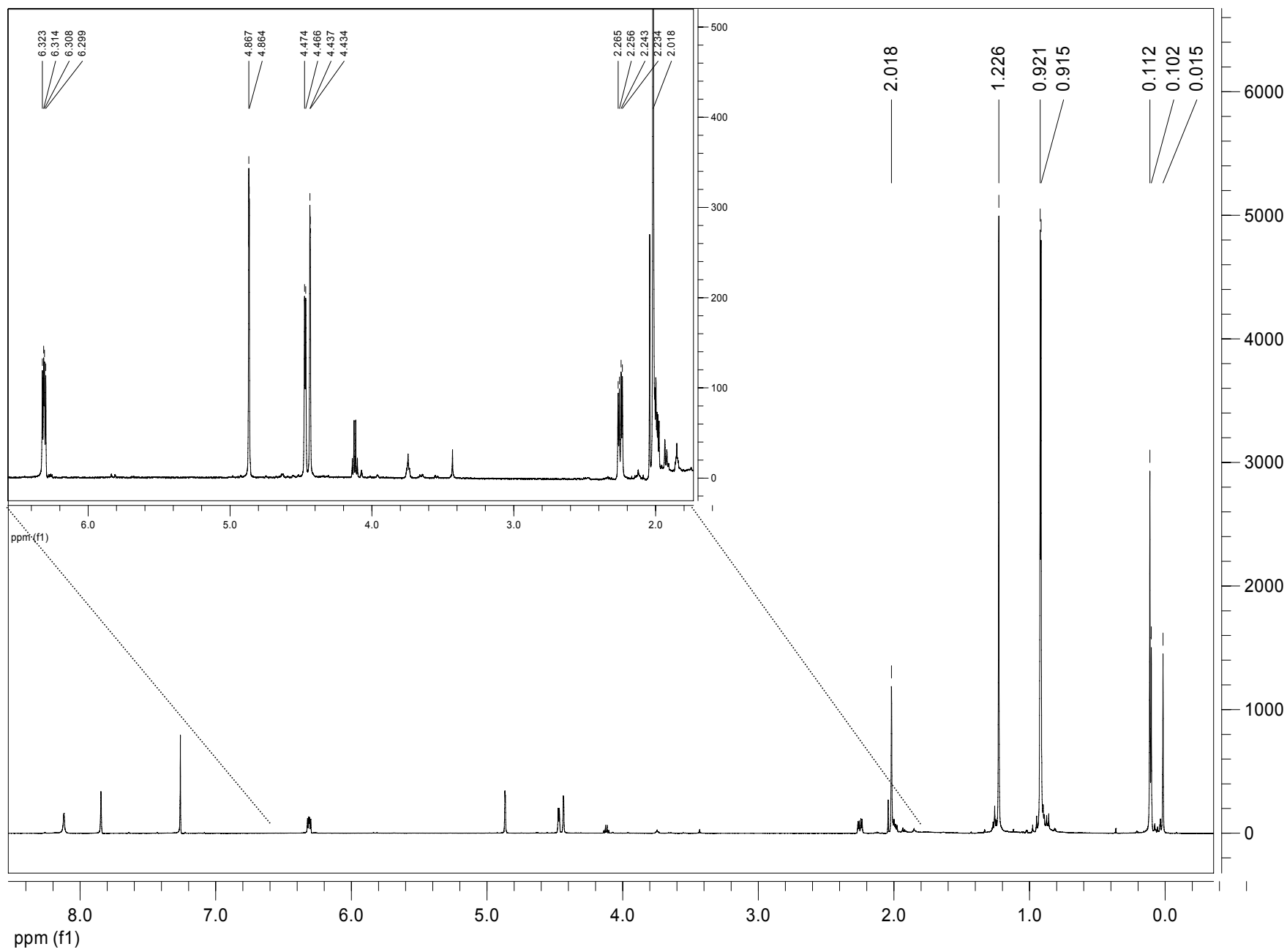
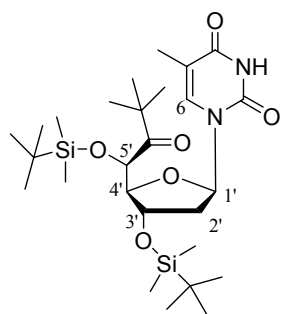
To a solution of 3'-OH, 5'-TBDMS-ketone **1.83** (73 mg, 0.2 mmol) in dry pyridine (2 mL) was added 35 μ L (0.38 mmol) of acetic anhydride. The mixture was stirred at r.t. for 24 h. The solvent was removed by rotary evaporation and the residue co-evaporated three times with 1 mL of toluene. The ketone **1.84** was obtained in 82 % of yield as white powder and was characterized. The 5'(*R*) configuration was assigned by resolution of the crystal obtained from a saturated EtOAc solution of **1.84**.

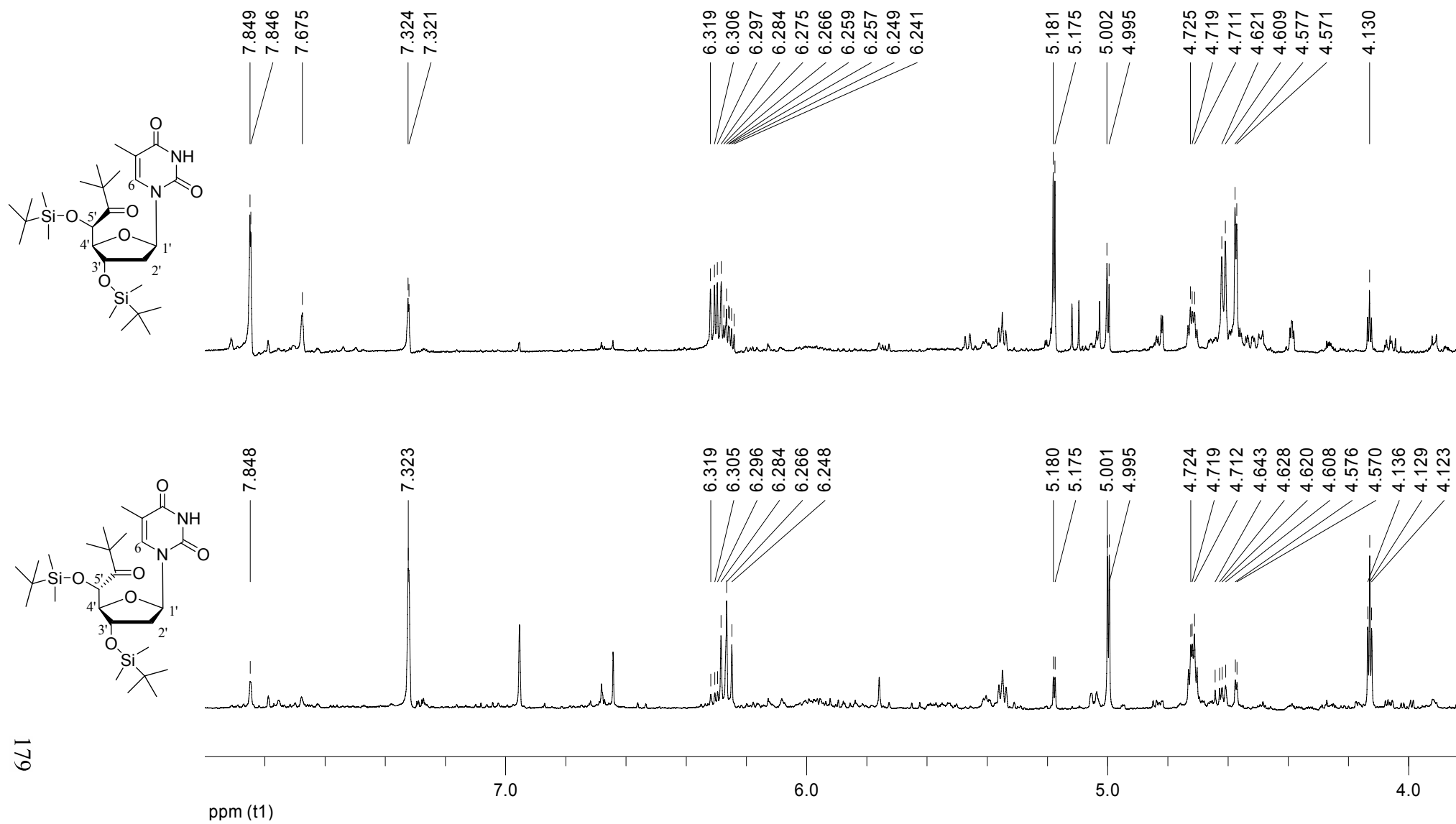
$^1\text{H NMR}$ (600 MHz, CDCl_3): δ = 8.06 (s, 1H, H3 (NH)), 7.87 (d, 1H, H6, J = 1.1 Hz), 6.30 (dd, 1H, H1', J_1 = 9.2 Hz, J_2 = 5.4 Hz), 5.22 (d, 1H, H3', J = 5.9 Hz), 5.08 (d, 1H, H5', J = 2.1 Hz), 4.51 (d, 1H, H4', J = 1.8 Hz), 2.48 (dd, 1H, H2', J_1 = 13.8 Hz, J_2 = 5.4 Hz), 2.13 (m, 1H, H2'), 2.14 (s, 3H, Ac), 2.03 (d, 3H, CH_3 -5, J = 1.0 Hz), 1.21 (s, 9H, ^tBu -CO), 0.92 (s, 9H, ^tBu -Si), 0.11 (s, 3H, CH_3 -Si), 0.06 ppm (s, 3H, CH_3 -Si). **$^{13}\text{C NMR}$** (150.8 MHz, CDCl_3): δ = 210.59 (C), 171.01 (C), 163.54 (C), 150.12 (C), 136.03 (CH), 111.12 (C), 85.50 (CH), 85.53 (CH), 74.81 (CH), 43.08 (C), 37.57 (CH_2), 27.43 (CH_3), 25.80 (CH_3), 21.02 (CH_3), 18.38 (C), 12.47 (CH_3), -4.54 (CH_3), -5.41 ppm (CH_3). **FT-MS** calc.: M = 482.2448, (+ c ESI) found 483.2502 [$M + \text{H}$] $^+$, 505.2326 [$M + \text{Na}$] $^+$, (- c ESI) found 481.2425 [$M - \text{H}$] $^-$, 517.2202 [$M + \text{Cl}$] $^-$. **R_f** (EtOAc : *i*-Hex, 2:3) = 0.42.

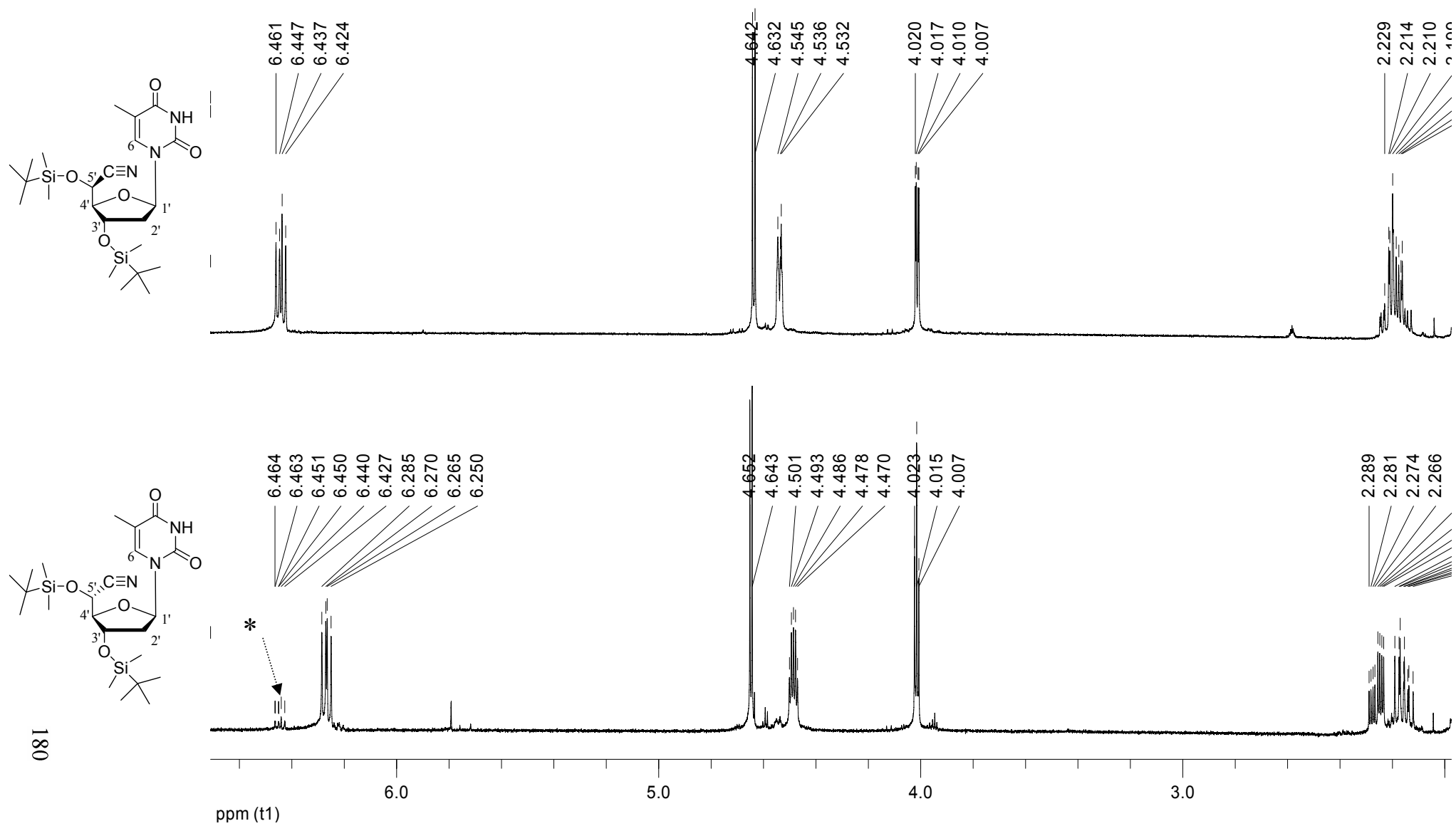
X-ray crystal structure determination

Crystal structure of **1.84**, hydrogen atoms are omitted for clarity; selected distances [\AA] and angles [$^\circ$] (standard deviation in parenthesis): Si2 O8 1.659(4), O8 C30 1.419(6), O9 C31 1.206(6), O10 C39 1.412(6), O11 C37 1.433(7), N3 C39 1.466(7), C30 C36 1.500(7), C30 C31 1.552(7); C30 O8 Si2 126.5(3), O8 C30 C36 108.3(4), O8 C30 C31 109.3(4), C36 C30 C31 110.8(4), O9 C31 C30 119.1(5), O11 C37 C38 107.2(4), O11 C37 C36 112.4(5), N3 C39 C38 113.5(5), N4 C42 N3 114.6(5), N4 C43 C44 114.1(5).

X-Ray data were collected at 200 K with a Nonius KappaCCD diffractometer equipped with a rotating anode and a graded multilayer x-ray optics to get monochrome MoK α radiation ($\lambda = 0.71073 \text{ \AA}$). The structure was solved with direct methods with SIR97^[314] and refined with SHELXL-97.^[315] Hydrogen atoms were calculated in idealized positions riding on their parent atoms. One of the *tert*-Butyl groups is disordered; a split model was applied with isotropic refinement of the split atoms. Data for compound **1.84**: C₂₃H₃₈N₂O₇Si, Fw = 482.643, colourless block, 0.18 · 0.15 · 0.11 mm³, monoclinic, *P*21 (no. 4), $a = 14.1327(4) \text{ \AA}$, $b = 10.9042(3) \text{ \AA}$, $c = 17.7449(6) \text{ \AA}$, $\beta = 93.3188(11)^\circ$, $V = 2730.01(14) \text{ \AA}^3$, $Z = 4$, 7119 unique reflections, 593 parameters were refined, $R1 (I > 2\sigma(I)) = 0.0621$, $wR2$ (all reflections) = 0.1774, $S = 1.062$. Residual electron density between 0.763 and $-0.316 \text{ e \AA}^{-3}$. Further details are available under the depository number CCDC **618360** from the Cambridge Crystallographic Data Centre.

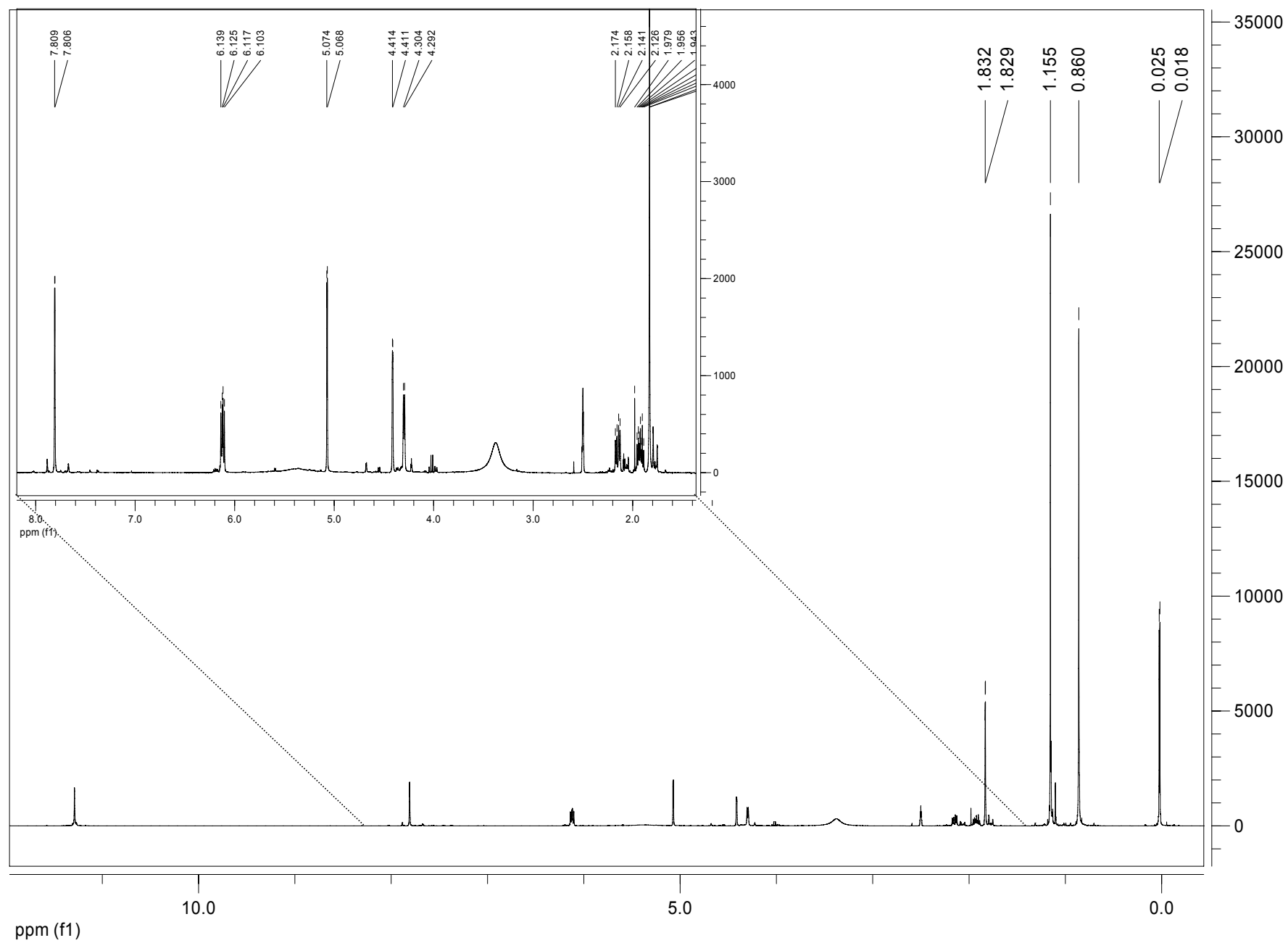
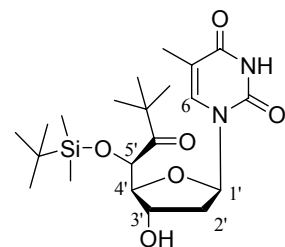
1.77a in CDCl₃

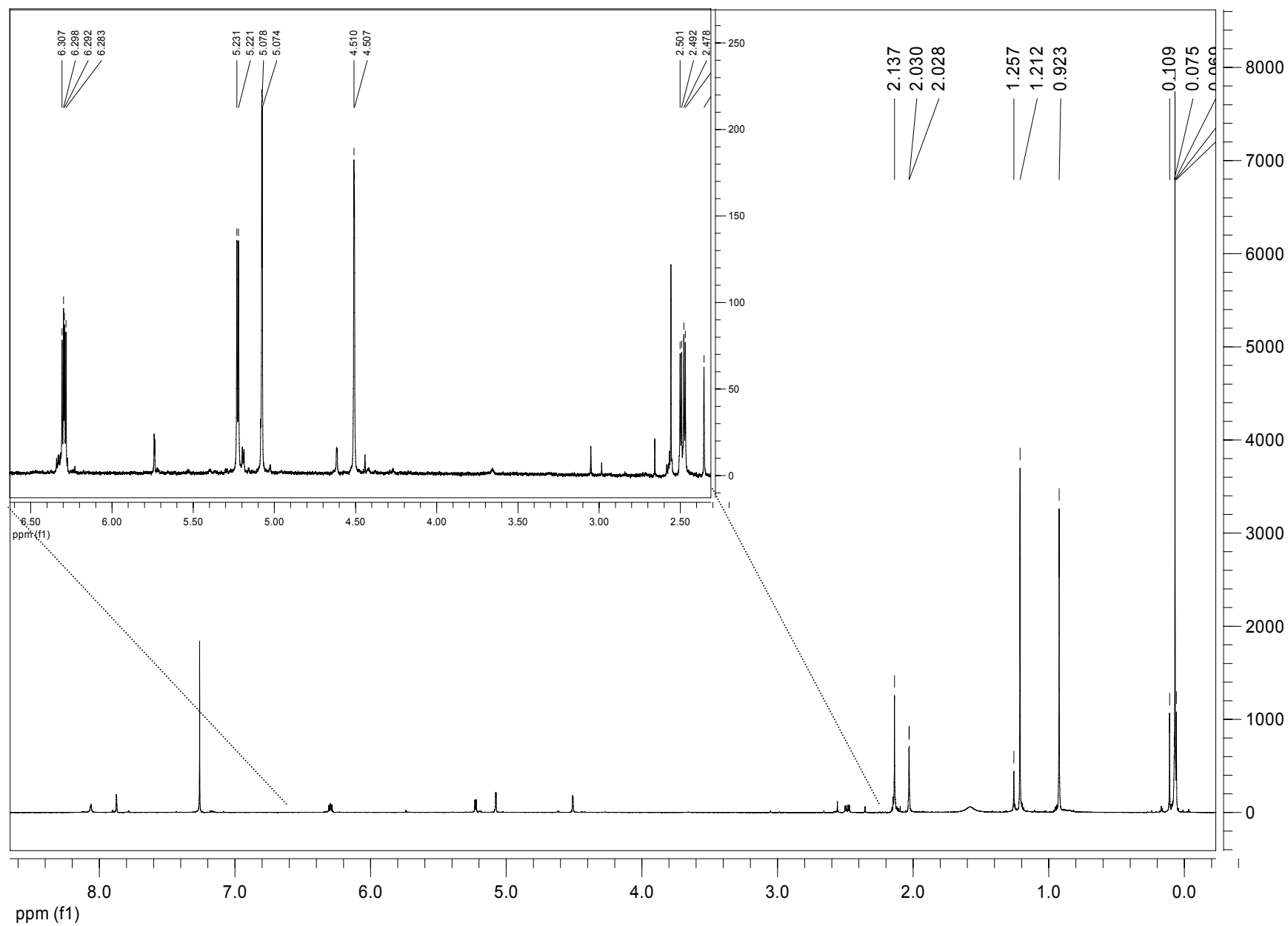
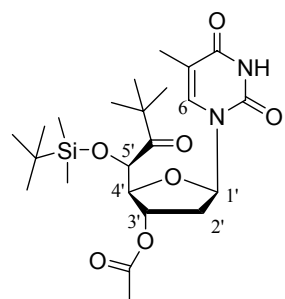
1.77a and 1.77b in Acetone-d₆

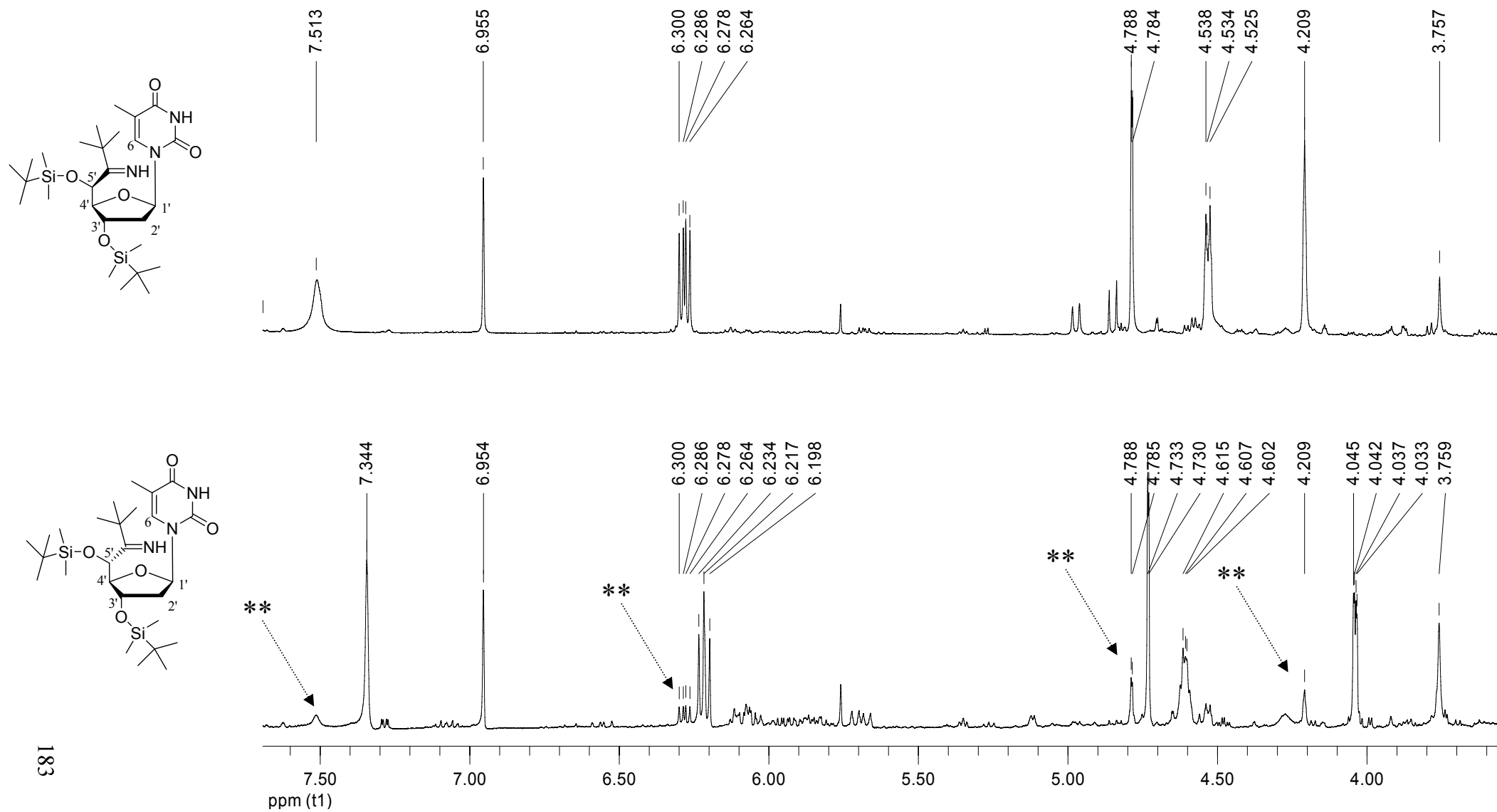
1.80a and **1.80b** in CDCl₃

* **1.80a** present in trace in **1.80b**.

1.83 in DMSO

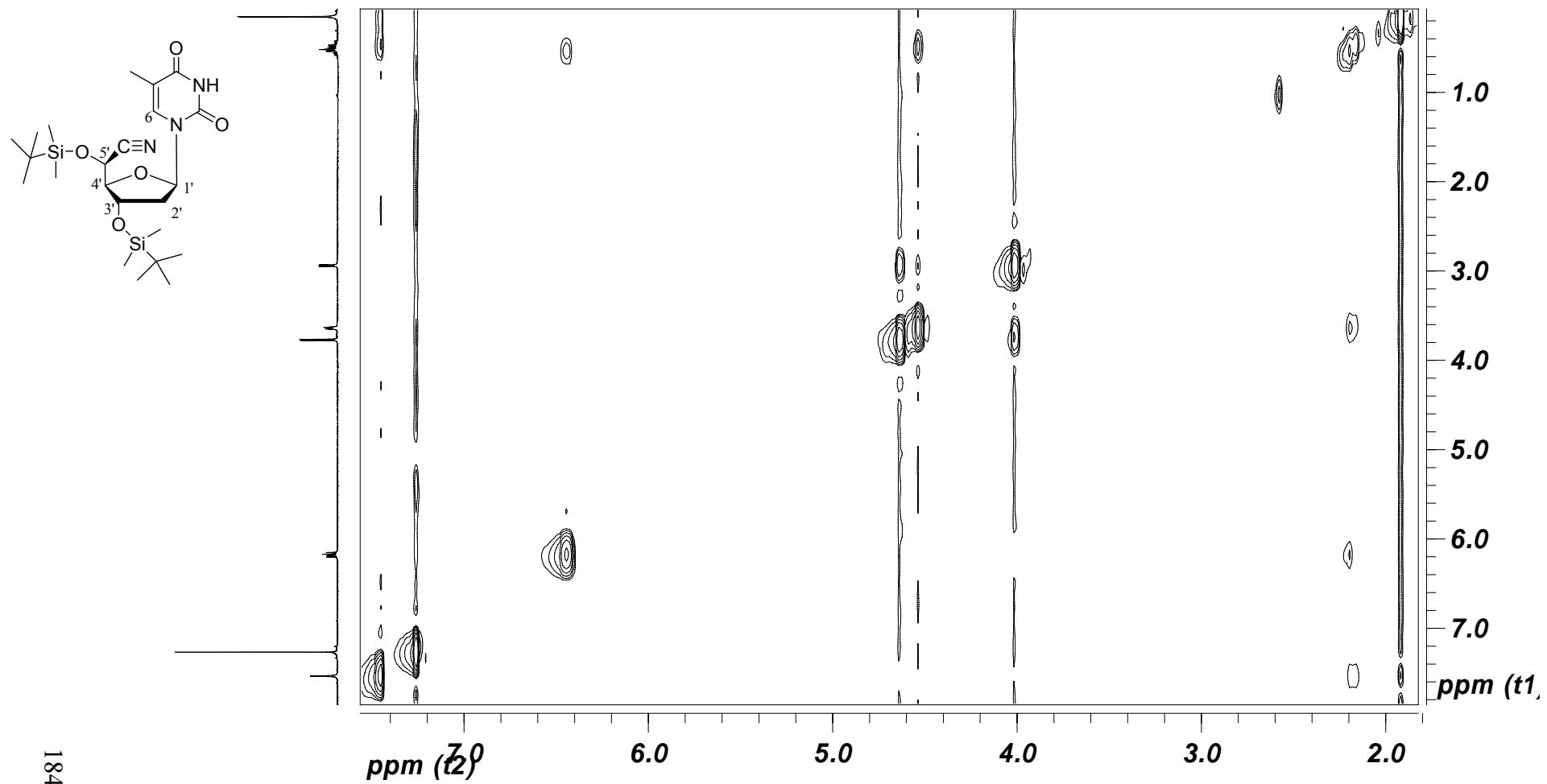


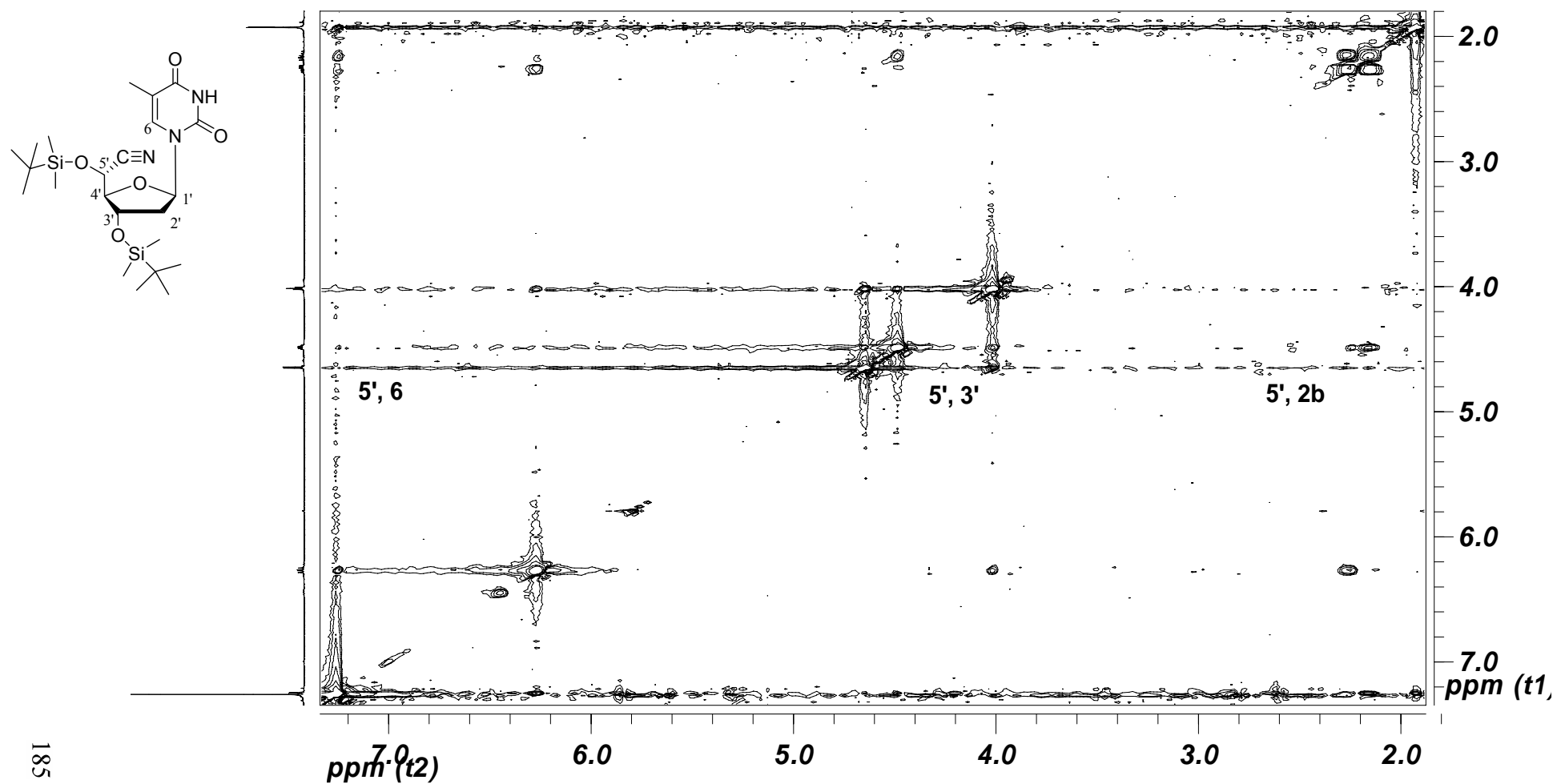
1.84 in CDCl₃

1.81a and **1.81b** in acetone- d_6 

181

**** 1.81a** from **1.80a** present in trace in **1.81b** (see spectra **1.80b**).

NOESY experiment. **1.80a** in CDCl₃

NOESY experiment. **1.80b** in CDCl₃

4.2 Electron Transfer through DNA

DNA synthesis and purification

Solid phase DNA synthesis was carried out on a *Perseptive Biosystems Expedite 8900* Synthesizer using *Ultramild* bases and reagents (*Glen Research*) and following standard phosphoramidite or phosphoramidite/*H*-phosphonate protocols. Coupling times for Br-nucleotides building blocks were increased to 10 min. Oligonucleotides were cleaved from the solid support as described in the text with conc. Ammonia (25 %) for times between 1 day and 5 days generally at 25°C due to the base lability of the nucleotides used. Analytical and preparative HPLC was performed with a *Merck LaChrom* system using 3 μ or 5 μ C₁₈-reversed phase columns by *Macherey-Nagel* and 0.1 M NH₄OAc in water : acetonitrile as eluent. After concentration *in vacuo* the strands were desalted on *Waters SepPak*TM-C₁₈-cartridges and concentrated again. The final DNA concentration was estimated by UV absorption measured on a *Cary 100* UV-Vis spectrometer following standard procedures. The strands were further characterized by MALDI-ToF-MS. MALDI mass spectra were recorded on a *Bruker Autoflex II* mass spectrometer using 3-hydroxypicolinic acid as matrix substance and measuring in the negative or positive polarity mode.

4.2.1 Sequence dependence studies

Irradiation experiments

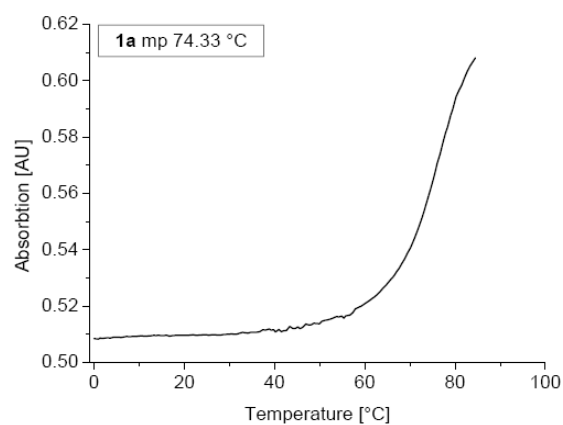
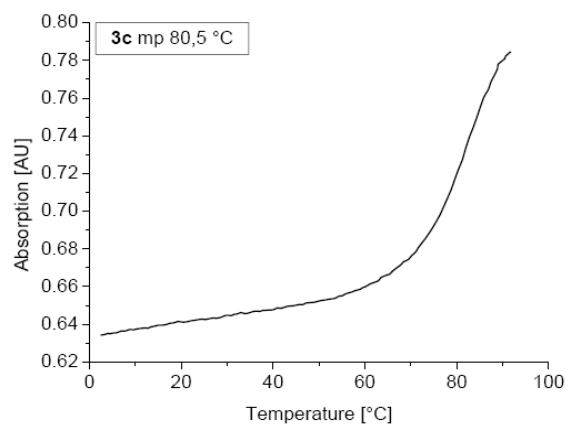
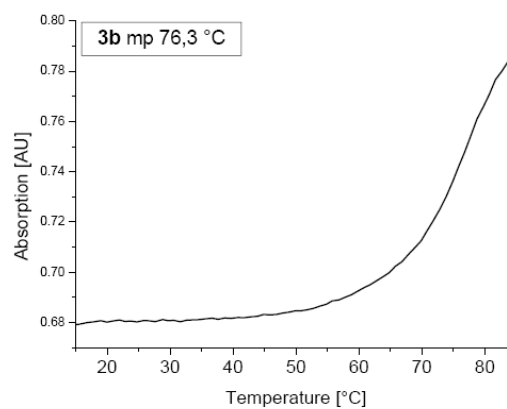
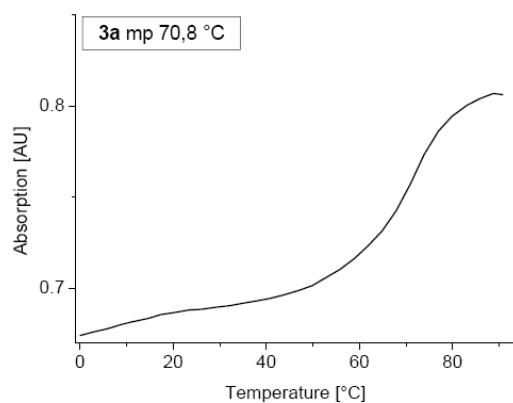
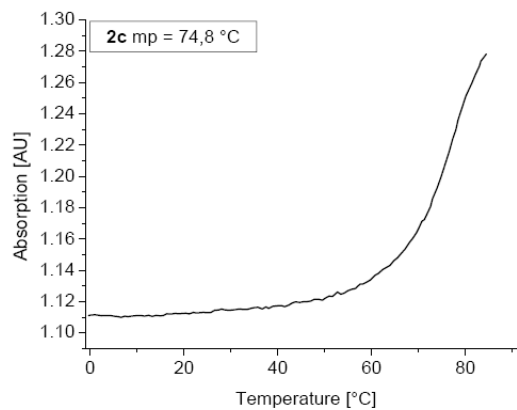
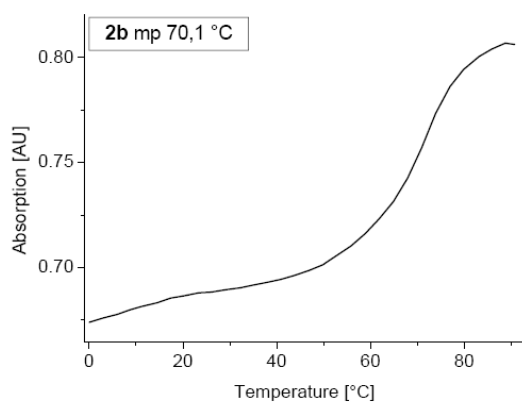
In a typical irradiation experiment a solution of the oligonucleotide (3-30 μ M) containing 150 mM NaCl and 10 mM Tris-HCl (pH 7.4, total volume 150 μ L) was transferred to a 1 mL quartz fluorescence cuvette sealed with a rubber septum. The solution was degassed by sparging with argon for 20 min. For reduction of the flavin two different procedures were used. For one part of the experiments 15 μ L of an alkaline solution of sodium dithionite (87 mg dithionite in 5 g water + 75 μ L 5 M NaOH, pH ~ 8) was added. Alternatively an EDTA-mediated photoreduction was used. For this purpose EDTA 0.2M was added and the solution pre-irradiated under anaerobic conditions for 1 minute with white light to photoreduce the flavin (monitored by fluorescence spectroscopy). After reduction the samples were further irradiated at 10 °C with a *Thermo Oriel* 1000 W Xe-lamp, equipped with a cooled 340 nm cut-off filter. For the analysis 10 μ L aliquots were removed from the assay solution after defined time intervals, aerated for 30 min and analysed. Analysis of the data

was performed by HPLC (3 μ C₁₈-reversed phase columns by *Macherey-Nagel* and 0.1 M NH₄Et₃OAc in water : acetonitrile as eluent) and MALDI-Tof-MS, or by capillary electrophoresis (*Beckman Coulter P/ACE-MDQ* DNA system, UV detection at 254 nm, 30 cm fused silica capillary filled with 6% polyacrylamide gel in 0.1 M Tris-borate, 2 mM EDTA, pH 8.4, electrokinetic injection by applying 10 kV for 2-5 s, separation at 9 kV for 45 min). The integration of the peaks was achieved using the instrument software. The data were plotted and a linear regression was applied to the points using *Microcal Origin*.

In the following pages are reported a selection of melting point curves, CD-spectra and curves relative to the irradiation experiments of the hairpins used in the EET study.

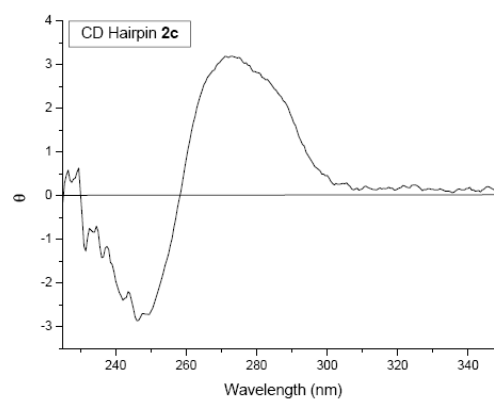
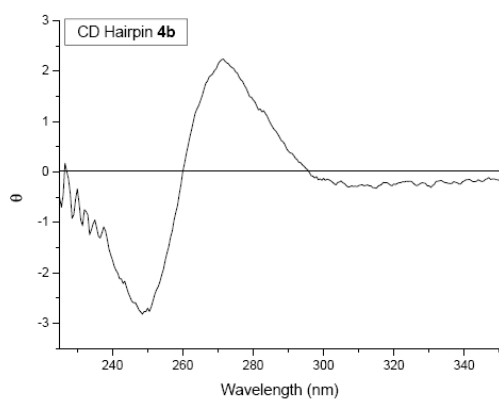
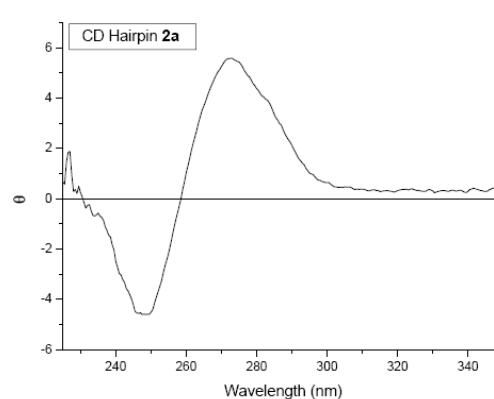
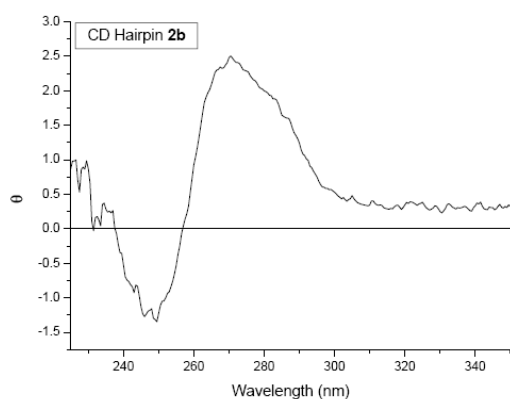
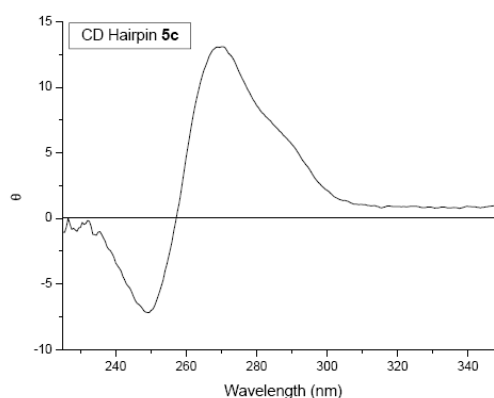
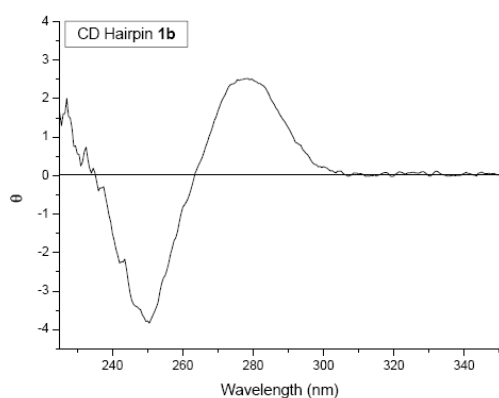
Melting point experiments

UV melting points were measured on a *Cary 100* UV-Vis spectrometer using 1 mL quartz cuvettes with 1 cm pathlength. The samples contained 150 mM NaCl, 10 mM Tris-HCl (pH 7.4) and 3 μ M of the oligonucleotide. For every strand five temperature cycles from 85 °C to 0 °C were recorded, the average melting point was calculated computationally using *Microcal Origin*.

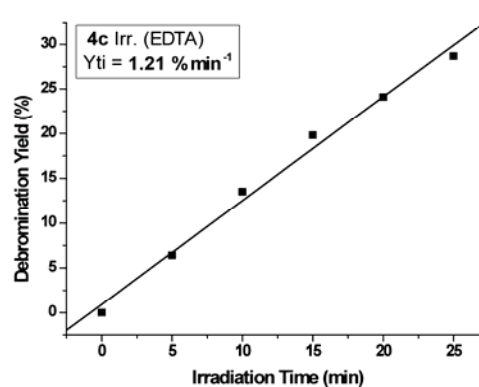
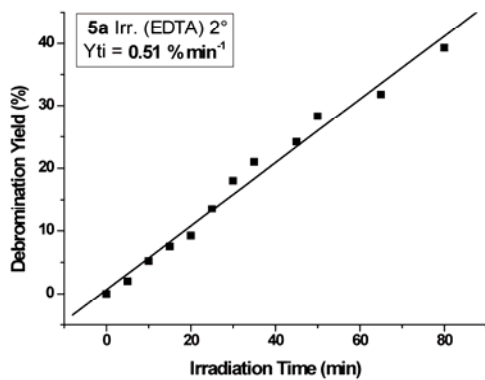
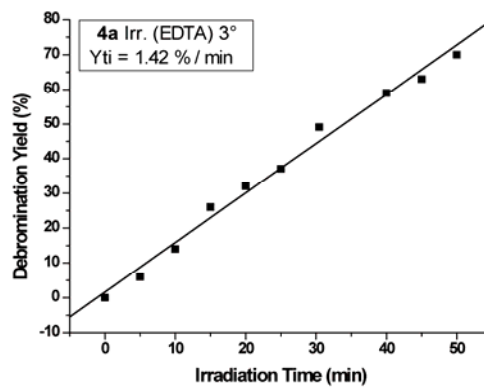
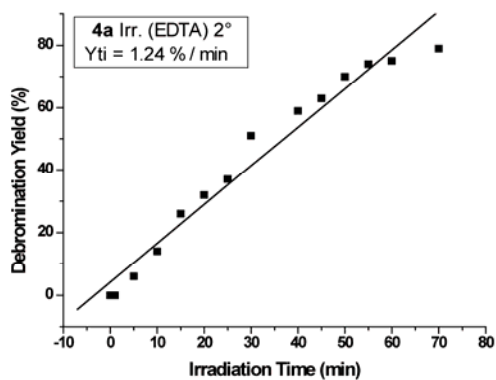
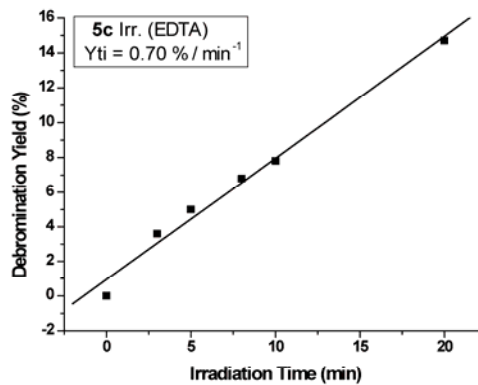
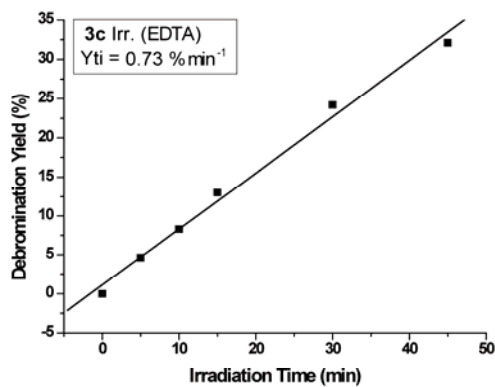


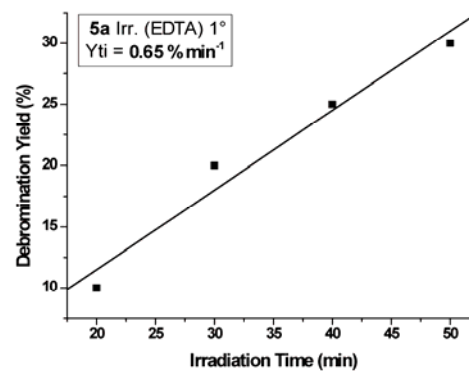
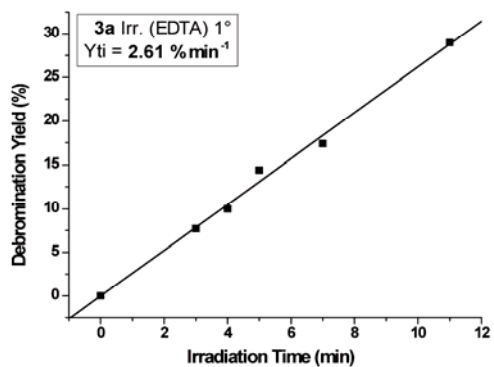
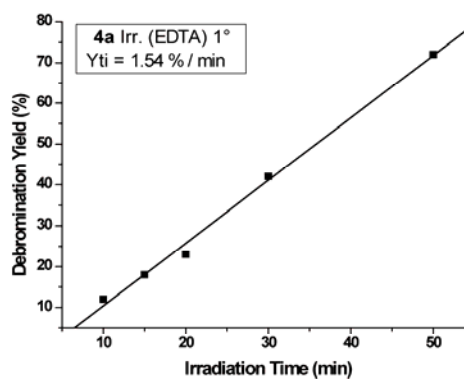
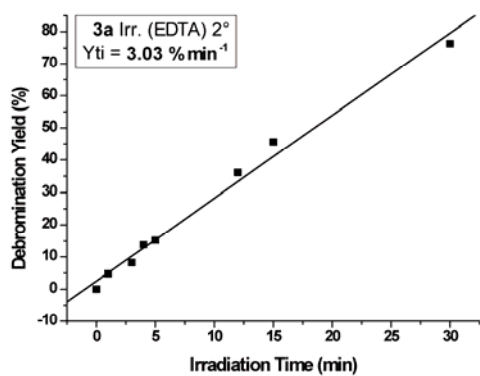
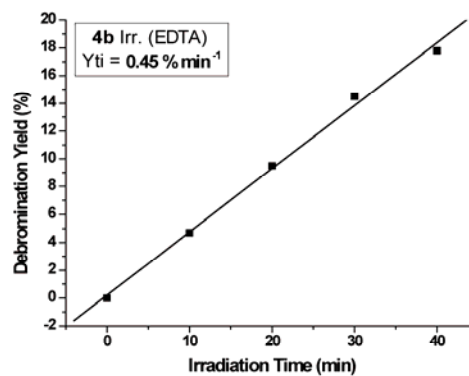
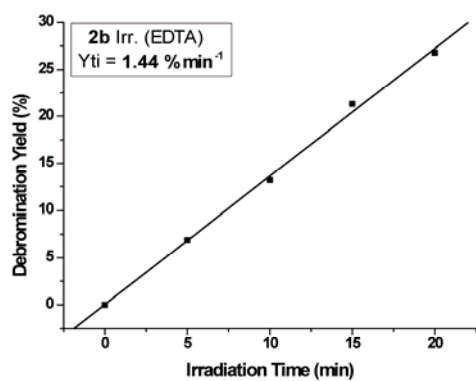
CD experiments

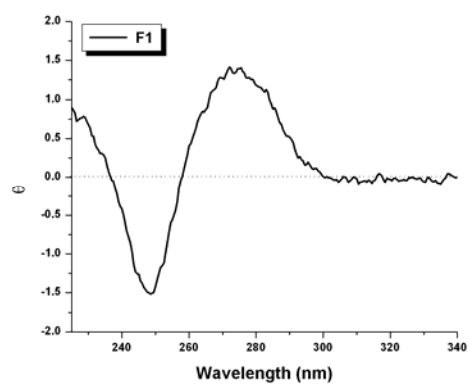
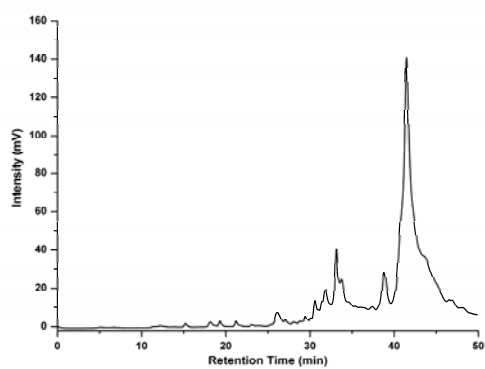
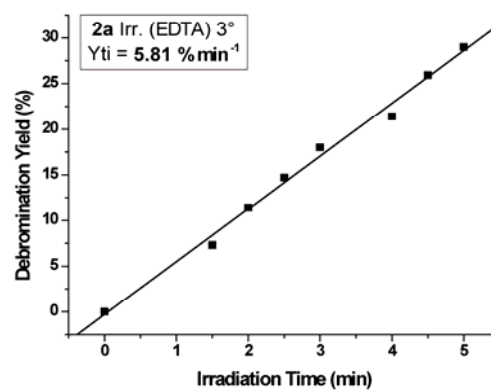
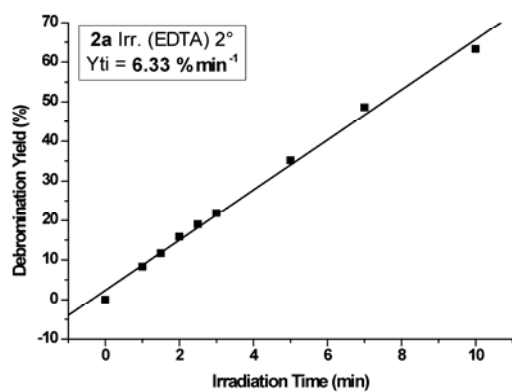
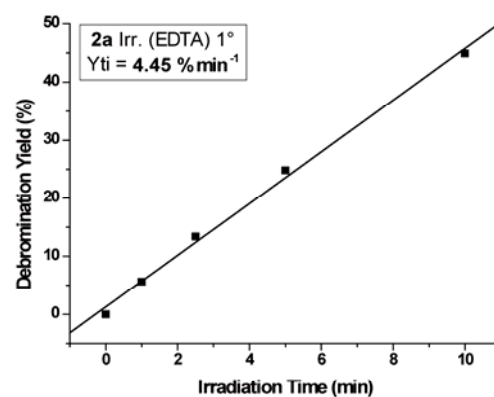
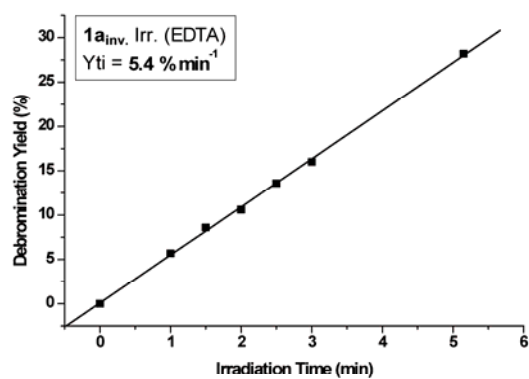
CD spectra were recorded on a *Jasco J-810* spectropolarimeter equipped with a *Peltier* temperature controller using 2 mL quartz cuvettes with 1 cm pathlength. The samples contained 150 mM NaCl, 10 mM Tris-HCl (pH 7.4) and 2-8 μM of the oligonucleotide. The hairpins containing the flavin were also measured in the irradiation buffer ($c_{\text{DNA}} = 2\text{-}8 \mu\text{M}$, 0.01 M Tris, pH = 7.4, 0.15 M NaCl, 0,02 M EDTA)



Irradiation curves



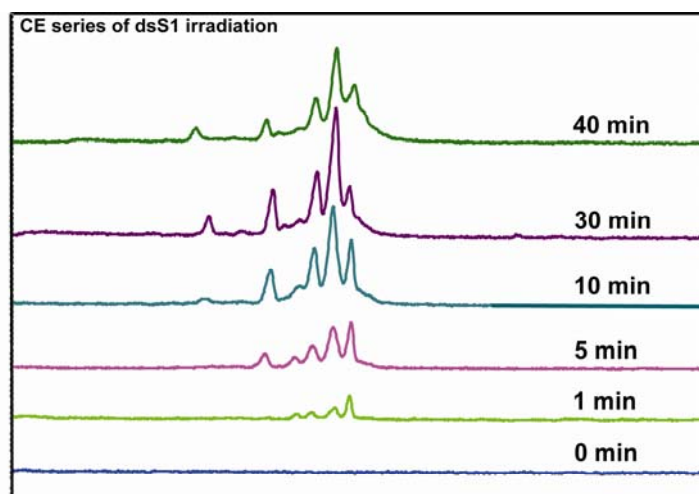


HPLC chromatogram and CD spectrum of **F1**.

4.2.2 Single electron donor and two acceptors

Irradiation experiments

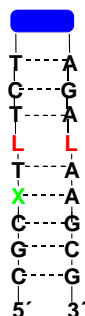
In a typical irradiation experiment a solution of the oligonucleotide (3-30 μM) containing 150 mM NaCl and 10 mM Tris-HCl (pH 7.4, total volume 150 μL) was transferred to a 1 mL quartz fluorescence cuvette sealed with a rubber septum. The solution was degassed by sparging with argon for 20 min. The samples were irradiated at 10 $^{\circ}\text{C}$ with a *Thermo Oriol* 1000 W Xe-lamp, equipped with a cooled 320 nm cut-off filter. For the analysis 10 μL aliquots were removed from the assay solution after defined time intervals and analysed. Analysis of the data was performed by HPLC (3 μC_{18} -reversed phase columns by *Macherey-Nagel* and 0.1 M NH_4OAc in water : acetonitrile as eluent) and MALDI-Tof-MS, or by capillary electrophoresis (*Beckman Coulter* P/ACE-MDQ DNA system, UV detection at 254 nm, 30 cm fused silica capillary filled with 6% polyacrylamide gel in 0.1 M Tris-borate, 2 mM EDTA, pH 8.4, electrokinetic injection by applying 10 kV for 2-5 s, separation at 9 kV for 45 min).



Enlargement (fragment-peaks) of a section from the CE series of irradiated dsS1.

4.3 M-MEET. High resolution mass

H2



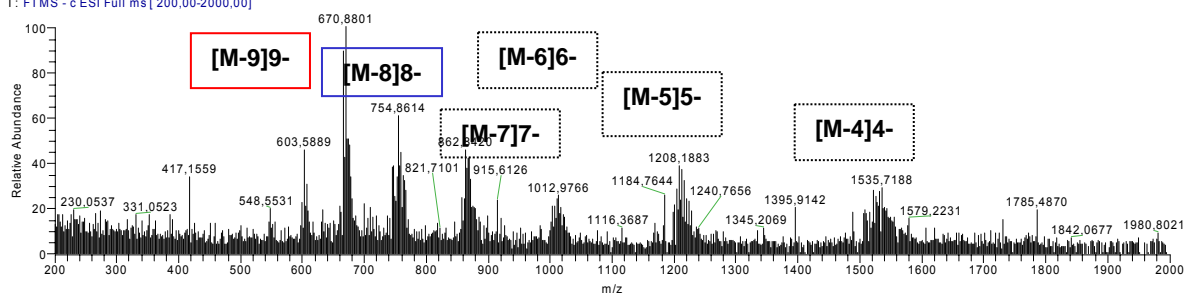
[M-3]3-	[M-4]4-	[M-5]5-	[M-6]6-	[M-7]7-	[M-8]8-	[M-9]9-	[M-10]10-
2000,6747	1500,2540	1200,0016	999,8333	856,8560	749,6230	666,2196	599,3960

1cle_antonio_EM2a-c_EM2Cua-c_06020218...
200 ul/min, H2O:MeCN=90:10, LTQ FT, Spahi

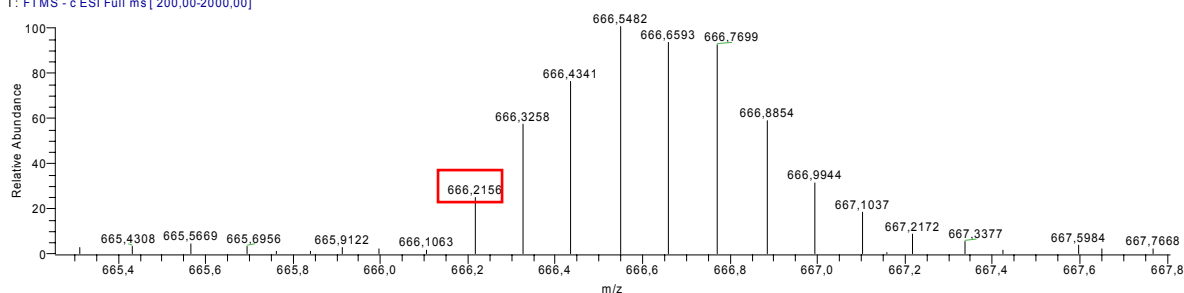
02.02.2006 18:45:10

Clever, Carell

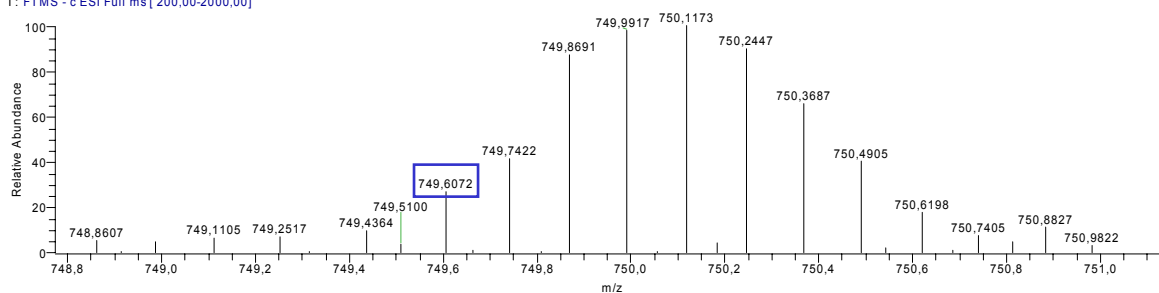
1cle_antonio_EM2a-c_EM2Cua-c_060202183534 #18-23 RT: 0,49-0,58 AV: 6 NL: 4,27E4
T: FTMS - c ESI Full ms [200,00-2000,00]



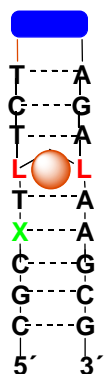
1cle_antonio_EM2a-c_EM2Cua-c_060202183534 #25-32 RT: 0,61-0,73 AV: 8 NL: 3,79E4
T: FTMS - c ESI Full ms [200,00-2000,00]



1cle_antonio_EM2a-c_EM2Cua-c_060202183534 #25-32 RT: 0,61-0,73 AV: 8 NL: 1,23E4
T: FTMS - c ESI Full ms [200,00-2000,00]

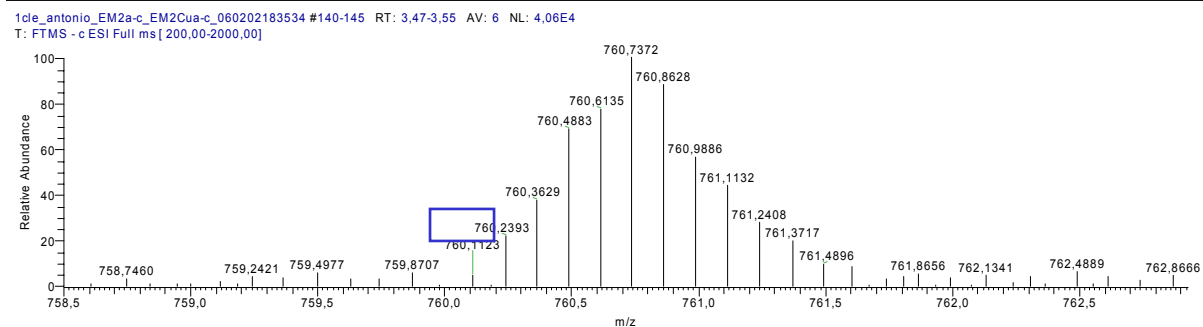
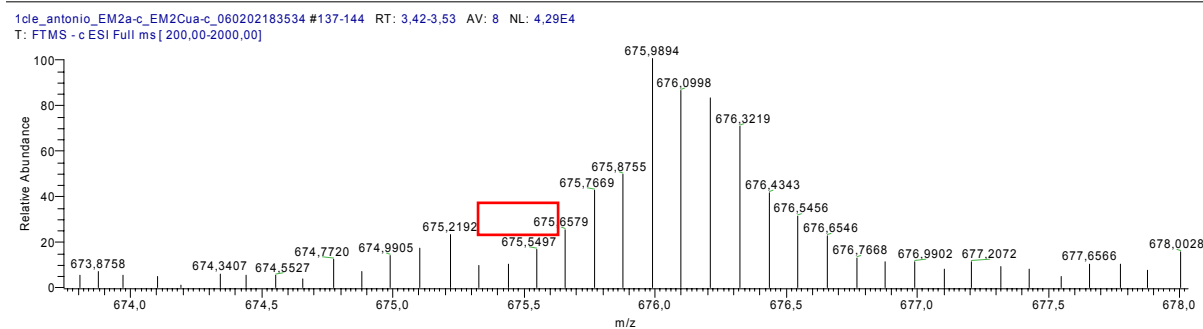
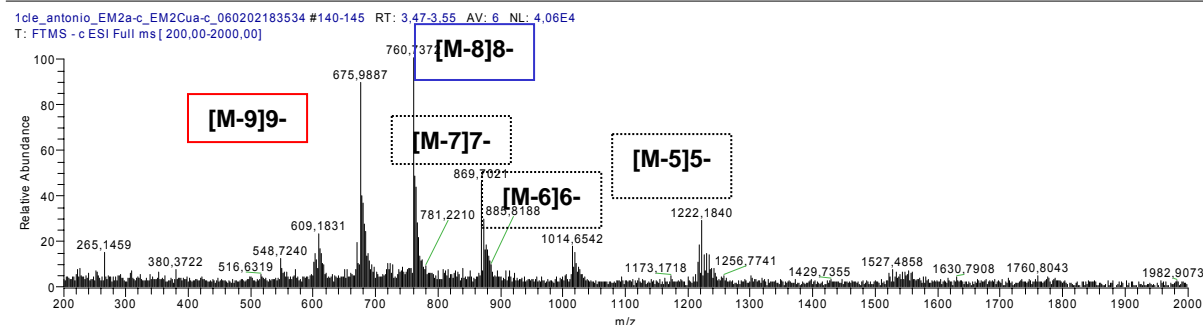


H2-Cu

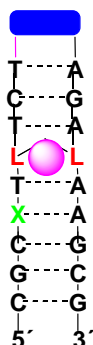


[M-3]3-	[M-4]4-	[M-5]5-	[M-6]6-	[M-7]7-	[M-8]8-	[M-9]9-	[M-10]10-
2028,9952	1521,4944	1216,9939	1013,9936	868,9934	760,2432	675,6597	607,8922

1cle_antonio_EM2a-c_EM2Cua-c_060202183534 #140-145 RT: 3.47-3.55 AV: 6 NL: 4.06E4
 200 ul/min, H2O:MeCN=90:10, LTQ FT, Spahl 02.02.2006 18:45:10 Clever, Carell



H2-Mn



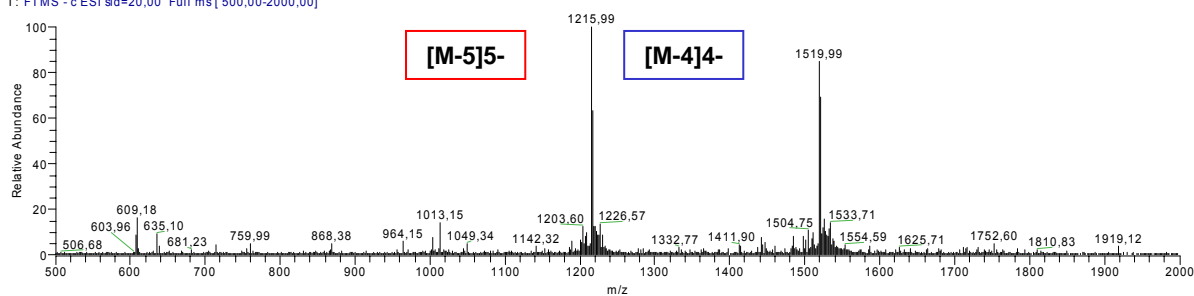
[M-3]3-	[M-4]4-	[M-5]5-	[M-6]6-	[M-7]7-	[M-8]8-	[M-9]9-	[M-10]10-
2025,9948	1519,2441	1215,1937	1012,4934	867,7075	759,1181	674,6596	606,9920

3cle_EM2_enMn_just_desalt_060306161448
200 ul/min, H2O:MeCN=80:20, LTQ FT, Spahl

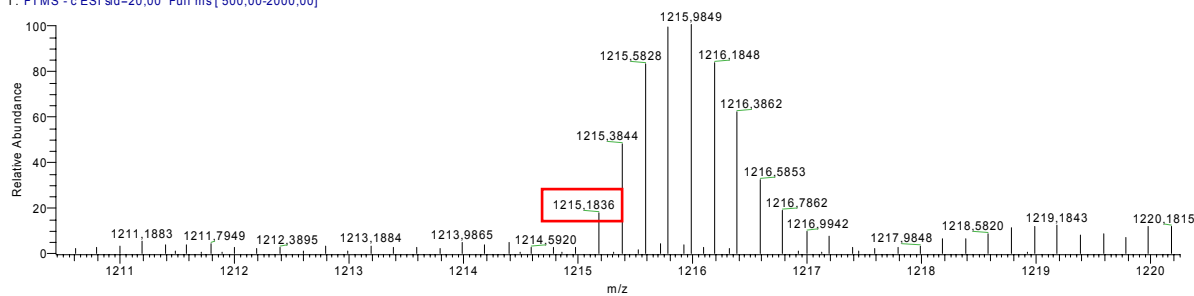
07.03.2006 16:26:33

Clever, Carell

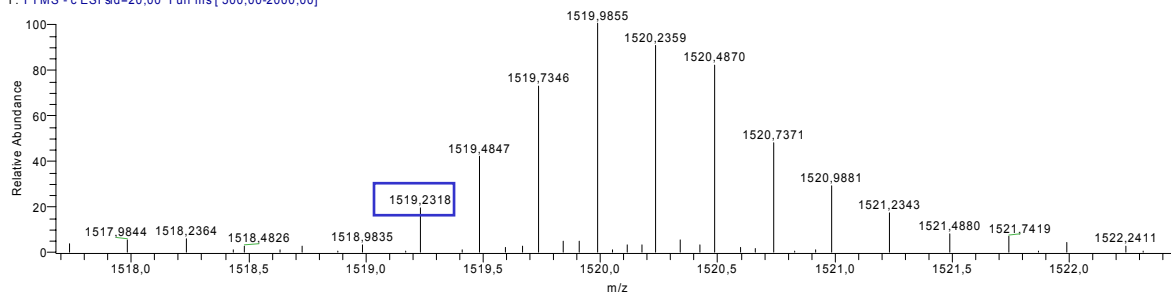
3cle_EM2_enMn_just_desalt_060306161448 #133-142 RT: 3.70-3.94 AV: 10 NL: 7,20E3
T: FTMS - c ESI sid=20,00 Full ms [500,00-2000,00]



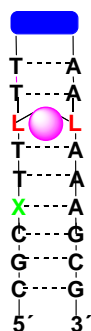
3cle_EM2_enMn_just_desalt_060306161448 #133-142 RT: 3.70-3.94 AV: 10 NL: 7,34E3
T: FTMS - c ESI sid=20,00 Full ms [500,00-2000,00]



3cle_EM2_enMn_just_desalt_060306161448 #133-142 RT: 3.70-3.94 AV: 10 NL: 6,09E3
T: FTMS - c ESI sid=20,00 Full ms [500,00-2000,00]



H1-Mn



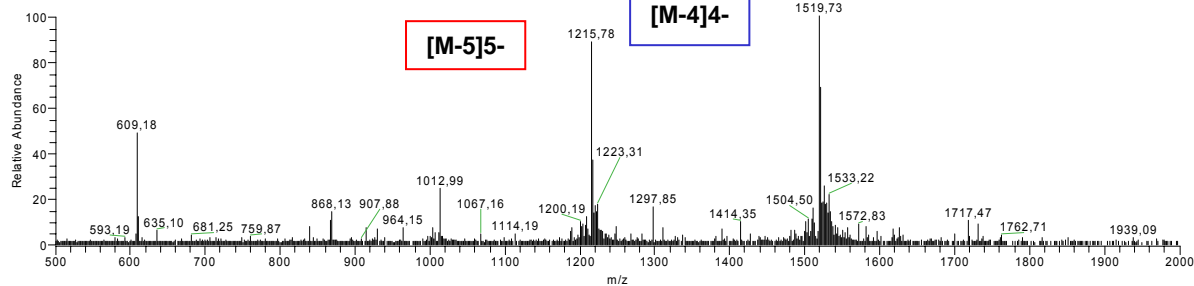
[M-3]3-	[M-4]4-	[M-5]5-	[M-6]6-	[M-7]7-	[M-8]8-	[M-9]9-	[M-10]10-
2025,6631	1518,9954	1214,9947	1012,3276	867,5653	758,9937	674,5490	606,8925

3cle_EM3_enMn_just_desalt_060306161448
200 ul/min, H2O:MeCN=80:20, LTQ FT, Spahl

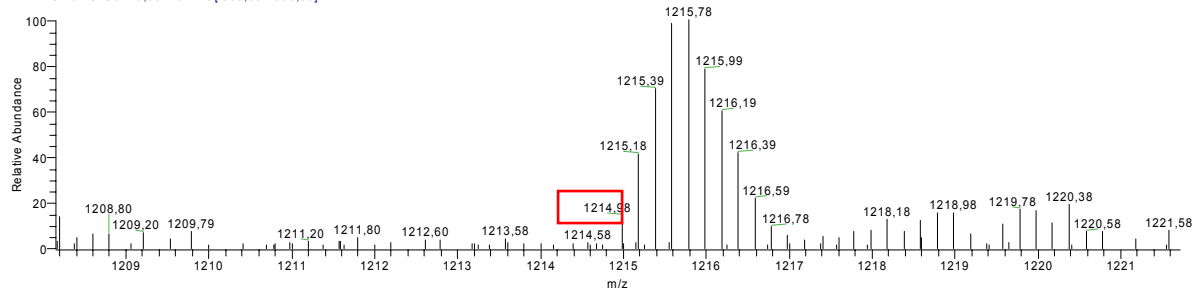
07.03.2006 16:31:44

Clever, Carell

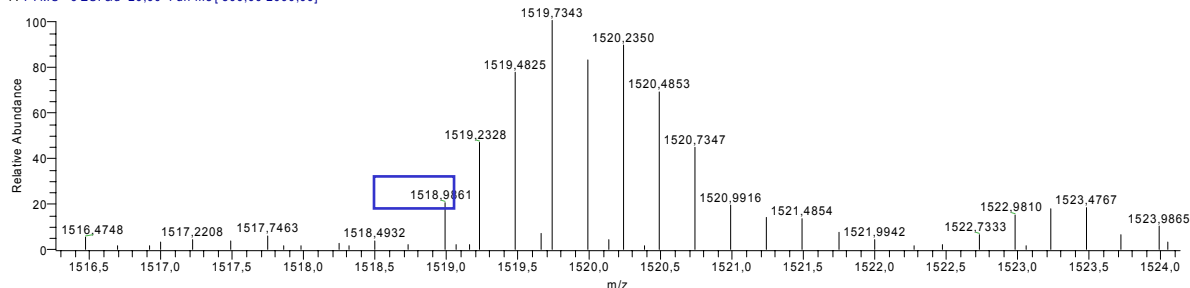
3cle_EM3_enMn_just_desalt_060306161448 #46-50 RT: 1.26-1.38 AV: 5 NL: 3.19E3
T: FTMS - c ESI sid=20,00 Full ms [500,00-2000,00]



3cle_EM3_enMn_just_desalt_060306161448 #46-50 RT: 1.26-1.38 AV: 5 NL: 2.83E3
T: FTMS - c ESI sid=20,00 Full ms [500,00-2000,00]



3cle_EM3_enMn_just_desalt_060306161448 #46-50 RT: 1.26-1.38 AV: 5 NL: 3.19E3
T: FTMS - c ESI sid=20,00 Full ms [500,00-2000,00]



4.4 Molecular beacon for DNA-photography

General Procedure for Photography Experiments

The following steps were all carried out under darkroom conditions: 1 μL aliquots of each solution of the MB-experiments were spotted onto black and white photographic paper (Ilfospeed RC Deluxe, Ilford) along with 1 μL of a solution reference. During the spotting procedure the contact between the micropipette tips and the photopaper must be avoided. A custom-made tips guide was used in order to avoid this contact and to ease the spotting of up to 96 different samples in few minutes, when needed. The strips of photopaper spotted with the solutions were then placed in a cupboard and kept in darkness for 20 min or until all of the solution had been absorbed into the emulsion. Alternatively, the strips were placed on a warm surface ($< 40\text{ }^\circ\text{C}$) in the dark for 1-3 min for a faster absorption process. One strip was then taken and placed into a filter cassette containing a 570 nm cut-off filter and a 0.5 OD density filter. This was then exposed to a white light source (24V, 250W) for 5, 15, 20 or 25 sec. The photopaper was then developed, stopped and fixed in standard solutions (Phenisol Developer, 2% AcOH in H_2O and Hypam Fixer from Ilford) according to the manufacturer's instructions (1 min in total), washed with running water for 3-5 min and then finally dried (5-10 min). The last two steps do not need dark conditions.

Materials and Fluorescence measurements

MB1 (5'-Cy3-CGCTGCCCTTGAGGCGTGGCTGCAGCG-BHQ2-3') and the target **T** (*Y. pestis* gene, 5'-AGCCACGCCTCAAGGG-3') were purchased from *Metabion*. Fluorescence measurements of the solutions were performed prior photographic analysis as control. Fluorescence kinetics and thermal denaturation curves were measured using a *Jasco Fluorescence Spectrometer F-750* and fluorescence quartz cuvettes ($\lambda_{\text{ex}} = 545\text{ nm}$; $\lambda_{\text{em}} = 570\text{ nm}$ for Cy3). Two different aqueous solutions were used as buffers: 5 mM tris-HCl pH 8, 5 mM KCl and 0.5 mM MgCl_2 for high concentration assays (i.e. for **MB1** 1 μM) and 5 mM tris-HCl pH 8, 0.5 mM MgCl_2 for low concentration assays (i.e. for **MB1** 0.2 μM). Prior analysis, the samples were heated to the maximum temperature of 85 $^\circ\text{C}$ and cooled down slowly to the starting temperature of 20 $^\circ\text{C}$.

Cell line and cell culture

A human colon carcinoma cell line, HCT116, obtained from DSMZ (DSMZ no. ACC 581), was routinely grown in DMEM medium supplemented with 10% fetal bovine serum and antibiotics. Once the cells reached confluence, they were harvested and subjected to genomic DNA isolation. Extraction was carried out using the E.Z.N.A.® Tissue DNA Mini Kit (Peqlab Biotechnologie GmbH). DNA fractions were pooled in a 15 mL Falcon™ Tube and concentrated to approx. 1 µg/µL in the SpeedVac. The genomic DNA was fragmented by sonification. The majority of the resulting fragments ranged from less than 0.5 kb up to 2 kb.

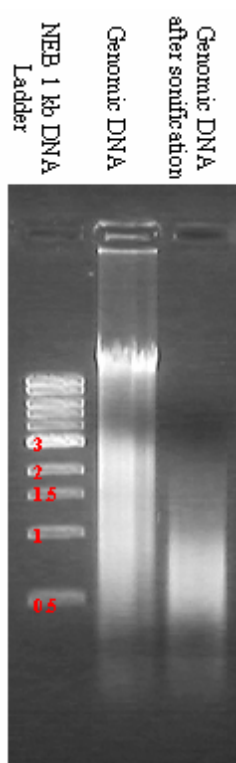


Figure S15 1% agarose gel, stained with ethidium bromide, total amount of genomic DNA per lane 2.5 µg

5 Abbreviations

A	adenine (adenosine)
Å	Angstrom, 10^{-10} m
Abs	absorption
Ac ₂ O	Acetylanhydride
acac	acetylacetonate
AcOH	Acetic acid
AFM	Atomic Force Microscopy
AIBN	azobisisobutyronitrile
A _{max}	absorption maximum
A _{norm}	normed absorption
BER	Base excision repair
bp	base pair(s)
Bu	butyl
BuSH	1-Butanethiol
C	cytosine (cytidine)
cat.	catalytic
CD	Circular Dichroism
CE	Capillary electrophoresis
CED	cianoethyl- <i>N,N</i> -diisopropyl
CIP	Cahn-Ingold-Prelog priority rule
CPD	Cyclobutane-pyrimidine dimer
CT	Charge transfer
Cyclo-dhT	Cyclo-dehydrothymidine
d	day(s)
dA	2'-deoxyribo-adenosine
Da	Dalton
dC	2'-deoxy-cytidine
dG	2'-deoxy-guanosine
DMAP	4- <i>N,N</i> -dimethylaminopyridine
DMBz	dimethoxybenzoyl
DMC	dichloromethane
DMF	dimethylformamide
DMSO	dimethylsulfoxide
DMT	4,4'-dimethoxytrityl
DNA	deoxyribonucleic acid
DP	DNA-photography
ds	Double strand
dT	2'-deoxy-thymidine
DTBP	di- <i>tert</i> -butyl peroxide
dU	2'-deoxy-uridine
EA	Elementary Analysis
Ed.	editor(s)
EDTA	ethylenediamine-tetra-acetate
EET	Excess electron transfer
EI	Electron Impact
en	ethylenediamine
EPR	Electron Paramagnetic Resonance
equ	equivalent(s)
ESI	Electro Spray Ionisation
Et	ethyl
eV	electronvolt

Abbreviations

FAB	Fast Atom Bombardement
FAD	Flavin adenine dinucleotide
FT	Fourier Transformation
G	guanine (guanosine)
GSH	gluthatione
h	hour(s)
HDF	8-hydroxy-5-deazaflavin
HOMO	Highest occupied molecular orbital
HPLC	High Performance Liquid Chromatography
HRMS	High Resolution Mass Spectrometry
HT	Hole transfer
I	intensity
iPr	iso-propyl
IR	Infrared (spectroscopy)
<i>J</i>	coupling constant
LC-MS	Liquid Chromatography-Mass Spectrometry
LUMO	Lowest unoccupied molecular orbital
M	molecule or molar
m/z	mass/charge
MALDI	Matrix Assisted Laser Desorption Ionisation
MB	Molecular beacon
MBDP	Molecular beacon for DNA-photography
mdeg	milli degree (ellipticity)
Me	methyl
MeCN	acetonitrile
MeOH	methanol
MF	5-methylene furanone
min	minute(s)
M-MEET	Metal-mediated excess electron transfer
MS	Mass Spectrometry
mV	millivolt
NER	Nucleotide excision repair
NHE	Normal hydrogen electrode
NMR	Nuclear Magnetic Resonance
NOESY	Nuclear Overhauser Effect Spectroscopy
OAc	acetyl
ODN	Oligo-2'-deoxy-nucleotide
PCR	Polymerase chain reaction
Ph	phenyl
Py	pyridine
R	organic residue
r.t.	room temperature
rel. int.	relative intensity
RF	retention factor
RNA	ribonucleic acid
ROS	Reactive oxygen specie

Abbreviations

RP	Reverse Phase
RP HPLC	Reverse phase HPLC
s	second
salen	N,N-bis-salicylidene-ethylenediamine
sat.	saturated
SCE	Standard hydrogen electrode
SED	Single electron donor
SET	Single electron transfer
ss	Single strand
STM	Scanning Tunneling Microscopy
T	thymine (thymidine)
TBAF	tetra-n-butylammonium fluoride
TBDMS	<i>tert</i> -Butyldimethylsilyl
TBDPS	<i>tert</i> -Butyldiphenylsilyl
TBHN	di- <i>tert</i> -butyl hyponitrite
TBPB	<i>tert</i> -butyl peroxybenzoate
THF	tetrahydrofuran
TLC	thin layer chromatography
T _M	melting temperature
TMS	trimethylsilyl
Tof	time of flight
Tol	toluoyl
TRIS	tris(hydroxymethyl)aminomethane
TTMSS	tris-trimethylsilyl-silane
U	Uracil, uridine
UV	Ultraviolet (spectroscopy)
V	Volt
Vis	Visible (spectroscopy)
Y	Debromination yield per time of irradiation
z	charge
ε	extinction coefficient
λ	wavelength
λ _{max}	maximum abs wavelength

6 References

- (1) Watson, J. D.; Crick, F. H. C., A structure for deoxyribose nucleic acid. *Nature*, **1953**, *171*, 737-738.
- (2) Miescher, F., Ueber die chemische Zusammensetzung der Eiterzellen. *Hoppe-Seyler's medizinisch-chemische Untersuchungen*, **1871**, *4*, 441-460.
- (3) Levene, P. A., The structure of yeast nucleic acid. *J. Biol. Chem.*, **1917**, *31*, 591-8.
- (4) Levene, P. A., Properties of the nucleotides obtained from yeast nucleic acid. *J. Biol. Chem.*, **1920**, *41*, 483-92.
- (5) Lythgoe, B.; Todd, A. R., Structure of adenosine di- and triphosphate. *Nature*, **1945**, *155*, 695-6.
- (6) Todd, A. R., Synthesis of nucleotides. *Bulletin de la Societe Chimique de France*, **1948**, 933-8.
- (7) Chargaff, E., Chemical specificity of nucleic acids and mechanism of their enzymatic degradation. *Experientia*, **1950**, *6*, 201-209.
- (8) Franklin, R. E.; Gosling, R. G., Evidence for 2-chain helix in crystalline structure of sodium deoxyribonucleate. *Nature*, **1953**, *172*, 156-7.
- (9) Halliwell, B.; Aruoma, O. I., *DNA and Free Radicals*; Ellis Horwood: Chichester, **1993**, the whole volume.
- (10) O'Neill, P.; Fielden, E. M., Primary free radical processes in DNA. *Adv. Radiat. Biol.*, **1993**, *17*, 53-120.
- (11) Pratiel, G.; Bernadou, J.; Meunier, B., Carbon - Hydrogen Bonds of DNA Sugar Units as Targets for Chemical Nucleases and Drugs. *Angew. Chem. Int. Ed.*, **1995**, *34*, 746-769.
- (12) Cadet, J.; Douki, T.; Gasparutto, D.; Ravanat, J.-L., Radiation-induced damage to cellular DNA: measurement and biological role. *Radiat. Phys. Chem.*, **2005**, *72*, 293-299.
- (13) Cadet, J.; Douki, T.; Ravanat, J.-L.; In *Redox-Genome Interactions in Health and Disease*; Fuchs, J., Podda, M., Packer, L., Eds.; Dekker: New York, **2003**; pp 143-189.
- (14) Chatgililoglu, C.; O'Neill, P., Free radicals associated with DNA damage. *Exp. Gerontol.*, **2001**, *36*, 1459-1471.
- (15) Dizdaroglu, M.; Jaruga, P.; Birincioglu, M.; Rodriguez, H., Free radical-induced damage to DNA: mechanisms and measurement. *Free Rad. Biol. Med.*, **2002**, *32*, 1102-1115.
- (16) Dizdaroglu, M.; Jaruga, P.; Rodriguez, H.; In *Critical Reviews of Oxidative Stress and Aging: Advances in Basic Science Diagnostics and Intervention*; Gutler, R. G., Rodriguez, H., Eds.; World Scientific: London, **2003**; Vol. 1; pp 165-189.
- (17) Birincioglu, M.; Jaruga, P.; Chowdhury, G.; Rodriguez, H.; Dizdaroglu, M.; Gates, K. S., DNA Base Damage by the Antitumor Agent 3-Amino-1,2,4-benzotriazine 1,4-Dioxide (Tirapazamine). *J. Am. Chem. Soc.*, **2003**, *125*, 11607-11615.

- (18) Dizdaroglu, M.; Jaruga, P.; Rodriguez, H., Identification and quantification of 8,5'-cyclo-2'-deoxy-adenosine in DNA by liquid chromatography/ mass spectrometry. *Free Rad. Biol. Med.*, **2001**, *30*, 774-784.
- (19) Jaruga, P.; Birincioglu, M.; Rodriguez, H.; Dizdaroglu, M., Mass Spectrometric Assays for the Tandem Lesion 8,5'-Cyclo-2'-deoxyguanosine in Mammalian DNA. *Biochemistry*, **2002**, *41*, 3703-3711.
- (20) Pogozelski, W. K.; Tullius, T. D., Oxidative Strand Scission of Nucleic Acids: Routes Initiated by hydrogen abstraction from the sugar moiety. *Chem. Rev.*, **1998**, *98*, 1089-1107.
- (21) Drew, H. R.; Wing, R. M.; Takano, T.; Broka, C.; Tanaka, S.; Itakura, K.; Dickerson, R. E., Structure of a B-DNA Dodecamer: Conformation and Dynamics. *Proc. Natl. Acad. Sci. USA*, **1981**, *78*, 2179-2183.
- (22) Pardo, L.; Banfelder, J. T.; Osman, R., Theoretical studies of the kinetics, thermochemistry, and mechanism of hydrogen-abstraction from methanol and ethanol. *J. Am. Chem. Soc.*, **1992**, *114*, 2382-2390.
- (23) Colson, A.-O.; Sevilla, M. D., Structure and Relative Stability of Deoxyribose Radicals in a Model DNA Backbone: Ab Initio Molecular Orbital Calculations. *J. Phys. Chem.*, **1995**, *99*, 3867-3874.
- (24) Miaskiewicz, K.; Osman, R., Theoretical study on the deoxyribose radicals formed by hydrogen abstraction. *J. Am. Chem. Soc.*, **1994**, *116*, 232-238.
- (25) Chatgililoglu, C.; Guerra, M.; Mulazzani, Q. G., Model Studies of DNA C5' Radicals. Selective Generation and Reactivity of 2'-Deoxyadenosin-5'yl Radical. *J. Am. Chem. Soc.*, **2003**, *125*, 3839-3848.
- (26) Flyunt, R.; Bazzanini, R.; Chatgililoglu, C.; Mulazzani, Q. G., Fate of the 2'-Deoxyadenosin-5'yl Radical under Anaerobic Conditions. *J. Am. Chem. Soc.*, **2000**, *122*, 4225-4226.
- (27) Jimenez, L. B.; Encinas, S.; Miranda, M. A.; Navacchia, M. L.; Chatgililoglu, C., The photochemistry of 8-bromo-2-deoxyadenosine. A direct entry to cyclopurine lesions. *Photochem. Photobiol. Sci.*, **2004**, *3*, 1042-1046.
- (28) von Sonntag, C., *Free-Radical-Induced DNA damage and its Repair*; Springer-Verlag: Berlin, **2006**, pp. 366-371.
- (29) Goodman, B. K.; Greenberg, M. M., Independent Generation and Reactivity of 2'-Deoxyurid-1'-yl. *J. Org. Chem.*, **1996**, *61*, 2-3.
- (30) Chatgililoglu, C.; Gimisis, T., Fate of the C-1 peroxy radical in the 2-deoxyuridine system. *Chem. Commun.*, **1998**, 1249-1250.
- (31) Greenberg, M. M., Elucidating DNA damage and repair processes by independently generating reactive and metastable intermediates. *Organic & Biomolecular Chemistry*, **2007**, *5*, 18-30.
- (32) Greenberg, D. A.; Jin, K., From angiogenesis to neuropathology. *Nature*, **2005**, *438*, 954-959.
- (33) Ito, T.; Rokita, S. E., Excess Electron Transfer from an Internally Conjugated Aromatic Amine to 5-Bromo-2'-deoxyuridine in DNA. *J. Am. Chem. Soc.*, **2003**, *125*, 11480-11481.

- (34) Wagenknecht, H.-A., Reductive electrontransfer and transport of excess electrons in DNA. *Angew. Chem. Int. Ed.*, **2003**, *42*, 2454-2460.
- (35) Manetto, A.; Breeger, S.; Chatgililoglu, C.; Carell, T., Complex Sequence Dependence by Excess-Electron Transfer through DNA with Different Strength Electron Acceptors. *Angew. Chem. Int. Ed.*, **2006**, *45*, 318-321.
- (36) Xu, Y.; Sugiyama, H., Photochemical Approach to Probing Different DNA Structures. *Angew. Chem. Int. Ed.*, **2006**, *45*, 1354-1362.
- (37) Adhikary, A.; Malkhasian, A. Y. S.; Collins, S.; Koppen, J.; Becker, D.; Sevilla, M. D., UVA-visible photo-excitation of guanine radical cations produces sugar radicals in DNA and model structures. *Nucl. Acids Res.*, **2005**, *33*, 5553-5564.
- (38) Lesiak, K. B.; Wheeler, K. T., Formation of α -deoxyadenosine in polydeoxynucleotides exposed to ionising radiation under anoxic conditions. *Radiat. Res.*, **1990**, *121*, 328-337.
- (39) Ide, H.; Yamaoka, T.; Kimura, Y., Replication of DNA Templates Containing the α -Anomer of Deoxyadenosine, a Major Adenine Lesion Produced by Hydroxyl Radicals. *Biochemistry*, **1994**, *33*, 7127-7133.
- (40) Sitlani, A.; Long, E. C.; Pyle, A. M.; Barton, J. K., DNA photocleavage by phenanthrenequinone diimine complexes of rhodium(III): shape-selective recognition and reaction. *J. Am. Chem. Soc.*, **1992**, *114*, 2303-2312.
- (41) Mohler, D. L.; Downs, J. R.; Hurley-Predecki, A. L.; Sallman, J. R.; Gannett, P. M.; Shi, X., DNA Cleavage by the Photolysis of Cyclopentadienyl Metal Complexes: Mechanistic Studies and Sequence Selectivity of Strand Scission by CpW(CO)₃CH₃. *J. Org. Chem.*, **2005**, *70*, 9093-9102.
- (42) Giese, B.; Burger, J.; Kang, T. W.; Kesselheim, C.; Wittmer, T., Model studies on the radical induced DNA-strand cleavage. *J. Am. Chem. Soc.*, **1992**, *114*, 7322-7324.
- (43) Dussy, A.; Meggers, E.; Giese, B., Spontaneous Cleavage of 4'-DNA Radicals under Aerobic Conditions: Apparent Discrepancy between Trapping Rates and Cleavage Products. *J. Am. Chem. Soc.*, **1998**, *120*, 7399-7403.
- (44) Giese, B.; Beyrich-Graf, X.; Erdmann, P.; Giraud, L.; Imwinkelried, P.; Mueller, S. N.; Schwitter, U., Cleavage of Single-Stranded 4'-Oligonucleotide Radicals in the Presence of O₂. *J. Am. Chem. Soc.*, **1995**, *117*, 6146-6147.
- (45) Criegee, R., Ein neuer Weg in die Cyclodecanreihe. *Chem. Ber.*, **1945**, *77*, 722-726.
- (46) Introduction Dirksen, M. L.; Blakely, W. F.; Holwitt, E.; Dizdaroglu, M., Effect Of Dna Conformation On The Hydroxyl Radical-Induced Formation Of 8,5'-Cyclopurine 2'-Deoxyribonucleoside Residues In Dna. *Int. J. Radiat. Biol.*, **1988**, *54*, 195-204. International Journal Of Radiation Biology.
- (47) Karakaya, A.; Jaruga, P.; Bohr, V. A.; Grollman, A. P.; Dizdaroglu, M., Kinetics of excision of purine lesions from DNA by *Escheria coli* Fpg protein. *Nucl. Acids Res.*, **1997**, *25*, 474-479.
- (48) Randerath, K.; Zhou, G.-D.; Somers, R. L.; Robbins, J. H.; Brooks, P. J., A 32P-Postlabeling Assay for the Oxidative DNA Lesion 8,5'-Cyclo-2'-deoxyadenosine in Mammalian Tissues. Evidence that Four Type II I-compounds are Dinucleotides Containing the Lesion in the 3' Nucleotide. *J. Biol. Chem.*, **2001**, *276*, 36051-36057.

- (49) Kuraoka, I.; Bender, C.; Romieu, A.; Cadet, J.; Wood, R. D.; Lindahl, T., Removal of oxygen free-radical-induced 5',8-purine cyclodeoxynucleosides from DNA by the nucleotide excision-repair pathway in human cells. *PNAS*, **2000**, *97*, 3832-3837.
- (50) Kuraoka, I.; Kobertz, W. R.; Ariza, R. R.; Biggerstaff, M.; Essigmann, J. M.; Wood, R. D., Repair of an interstrand DNA cross-link initiated by ERCC1-XPF repair/recombination nuclease. *J. Biol. Chem.*, **2000**, *275*, 26632-26636.
- (51) Brooks, P. J.; Wise, D. S.; Berry, D. A.; Kosmoski, J. V.; Smerdon, M. J.; Somers, R. L.; Mackie, H.; Spoonde, A. Y.; Ackerman, E. J.; Coleman, K.; Tarone, R. E.; Robbins, J. H., The Oxidative DNA Lesion 8,5'-(S)-Cyclo-2'-deoxyadenosine Is Repaired by the Nucleotide Excision Repair Pathway and Blocks Gene Expression in Mammalian Cells. *J. Biol. Chem.*, **2000**, *275*, 22355-22362.
- (52) Kuraoka, I.; Robins, P.; Masutani, C.; Hanaoka, F.; Gasparutto, D.; Cadet, J.; Wood, R. D.; Lindahl, T., Oxygen Free Radical Damage to DNA. Translesion Synthesis by Human DNA Polymerase eta and Resistance to Exonuclease Action at Cyclopurine Deoxynucleoside Residues. *J. Biol. Chem.*, **2001**, *276*, 49283-49288.
- (53) Ioele, M.; Bazzanini, R.; Chatgililoglu, C.; Mulazzani, Q. G., Chemical Radiation Studies of 8-Bromoguanosine in Aqueous Solutions. *J. Am. Chem. Soc.*, **2000**, *122*, 1900-1907.
- (54) Chatgililoglu, C.; Caminal, C.; Guerra, M.; Mulazzani, Q. G., Tautomers of One-Electron-Oxidized Guanosine. *Angew. Chem. Int. Ed.*, **2005**, *44*, 2-4.
- (55) Manetto, A.; Georganakis, D.; Gimisis, T.; Leondiadis, L.; Carell, T.; Chatgililoglu, C., Independent Generation of C5'-Nucleosidyl Radicals in Thymidine and 2'-Deoxyguanosine. *J. Org. Chem.*, **2007**, Accepted.
- (56) Kodama, T.; Greenberg, M. M., Preparation and Analysis of Oligonucleotides Containing Lesions Resulting from C5'-Oxidation. *J. Org. Chem.*, **2005**, *70*, 9916-9924.
- (57) Goldberg, I. H., Mechanism of neocarzinostatin action: role of DNA microstructure in determination of chemistry of bistranded oxidative damage. *Acc. Chem. Rev.*, **1991**, *24*, 191-198.
- (58) Goldberg, I. H., Free radical mechanisms in neocarzinostatin-induced DNA damage. *Free Radical Biol. Med.*, **1987**, *3*, 41-54.
- (59) Myers, A. G.; Kuo, E. Y.; Finney, N. S., Thermal generation of .alpha.,3-dehydrotoluene from (Z)-1,2,4-heptatrien-6-yne. *J. Am. Chem. Soc.*, **1989**, *111*, 8057-8059.
- (60) Nagata, R.; Yamanaka, H.; Okazaki, E.; Saito, I., Biradical formation from acyclic conjugated eneyne-allene system related to neocarzinostatin and esperamicin-calicheamicin. *Tetrahedron Lett.*, **1989**, *30*, 4995-4998.
- (61) Sugiyama, H.; Fujiwara, T.; Kawabata, H.; Yoda, N.; Hirayama, N.; Saito, I., Chemistry of neocarzinostatin-mediated cleavage of oligonucleotides. Competitive ribose C5' and C4' hydroxylation. *J. Am. Chem. Soc.*, **1992**, *114*, 5573-5578.
- (62) Kappen, L. S.; Goldberg, I. H., Deoxyribonucleic acid damage by neocarzinostatin chromophore: strand breaks generated by selective oxidation of C-5' of deoxyribose. *Biochemistry*, **1983**, *22*, 4872-4878.
- (63) Gu, F.; Xi, Z.; Goldberg, I. H., DNA Damage by Thiol-Activated Neocarzinostatin Chromophore at Bulged Sites. *Biochemistry*, **2000**, *39*, 4881-4891.

- (64) Breen, A. P.; Murphy, J. A., Reactions of Oxyl Radicals With DNA. *Free Rad. Biol. Med.*, **1995**, *18*, 1033-1077.
- (65) Kawabata, H.; Takeshita, H.; Fujiwara, T.; Sugiyama, H.; Matsuura, T.; Saito, I., Chemistry of neocarzinostatin-mediated degradation of d(GCATGC). Mechanism of spontaneous thymine release. *Tetrahedron Lett.*, **1989**, *30*, 4263-4266.
- (66) Kappen, L. S.; Goldberg, I. H., Nitroaromatic Radiation Sensitizers Substitute for Oxygen in Neocarzinostatin-Induced DNA Damage. *Proc. Natl. Acad. Sci. USA*, **1984**, *81*, 3312-3316.
- (67) Chin, D.-H.; Kappen, L. S.; Goldberg, I. H., 3'-formyl Phosphate-Ended DNA: High-Energy Intermediate in Antibiotic-Induced DNA Sugar Damage. *Proc. Natl. Acad. Sci. USA*, **1987**, *84*, 7070-7074.
- (68) Jagannadham, V.; Steenken, S., One-electron reduction of nitrobenzenes by .alpha.-hydroxyalkyl radicals via addition/elimination. An example of an organic inner-sphere electron-transfer reaction. *J. Am. Chem. Soc.*, **1984**, *106*, 6542-6551.
- (69) Steenken, S.; Jagannadham, V., Reaction of 6-yl radicals of uracil, thymine, and cytosine and their nucleosides and nucleotides with nitrobenzenes via addition to give nitroxide radicals. Hydroxide ion-catalyzed nitroxide heterolysis. *J. Am. Chem. Soc.*, **1985**, *107*, 6818-6826.
- (70) De Mico, A.; Margarita, R.; Parlanti, L.; Vescovi, A.; Piancatelli, G., A Versatile and Highly Selective Hypervalent Iodine (III)/2,2,6,6-Tetramethyl-1-piperidinyloxyl-Mediated Oxidation of Alcohols to Carbonyl Compounds. *J. Org. Chem.*, **1997**, *62*, 6974-6977.
- (71) Ando, W., *Organic Peroxides*; Wiley: New York, **1992**, pp 425-478.
- (72) Corey, E. J.; Snider, B. B., Total synthesis of (+)-fumagillin. *J. Am. Chem. Soc.*, **1972**, *94*, 2549-2550.
- (73) Zavitsas, A. A., Energies of Activation. The Paradigm of Hydrogen Abstractions by Radicals. *J. Am. Chem. Soc.*, **1995**, *117*, 10645-10654.
- (74) Engstrom, J. P.; Greene, F. D., Stereochemistry of free-radical recombination reactions. Cage effect in decomposition of (S)(+)-tert-butyl 2-phenylperpropionate. *J. Org. Chem.*, **1972**, *37*, 968-972.
- (75) Pryor, W. A.; Hendrickson, W. H., Reaction of nucleophiles with electron acceptors by SN₂ or electron transfer (ET) mechanisms: tert-butyl peroxybenzoate/dimethyl sulfide and benzoyl peroxide/N,N-dimethylaniline systems. *J. Am. Chem. Soc.*, **1983**, *105*, 7114-7122.
- (76) Kim, S. S.; Tuchkin, A.; Kim, C. S., Induced Thermolysis of tert-Butyl Phenylperacetates by Thiophenol: Simultaneous Occurrence of Homolysis and Single Electron Transfer. *J. Org. Chem.*, **2001**, *66*, 7738-7740.
- (77) Emanuel, C. J.; Newcomb, M.; Ferreri, C.; Chatgililoglu, C., Kinetics of 2'-Deoxyuridin-1'-yl Radical Reactions. *J. Am. Chem. Soc.*, **1999**, *121*, 2927-2928.
- (78) Navacchia, M. L.; Manetto, A.; Montecvecchi, P. C.; Chatgililoglu, C., Radical Cyclization Approach to Cyclonucleosides. *Eur. J. Org. Chem.*, **2005**, 4640-4648.
- (79) Romieu, A.; Gasparutto, D.; Cadet, J., Synthesis and Characterization of Oligodeoxynucleotides Containing the two 5R and 5S Diastereomers of (5S,6S)-5,6-cyclo-5,6-dihydrothymidine; Radiation-induced Tandem Lesions of Thymidine. *J. Chem. Soc., Perkin Trans. 1*, **1999**, 1257-1264.

- (80) Romieu, A.; Gasparutto, D.; Cadet, J., Synthesis and Characterization of Oligonucleotides Containing 5',8-Cyclopurine 2'-Deoxyribonucleosides: (5'R)-5',8-Cyclo-2'-deoxyadenosine, (5'S)-5',8-Cyclo-2'-deoxyguanosine, and (5'R)-5',8-Cyclo-2'-deoxyguanosine. *Chem. Res. Toxicol.*, **1999**, *12*, 412-421.
- (81) Romieu, A.; Gasparutto, D.; Molko, D.; Cadet, J., Site-Specific Introduction of (5'S)-5',8-Cyclo-2'-deoxyadenosine into oligodeoxyribonucleotides. *J. Org. Chem.*, **1998**, *63*, 5245-5249.
- (82) Muller, E.; Gasparutto, D.; Cadet, J., Chemical Synthesis and Biochemical Properties of Oligonucleotides that Contain the (5primeS,5S,6S)-5prime,6-Cyclo-5-hydroxy-5,6-dihydro-2prime-deoxyuridine DNA Lesion. *ChemBioChem*, **2002**, *3*, 534-542.
- (83) Muller, E.; Gasparutto, D.; Jaquinod, M.; Romieu, A.; Cadet, J., Chemical and Biochemical Properties of Oligonucleotides that Contain (5'S,6S)-Cyclo-5,6-dihydro-2'-deoxyuridine and (5'S,6S)-Cyclo-5,6-dihydrothymidine, Two Main Radiation-Induced Degradation Products of Pyrimidine 2'-Deoxyribonucleosides. *Tetrahedron*, **2000**, *56*, 8689-8701.
- (84) Kuraoka, I.; Bender, C.; Romieu, A.; Cadet, J.; Wood, R. D.; Lindahl, T., Removal of oxygen free-radical-induced 5',8-purine cyclodeoxynucleosides from DNA by the nucleotide excision-repair pathway in human cells. *Proc. Natl. Acad. Sci. USA*, **2000**, *97*, 3832-3837.
- (85) Jaruga, P.; Theruvathu, J.; Dizdaroglu, M.; Brooks, P. J., Complete release of (5'S)-8,5'-cyclo-2'-deoxyadenosine from dinucleotides, oligodeoxynucleotides and DNA, and direct comparison of its levels in cellular DNA with other oxidatively induced DNA lesions. *Nucl. Acids Res.*, **2004**, *32*, e87-.
- (86) Chatgililoglu, C., *Organosilanes in radical chemistry*; Wiley: Chichester, **2004**,
- (87) Chatgililoglu, C.; In *Radicals in Organic Synthesis*; Renaud, P., Sibi, M. P., Eds.; Wiley-VCH: Weinheim, **2001**; Vol. 1; pp 28-49.
- (88) Griller, D.; Ingold, K. U., Free-radical clocks. *Acc. Chem. Res.*, **1980**, *13*, 317-323.
- (89) Newcomb, M., Competition Methods and Scales for Alkyl Radical Reaction Kinetics. *Tetrahedron*, **1993**, *49*, 1151-1176.
- (90) Angeloff, A.; Dubey, I.; Pratviel, G.; Bernadou, J.; Meunier, B., Characterization of a 5'-Aldehyde Terminus Resulting from the Oxidative Attack at C5' of a 2-Deoxyribose on DNA. *Chem. Res. Toxicol.*, **2001**, *14*, 1413-1420.
- (91) Brook, M. A.; Balduzzi, S.; Mohamed, M.; Gottardo, C., The photolytic and hydrolytic lability of silyl (Si(SiMe₃)₃) ethers, an alcohol protecting group. *Tetrahedron*, **1999**, *55*, 10027-10040.
- (92) Chatgililoglu, C.; Ballestri, M.; Vecchi, D.; Curran, D. P., Synthesis of 2-functionalized allyl tris(trimethylsilyl)silanes. *Tetrahedron Lett.*, **1996**, *37*, 6383-6386.
- (93) Chatgililoglu, C., The Tris(trimethylsilyl)silane/Thiol Reducing System: A Tool for Measuring Rate Constants for Reactions of Carbon-Centered Radicals with Thiols. *Helv. Chim. Acta*, **2006**, *89*, 2387-2398.
- (94) Roberts, B. P., Polarity-reversal catalysis of hydrogen-atom abstraction reactions: concepts and applications in organic chemistry. *Chem. Soc. Rev.*, **1999**, *28*, 25-35.

- (95) Richard, L. H., Kinetics and mechanism of the trialkylboron-catalyzed polymerization of methyl methacrylate in the presence of oxygen. *Journal of Polymer Science Part A: General Papers*, **1964**, *2*, 4215-4230.
- (96) Tronche, C.; Martinez, F. N.; Horner, J. H.; Newcomb, M.; Senn, M.; Giese, B., Polar substituent and solvent effects on the kinetics of radical reactions with thiols. *Tetrahedron Lett.*, **1996**, *37*, 5845-5848.
- (97) Newcomb, M.; Choi, S. Y.; Horner, J. H., Adjusting the Top End of the Alkyl Radical Kinetic Scale. Laser Flash Photolysis Calibrations of Fast Radical Clocks and Rate Constants for Reactions of Benzeneselenol. *J. Org. Chem.*, **1999**, *64*, 1225-1231.
- (98) For 5-*exo-trig* radical cyclizations in uracil derivatives, see: Fenick, D. J.; Falvey, D. E., Free Radical Rearrangements in Uracil Derivatives. *J. Org. Chem.*, **1994**, *59*, 4791-4799.
- (99) Greenberg, M. M.; Barvian, M. R.; Cook, G. P.; Goodman, B. K.; Matray, T. J.; Tronche, C.; Venkatesan, H., DNA damage induced via 5,6-dihydrothymid-5-yl in single-stranded oligonucleotides. *J. Am. Chem. Soc.*, **1997**, *119*, 1828-1839.
- (100) Meggers, E.; Michel-Beyerle, M. E.; Giese, B., Sequence dependent long range hole transport in DNA. *J. Am. Chem. Soc.*, **1998**, *120*, 12950-12955.
- (101) Montevecchi, P. C.; Manetto, A.; Navacchia, M. L.; Chatgililoglu, C., Thermal decomposition of the tert-butyl perester of thymidine-5'-carboxylic acid. Formation and fate of the pseudo-C4' radical. *Tetrahedron*, **2004**, *60*, 4303-4308.
- (102) Chen, Y.; Wang, M. S.; Mao, C. D., An autonomous DNA nanomotor powered by a DNA enzyme. *Angew. Chem.-Int. Ed.*, **2004**, *43*, 3554-3557.
- (103) Thymidine: Dess Martin oxidation to the Aldehyde Tronchet, J. M. J.; Kovacs, I.; Dilda, P.; Seman, M.; Andrei, G.; Snoeck, R.; De Clereq, E.; Balzarini, J., Synthesis and anti-HIV activity of thymidine analogues bearing a 4'-cyanovinyl group and some derivatives thereof. *Nucleosides Nucleotides Nucleic Acids*, **2001**, *20*, 1927-1939. *Nucleosides Nucleotides & Nucleic Acids*.
- (104) Chatgililoglu, C.; Crich, D.; Komatsu, M.; Ryu, I., Chemistry of Acyl Radicals. *Chem. Rev.*, **1999**, *99*, 1991-2070.
- (105) Cecchini, S.; Masson, C.; La Madeleine, C.; Huels, M. A.; Sanche, L.; Wagner, J. R.; Hunting, D. J., Interstrand Cross-Link Induction by UV Radiation in Bromodeoxyuridine-Substituted DNA: Dependence on DNA Conformation. *Biochemistry*, **2005**, *44*, 16957-16966.
- (106) Galanski, M.; Baumgartner, C.; Meelich, K.; Arion, V. B.; Fremuth, M.; Jakupec, M. A.; Schluga, P.; Hartinger, C. G.; Keyserlingk, N. G. v.; Keppler, B. K., Synthesis, Crystal Structure and pH Dependent Cytotoxicity of (SP-4-2)-bis(2-aminoethanolato-κ2N,O)platinum(II) – a Representative of Novel pH Sensitive Anticancer Platinum Complexes. *Inorg. Chim. Acta*, **2004**, *357*, 3237-3244.
- (107) Eley, D. D.; Spivey, D. I., Nucleic Acid in the Dry State. *Trans. Faraday Soc.*, **1962**, *58*, 411-415.
- (108) Murphy, C. J.; Arkin, M. R.; Jenkins, Y.; Ghatlia, N. D.; Bossmann, S. H.; Turro, N. J.; Barton, J. K., Long-range photoinduced electron transfer through a DNA helix. *Science*, **1993**, *262*, 1025-1029.

- (109) Arkin, M. R.; Stemp, E. D. A.; Holmlin, R. E.; Barton, J. K.; Hörmann, A.; Olson, E. J. C.; Barbara, P. F., Rates of DNA-mediated electron transfer between metallointercalators. *Science*, **1996**, *273*, 475-480.
- (110) Hess, S.; Götz, M.; Davis, W. B.; Michel-Beyerle, M.-E., On the apparently anomalous distance dependence of charge transfer rates in 9-amino-6-chloro-2-methoxyacridine-modified DNA. *J. Am. Chem. Soc.*, **2001**, *123*, 10046-10055.
- (111) Giese, B., Long distance charge transport through DNA: quantification and extension of the hopping model. *Chem. Phys. Chem.*, **2000**, *1*, 195-198.
- (112) Bixon, M.; Jortner, J., Charge transport in DNA via thermally induced hopping. *J. Am. Chem. Soc.*, **2001**, *123*, 12556-12567.
- (113) Jortner, J.; Bixon, M.; Langenbacher, T.; Michel-Beyerle, M. E., Charge transfer and transport in DNA. *Proc. Natl. Acad. Sci. U S A*, **1998**, *95*, 12759-12765.
- (114) Pouget, J. P.; Douki, T.; Richard, M. J.; Cadet, J., DNA damage induced in cells by gamma and UVA radiation as measured by HPLC/GC-MS and HPLC-EC and comet assay. *Chem. Res. Toxicol.*, **2000**, *13*, 541-549. *Chem. Res. Toxicol.*
- (115) Seidel, C. A. M.; Schulz, A.; Sauer, M. H. M., Nucleobase-specific quenching of fluorescent dyes. 1. Nucleobase One-electron redox potentials and their correlation with static and dynamic quenching efficiencies. *J. Phys. Chem.*, **1996**, *100*, 5541-5553.
- (116) Steenken, S.; Jovanovic, S. V., How easily oxidizable is DNA? One-electron reduction potentials of adenosine and guanosine radicals in aqueous solution. *J. Am. Chem. Soc.*, **1997**, *119*, 617-618.
- (117) Melvin, T.; Botchway, S.; Parker, A. W.; O'Neill, P., Migration of Photoinduced oxidative damage in Models for DNA. *Chem. Comm.*, **1995**, 653-654.
- (118) Debije, M. G.; Milano, M. T.; Bernhard, W. A., DNA responds to ionizing radiation as an insulator, not as a "molecular wire". *Angew. Chem. Int. Ed.*, **1999**, *38*, 2752-2755.
- (119) Holmlin, R. E.; Dandlicker, P. J.; Barton, J. K., Charge transfer through the DNA base stack. *Angew. Chem. Int. Ed.*, **1997**, *36*, 2715-2730. *Angew. Chem. Int. Ed. Engl.* **1997**, *36*, 2715-2730.
- (120) Giese, B., Long-distance charge transport in DNA: The hopping mechanism. *Acc. Chem. Res.*, **2000**, *33*, 631-636.
- (121) Lewis, F. D.; Letsinger, R. L.; Wasielewski, M. R., Dynamics of photoinduced charge transfer and hole transport in synthetic DNA hairpins. *Acc. Chem. Res.*, **2001**, *34*, 159-170.
- (122) Schuster, G. B., Long-range charge transport in DNA: Transient structural distortions control the distance dependence. *Acc. Chem. Res.*, **2000**, *33*, 253-260.
- (123) Giese, B.; Amaudrut, J.; Köhler, A.-K.; Spormann, M.; Wessely, S., Direct observation of hole transfer through DNA by hopping between adenine bases and by tunneling. *Nature*, **2001**, *412*, 318-320.
- (124) Nadeau, J. G.; Crothers, D. M., Structural Basis for DNA Bending. *Proc. Natl. Acad. Sci. USA*, **1989**, *86*, 2622-2626.

- (125) Marcus, R. A.; Eyring, H., Chemical and electrochemical electron-transfer theory. *Ann. Rev. Phys. Chem.*, **1964**, *15*, 155-96.
- (126) Kestner, N. R.; Logan, J.; Jortner, J., Thermal electron transfer reactions in polar solvents. *J. Phys. Chem.*, **1974**, *78*, 2148-66.
- (127) Ulstrup, J.; Jortner, J., Effect of intramolecular quantum modes on free energy relations for electron transfer reactions. *J. Chem. Phys.*, **1975**, *63*, 4358-68.
- (128) Jortner, J., Temperature dependent activation energy for electron transfer between biological molecules. *J. Chem. Phys.*, **1976**, *64*, 4860-7.
- (129) Efrima, S.; Bixon, M., Vibrational effects in outer-sphere electron-transfer reactions in polar media. *Chem. Phys.*, **1976**, *13*, 447-60.
- (130) Newton, M. D.; Sutin, N., Electron transfer reactions in condensed phases. *Ann. Rev. Phys. Chem.*, **1984**, *35*, 437-80.
- (131) Jortner, J.; Bixon, M.; Langenbacher, T.; Michel-Beyerle, M. E., Charge transfer and transport in DNA. *Proceedings of the National Academy of Sciences of the United States of America*, **1998**, *95*, 12759-12765.
- (132) Marcus, R. A.; Sutin, N., Electron transfers in chemistry and biology. *Biochim. Biophys. Acta (BBA) - Reviews on Bioenergetics*, **1985**, *811*, 265-322.
- (133) Bixon, M.; Giese, B.; Wessely, S.; Langenbacher, T.; Michel-Beyerle, M. E.; Jortner, J., Long-range charge hopping in DNA. *Proc. Natl. Acad. Sci. USA*, **1999**, *96*, 11713-11716.
- (134) Schuster, G. B.; Landman, U., The mechanism of long-distance radical cation transport in duplex DNA: Ion-gated hopping of polaron-like distortions. *Top. Curr. Chem.*, **2004**, *236*, 139-161.
- (135) O'Neill, M. A.; Barton, J. K., DNA-mediated charge transport chemistry and biology. *Top. Curr. Chem.*, **2004**, *236*, 67-115.
- (136) Lewis, F. D.; Wasielewski, M. R., Dynamics and equilibrium for single step hole transport processes in duplex DNA. *Top. Curr. Chem.*, **2004**, *236*, 45-65.
- (137) Giese, B., Hole injection and hole transfer through DNA: The hopping mechanism. *Top. Curr. Chem.*, **2004**, *236*, 27-44.
- (138) Lewis, F. D.; Liu, X.; Liu, J.; Miller, S. E.; Hayes, R. T.; Wasielewski, M. R., Direct measurement of hole transport dynamics in DNA. *Nature*, **2000**, *406*, 51-53.
- (139) Pascaly, M.; Yoo, J.; Barton, J. K., DNA mediated charge transport: Characterization of a DNA radical localized at an artificial nucleic acid base. *J. Am. Chem. Soc.*, **2002**, *124*, 9083-9092. *J. Am. Chem. Soc.*
- (140) Takada, T.; Kawai, K.; Cai, X.; Sugimoto, A.; Fujitsuka, M.; Majima, T., Charge Separation in DNA via Consecutive Adenine Hopping. *J. Am. Chem. Soc.*, **2004**, *126*, 1125-1129.
- (141) Kendrick, T.; Giese, B., Charge transfer through DNA triggered by site selective charge injection into adenine. *Chem. Comm.*, **2002**, 2016-2017.
- (142) Kendrick, T.; Giese, B., Charge transfer through DNA triggered by site selective charge injection into adenine. *Chem. Commun.*, **2002**, 2016-2017.

- (143) Lewis, F. D.; Zhu, H.; Daublain, P.; Cohen, B.; Wasielewski, M. R., Hole Mobility in DNA A Tracts. *Angew. Chem. Int. Ed.*, **2006**, *45*, 7982-7985.
- (144) Steenken, S., Electron transfer in DNA? competition by ultra-fast proton transfer. *Biol. Chem.*, **1997**, *378*, 1293-1297.
- (145) Steenken, S., Electron-transfer-induced acidity/basicity and reactivity changes of purine and pyrimidine bases. Consequences of redox processes for DNA base pairs. *Free Rad. Res. Comms.*, **1992**, *16*, 349-79.
- (146) Lewis, F. D.; Miller, S. E.; Hayes, R. T.; Wasielewski, M. R., Dynamics of electron injection in DNA hairpins. *J. Am. Chem. Soc.*, **2002**, *124*, 11280-11281.
- (147) Barnett, R. N.; Cleveland, C. L.; Joy, A.; Landman, U.; Schuster, G. B., Charge migration in DNA: Ion-gated transport. *Science*, **2001**, *294*, 567-570.
- (148) Lewis, F. D.; Wu, T.; Zhang, Y.; Letsinger, R. L.; Greenfield, S. R.; Wasielewski, M. R., Distance-dependent electron transfer in DNA hairpins. *Science*, **1997**, *277*, 673-676.
- (149) Dotse, A. K.; Boone, E. K.; Schuster, G. B., Remote *cis-syn* thymine [2+2] dimers are not repaired by radical cations migrating in duplex DNA. *J. Am. Chem. Soc.*, **2000**, *122*, 6825-6833.
- (150) Santhosh, U.; Schuster, G. B., Long-Range Charge Transport in Duplex DNA: Anthraquinone Sensitization Results Are Independent of Terminal Ionic Distribution. *J. Am. Chem. Soc.*, **2002**, *124*, 10986-10987.
- (151) Vivic, D. A.; Odom, D. T.; Nunez, M. E.; Gianolio, D. A.; McLaughlin, L. W.; Barton, J. K., Oxidative repair of a thymine dimer in DNA from a distance by a covalently linked organic intercalator. *J. Am. Chem. Soc.*, **2000**, *122*, 8603-8611.
- (152) Williams, T. T.; Barton, J. K., The effect of varied ion distributions on long-range DNA charge transport. *J. Am. Chem. Soc.*, **2002**, *124*, 1840-1841. *J. Am. Chem. Soc.*
- (153) Burrows, C. J.; Muller, J. G., Oxidative nucleobase modifications leading to strand breaks. *Chemical Reviews*, **1998**, *98*, 1109-1151.
- (154) Friedberg, E. C.; Walker, G. C.; Siede, W., *DNA repair and mutagenesis*; ASM Press: Washington, D.C., **1995**,
- (155) Nunez, M.; Hall, D. B.; Barton, J. K., Long-range oxidative damage to DNA: effects of distance and sequence. *Chem. Biol.*, **1999**, *6*, 85-97.
- (156) Lewis, F. D.; Liu, X.; Wu, Y.; Miller, S. E.; Wasielewski, M. R.; Letsinger, R. L.; Sanishvili, R.; Joachimiak, A.; Tereshko, V.; Egli, M., Structure and photoinduced electron transfer in exceptionally stable synthetic DNA hairpins with stilbenediethyl linkers. *J. Am. Chem. Soc.*, **1999**, *121*, 9905-9906.
- (157) Giese, B.; Wessely, S.; Sporman, M.; Lindemann, U.; Meggers, E.; Michel-Beyerle, M. E., On the mechanism of long-range electron transfer through DNA. *Angew. Chem. Int. Ed.*, **1999**, *38*, 996-998. *Angew. Chem. Int. Ed. Engl.* **1999**, *38*, 996-998.
- (158) Cai, L.; Tabata, H.; Kawai, T., Self-assembled DNA networks and their electrical conductivity. *Appl. Phys. Lett.*, **2000**, *77*, 3105-3106.

- (159) Yoo, K.-H.-.; Ha, D. H.; Lee, J.-O.; Park, J. W.; Kim, J.; Kim, J. J.; Lee, H.-Y.; Kawai, T.; Choi, H. Y., Electrical conduction through poly(dA)-poly(dT) and poly(dG)-poly(dC) DNA molecules. *Phys. Rev. Lett.*, **2001**, *87*, 1981021-1981024.
- (160) Fink, H.-W.; Schönenberger, C., Electrical conduction through DNA molecules. *Nature*, **1999**, *398*, 407-410.
- (161) Porath, D.; Bezryadin, A.; De Vries, S.; Dekker, C., Direct measurement of electrical transport through DNA molecules. *Nature*, **2000**, *403*, 635-638.
- (162) Storhoff, J. J.; Mirkin, C. A., Programmed Materials Synthesis with DNA. *Chem. Rev.*, **1999**, *99*, 1849-1862.
- (163) Seeman, N. C. *Nature*, **2003**, *421*, 427-431.
- (164) Seeman, N. C., Nanostrukturen und Topologien von Nucleinsäuren. *Angew. Chem. Int. Ed.*, **1998**, *37*, 3220-3238. *Angewandte Chemie* 110 3408-3428.
- (165) Yan, H.; Zhang, X.; Shen, Z.; Seeman, N. C., A robust DNA mechanical device controlled by hybridization topology. *Nature*, **2002**, *415*, 62-65.
- (166) Braun, E.; Eichen, Y.; Sivan, U.; Ben-Yoseph, G., DNA templated assembly and electrode attachment of a conductive silver wire. *Nature*, **1998**, *391*, 775-778.
- (167) Keren, K.; Berman, R. S.; Buchstab, E.; Sivan, U.; Braun, E., DNA-Templated Carbon Nanotube Field-Effect Transistor. *Science*, **2003**, *21*, 1380-1382.
- (168) Fahlman, R. P.; Sen, D., DNA Conformational Switches as Sensitive Electronic Sensors of Analytes. *J. Am. Chem. Soc.*, **2002**, *124*, 4610-4616.
- (169) Rothmund, P. W. K., Folding DNA to create nanoscale shapes and patterns. **2006**, *440*, 297-302. *Nature*.
- (170) Wagenknecht, H.-A., Reductive electrontransfer and transport of excess electrons in DNA. *Angew. Chem.*, **2003**, *115*, 2558-2565. *Angew. Chem. Int. Ed.* **2003**, *42*, 2454-2460.
- (171) Todo, T.; Takemori, H.; Ryo, H.; Ihara, M.; Matsunaga, T.; Nikaido, O.; Sato, K.; Nomura, T., A new photoreactivating enzyme that specifically repairs ultraviolet light-induced (6-4)photoproducts. *Nature*, **1993**, *361*, 371-374.
- (172) Sancar, A., Structure and function of DNA photolyase and cryptochrome blue-light photoreceptors. *Chem. Rev.*, **2003**, *103*, 2203-2238.
- (173) Kim, S.-T.; Malhotra, K.; Smith, C. A.; Taylor, J.-S.; Sancar, A., Characterization of a (6-4) photoproduct DNA photolyase. *Journal of Biological Chemistry*, **1994**, *269*, 8535-8540.
- (174) Taylor, J.-S., Unraveling the molecular pathway from sunlight to skin cancer. *Acc. Chem. Res.*, **1994**, *27*, 76-82.
- (175) Carell, T.; Burgdorf, L. T.; Kundu, L.; Cichon, M., The mechanism of action of DNA photolyases. *Curr. Opin. Chem. Biol.*, **2001**, *5*, 491-498.
- (176) Okamoto, A.; Tanaka, K.; Saito, I. *J. Am. Chem. Soc.*, **2003**, *125*, 5066-5071.

- (177) Niemeyer, C. M., Nanopartikel, Proteine und Nucleinsäuren: Die Biotechnology gegenet den Materialwissenschaften. *Angew. Chem. Int. Ed.*, **2001**, *40*, 4128-4158. *Angew. Chem.* 113 4254-4287.
- (178) Sancar, A., Structure and Function of DNA Photolyase. *Biochemistry*, **1994**, *33*, 2-9.
- (179) Mees, A.; Klar, T.; Gnau, P.; Hennecke, U.; Eker, A. P. M.; Carell, T.; Essen, L. O., Crystal structure of a photolyase bound to a CPD-like DNA lesion after in situ repair. *Science*, **2004**, *306*, 1789-1793.
- (180) Heelis, P. F.; Hartman, R. F.; Rose, S. D., Photoenzymatic Repair of UV-Damaged DNA: A Chemist's Perspective. *Journal of the Chemical Society, Chemical Reviews*, **1995**, 289-297.
- (181) Carell, T., Sunlight-Damaged DNA Repaired with Sunlight. *Angew. Chem. Int. Ed.*, **1995**, *34*, 2491-2493. *Angew. Chem. Int. Ed. Engl.* **1995**, *34*, 2491-2494.
- (182) Begley, T. P., Photoenzymes: A Novel Class of Biological Catalysts. *Acc. Chem. Res.*, **1994**, *27*, 394-401.
- (183) Song, Q. H.; Xiaoming, H.; Zhixiu, X.; Xiang, Z.; Qingxiang, G. *Bioorganic Chemistry*, **2003**, *31*, 357-366.
- (184) Jorns, M. S., Photosensitized Cleavage of Thymine Dimer with Reduced Flavin: A Model for Enzymic Photorepair of DNA. *J. Am. Chem. Soc.*, **1987**, *109*, 3133-3136.
- (185) Epple, R.; Wallenborn, E.-U.; Carell, T., Investigation of Flavin-Containing DNA-Repair Model Compounds. *J. Am. Chem. Soc.*, **1997**, *119*, 7440-7451.
- (186) Epple, R.; Carell, T., Charakterisierung des Energietransfers in DNA-Photolyasen von Typ II mit Flavin und Desazaflavin enthaltenden Modellverbindungen. *Angew. Chem.*, **1998**, *110*, 986-989.
- (187) Epple, R.; Carell, T., Efficient Light-dependent DNA repair requires a large cofactor separation. *J. Am. Chem. Soc.*, **1999**, *121*, 7318-7329.
- (188) Cichon, M. K.; Arnold, S.; Carell, T., A (6-4) Photolyase Model: Repair of DNA (6-4) Lesions requires a reduced and deprotonated flavin. *Angew. Chem. Int. Ed.*, **2002**, *51*, 767-770.
- (189) Zhang, J.; Song, S.; Zhang, L.; Wang, L.; Wu, H.; Pan, D.; Fan, C., Sequence-Specific Detection of Femtomolar DNA via a Chronocoulometric DNA Sensor (CDS): Effects of Nanoparticle-Mediated Amplification and Nanoscale Control of DNA Assembly at Electrodes. *J. Am. Chem. Soc.*, **2006**, *128*, 8575-8580.
- (190) Stafforst, T.; Diederichsen, U., (6-4)-Photolyase activity requires a charge shift reaction. *Chem. Comm.*, **2005**, 3430-3432.
- (191) Yeh, S.-R.; Falvey, D. E., Model Studies of DNA Photorepair: Energetic Requirements for the Radical Anion Mechanism Determined by Fluorescence Quenching. *J. Am. Chem. Soc.*, **1992**, *114*, 7313-7314.
- (192) Scannel, M. P.; Fenick, D. J.; Yeh, S.-R.; Falvey, D. E., Model Studies of DNA Photorepair: Reduction Potentials of Thymine and Cytosine Cyclobutane Dimers Measured by Fluorescence Quenching. *J. Am. Chem. Soc.*, **1997**, *119*, 1971-1977.

- (193) Scannel, M. P.; Prakash, G.; Falvey, D. E., Photoinduced electron transfer to pyrimidines and 5,6-dihydropyrimidine derivatives: Reduction potentials determined by fluorescence quenching kinetics. *Journal of Physical Chemistry A*, **1997**, *101*, 4332-4337.
- (194) Steenken, S.; Telo, J. P.; Novais, H. M.; Candeias, L. P., One-electron reduction potentials of pyrimidine bases, nucleosides, and nucleotides in aqueous solution. Consequences for DNA redox chemistry. *J. Am. Chem. Soc.*, **1992**, *114*, 4701-4709.
- (195) Richardson, N. A.; Gu, J.; Wang, S.; Xie, Y.; Schaefer III, H. F., DNA Nucleosides and Their Radical Anions: Molecular Structures and Electron Affinities. *J. Am. Chem. Soc.*, **2004**, *126*, 4404-4411.
- (196) Li, X.; Cai, Z.; Sevilla, M. D., Investigation of Proton Transfer within DNA Base Pair Anion and Cation Radicals by Density Functional Theory (DFT). *Journal of Physical Chemistry B*, **2001**, *105*, 10115-10123.
- (197) Razskazovskiy, Y.; Roginskaya, M.; Jacobs, A.; Sevilla, M. D., Reductively activated cleavage of DNA mediated by o,o'-Diphenylenehalonium compounds. *Radiation Research*, **2000**, *154*, 319-325.
- (198) Amann, N.; Pandurski, E.; Fiebig, T.; Wagenknecht, H.-A., Electron Injection into DNA: Synthesis and Spectroscopic Properties of Pyrenyl-modified Oligonucleotides. *Chem. Eur. J.*, **2002**, *8*, 4877-4883.
- (199) Fiebig, T.; Wan, C.; Zewail, A. H., Femtosecond charge transfer dynamics of a modified DNA base: 2-Aminopurine in complexes with nucleotides. *ChemPhysChem.*, **2002**, *3*, 781-788.
- (200) Carell, T.; von Meltzer, M.; In *Charge Transfer in DNA*; Wagenknecht, H.-A., Ed.; VCH: Weinheim, **2005**.
- (201) Behrens, C.; Carell, T.; In *Top. Curr. Chem.*; Springer Verlag: Heidelberg, **2004**; Vol. 236; pp 187-204.
- (202) Schwögler, A.; Burgdorf, L. T.; Carell, T., Self-repairing DNA based on a reductive electron transfer through the base stack. *Angew. Chem. Int. Ed.*, **2000**, *39*, 3918-3920.
- (203) Behrens, C.; Burgdorf, L. T.; Schwögler, A.; Carell, T., Weak distance dependence of excess electron transfer in DNA. *Angew. Chem. Int. Ed.*, **2002**, *41*, 1763-1766.
- (204) Cai, Z.; Gu, Z.; Sevilla, M. D., Electron spin resonance study of the temperature dependence of electron transfer in DNA: competitive processes of tunneling, protonation at carbon, and hopping. *J. Phys. Chem. B*, **2000**, *104*, 10406-10411.
- (205) Messer, A.; Carpenter, K.; Forzley, K.; Buchanan, J.; Yang, S.; Razskazovskii, Y.; Cai, Z.; Sevilla, M. D., Electron spin resonance study of electron transfer rates in DNA: determination of the tunneling constant β for single-step excess electron transfer. *Journal of Physical Chemistry B*, **2000**, *104*, 1128-1136.
- (206) Bonnet, G.; Krichevsky, O.; Libchaber, A., Kinetics of conformational fluctuations in dna hairpin-loops. *Proc. Natl. Acad. Sci. USA*, **1998**, *95*, 8602-8606.
- (207) Haasnoot, C. A. G.; de Bruin, S. H.; Berendsen, R. G.; Janssen, H. G. J. M.; Binnendijk, T. J. J.; Holbers, C. W.; van der Marel, G. A.; van Boom, J. H., Structure, kinetics and thermodynamics of DNA hairpin fragments in solution. *J. Biomol. Struct. Dyn.*, **1983**, *1*, 115-129.

- (208) Grunwell, J. R.; Glass, J. L.; Lacoste, T. D.; Deniz, A. A.; Chemla, D. S.; Schultz, P. G., Monitoring the conformational fluctuations of DNA hairpins using single-pair fluorescence resonance energy transfer. *J. Am. Chem. Soc.*, **2001**, *123*, 4295-4303.
- (209) Behrens, C.; Carell, T., Excess electron transfer in flavin-capped, thymine dimer-containing DNA hairpins. *Chem. Comm.*, **2003**, 1632-1633.
- (210) Jortner, J.; Bixon, M.; Langenbacher, T.; Michel-Beyerle, M. E., Charge transfer and transport in DNA. *Proc. Natl. Acad. Sci. USA*, **1998**, *95*, 12759-12765.
- (211) Ito, T.; Rokita, S. E., Criteria for Efficient Transport of Excess Electrons in DNA. *Angew. Chem. Int. Ed.*, **2004**, *116*, 1875-1878.
- (212) Haas, C. H.; Kräling, K.; Cichon, M.; Rahe, N.; Carell, T., Excess electron transfer driven DNA does not depend on the transfer direction. *Angew. Chem. Int. Ed.*, **2004**, *14*, 1842-1844.
- (213) *Peptide Nucleic Acids*; Nielsen, P. E.; Egholm, M., Eds.; Horizon Scientific Press: Norfolk, **1999**.
- (214) Cichon, M. K.; Haas, C. H.; Grolle, F.; Mees, A.; Carell, T., Efficient Intrastrand excess electron transfer in PNA:DNA hybrids. *J. Am. Chem. Soc.*, **2002**, *124*, 13984-13985.
- (215) Ito, T.; Rokita, S. E., Reductive Electron Injection into Duplex DNA by Aromatic Amines. *J. Am. Chem. Soc.*, **2004**, *126*, 15552-15559.
- (216) O'Neill, M. A.; Barton, J. K., Effects of strand and directional asymmetry on base-base coupling and charge transfer in double-helical DNA. *Proc. Natl. Acad. Sci. USA*, **2002**, *99*, 16543-16550.
- (217) Breger, S.; Hennecke, U.; Carell, T., Excess electron transfer based repair of a cis-syn thymine dimer in DNA is only weakly sequence dependent. *J. Am. Chem. Soc.*, **2004**, *126*, 1302-1303.
- (218) Wagner, C.; Wagenknecht, H.-A., Reductive Electron Transfer in Phenothiazine-Modified DNA Is Dependent on the Base Sequence. *Chem. Eur. J.*, **2005**, *11*, 1871-1876.
- (219) Ito, T.; Rokita, S. E. *Angew. Chem. Int. Ed.*, **2004**, *116*, 1875.
- (220) Brun, A. M.; Harriman, A., Energy- and Electron-Transfer Processes involving palladium porphyrins bound to DNA. *J. Am. Chem. Soc.*, **1994**, *116*, 10383-10393.
- (221) Breger, S.; von Meltzer, M.; Hennecke, U.; Carell, T., Investigation of the Pathways of Excess Electron Transfer in DNA with Flavin-Donor and Oxetane-Acceptor Modified DNA Hairpins. *Chem. Eur. J.*, **2006**, *12*, 6469-6477.
- (222) Prakash, G.; Falvey, D. E., Model Studies of the (6-4) Photoproduct DNA Photolyase: Synthesis and Photosensitized Splitting of a thymine-5,6-Oxetane. *J. Am. Chem. Soc.*, **1995**, *117*, 11375-11376.
- (223) Joseph, A.; Prakash, G.; Falvey, D. E., Model Studies of the (6-4) Photoproduct Photolyase Enzyme: Laser Flash Photolysis Experiments Confirm Radical Ion Intermediates in the Sensitized Repair of Thymine Oxetane Adducts. *J. Am. Chem. Soc.*, **2000**, *122*, 11219-11225.
- (224) Joseph, A.; Falvey, D. E., Photolysis of thymine oxetane produces triplet excited carbonyl compounds with high efficiency. *J. Am. Chem. Soc.*, **2001**, *123*, 3145-3146.

- (225) Joseph, A.; Falvey, D. E., Photoinduced electron transfer cleavage of oxetane adducts of uracil and cytosine. *Photochem. Photobiol. Sci.*, **2002**, *1*, 632-635.
- (226) Friedel, M.; Cichon, M.; Carell, T., Model compounds for (6-4) photolyases: a comparative flavin induced cleavage study of oxetanes and thietanes. *Org. Biomol. Chem.*, **2005**, *3*, 1937-1941.
- (227) Miranda, M. A.; Izquierdo, M. A., Stepwise cycloreversion of oxetane radical cations with initial C-O bond cleavage. *J. Am. Chem. Soc.*, **2002**, *124*, 6532-6533.
- (228) Miranda, M. A.; Izquierdo, M. A., Chemical and transient spectroscopic evidence for C₂-C₃ cleavage of 2,3-diaryloxetane radical cations. *J. Chem. Soc., Chem. Commun.*, **2003**, 364-365.
- (229) Mozziconacci, O.; Bobrowski, K.; Ferreri, C.; Chatgililoglu, C., Reactions of Hydrogen Atoms with Met-Enkephalin and Related Peptides. *Chem. Eur. J.*, **2007**, *13*, 2029-2033.
- (230) Giese, B.; Carl, B.; Carl, T.; Carell, T.; Behrens, C.; Hennecke, U.; Schiemann, O.; Feresin, E., Excess electron transport through DNA: A single electron repairs more than one UV-induced lesion. *Angew. Chem. Int Ed.*, **2004**, *14*, 1848-1851.
- (231) Wesolowski, S. S.; Leininger, M. L.; Pentchev, P. N.; III, H. F. S., Electron affinities of the DNA and RNA bases. *J. Am. Chem. Soc.*, **2001**, *123*, 4023-4028.
- (232) Schwarz, H. A.; Dodson, R. W. *J. Phys. Chem.*, **1989**, *93*, 409.
- (233) Chatgililoglu, C.; Carell, T. *Not yet published*,
- (234) Kaden, P.; Mayer-Enthart, E.; Trifonov, A.; Fiebing, T.; Wagenknecht, H.-A., Real-Time Spectroscopic and Chemical Probing of Reductive Electron Transfer in DNA. *Angew. Chem. Int Ed.*, **2005**, *44*, 1636-1639.
- (235) Saito, I.; Matsuura, T., Chemical aspects of UV-induced crosslinking of proteins to nucleic acids. Photoreactions with lysine and tryptophan. *Acc. Chem. Res.*, **1985**, *18*, 134-141.
- (236) Sugiyama, H.; Tsutsumi, Y.; Saito, I., Highly sequence-selective photoreaction of 5-bromouracil-containing deoxyhexanucleotides. *J. Am. Chem. Soc.*, **1990**, *112*, 6720-6721.
- (237) Cook, G. P.; Greenberg, M. M., A novel Mechanism for the Formation of Direct Strand Breaks upon Anaerobic Photolysis of Duplex DNA Containing 5-Bromodeoxyuridine. *J. Am. Chem. Soc.*, **1996**, *118*, 10025-10030.
- (238) Graham, D.; Parkinson, J. A.; Brown, T., DNA duplexes stabilized by modified monomer residues: synthesis and stability. *J. Chem. Soc., Perk. Trans. 1*, **1998**, *6*, 1131-1138.
- (239) Simpson, R. T.; Seale, R. L., Characterization of chromatin extensively substituted with 5-bromodeoxyuridine. *Biochemistry*, **1974**, *13*, 4609-4616.
- (240) Yu, H.; Eritja, R.; Bloom, L. B.; Goodman, M. F., Ionization of bromouracil and fluorouracil stimulates base mispairing frequencies with guanine. *J. Biol. Chem.*, **1993**, 15935-15943.
- (241) Sugiyama, H.; Tsutsumi, Y.; Fujimoto, K.; Saito, I., Photoinduced deoxyribose C2' oxidation in DNA. Alkali-dependent cleavage of erythrose-containing sites via a retroaldol reaction. *J. Am. Chem. Soc.*, **1993**, *115*, 4443-4448.

- (242) Chen, T.; Cook, G. P.; Koppisch, A. T.; Greenberg, M. M., Investigation of the Origin of the Sequence Selectivity for the 5-Halo-2'-deoxyuridine Sensitization of DNA to Damage by UV-Irradiation. *J. Am. Chem. Soc.*, **2000**, *122*, 3861-3866.
- (243) Li, X.; Sevilla, M. D.; Sanche, L., DFT Investigation of Dehalogenation of Adenine-Halouracil Base Pairs upon Low-Energy Electron Attachment. *J. Am. Chem. Soc.*, **2003**, *125*, 8916-8920.
- (244) Rivera, E.; Schuler, R. H., Intermediates in the Reduction of 5-Halouracils by e_{aq}^- . *J. Phys. Chem.*, **1983**, *87*, 3966-3971.
- (245) Li, X.; Sanche, L.; Sevilla, M. D., Dehalogenation of 5-Halouracils after Low Energy Electron Attachment: A Density Functional Theory Investigation. *J. Phys. Chem. A*, **2002**, *106*, 11248-11253.
- (246) Liu, J.; Verdine, G. L., Synthesis of photoactive DNA: incorporation of 8-bromo-2'-deoxyadenosine into synthetic oligodeoxynucleotides. *Tetrahedron Lett.*, **1992**, *33*, 4265-4268.
- (247) Kimura, T., Kawai, K., Tojo S., Majima, T., One-Electron Attachment Reaction of B- and Z-DNA Modified by 8-Bromo-2'-deoxyguanosine. *J. Org. Chem*, **2004**, *69*, 1169-1173.
- (248) Chatgililoglu, C.; Caminal, C.; Altieri, A.; Vougioukalakis, G. C.; Mulazzani, Q. G.; Gimisis, T.; Guerra, M., Tautomerism in the Guanyl Radical. *J. Am. Chem. Soc.*, **2006**, *128*, 13796-13805.
- (249) de Campore', M.; De Napoli, L.; Montesarchio, D.; Piccialli, G.; Caminal, C.; Mulazzani, Q. G.; Navacchia, M. L.; Chatgililoglu, C., Excess electron transfer in G-quadruplex. *Chem. Commun.*, **2004**, 1756-1757.
- (250) Schmidt, K. H.; Han, P.; Bartels, D. M., Radiolytic Yields of the Hydrated Electron from Transient Conductivity: Improved Calculation of the Hydrated Electron Diffusion Coefficient and Analysis of Some Diffusion-Limited (e⁻)_{aq} Reaction Rates. *J. Phys. Chem.*, **1995**, *99*, 10530-10539.
- (251) Patterson, L. K.; Bansal, K. M., Pulse Radiolysis Studies of 5-Halouracil in Aqueous Solutions. *J. Phys. Chem.*, **1972**, *76*, 2392-2399.
- (252) Buxton, G. V.; Greenstock, C. L.; Helman, W. P.; Ross, A. B., Critical Review of Rate Constants for Reactions of Hydrated Electrons, Hydrogen Atoms and Hydroxyl Radicals (OH/0) in Aqueous Solution. *J. Phys. Chem. Ref. Data*, **1988**, *17*, 513-886.
- (253) Gaballah, S. T.; Collier, G.; Netzel, T. L., Charge Transfer Excited-State Dynamics in DNA Duplexes Substituted with an Ethynylpyrenyldeoxyuridine Electron Source and a Fluorodeoxyuridine Electron Trap. *J. Phys. Chem. B*, **2005**, *109*, 12175-12181.
- (254) Frier, C.; Mouscadet, J.-F.; Décout, J.-L.; Auclair, C.; Fontecave, M., Flavin-oligonucleotide conjugates: sequence specific photocleavage of DNA. *Journal of Chemical Society, Chemical Communication*, **1998**, 2457-2458.
- (255) Frier, C.; Décout, J.-L.; Fontecave, M., Methods for Preparing New Flavin Derivatives: Synthesis of Flavin-Thymine Nucleotides and Flavin-Oligonucleotide Adducts. *Journal of Organic Chemistry*, **1997**, *62*, 3520.
- (256) Behrens, C.; Ober, M.; Carell, T., Excess electron transfer in flavin-capped DNA-hairpins. *Eur. J. Org. Chem.*, **2002**, 3281-3289.

- (257) Schwögler, A.; Carell, T., Towards catalytically active oligonucleotides: Synthesis and properties of a flavin nucleotide and its incorporation into DNA. *Organic Letters*, **2000**, *2*, 1415-1418.
- (258) Cantor, C. R.; Warshaw, M. M.; Shapiro, H., Oligonucleotide Interactions. III. Circular Dichroism Studies of the Conformation of Deoxyoligonucleotides. *Biopolymers*, **1970**, *9*, 1059-1077.
- (259) Rinker, R. G.; Lynn, S., The formation of the $S_2O_4^-$ free radical in dimethylformamide. *J. Phys. Chem.*, **1968**, *72*, 4706-4707.
- (260) Janzen, E. G., ESR studies of thermal decomposition mechanisms. II. Electron spin resonance study of the SO_2^- formation in the thermal decomposition of sodium dithionite, sodium and potassium metabisulfite, and sodium hydrogen sulfite. *J. Phys. Chem.*, **1972**, *76*, 157-1622.
- (261) Leontiev, A. V.; Rudkevich, D. M., Revisiting Noncovalent SO_2 -Amine Chemistry: An Indicator-Displacement Assay for Colorimetric Detection of SO_2 . *J. Am. Chem. Soc.*, **2005**, *127*, 14126-14127.
- (262) Hara, K.; Sayama, K.; Arakawa, H., UV photoinduced reduction of water to hydrogen in Na_2S , Na_2SO_3 , and $Na_2S_2O_4$ aqueous solutions. *J. Photochem. Photobiol. A: Chemistry*, **1999**, *128*, 27-31.
- (263) Traber, R.; Kramer, H. E. A.; Hemmerich, P., Mechanism of light-induced reduction of biological redox centers by amino acids. A flash photolysis study of flavin photoreduction by EDTA and nitrilotriacetate. *Biochemistry*, **1982**, *21*, 1687-1693.
- (264) Carl, B., Entwicklung einer neuen Methode zur Injektion von Elektronen in DNA (Development of a new method for the electron injection in DNA), *Universität Basel*, **2004**.
- (265) Carl, T., Chemie auf Distanz: Reduktiver Elektronentransport in DNA (Chemistry at Distance: Reductive Electron Transfer in DNA), *Universität Basel*, **2004**.
- (266) Richter, J., Metallization of DNA. *Physica E*, **2003**, *16*, 157-173.
- (267) Porath, D.; Cuniberti, G.; Di Felice, R., Charge Transport in DNA-Based Devices. *Top. Curr. Chem.*, **2004**, *237*, 183-227.
- (268) Braun, E.; Eichen, Y.; Sivan, U.; Ben-Yoseph, G., DNA-templated assembly and electrode attachment of a conducting silver wire. *Nature*, **1998**, *391*, 775-778.
- (269) Burley, G. A.; Gierlich, J.; Mofid, M. R.; Nir, H.; Tal, S.; Eichen, Y.; Carell, T., Directed DNA Metallization. *J. Am. Chem. Soc.*, **2006**, *128*, 1398-1399.
- (270) De Cola, L., Molecular Wires. *Top. Curr. Chem.*, **2005**, *257*, The whole volume.
- (271) Clever, G. H.; Polborn, K.; Carell, T., A Highly DNA-Duplex-Stabilizing Metal-Salen Base Pair. *Angew. Chem. Int. Ed.*, **2005**, *44*, 7204-7208.
- (272) Clever, G. H.; Sötl, Y.; Burks, H.; Spahl, W.; Carell, T., Metal-Salen-Base-Pair Complexes Inside DNA: Complexation Overrides Sequence Information. *Chem. Eur. J.*, **2006**, *12*, 8708-8718.
- (273) Tanaka, K.; Tengeiji, A.; Kato, T.; Toyama, N.; Shionoya, M., A Discrete Self-Assembled Metal Array in Artificial DNA. *Science*, **2003**, *299*, 1212-1213.

- (274) Tanaka, K.; Shionoya, M., Bio-inspired programmable self-assembly on DNA templates. *Chemistry Letters*, **2006**, *35*, 694-699.
- (275) Tanaka, K.; Shionoya, M., Synthesis of a Novel Nucleoside for Alternative DNA Base Pairing through Metal Complexation. *J. Org. Chem.*, **1999**, *64*, 5002-5003.
- (276) Meggers, E.; Holland, P. L.; Tolman, W. B.; Romesberg, F. E.; Schultz, P. G., A Novel Copper-Mediated DNA Base Pair. *J. Am. Chem. Soc.*, **2000**, *122*, 10714-10715.
- (277) Clever, G. H.; Carell, T., Controlled Stacking of 10 Transition-Metal Ions Inside a DNA Duplex. *Angew. Chem. Int. Ed.*, **2006**, in press.
- (278) Tanaka, K.; Clever, G. H.; Takezawa, Y.; Yamada, Y.; Kaul, C.; Shionoya, M.; Carell, T., Programmable self-assembly of metal ions inside artificial DNA duplexes. *Nature Nanotech.*, **2006**, *1*, 190-194.
- (279) Katz, S., The Reversible Reaction of Sodium Thymonucleate and Mercuric Chloride. *J. Am. Chem. Soc.*, **1952**, *74*, 2238-2245.
- (280) Kosturko, L. D.; Folzer, C.; Stewart, R. F., Crystal and molecular structure of a 2:1 complex of 1-methylthymine-mercury(II). *Biochemistry*, **1974**, *13*, 3949-3952.
- (281) R. K. Saiki, S. S., F. Faloona, K. B. Mullis, G. T. Horn, H. A. Erlich, N. Arnheim, Enzymatic amplification of beta-globin genomic sequences and restriction site analysis for diagnosis of sickle cell anemia. *Science*, **1985**, *230*, 1350-1354.
- (282) Taton, T. A.; Mirkin, C. A.; Letsinger, R. L., Scanometric DNA Array Detection with Nanoparticle Probes. *Science*, **2000**, *289*, 1757-1760.
- (283) Park, S.-J.; Taton, T. A.; Mirkin, C. A., Array-Based Electrical Detection of DNA with Nanoparticle Probes. *Science*, **2002**, *295*, 1503-1506.
- (284) Zhao, X.; Tapecc-Dytioco, R.; Tan, W., Ultrasensitive DNA Detection Using Highly Fluorescent Bioconjugated Nanoparticles. *J. Am. Chem. Soc.*, **2003**, *125*, 11474-11475.
- (285) Nam, J. M.; Stoeva, S. I.; Mirkin, C. A., Bio-Bar-Code-Based DNA Detection with PCR-like Sensitivity. *J. Am. Chem. Soc.*, **2004**, *126*, 5932-5933.
- (286) Rosi, N. L.; Mirkin, C. A., Nanostructures in Biodiagnostics. *Chem. Rev.*, **2005**, *105*, 1547-1562.
- (287) Baker, E. S.; Hong, J. W.; Gaylord, B. S.; Bazan, G. C.; Bowers, M. T., PNA/dsDNA Complexes: Site Specific Binding and dsDNA Biosensor Applications. *J. Am. Chem. Soc.*, **2006**, *128*, 8484-8492.
- (288) Hammond, D. M.; Manetto, A.; Gierlich, J.; Azov, V. A.; Gramlich, P. M. A.; Burley, G. A.; Carell, T., DNA Photography: An Ultra-Sensitive DNA Detection Method Based on the Chemistry of Photography. *Angew. Chem. Int. Ed.*, Submitted.
- (289) Tani, T., *Photographic Sensitivity, Theory and Mechanisms*; OUP, **1995**,
- (290) Vogel, H. M. *Berichte*, **1873**, *6*, 1302.
- (291) West, W.; Gilman, P. B., *The Theory of the Photographic Process*; T. H. James ed.; Macmillan: New York, **1977**, 251.

- (292) Rostevtsev, V. V.; Green, L. G.; Fokin, V. V.; Sharpless, K. B. *Angew. Chem., Int. Ed.*, **2002**, *41*, 2596-2598.
- (293) Kolb, H. C.; Finn, M. G.; Sharpless, K. B. *Angew. Chem., Int. Ed.*, **2001**, *40*, 2004-2021.
- (294) Tornøe, C. W.; Christensen, C.; Meldal, M., Peptidotriazoles on solid phase: [1,2,3]-triazoles by regiospecific copper(I)-catalyzed 1,3-dipolar cycloadditions of terminal alkynes to azides. *J. Org. Chem.*, **2002**, *67*, 3057-3064.
- (295) Burley, G. A.; Gierlich, J.; Mofid, M. R.; Nir, H.; Tal, S.; Eichen, Y.; Carell, T. *J. Am. Chem. Soc.*, **2006**, *128*, 1398-1399.
- (296) Gierlich, J.; Burley, G. A.; Gramlich, P. M. E.; Hammond, D. M.; Carell, T. *Org. Lett.*, **2006**, *8*, 3639-3642.
- (297) Tyagi, S.; Kramer, F. R., Molecular Beacons: Probes that Fluoresce upon Hybridization. *Nat. Biotechnol.*, **1996**, *14*, 303-308.
- (298) Marras, S. A. E.; Kramer, F. R.; Tyagi, S., Efficiencies of fluorescence resonance energy transfer and contact-mediated quenching in oligonucleotide probes. *Nucl. Ac. Res.*, **2002**, *30*, e122.
- (299) Campbell, G. L.; Dennis, D. T.; In *Harrison's principles of internal medicine.*; 14th ed.; McGraw Hill: New York, **1998**; pp 975-983.
- (300) Varma-Basil, M.; El-Hajj, H.; Marras, S. A. E.; Hazbon, M. H.; Mann, J. M.; Connell, N. D.; Kramer, F. R.; Alland, D., Molecular Beacons for Multiplex Detection of Four Bacterial Bioterrorism Agents. *Clin Chem*, **2004**, *50*, 1060-1062.
- (301) Tan, W.; Wang, K.; Drake, T. J., Molecular beacons. *Current Opinion in Chemical Biology*, **2004**, *8*, 547-553.
- (302) Marras, S. A. E.; Tyagi, S.; Kramer, F. R., Real-time assays with molecular beacons and other fluorescent nucleic acid hybridization probes. *Clinica Chimica Acta*, **2006**, *363*, 48-60.
- (303) Dubertret, B.; Calame, M.; Libchaber, A. J., Single-mismatch detection using gold-quenched fluorescent oligonucleotides. *Nat Biotech*, **2001**, *19*, 365-370.
- (304) Wang, L.; Yang, C. J.; Medley, C. D.; Benner, S. A.; Tan, W., Locked Nucleic Acid Molecular Beacons. *J. Am. Chem. Soc.*, **2005**, *127*, 15664-15665.
- (305) Yang, C. J.; Lin, H.; Tan, W., Molecular Assembly of Superquenchers in Signaling Molecular Interactions. *J. Am. Chem. Soc.*, **2005**, *127*, 12772-12773.
- (306) Zemlicka, J.; Gasser, R.; Freisler, J. V.; Horwitz, J. P., Nucleosides. XV. Decarboxylative elimination of 2'-deoxynucleoside uronic acids. *J. Am. Chem. Soc.*, **1972**, *94*, 3213-3218.
- (307) Yang, T.-F.; Kotra, L. P.; Teng, Q.; Naguib, F. N. M.; Sommadossi, J.-P.; el Kouni, M.; Chu, C. K., Synthesis of [4-(hydroxy)tetrahydrofuran-2-yl]nucleosides as a novel class of uridine phosphorylase inhibitors. *Tetrahedron Lett.*, **1995**, *36*, 983-986.
- (308) Buchko, G. W.; Hruska, F. E.; Sadana, K. L., An NMR study of dinucleoside monophosphates with an O4-ethylated thymine. d(e⁴TpT) and d(Tpe⁴T). *Canadian Journal of Chemistry*, **1989**, *67*, 109-119.

- (309) Hakimelahi, G. H.; Proba, Z. A.; Ogilvie, K. K., New catalysts and procedures for the dimethoxytritylation and selective silylation of ribonucleosides. *Can. J. Chem.*, **1982**, 1106-1113.
- (310) Ogilvie, K. K., The *tert*-Butyldimethylsilyl Group as a Protection Group in Deoxynucleosides. *Can. J. Chem.*, **1973**, 51, 3799-3807.
- (311) White, J. D.; Kawasaki, M., Total synthesis of (+)-latrunculin A. *J. Am. Chem. Soc.*, **1990**, 112, 4991-4993.
- (312) Zhang, J.; Matteucci, M. D., Synthesis of a N-acylsulfamide linked dinucleoside and its incorporation into an oligonucleotide. *Bioorg. Med. Chem. Lett.*, **1999**, 9, 2213-2216.
- (313) Jung, M. E.; Xu, Y., Efficient synthesis of specifically deuterated nucleosides: Preparation of 4'-deuteriothymidine. *Heterocycles*, **1998**, 47, 349-356.
- (314) Altomare, A.; Burla, M. C.; Camalli, M.; Cascarano, G. L.; Giacovazzo, C.; Guagliardi, A.; Moliterni, A. G. G.; Polidori, G.; Spagna, R., SIR97: a new tool for crystal structure determination and refinement. *J. Appl. Crystallogr.*, **1999**, 32, 115-119.
- (315) Sheldrick, G. M., SHELXL-97. *University of Goettingen*, 97-2 version.

7 Curriculum Vitae

A N T O N I O M A N E T T O

PERSONAL DETAILS

Nationality: Italian
 Birth date: 14.11.1975
 Birth place: Messina, Italy
 Living address: Endelhauserstr., 28 80686 München, Germany
 Marital status: married with one daughter
 E-mail: antonio.manetto@cup.uni-muenchen.de
 Telephone: +49 89 2180 77849 (W), +49 176 27165298 (M), +49 89 57952984 (H)
 Fax: +49 89 2180 77756 (W)

EDUCATION

2004-2007 EU-scholarship "Marie Curie" for an "Early Stage Researcher" within the Network "CLUSTOXDNA". LMU, München, Germany.
2004 EU-Mobility scholarship "Marco Polo", Alma Mater, Bologna, Italy.
2002-2004 Italian ministerial scholarship for the "Dottorato di Ricerca in Scienze Chimiche XVII Ciclo". "CNR" and "Università di Bologna", Bologna, Italy.
2002 Qualification for the Order of Italian Chemists, II session 2001/02, Ferrara, Italy.
1995-2001 "Laurea in Chimica Industriale", Università degli studi di Bologna, Italy. Ranking: 106/110.
1989-1994 High school in the Liceo Scientifico "Archimede", Messina, Italy. Ranking 44/60

CONTRIBUTION TO CONGRESSES

CLUSTOXDNA V EU-Meeting, Oct. 2006, Gandia, Spain.

Authors: Manetto, A. Gimisis, T. Chatgililoglu, C. Carell, T.
Titel: "Independent Generation of C5'-Nucleosidyl Radicals in Thymidine and 2'-Deoxyguanosine"
Contribution: Oral talk

CLUSTOXDNA Mid-Term EU-Meeting, May. 2006, Oxford, UK.

Authors: Manetto, A. Carell, T.
Titel: "EET and M-MEET. through DNA"
Contribution: Oral talk

Cerlib 2006, Mar. 2006, Annecy, France.

Authors: Manetto, A. Breeger, S. Chatgililoglu, C. Carell, T.
Titel: "EET. through DNA Investigated with Differently Strong Electron Acceptors"
Contribution: Poster

CLUSTOXDNA IV EU-Meeting, Mar. 2006, Annecy, France.

Authors: Manetto, A. Clever, G. Carell, T.
Titel: "M-MEET. Metal mediated excess electron transfer through DNA"
Contribution: Oral talk

CLUSTOXDNA III EU-Meeting, Oct. 2005, Athens, Greece.

Authors: Manetto, A. Breeger, S. Chatgililoglu, C. Carell, T.
Titel: "Excess Electron Transfer Through DNA Investigated with Differently Strong Electron Acceptors Reveals Complex Sequence Dependence"
Contribution: Oral talk

CLUSTOXDNA II EU-Meeting, Feb. 2005, München, Germany.

Authors: Manetto, A. Breeger, S. Chatgililoglu, C. Carell, T.

Titel: "8-Br-purines: new electron acceptors for the EET in DNA"

Contribution: Oral talk

ISOFR 9th, June 2004, Porto Vecchio, Corsica, France.

Authors: Manetto, A. Montevecchi, P. C. Navacchia, M. L. Chatgililoglu, C.

Titel: "Radical Cyclization Approach to Cyclonucleosides"

Contribution: Poster

3th SAYCS and COFEM 2003, May 2003, Riccione, Italy.

Authors: Manetto, A.

Titel: "Radical decomposition of the *tert*-butyl perester of the thymidinoic acid: the fate of *pseudo*-C4' radical."

Contribution: Oral communication and Poster

XV International Round Table Nucleosides, Nucleotides and Nucleic acids Sept. 2002, Leuven, Belgium.

Authors: Manetto, A. Montevecchi, P. C. Navacchia, M. L. Chatgililoglu, C.

Titel: "Model studies on the fate of C-5' radicals under aerobic conditions: the case of *pseudo*-C4' radical"

Contribution: Poster

SCIENTIFIC PUBLICATIONS

Manetto, A; Chatgililoglu, C.; Giese, B.; Carell, T.; The Kind of Electron Injection into DNA Determines the Chemistry: Only Ground state Donors Trigger with one Electron two Reaction. *Manuscript in preparation.*

Hammond, D. M.;* **Manetto, A.;*** Gierlich, J.; Azov, V. A.; Gramlich, P. M. A.; Burley, G. A.; Maul, M.; Carell, T., Click-Chemistry Combined with Black-and-White Photography allows Ultra-sensitive DNA Detection by Eye. *Angew. Chem. Int. Ed.*, **2007**, *46*, 4184-4187.

Manetto, A.; Georganakis, D.; Gimisis, T.; Leondiadis, L.; Carell, T.; Chatgililoglu, C., Independent Generation of C5'-Nucleosidyl Radicals in Thymidine and 2'-Deoxyguanosine. *J. Org. Chem.*, **2007**, *72*, 3659-3666.

Manetto, A.; Breeger, S.; Chatgililoglu, C.; Carell, T., Complex Sequence Dependence by Excess-Electron Transfer through DNA with Different Strength Electron Acceptors. *Angew. Chem. Int. Ed.*, **2006**, *45*, 318-321.

Navacchia, M. L.; **Manetto, A.;** Montevecchi, P. C.; Chatgililoglu, C., Radical Cyclization Approach to Cyclonucleosides. *Eur. J. Org. Chem.*, **2005**, 4640-4648.

Montevecchi, P. C.; **Manetto, A.;** Navacchia, M. L.; Chatgililoglu, C., Thermal decomposition of the *tert*-butyl perester of thymidine-5'-carboxylic acid. Formation and fate of the *pseudo*-C4' radical. *Tetrahedron*, **2004**, *60*, 4303-4308.

Peri, F.; Binassi, E.; **Manetto, A.;** Marotta, E.; Mazzanti, A.; Righi, P.; Scardovi, N.; Rosini, G., Preparation of Bicyclo[3.2.0]heptane-2-endo,7-endo-diols: 1,3-Diols with a Chiral Rigid Backbone. *J. Org. Chem.*, **2004**, *69*, 1353-1356. Also in *ChemInform*, **2004**, *35*, 42-43.

LANGUAGES

Italian: Native speaker
English: Fluently spoken and written
German: Intermediate spoken and written
Spanish: Basic knowledge